**UNIVERSIDADE DE BRASÍLIA**
**PROGRAMA DE PÓS-GRADUAÇÃO EM PATOLOGIA MOLECULAR**

**ANA CLARA BARBOSA ANTONELLI**

# Desenvolvimento de Anticorpos Monoclonais Anti-*Fusion Loop* de Ortoflavivírus a partir de uma Biblioteca Combinatória Apresentada em Fago (*Phage Display*) Derivada de Células B de Memória

**Brasília**
**2025**

**ANA CLARA BARBOSA ANTONELLI**

# Desenvolvimento de Anticorpos Monoclonais Anti-*Fusion Loop* de Ortoflavivírus a partir de uma Biblioteca Combinatória Apresentada em Fago (*Phage Display*) Derivada de Células B de Memória

Tese de Doutorado apresentada ao Programa de Pós-Graduação em Patologia Molecular da Universidade de Brasília como requisito para obtenção do título de Doutora em Patologia Molecular.
Orientadora: Prof.ª Dr.ª Andrea Queiroz Maranhão
Coorientador: Prof. Dr. Marcelo de Macedo Brígido

**Brasília**
**2025**

Ficha catalográfica elaborada automaticamente,
com os dados fornecidos pelo(a) autor(a)

BA635dd

Barbosa Antonelli, Ana Clara
Desenvolvimento de Anticorpos Monoclonais Anti-Fusion Loop de Ortoflavivírus a partir de uma Biblioteca Combinatória Apresentada em Fago (Phage Display) Derivada de Células B de Memória / Ana Clara Barbosa Antonelli; orientador Andrea Queiroz Maranhão; co-orientador Marcelo da Macedo Brígido. Brasília, 2025.
134 p.

Tese(Doutorado em Patologia Molecular) Universidade de Brasília, 2025.

1. Anticorpos monoclonais. 2. Phage Display. 3. Ortoflavivírus. 4. Fusion loop. 5. Anticorpos terapêuticos. I. Queiroz Maranhão, Andrea, orient. II. da Macedo Brígido, Marcelo, co-orient. III. Título.

**PROGRAMA DE PÓS-GRADUAÇÃO EM PATOLOGIA MOLECULAR**
**UNIVERSIDADE DE BRASÍLIA**

**Banca Examinadora da Tese De Doutorado**

**Aluna: Ana Clara Barbosa Antonelli**

**Orientadora: Profª. Drª. Andrea Queiroz Maranhão**

**Coorientador: Prof. Dr. Marcelo De Macedo Brígido**

**Membros da Banca**

**Prof. Dr. Gilvan Pessoa Furtado (Membro Titular)**

**Profª. Drª. Kelly Grace Magalhães (Membro Titular)**

**Prof. Dr. Carlos Roberto Prudêncio (Membro Titular)**

**Profª. Drª. Juliana Franco de Almeida (Suplente)**

Aos meus pais,

pelo amor e apoio incondicional que me sustentaram até aqui.

**AGRADECIMENTOS**

Este trabalho é fruto do esforço coletivo e da colaboração de muitas pessoas que generosamente dedicaram seu tempo e contribuíram de forma essencial em cada etapa. A ciência não se faz sozinha, ela é construída na parceria, no compartilhamento e no apoio mútuo.

Agradeço aos meus orientadores Andréa e Marcelo pela confiança e todo o conhecimento compartilhado. Me sinto privilegiada de fazer parte de um laboratório leve, acolhedor e divertido, um ambiente que existe, em grande parte, graças à parceria harmoniosa dos dois. Individualmente, são pesquisadores excepcionais; juntos, formam uma dupla rara e admirável no meio acadêmico. Marcelo combina uma mente brilhante com uma tranquilidade invejável, enquanto Andréa traz energia, determinação e a capacidade de encontrar soluções para qualquer desafio que apareça. Sou imensamente grata por todo o cuidado, incentivo e apoio que recebi ao longo desses anos. Admiro-os muito, e na Andréa encontrei uma inspiração do tipo de pesquisadora e professora que desejo me tornar "quando crescer".

Aos todos os amigos do Lab1. À safra atual do lab, Lucas, Pietra, Maria, Renato Oliveira, Sylvia, Luísa, Dy, Werneck, Igor, Manu, Bel e Paulo por fazerem do nosso lab um ambiente descontraído e de parceria. Vocês são incríveis! Em especial, agradeço ao Lucas, minha "duplinha", pela amizade e pela imensa parceria ao longo desses anos. Obrigada por recuperar minhas células eletroporadas dia após dia, e por cada phage, transfecção, purificação, ELISA e PRNT realizados juntos. Obrigada também pelo apoio moral sempre que eu preciso pedir algo em outro laboratório, por me ensinar a lidar com proteínas, por me ouvir tagarelar diariamente e pelos comentários pontuais e certeiros. A ele e à Maria, agradeço pela parceria nos projetos com vírus, mesmo em meio a uma grande onda de CAR-T! Agradeço também ao Hítallo, que passou pouco tempo no laboratório, mas que, por ser meu vizinho, acabou se tornando um grande apoio em Brasília. A Jacy, que foi quem me trouxe para o lab, e sempre me deu muito apoio desde antes do doutorado, quando eu era IC dela que era mestranda na UFG. A Dayane Prado e Luiz pela amizade dentro e fora do lab.

A todos os colegas que passaram pelo laboratório ao longo desses anos e aos que ainda estão aqui, deixo minha sincera gratidão. Ao Pedro, pela condução cuidadosa das análises de bioinformática; ao Renato Kaylan, que me ensinou tanto quando cheguei ao laboratório no primeiro ano do doutorado, completamente inexperiente em biologia molecular; a todos os ICs que se dedicam aos seus primeiros anos na ciência e completam nosso laboratório; e a tantos outros que me ajudaram, seja tirando uma placa da estufa, seja compartilhando momentos de descontração na copa;

Ao professor Brandon DeKosky, do Ragon Institute of MGH, MIT and Harvard, agradeço pela abertura e receptividade desde o primeiro contato, permitindo que eu realizasse o doutorado sanduíche em seu laboratório. Graças a essa oportunidade, vivi experiências que jamais imaginei que seriam possíveis. A todos os colegas e amigos do DeKosky Lab, Matheus, Ahmed, Jihwan, Matias, Gene, Emily, Shelbe, Blythe, Azady, Evan, Shawn, Anurag, Camila e Katerina. Em especial, agradeço ao Matheus, que foi um mentor e amigo, e Ahmed e Matias, pela disponibilidade de ajudar e orientação nos experimentos. Agradeço também aos amigos Jihwan e sua esposa, Jiin, por serem algumas das pessoas mais gentis que já conheci.

A todos os responsáveis por tornar possível, ano após ano (por mais de duas décadas), o curso de Phage Display do Cold Spring Harbor Laboratory. Participar desse curso foi uma das experiências mais incríveis que vivi, chegando para reacender meu brilho nos olhos pela ciência em um momento especialmente difícil, marcado por obstáculos experimentais e resultados desafiadores. Aos instrutores e co-instrutores Gregg Silverman, Gianluca Veggiani, Johannes Yeh e Jason (Qichen) Tang, agradeço imensamente por todo o conhecimento compartilhado com tanta generosidade. Aos quinze colegas de curso e aos palestrantes convidados, em especial George Smith, que mesmo laureado com um Prêmio Nobel, é uma pessoa extremamente humilde e gentil. E aos amigos que ganhei ali, Paula, Josh e Ryan, que levo comigo com muito carinho, mesmo à distância.

Aos alunos e professores dos laboratórios da “Biomol” e “Biofísica”, que colaboraram com linhagens celulares, reagentes, equipamentos e tempo.

A professora Lucimeire  pelo tempo e espaço dedicados ao aprendizado e realização dos ensaios de neutralização (PRNT) na Universidade Federal de Goiás.

Aos membros da banca por disponibilizar tempo para a avaliação e contribuição com esse trabalho.

À Universidade de Brasília e ao Programa de Pós-Graduação em Patologia Molecular, agradeço pela estrutura necessária à execução deste projeto e pelas oportunidades de crescimento acadêmico. Também agradeço às agências de fomento CAPES e FAP-DF pelo suporte financeiro que possibilitou o desenvolvimento desta pesquisa.

À minha família, minha base. Aos meus pais, Wilson e Lucimeire, minhas maiores fontes de inspiração e encorajamento, cujo amor e apoio incondicional me fortalecem todos os dias. Ao meu irmão Lucas, um dos maiores parceiros que a vida poderia me dar. Sinto-me profundamente privilegiada por pertencer a uma família tão estruturada, presente e amorosa. Aos meus tios, primos e avós, que completam essa família que me faz tão bem, agradeço pelo carinho e apoio de sempre. Cada almoço de família me relembra os motivos do meu esforço e da minha dedicação. Em especial à Laíza e Nara, minhas primas-irmãs. Em "família", incluo também os amigos da vida, Ana Tereza, Thaiz, Leonardo e Luísa, que me ouviram e me incentivaram tanto ao longo desses anos de doutorado. E aos amigos um pouco mais distantes, mas sempre presentes, Luiz, Luizinho, Anthony e Antônio, agradeço pelo cuidado e pela dedicação em me ajudar tantas vezes.

Por fim, agradeço a todos que, de alguma forma, contribuíram para que eu chegasse até aqui, seja com uma palavra de apoio, uma sugestão, ou simplesmente com presença. Cada gesto fez diferença.

**SUMÁRIO**

**LISTA DE ABREVIATURAS**

| | |
|---|---|
| BCR | Receptor de células B |
| CBM | Células B de memória |
| cDNA | Ácido desoxirribonucléico complementar |
| CDR | Região determinante de complementaridade |
| CH | Domínio constante da cadeia pesada de um anticorpo |
| CL | Domínio constante da cadeia leve de um anticorpo |
| C-terminal | Extremidade carboxi - terminal |
| $CT_{HF}$ | Célula T auxiliar folicular |
| DENV | Dengue Virus |
| DNA | Ácido desoxirribonucléico |
| Fab | Fragmento de anticorpo de ligação ao antígeno |
| Fc | Fragmento cristalizável de anticorpo (porção constante) |
| FR | Arcabouço (*Framework*) |
| Fv | Fragmento variável do anticorpo |
| GC | Centro germinativo |
| Ig | Imunoglobulina |
| IL | Interleucina |
| JEV | Vírus da encefalite japonesa |
| NGS | *Next-Generation Sequencing* |
| NS | Proteínas não-estruturais |
| PBMC | Células Mononucleares de Sangue Periférico |
| PCR | Reação em cadeia da polimerase |
| PRR | Pattern recognition receptors |
| PVZ | Positivo para ZIKV |
| PZD | Positivo para ZIKV e DENV |
| RE | Retículo Endoplasmático |
| RNA | Ácido ribonucléico |
| rpm | Rotações por minuto |
| scFv | Fragmento variável de anticorpo cadeia única (*Single chain Fragment Variable*) |
| ssRNA | *Single-standed* RNA |
| TLR | *Toll Like Receptors* |

| | |
|---|---|
| VH | Domínio variável da cadeia pesada de um anticorpo |
| VL | Domínio variável da cadeia leve de um anticorpo |
| WNV | *West Nile Virus* |
| YFV | *Yellow Fever Virus* |
| ZIKV | *Zika Virus* |

**LISTA DE FIGURAS**

**LISTAS DE TABELAS**

**RESUMO**

Os ortoflavivírus, como dengue (DENV), zika (ZIKV) e febre amarela (YFV), constituem um importante problema de saúde pública, e ainda não há terapias antivirais específicas disponíveis. Diante desse cenário, anticorpos monoclonais humanos surgem como ferramentas promissoras para o desenvolvimento de terapias direcionadas e estratégias profiláticas. Este trabalho teve como objetivo a geração e aplicação de uma biblioteca apresentada em fago (*phage display*) derivada de células B de memória humanas para a seleção de anticorpos monoclonais contra o fusion loop (FL), uma região altamente conservada da proteína de envelope (E) dos ortoflavivírus que pode favorecer a recuperação de clones com amplo espectro de neutralização. A biblioteca foi construída no formato single-chain variable fragment (scFv), utilizando o vetor pComb3XSS, e apresentou diversidade estimada de $7{,}8 \times 10^6$ transformantes. O repertório foi obtido a partir de células mononucleares de sangue periférico de indivíduos previamente expostos a DENV e/ou ZIKV, estimuladas *in vitro* para a expansão de células B de memória. O processo de seleção foi realizado com um peptídeo mimético do *fusion loop* do envelope viral, e os clones enriquecidos foram analisados por sequenciamento de nova geração (NGS) e convertidos para os formatos FvFc e IgG1, visando expressão em células Expi293. Dois anticorpos, FH2 e FH4, foram expressos e purificados com sucesso no formato IgG1. Ambos apresentaram ligação a ZIKV e aos quatro sorotipos de DENV, com diferentes perfis de afinidade, e demonstraram neutralização efetiva contra ZIKV e DENV-2. Esses resultados confirmam que o *loop* de fusão é um alvo funcional capaz de induzir anticorpos humanos de ampla reatividade e neutralização cruzada. O conjunto de dados obtido validam a abordagem experimental empregada, demonstrando que a combinação entre *phage display* e repertórios de memória humana é capaz de gerar anticorpos de alta afinidade e relevância funcional, e que a utilização do *fusion loop* como alvo favoreceu a seleção de anticorpos de ligação cruzada. Esses achados contribuem para o avanço do desenvolvimento de anticorpos terapêuticos contra ortoflavivírus.

**Palavras-chave:** anticorpos monoclonais humanos; *phage display*; ortoflavivírus; *fusion loop*; anticorpos terapêuticos.

**ABSTRACT**

Orthoflaviviruses, such as dengue virus (DENV), Zika virus (ZIKV), and yellow fever virus (YFV), represent a major public health concern, and there are still no specific antiviral therapies available. In this context, human monoclonal antibodies have emerged as promising tools for the development of targeted therapies and prophylactic strategies. This study aimed to generate and apply a phage-displayed library derived from human memory B cells for the selection of monoclonal antibodies targeting the fusion loop (FL), a highly conserved region of the orthoflavivirus envelope (E) protein that may favor the recovery of clones with broad neutralization potential. The library was constructed in the single-chain variable fragment (scFv) format using the pComb3XSS vector and exhibited an estimated diversity of $7.8 \times 10^6$ transformants. The antibody repertoire was obtained from peripheral blood mononuclear cells of individuals previously exposed to DENV and/or ZIKV, which were stimulated in vitro to expand memory B cells. The selection process was performed using a mimetic peptide corresponding to the viral envelope fusion loop, and enriched clones were analyzed by next-generation sequencing (NGS) and converted into FvFc and IgG1 formats for expression in Expi293 cells. Two antibodies, FH2 and FH4, were successfully expressed and purified in the IgG1 format. Both antibodies bound to ZIKV and all four DENV serotypes, displaying distinct affinity profiles, and demonstrated effective neutralization against ZIKV and DENV-2. These results confirm that the fusion loop is a functional target capable of eliciting human antibodies with broad reactivity and cross-neutralizing activity. The data obtained validate the experimental approach employed, demonstrating that the combination of phage display and human memory repertoires can generate antibodies with high affinity and functional relevance, and that targeting the fusion loop favored the selection of cross-reactive antibodies. Collectively, these findings contribute to the advancement of therapeutic antibody development against orthoflaviviruses.

**Keywords:** human monoclonal antibodies; phage display; orthoflaviviruses; fusion loop; therapeutic antibodies.

# 1 INTRODUÇÃO

## 1.1 Aspectos gerais, origem e epidemiologia das infecções por ortoflavivírus

O gênero Ortoflavivírus corresponde ao maior dos quatro gêneros da família Flaviviridae. Os ortoflavivírus são vírus de RNA de cadeia simples e polaridade positiva (ssRNA+), transmitidos principalmente por vetores artrópodes como mosquitos e carrapatos (Lindenbach; Rice, 2003). O subgrupo de ortoflavivírus transmitidos por mosquitos inclui vírus de significativo impacto na saúde pública global, sendo os mais típicos os vírus da dengue (DENV), da febre amarela (YFV), Zika (ZIKV), do Nilo Ocidental (WNV) e da Encefalite japonesa (JEV). Estes vírus são transmitidos principalmente por mosquitos do gênero Aedes (DENV, YFV, ZIKV) e Culex (WNV e JEV), apesar do ZIKV ser também transmitido por vias sexual, vertical e por transfusões sanguíneas (Barjas-Castro et al., 2016; Calvet et al., 2016; Kramer; Styer; Ebel, 2008; Petersen; Marfin, 2008; Van den Hurk; Ritchie; Mackenzie, 2009).

A dengue é uma doença infecciosa reemergente e negligenciada, causada por 4 sorotipos de DENV geneticamente distintos e biologicamente semelhantes entre si (Guzman; Harris, 2015; Halstead, 2019). Dentre os ortoflavivírus, os DENVs destacam-se pela maior distribuição geográfica, tendo causado infecções em cerca de 128 países (Bhatt et al., 2013; Messina et al., 2014). Aproximadamente 400 milhões de casos de infecção pelo DENV ocorrem globalmente a cada ano, resultando em cerca de 40 mil óbitos, principalmente associados às formas graves da doença (CDC, 2023). No Brasil, em 2025, foram registrados 1.661.001 casos prováveis de dengue, com um coeficiente de incidência de 781,3 casos por 100 mil habitantes. No mesmo período, 1.786 óbitos por dengue foram confirmados, além de 184 óbitos ainda em investigação, refletindo o elevado impacto da doença no país. A letalidade observada foi de 0,11% entre os casos prováveis, alcançando 4,98% nos casos graves, evidenciando a gravidade clínica e o desafio contínuo para o sistema de saúde brasileiro (Ministério da Saúde, 2025).

O Zika vírus (ZIKV) foi primeiramente isolado de macacos Rhesus em 1947 na floresta Zika em Uganda (Dick; Kitchen; Haddow, 1952). Os primeiros relatos de infecções em humanos pelo ZIKV ocorreram na década de 60 em países da África e Ásia (Simpson, 1964; Marchette; Garcia; Rudnick, 1969), no entanto, apenas em 2013 na Polinésia Francesa e em 2015 no Brasil, o vírus foi associado a complicações neurológicas em adultos e fetos de grávidas infectadas, respectivamente (De Araújo et al., 2016; Musso; Nilles; Cao-Lormeau, 2014). No Brasil, entre 2015 e 2017,

aproximadamente 270 mil casos prováveis de infecção por ZIKV foram notificados, incluindo cerca de 20 mil casos em gestantes (Ministério da Saúde, 2018). Um estudo epidemiológico conduzido em 2016 demonstrou que, entre 116 gestantes acompanhadas, 42% tiveram bebês com malformações congênitas, evidenciando o elevado impacto da infecção durante a gestação (Brasil et al., 2016). Após 2017, o número de casos de ZIKV diminuiu consideravelmente e o período emergencial foi oficialmente encerrado. No entanto, a circulação viral persiste no país, e em 2025 foram registrados 4.119 casos prováveis de Zika, com coeficiente de incidência de 1,9 casos por 100 mil habitantes e registro de um óbito, indicando que, apesar da redução expressiva em relação aos anos epidêmicos, o ZIKV continua representando um risco à saúde pública no Brasil (Ministério da Saúde, 2025).

## 1.2 Manifestações clínicas das infecções por ortoflavivírus

Aproximadamente 50-80% das infecções por ortoflavivírus são assintomáticas ou caracterizadas por sintomas leves (Pierson; Diamond, 2020). A maioria das infecções sintomáticas por ortoflavivírus resulta em doenças autolimitadas, causando sintomas leves a moderados como febre, cefaleia, mialgia e artralgia (Guarner; Hale, 2019; Higuera; Ramírez, 2019). No entanto, a depender de fatores específicos do vírus (virotipos, virulência, mecanismos de evasão do sistema imunológico) e do hospedeiro (comorbidades, idade, exposição prévia, estado imunológico, características genéticas), diferentes complicações no curso da doença podem ocorrer (Aguiar et al., 2020; Boonak et al., 2011; Lim et al., 2008; Loke et al., 2017; Murray et al., 2006; Pierson; Diamond, 2020). Alguns ortoflavivírus como ZIKV, WNV e JEV são neurotrópicos, podendo atravessar a barreira hematoencefálica e causar complicações neurológicas (Chen et al., 2021; Guarner; Hale, 2019; Jr et al., 2014; Oliveira Melo et al., 2016). Já os vírus da dengue e febre amarela são viscerotrópicos, podendo causar lesões em órgãos relevantes como fígado e rins (Monath; Vasconcelos, 2015; Pang; Zhang; Cheng, 2017).

O neurotropismo do ZIKV pode desencadear complicações graves como a Síndrome de Guillain-Barré, uma neuropatia aguda que pode levar a paralisia (Créange, 2016; Musso; Nilles; Cao-Lormeau, 2014), e Síndrome congênita do ZIKV (SCZ) (Musso; Nilles; Cao-Lormeau, 2014; Oliveira Melo et al., 2016). Esta última é caracterizada por má formação neurológica, morfológica, auditiva e oftalmológica em fetos de gestantes infectadas. Dentre essas alterações, destacam-se a microcefalia,

problemas de deglutição, anormalidades auditivas, hipoplasia ou atrofia do nervo óptico, hipoplasia do tronco cerebral e ventriculomegalia (CDC, 2019; De Barros Miranda-Filho et al., 2016; Oliveira Melo et al., 2016).

Em uma parcela dos indivíduos, a dengue evolui para doença grave com a infecção de órgãos e tecidos viscerais pelo vírus. A dengue grave é caracterizada por trombocitopenia e aumento da permeabilidade capilar, que levam ao choque hipovolêmico, podendo resultar em comprometimento de órgãos, hemorragia grave e choque cardiogênico (Guzman; Harris, 2015; Tayal; Kumar; Rakesh, 2023). Além disso, lesões imunomediadas, e os efeitos diretos do vírus nos rins podem levar a insuficiência renal, hepatomegalia e insuficiência hepática aguda (Leowattana; Leowattana, 2021; Tayal; Kumar; Rakesh, 2023). Apesar de o vírus da dengue não ser considerado um vírus neurotrópico clássico, complicações neurológicas, incluindo encefalopatia, já foram associadas à infecção, principalmente pelos sorotipos DENV-2 e DENV-3 (Trivedi; Chakravarty, 2022). Além disso, há relatos raros de infecção persistente do DENV no sistema nervoso central, culminando em um quadro de panencefalite crônica, mesmo na ausência de imunodeficiência aparente (Johnson et al., 2019).

### 1.3 Genética e estrutura da partícula viral

O material genético dos ortoflavivírus é de RNA fita simples de polaridade positiva (ssRNA +) com aproximadamente 11 kb de comprimento. Seu genoma contém uma única Open Reading Frame (ORF) que codifica uma poliproteína de aproximadamente 3400 resíduos, e duas regiões não-codificadoras (5’ e 3’ UTR – untranslated region). A extremidade 5’ possui cap, importante para a tradução do RNA viral, enquanto a extremidade 3’ não apresenta poliadenilação (Dey et al., 2021; Lindenbach; Rice, 2003). A poliproteína codificada pelo genoma viral é clivada por proteases celulares e virais em três proteínas estruturais (capsídio (C), proteína precursora de membrana (prM) e envelope (E)), e sete proteínas não-estruturais (NS1, NS2A, NS2B, NS3, NS4A, NS4B e NS5) (Dey et al., 2021; Lindenbach; Rice, 2003).

O capsídio dos ortoflavivírus possui morfologia icosaédrica e é envolto por um envelope lipídico esférico, tendo em torno de 50 nm de diâmetro. A proteína do capsídio está envolvida no empacotamento do genoma viral e na formação do nucleocapsídio. A prM atua no dobramento e estabilização da proteína E, e é posteriormente clivada dando origem ao peptídeo pr, que será secretado, e à proteína M (~75 aa).

A proteína E possui sítios de ligação a receptores celulares e um loop de fusão, que contribuem para o processo de adsorção e fusão do envelope viral à membrana endossomal da célula hospedeira (Dey et al., 2021; Lindenbach; Rice, 2003; Sirohi; Kuhn, 2017). A proteína E dos Ortoflavivírus é uma estrutura de três domínios: domínio I (DI), domínio II (DII) e domínio III (DIII). Os três domínios da proteína são conectados por dobradiças flexíveis que medeiam mudanças conformacionais da proteína durante o ciclo replicativo viral (Zhang et al., 2017). O domínio I é localizado centralmente na proteína E, atuando como uma ponte entre os domínios II e III. O domínio II contém o loop de fusão, região hidrofóbica e mais conservada da proteína E entre os ortoflavivírus, que é essencial para a fusão do vírus à célula hospedeira, e o domínio III é o local de ligação do vírus a receptores celulares (Heinz; Allison, 2001; Heinz; Stiasny, 2017; Zhang et al., 2017).

As proteínas não-estruturais compõem o complexo replicativo dos ortoflavivírus. A proteína NS3, por exemplo, é essencial para a replicação viral e processamento da poliproteína, uma vez que apresenta um domínios de protease e helicase (Lin et al., 2018). Já a NS5 possui uma RNA polimerase dependente de RNA (RdRp) no domínio C-terminal que desempenha papel central na síntese do RNA viral (Lu; Gong, 2017).

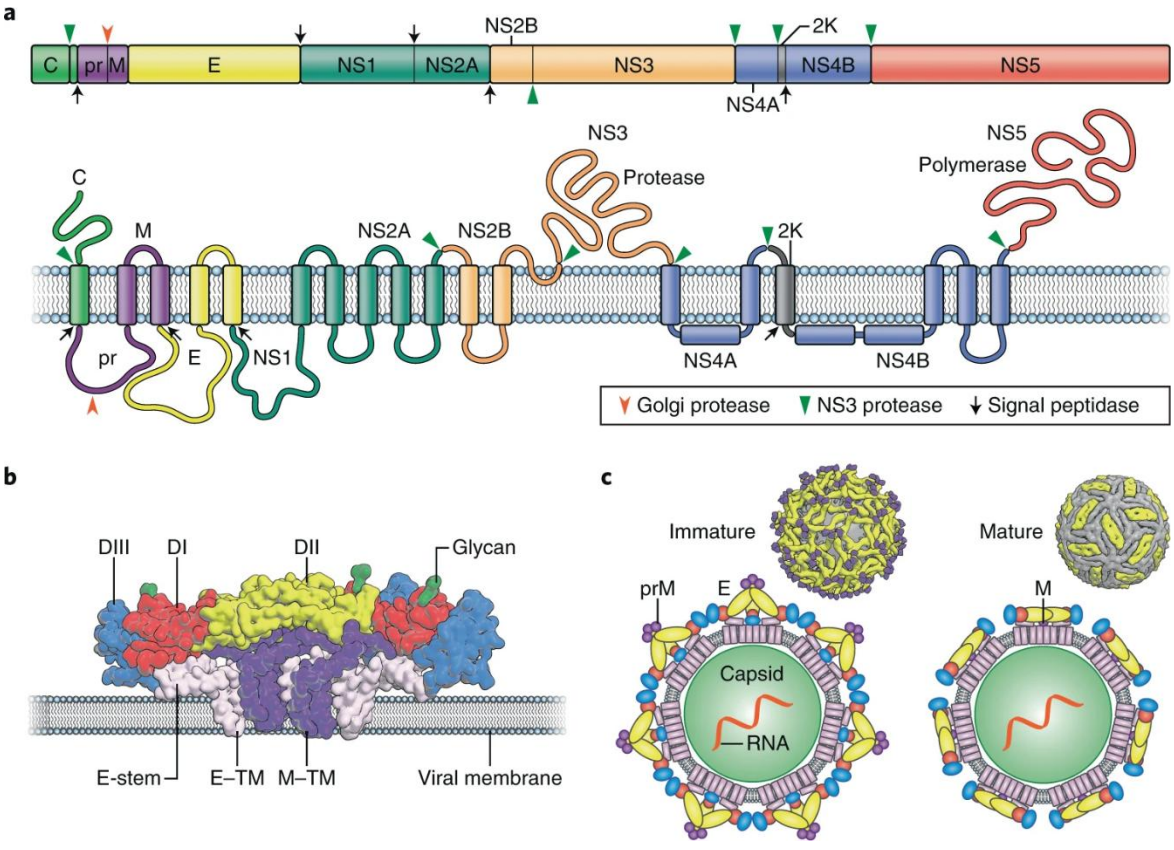


**Figura 1. Estrutura e organização genômica dos ortoflavivírus.** O material genético dos ortoflavivírus codifica uma única poliproteína que é clivada por proteases virais e da célula hospedeira, resultando em

três proteínas estruturais, C, prM e E, e sete proteínas não estruturais (A). As proteínas E dos ortoflavivírus possuem três domínios aderidos à membrana viral por uma haste e dois domínios transmembranares. Em roxo está representada a proteína M (B). Representação do arranjo das proteínas E e M nas formas imatura e madura do virion (C). Pierson e Diamond, 2020.

## 1.4 Ciclo replicativo dos ortoflavivírus

A adsorção dos ortoflavivírus à célula hospedeira é mediada pela interação da proteína E dos vírus a receptores de lectina do tipo C (CLRs), receptores de fosfatidilserina da família TIM (TIM-1, TIM-3, TIM-4) e TAM (TYRO3, AXL e MER) na superfície celular (Perera-Lecoin et al., 2013).

O ciclo replicativo dos ortoflavivírus se inicia com a entrada do vírus na célula hospedeira por meio da interação entre os receptores celulares mencionados e as proteínas do envelope viral, em um processo de endocitose mediada por clatrina. A vesícula endocítica que carrega o vírus é entregue aos endossomos iniciais, que amadurecem em endossomos tardios (Pierson; Diamond, 2020). O pH ácido do endossomo desencadeia alterações conformacionais na proteína E viral, expondo o peptídeo de fusão, que interage com a membrana endossomal permitindo a fusão do envelope viral e a membrana endossomal com a consequente liberação do RNA genômico no citoplasma (Chong et al., 2019; Pierson; Diamond, 2020). O processo de fusão está representado na figura 2.

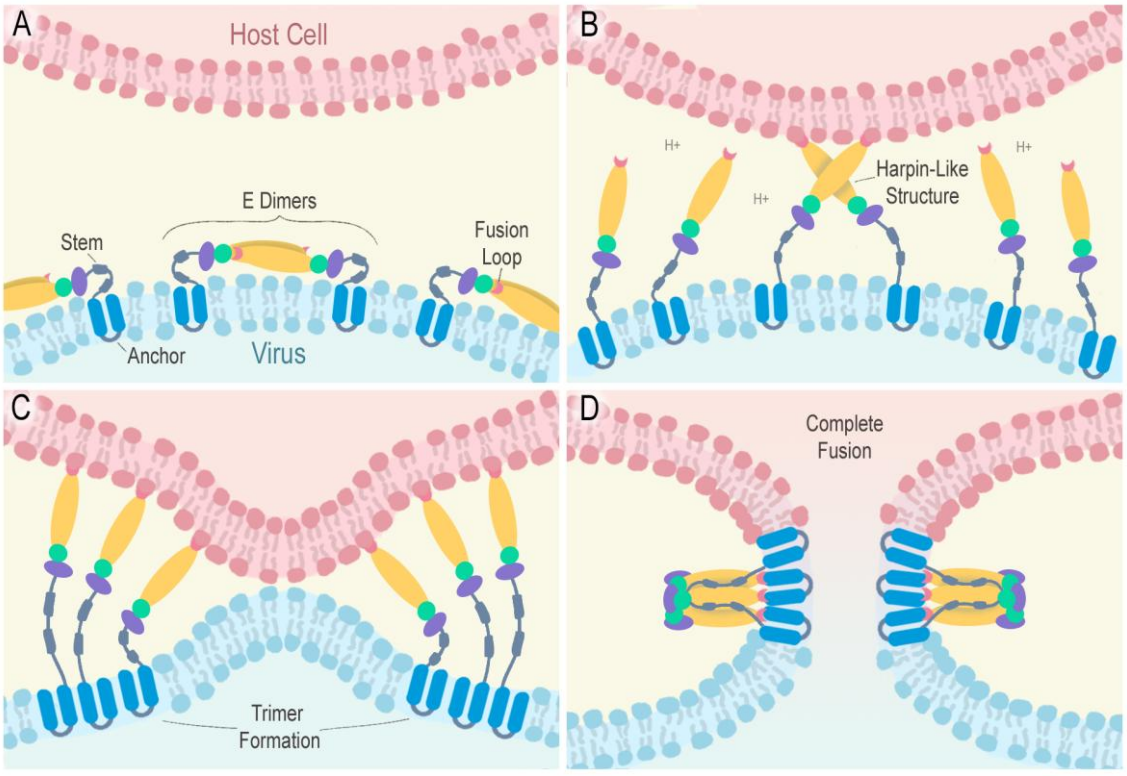


**Figura 2. Mecanismo de fusão de membranas mediado pela proteína de envelope (E) de ortoflavivírus.** Representação esquemática das etapas sequenciais do processo de fusão entre o

ortoflavivírus e a célula hospedeira, mediado pela glicoproteína de envelope. (A) No vírion maduro, as proteínas E formam dímeros antiparalelos que se dispõem de forma plana sobre a superfície viral, com os *fusion loops* (em rosa) enterrados na interface do dímero, impedindo a interação prematura com a membrana da célula hospedeira. (B) A acidificação endossomal (influxo de $H^+$) desencadeia mudanças conformacionais que dissociam os dímeros e expõem os *fusion loops*, que então se inserem na membrana da célula hospedeira. As proteínas E se estendem formando uma conformação intermediária em forma de grampo (*hairpin*). (C) A trimerização subsequente das proteínas E aproxima as membranas viral e endossomal, ancorando ambas por meio dos fusion loops inseridos e dos domínios transmembrana (TM1/TM2, em azul). (D) As proteínas E se rearranjam em um trímero estável, posicionando lado a lado os fusion loops e as âncoras de membrana, o que facilita a formação de um poro de fusão através do qual o genoma viral é liberado no citoplasma da célula hospedeira. Os domínios estruturais da proteína E estão codificados por cores: Domínio I (EDI) em verde, Domínio II (EDII) em amarelo, com o fusion loop em sua extremidade em rosa, Domínio III (EDIII) em roxo, a região da haste (stem) em cinza e os segmentos transmembrana TM1 e TM2 em azul. Antonelli et al. 2025.

No citoplasma, o RNA genômico é traduzido na poliproteína precursora, que é processada e origina as proteínas estruturais e as proteínas não-estruturais que compõem o complexo replicativo. A montagem do vírus ocorre na membrana do retículo endoplasmático (RE) e leva à formação de vírions imaturos e não infecciosos, que são transportados para o complexo de Golgi para processamento e maturação. O pH ácido no complexo de Golgi desencadeia o rearranjo do envelope viral e clivagem da prM pela protease celular furina em proteína M, dando origem aos vírions maduros infecciosos que serão liberados por vesículas exocíticas e poderão infectar novas células (Chong et al., 2019; Pierson; Diamond, 2020; Van Leur et al., 2021).

## 1.5 Resposta Imune aos Ortoflavivírus

A célula hospedeira possui receptores de reconhecimento de padrões (PRRs) nos compartimentos endossomais e no citoplasma capazes de detectar o material genético viral. O RNA viral de fita simples (ssRNA) dos ortoflavivírus que se replicam no citosol é detectado por receptores toll-like 7 (TLR7) e 8 (TLR8). A replicação do RNA viral gera RNA de fita dupla (dsRNA) que é detectado principalmente por RIG-I (Gene induzível por ácido retinóico I), TLR3 e MDA5 (Proteína 5 associada à diferenciação de melanoma) (Ngono; Shresta, 2018; Van Leur et al., 2021).

O reconhecimento do material genético viral pelos PRRs celulares desencadeia a ativação de fatores de transcrição como STAT1 e 2, e NF-κB, que induzem a síntese de interferons, principalmente do tipo I (IFN-α, β) e tipo III, além de outras citocinas e quimiocinas inflamatórias que modulam as respostas imunes inata e adaptativa (Ferraris; Yssel; Missé, 2019; Ngono; Shresta, 2018).

O sistema de interferon tipo I é um importante mediador da proteção contra infecções por ortoflavivírus, no entanto, os ortoflavivírus são capazes de antagonizar esta resposta imune inata antiviral. O ZIKV prejudica as vias de sinalização de IFNs inibindo a fosforilação de STAT1, e degradando as moléculas de sinalização JAK1 e STAT2 por meio de sua interação com proteínas NS2B e NS3, e NS5, respectivamente (Bowen et al., 2017; Grant et al., 2016; Serman; Gack, 2019; Xia et al., 2018). Similarmente, a proteína NS2A do WNV inibe a fosforilação de STAT1 e STAT2, e subsequente transcrição de genes antivirais (Liu et al., 2006).

As respostas imunes adaptativas celular e humoral são essenciais para o controle da infecção por ortoflavivírus. As respostas das células T apresentam um importante papel no controle da disseminação e eliminação do patógeno. Enquanto as células T CD4+ produzem citocinas importantes para a coordenação de diferentes elementos da resposta imune, as células T CD8+ citotóxicas são capazes de eliminar as células infectadas diretamente (Pardy; Richer, 2019). Já a resposta imune humoral contra infecções virais é imprescindível para neutralização viral. Além disso, os anticorpos desempenham um conjunto diverso de funções efetoras que contribuem para o controle de infecções virais.

Após a ativação de células B e o estabelecimento de respostas de centro germinativo, são gerados anticorpos com maior afinidade e diferentes subclasses capazes de mediar não apenas a neutralização, mas também processos como opsonização, citotoxicidade celular dependente de anticorpos (Antibody-dependent cellular cytotoxicity – ADCC), fagocitose (Antibody-dependent cellular phagocytosis – ADCP) e ativação do complemento (Complement-dependent cytotoxicity – CDC). Esses mecanismos, combinados, ampliam a capacidade do sistema imune de eliminar partículas virais e células infectadas, e desempenham papéis complementares à neutralização direta. Essas respostas efetoras foram majoritariamente descritas para anticorpos contra a proteína NS1 (Yu et al., 2021; Chung et al., 2007; Wessel et al., 2020).

### 1.5.1 Resposta Imune Humoral de Memória

A memória imunológica humoral é crítica para a proteção contra reinfecções por patógenos. Esta resposta é mediada por dois compartimentos celulares: células plasmáticas de vida longa e células B de memória (CBM) (Inoue; Tomohiro, 2023). Após encontro inicial com um antígeno, as células B podem se diferenciar em CBMs precoces expressando majoritariamente IgM (CBMs independentes de centro germinativo), bem

como em células plasmáticas de vida curta secretoras principalmente de IgM e células B do centro germinativo (GC). Estas últimas irão compor o Centro Germinativo (Germinal Center – GC), onde ocorre interação com células T helper foliculares (CTHF) e hipermutação somática. Nesta etapa, são geradas as CBMs de alta afinidade e células plasmáticas de vida longa. Após reencontro com o antígeno, as CBMs poderão se diferenciar em células plasmáticas de vida longa ou em células B GC, para gerar ainda mais células secretoras de anticorpos e CBMs (Inoue; Tomohiro, 2023; Seifert; Küppers, 2016).

Como as células plasmáticas de vida longa produzem anticorpos de alta afinidade para um antígeno primário, estes anticorpos atuam como uma primeira linha de defesa contra reinfecção por patógenos homólogos. Por outro lado, foi observado que as células B de memória apresentam maior flexibilidade de resposta, participando na defesa contra patógenos relacionados ou patógenos variantes que escapam da defesa mediada por células plasmáticas de longa duração (Inoue; Shinnakasu; Kurosaki, 2022). Estudos utilizando camundongos infectados pelo WNV mostraram o envolvimento das CBMs na proteção cruzada contra um sorotipo viral diferente da infecção primária (Purtha et al., 2011). Além disso, outros estudos em camundongos infectados por ortoflavivírus ou influenza mostraram que clones de reação cruzada pré-existentes de CBMs, mas não de células plasmáticas vida longa, são selecionados positivamente e diferenciam-se diretamente em células plasmáticas após novo desafio com variantes do vírus da primeira infecção (Leach et al., 2019; Wong et al., 2020). Esses estudos indicam que a população de células B de memória mais diversificada tem maior probabilidade de conter clones geralmente não imunodominantes, e que o processo de maturação de afinidade não necessariamente envolve perda drástica de diversidade, o que favorece a proteção cruzada (Inoue; Shinnakasu; Kurosaki, 2022; Inoue; Tomohiro, 2023).

#### *1.5.1.1 Estrutura e organização gênica dos anticorpos*

As imunoglobulinas são proteínas com organização simétrica compostas por duas cadeias pesadas e duas leves, que são conectadas por ligações dissulfeto. Cada cadeia leve pode consistir em uma cadeia κ ou uma cadeia λ, e possui duas regiões compostas por um domínio variável (VL) e um domínio constante (CL), enquanto cada cadeia pesada contém um domínio variável (VH) e pelo menos três domínios constantes (CH1–3). As cadeias pesadas apresentam uma região de dobradiça entre o primeiro (CH1) e o segundo

(CH2) domínio constante. As imunoglobulinas de mamíferos são classificadas em cinco isotipos/subtipos, IgA (IgA1 ou 2, que são encontradas na forma de monômeros no sangue e na forma de dímeros nas mucosas), IgD (monômeros), IgE (monômero), IgG (IgG1, 2, 3 ou 4, todos em forma monomérica) e IgM (pentâmero ou hexâmero) (Schroeder; Harry; Cavacini, 2010; Maranhão et al., 2015). Na figura 3, é possível observar uma representação esquemática de uma IgG, destacando cada um de seus domínios.

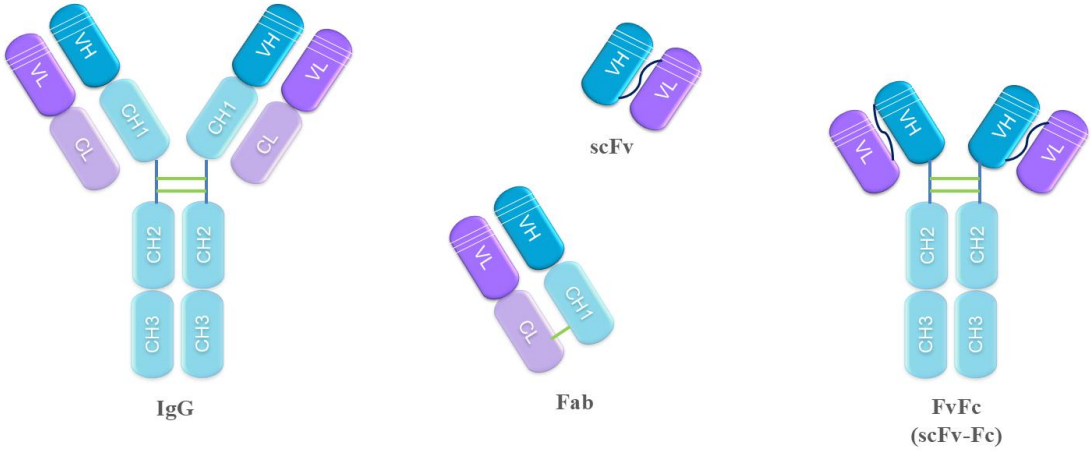


**Figura 3. Principais formatos estruturais de anticorpos monoclonais utilizados em aplicações terapêuticas e experimentais.** A IgG completa apresenta duas cadeias pesadas (CH1–CH3) e duas cadeias leves (CL), formando duas regiões Fab e uma região Fc responsável por funções efetoras. O fragmento Fab contém apenas o domínio variável (VH/VL) e o domínio constante CH1/CL, mantendo a capacidade de ligação ao antígeno. O formato scFv consiste na fusão dos domínios VH e VL conectados por um linker flexível. O formato FvFc (ou scFv-Fc) combina um scFv com a porção Fc da IgG, conferindo maior estabilidade, prolongamento da meia-vida e potencial de dimerização, preservando propriedades funcionais da região Fc.

As imunoglobulinas podem ser funcionalmente divididas em um fragmento Fc e um fragmento Fab. O fragmento Fab contém uma cadeia leve completa e a porção variável e CH1 da cadeia pesada. Seus domínios variáveis (VH e VL) constituem o fragmento Fv, responsável pelo reconhecimento do antígeno, enquanto CL e CH1 formam a parte constante do Fab. Já o fragmento Fc é constituído pelos domínios constantes CH2 e CH3 (e CH4 em IgM e IgA), sendo o principal mediador das interações com receptores Fc e componentes do complemento. Enquanto a porção Fc define o isotipo e subclasse de imunoglobulina e está relacionada a funções efetoras do anticorpo, a porção Fab, particularmente os domínios VH e VL contêm o paratopo de ligação a antígenos (Schroeder; Harry; Cavacini, 2010).

A diversidade de anticorpos é produzida durante dois estágios no desenvolvimento das células B, e é garantida pelo processo de rearranjo gênico que ocorre em nível cromossomal nos loci de imunoglobulinas. Nos estágios iniciais do desenvolvimento das

células B na medula óssea, o rearranjo de segmentos gênicos variáveis (V), diversidade (D) e junção (J), para o domínio VH e V e J para o domínio VL, ocorrem para produzir o repertório primário dos receptores de células B (BCRs), que são imunoglobulinas (Ig) associadas à membrana da célula B (Ig). Em células B maduras, após o reconhecimento do antígeno, os BCRs sofrem maturação de afinidade, mudança de classe, além de splicing alternativo convertendo parte dos BCRs em Igs secretadas. Esse processo culmina com a diferenciação dos linfócitos B em células plasmáticas e de memória e geração de um novo repertório de anticorpos (Maul; Gearhart, 2010).

Nos seres humanos, os loci das imunoglobulinas estão organizados de forma complexa: o locus da cadeia leve κ localiza-se no cromossomo 2, o da cadeia leve λ no cromossomo 22 e o locus principal da cadeia pesada no cromossomo 14 (Fell; Tucker, 1989). Nesses loci, a recombinação dos segmentos VH, D e JH (cadeia pesada) e VL e JL (cadeia leve) forma o éxon codificador dos respectivos domínios variáveis: VH e VL. A sequência resultante contém três regiões hipervariáveis conhecidas como regiões determinantes de complementaridade (CDRs), intercaladas por quatro regiões estruturalmente conservadas denominadas frameworks (FRs).

As CDR1 e CDR2 são integralmente codificadas pelo segmento gênico V, enquanto a CDR3 apresenta a maior variabilidade por resultar da junção dos segmentos VDJ na cadeia pesada e VJ na cadeia leve, associada a eventos de adição e remoção de nucleotídeos. Essa variabilidade destacada da CDR3 faz dessa região o principal determinante da especificidade e afinidade do anticorpo. Cada segmento gênico V possui seu próprio promotor, um éxon líder, um íntron intermediário e um éxon que codifica as três primeiras regiões estruturais (FR1, FR2 e FR3), as CDR1 e CDR2, a porção amino-terminal da CDR3 e uma sequência sinal de recombinação (RSS). De forma complementar, cada segmento gênico J inicia com seu próprio RSS e codifica a porção carboxi-terminal da CDR3 e o FR4 (Robertson, 1977; Schroeder; Harry; Cavacini, 2010).

Do ponto de vista filogenético, os segmentos VH humanos estão distribuídos em sete famílias (VH1–7), sendo VH3 a mais representada no repertório, seguida por VH1 e VH4 (Cook; Tomlinson, 1995; Kipps; Ghia; Rassenti, 2016). Já os genes Vk são divididos em seis famílias (Vk1–6) (Kipps; Ghia; Rassenti, 2016). Essa organização genética diversificada fundamenta a plasticidade da resposta humoral e permite a geração de repertórios capazes de reconhecer antígenos estruturalmente distintos.

*1.5.1.2 Resposta de anticorpos no contexto da infecção pelos ortoflavivírus*

A resposta imune mediada por anticorpos possui um importante papel na resposta antiviral, podendo atuar diretamente na neutralização da infecção ou na sinalização da presença do patógeno para células efetoras. A neutralização da infecção pelos anticorpos pode ocorrer de diferentes formas como mediante o bloqueio da ligação do vírus com o receptor celular e a inibição da fusão com a membrana celular por meio de interferência nas mudanças conformacionais proteicas necessárias para este processo (Hurtado-Monzón et al., 2020; Pierson et al., 2008). No contexto da infecção por ortoflavivírus, a produção de anticorpos é primariamente direcionada aos epítopos das proteínas prM, E e NS1 (Slon Campos; Mongkolsapaya; Screaton, 2018). Em especial, a proteína E é o alvo antigênico mais explorado para geração de anticorpos neutralizantes (Robbiani et al., 2017; Stettler et al., 2016).

Nas infecções por ortoflavivírus, a proteína de envelope (E) constitui o principal alvo de anticorpos neutralizantes devido ao seu papel essencial na entrada viral. O Domínio II (EDII) medeia a fusão de membranas, enquanto o Domínio III (EDIII) está envolvido no reconhecimento de receptores celulares, tornando ambas as regiões alvo atrativas para anticorpos neutralizantes (Pierson et al., 2008).

Além da neutralização, muitas funções efetoras dependem da interação de anticorpos com células do sistema imune por meio da região Fc. Na opsonização, anticorpos atuam como opsoninas, marcando patógenos para reconhecimento por fagócitos, que posteriormente os internalizam e degradam, prevenindo sua disseminação. Enquanto a região Fab é responsável pelo reconhecimento do antígeno e pela neutralização, a região Fc é essencial para a opsonização, pois interage com receptores Fc presentes na superfície de fagócitos. A ligação aos receptores Fc (FcR) supera forças de repulsão entre as membranas celulares, facilitando a internalização e subsequente destruição do alvo opsonizado (Winkelstein, 1973; Thau et al., 2025).

Outro mecanismo importante mediado por Fc é a ADCC, por meio da qual anticorpos promovem a eliminação de células infectadas ou tumorais através da interação com receptores Fc expressos em fagócitos, granulócitos e células NK. Esses efetores expressam três classes principais de receptores Fcγ, FcγRI (CD64), FcγRII (CD32) e FcγRIIIA (CD16), e contêm grânulos citotóxicos capazes de induzir morte celular. Após a ligação ao antígeno, anticorpos sofrem alterações conformacionais que aumentam a afinidade Fc–FcR, desencadeando vias de sinalização que culminam na eliminação da

célula-alvo por meio de perforina/granzima, FAS-L ou espécies reativas de oxigênio (ROS) e intermediários reativos (ROI) (Forthal; Finzi, 2018).

Além da ADCC, as interações Fc–FcR também direcionam a ADCP, na qual macrófagos e células dendríticas internalizam partículas virais ou células infectadas opsonizadas por anticorpos, conduzindo à degradação lisossômica e ao aumento da apresentação de antígenos (Kraivong, 2025; Brennan et al., 2025). Esse processo contribui tanto para a eliminação viral quanto para o fortalecimento das respostas adaptativas. Corroborando esse papel, estudos demonstraram que anticorpos monoclonais direcionados à proteína NS1 do WNV protegem camundongos por mecanismos dependentes de receptores Fc (Chung et al., 2007). Esses anticorpos induziram fagocitose mediada por FcγRI e/ou FcγRIV e eliminação de células infectadas, destacando a ADCP como mecanismo protetor chave in vivo (Chung et al., 2007). De forma semelhante, anticorpos anti-NS1 contra ZIKV induziram deposição de C3b em partículas recobertas com NS1, indicando ativação da via clássica do complemento, além de favorecerem a internalização desses alvos por monócitos e neutrófilos (Wessel et al., 2020).

Apesar de apresentarem papel essencial no controle da infecção por ortoflavivírus, os anticorpos podem também contribuir para a patogenia da doença. Na infecção primária por DENV, são produzidos anticorpos neutralizantes que conferem proteção de longo prazo contra o sorotipo infectante. No entanto, durante uma infecção secundária por um sorotipo heterólogo, os anticorpos de reação cruzada para o vírus primário tendem a apresentar baixa avidez e baixa atividade neutralizante, não sendo capazes de neutralizar o segundo vírus (Ngono; Shresta, 2018). Esses anticorpos não neutralizantes se ligam ao vírus formando imunocomplexos, que podem ser internalizados por células que expressam receptores FcγR, promovendo o aumento da carga viral e até a infecção de células que geralmente não são permissivas à infecção por ortoflavivírus (Slon Campos; Mongkolsapaya; Screaton, 2018; Van Leur et al., 2021). Este fenômeno, conhecido como Antibody Dependent Enhancement (ADE), pode resultar na evolução da doença para formas clínicas mais graves (Halstead; Nimmannitya; Cohen, 1970).

As respostas de anticorpos de reação cruzada ganharam destaque após os surtos de ZIKV em regiões epidemiológicas de DENV, uma vez que estes vírus apresentam aproximadamente 60% de similaridade na sequência de nucleotídeos (Ye et al., 2016). Esta similaridade levantou questionamentos quanto à ocorrência de ADE durante a infecção por ZIKV em indivíduos com exposição prévia ao DENV e vice-versa. Diferentes estudos mostraram aumento da infecção por DENV e ZIKV in vitro na

presença de anticorpos específicos para diferentes ortoflavivírus (Bardina et al., 2017; George et al., 2017; Priyamvada et al., 2016). Em camundongos fêmeas grávidas infectadas por ZIKV, foi observado que a presença de anticorpos específicos para DENV aumentaram significativamente o dano placentário, a restrição do crescimento fetal e o aumento da frequência de trofoblastos infectados. O mesmo estudo mostrou ainda que tecidos placentários humanos infectados com ZIKV também apresentaram aumento da replicação viral, dependente de FcγR, na presença de anticorpos DENV (Brown et al., 2019). Em contrapartida, outro estudo mostrou que anticorpos monoclonais humanos isolados de pacientes com DENV foram capazes de neutralizar o ZIKV in vitro e em modelo murino (Swanstrom et al., 2016). Além disso, em um estudo com coortes de macacos Rhesus, foi observado que a imunidade pré-existente para DENV resultou na redução no número de dias de viremia do ZIKV (Pantoja et al., 2017).

## 1.6 Abordagens terapêuticas e profiláticas contra infecções por ortoflavivírus

A vacina de vírus atenuado YFV-17D contra a febre amarela é atualmente a vacina com maior número de dados de eficácia e segurança já desenvolvida para uma infecção por ortoflavivírus. O sucesso da vacina se dá por sua capacidade de indução da imunidade inata e principalmente imunidade adaptativa de longa duração, caracterizada majoritariamente por anticorpos neutralizantes dirigidos à proteína do envelope viral e células T de memória que podem ser detectadas por até várias décadas após a vacinação (Fuertes Marraco et al., 2015; Gaucher et al., 2008; Gotuzzo; Yactayo; Córdova, 2013).

Apesar da eficácia da vacinação com a YFV-17D, a febre amarela ainda é um sério problema de saúde pública para áreas endêmicas. Por ser uma vacina de vírus atenuado, sua administração não é recomendada para gestantes e indivíduos imunossuprimidos (Silva et al., 2018). Além disso, resultados de um estudo de meta-análise mostraram que idosos, em comparação à população não idosa, apresentam risco três vezes maior de eventos adversos graves decorrentes da infecção pelo YFV, mesmo após a vacinação (De Abreu et al., 2022).

Os métodos profiláticos contra as infecções por DENV e ZIKV consistem principalmente no combate ao vetor, por meio da prevenção e eliminação de criadouros do mosquito Aedes aegypti (CDC, 2019). O laboratório Sanofi Pasteur, na França, desenvolveu a primeira vacina licenciada contra a dengue; entretanto, essa vacina apresenta como limitação a recomendação de uso restrita a indivíduos previamente

infectados pelo DENV, em função do risco aumentado de formas graves em soronegativos (HUANG et al., 2023; WU; QI; QIAN, 2023). Mais recentemente, a Takeda Pharmaceutical Company, do Japão, desenvolveu a vacina TAK-003 (QDENGA), que demonstrou perfil favorável de segurança e eficácia e foi aprovada pela Agência Nacional de Vigilância Sanitária (ANVISA) no Brasil (RIVERA et al., 2022). Além disso, o Instituto Butantan desenvolveu uma vacina tetravalente contra a dengue, de dose única, baseada em vírus vivos atenuados, que foi aprovada pela ANVISA para indivíduos de 2 a 59 anos, independentemente de infecção prévia, representando um avanço importante no cenário de prevenção da dengue no país (Kallás et al., 2024; ANVISA, 2025).

Apesar de uma série de vacinas para o ZIKV estarem atualmente em ensaio clínico (NCT03611946, NCT03008122, NCT02963909, NCT02952833, NCT02937233, NCT02887482, NCT02840487, NCT03014089, NCT04015648) nenhuma foi ainda licenciada.

O tratamento da infecção por ortoflavivírus baseia-se no controle do quadro sintomático, uma vez que não existem ainda terapias antivirais específicas aprovadas para nenhum desses vírus. Uma das principais estratégias no desenvolvimento de terapias antivirais específicas contra ortoflavivírus consiste na inibição de proteínas não estruturais que compõem o complexo replicativo destes vírus (Knyazhanskaya; Morais; Choi, 2021). Em especial, as proteínas NS3 e NS5 são os principais alvos desta estratégia terapêutica, uma vez que possuem inúmeras atividades enzimáticas essenciais para a replicação viral. No entanto, a maioria dos inibidores desenvolvidos até o momento se encontram na etapa de testes in vitro, e alguns estão sendo testados em modelo animal (Knyazhanskaya; Morais; Choi, 2021; Qian; Qi, 2022).

## 1.7 Anticorpos monoclonais terapêuticos

Desde a descoberta do potencial terapêutico do soro de animais imunizados contra difteria e tétano, no século XIX, houve um enorme progresso em pesquisas visando o desenvolvimento de terapias mediadas por anticorpos (Casadevall; Scharff, 1994). A partir da década de 1980, a comercialização de anticorpos monoclonais (mAbs) inovou o tratamento de câncer e doenças autoimunes e fortaleceu a integração desses biofármacos no repertório médico mundial (Akaishi; Nakashima, 2017). Alguns exemplos de mAbs comumente utilizados clinicamente incluem Adalimumabe e Infliximabe (anti-TNFα)

para tratamento de artrite reumatoide e doença de Crohn, Belimumabe (anti-Blys) para tratamento de Lúpus Eritematoso Sistêmico, e Rituximabe (anti-CD20) para tratamento de linfoma Non-Hodgkin (Maranhão et al., 2015).

Apesar do pioneirismo da terapia de anticorpos contra doenças infecciosas no século XIX, esta aplicação ainda era pouco explorada antes da pandemia de SARS-CoV-2 em 2020, quando plasma de indivíduos convalescentes da doença foi utilizado para tratamento de casos graves de internação (Casadevall; Pirofski; Joyner, 2021). Além disso, foram desenvolvidos diferentes mAbs específicos para a proteína Spike do SARS-CoV-2 que foram aprovados para o tratamento de casos leves e moderados pela FDA, apesar de não estarem atualmente autorizados para uso por não terem eficácia comprovada contra as variantes predominantemente circulantes no momento (FDA, 2022). Antes da pandemia de COVID-19, poucos mAbs haviam recebido aprovação da FDA para o tratamento de doenças infecciosas, dentre eles o palivizumabe, direcionado ao vírus sincicial respiratório (VSR), e ibalizumabe, para tratamento de infecção pelo HIV (Salazar et al., 2017).

Os anticorpos monoclonais podem ser produzidos em outros formatos, além da estrutura típica de imunoglobulina, como Fab, scFv e FvFc (scFv-Fc). A estrutura de cada um desses formatos está esquematizada na Figura 3. No formato Fragmento variável de cadeia simples (scFv), apenas as regiões variáveis VH e VL são produzidas, as quais são unidas por um peptídeo conector flexível (Maranhão et al., 2015). Este formato de anticorpo apresenta como vantagem melhor penetração tecidual, em decorrência do menor tamanho. No entanto, não são capazes de induzir respostas dependentes da porção Fc, como o ADCC (citotoxicidade mediada por células dependente de anticorpos), por exemplo (Monnier; Vigouroux; Tassew, 2013). O FvFc é também constituído por uma única cadeia polipeptídica contendo um scFv fusionado à região de dobradiça (hinge) e aos domínios constantes CH2 e CH3. Diferentemente do scFv, o FvFc possui como vantagens a presença de dois sítios ligantes (à semelhança da molécula de anticorpo inteira) e a preservação das funções efetoras de anticorpo (Maranhão et al., 2015).

Inicialmente, os mAbs eram produzidos pela tecnologia de hibridoma, no entanto, observou-se que a administração destes anticorpos de origem murina em humanos provoca uma resposta de anticorpos humanos contra os anticorpos de camundongos. Esta resposta acarreta na diminuição da meia-vida do anticorpo administrado, reduzindo sua eficácia e na possível ocorrência de efeitos colaterais graves como o choque anafilático, devido à natureza heteróloga dos anticorpos (Teillaud, 2012; Maranhão et al., 2015).

Abordagens moleculares e de engenharia genética passaram a ser utilizadas para substituir parte da sequência de anticorpos murinos por sequências humanas, resultando em moléculas quiméricas, humanizadas e, mais recentemente, humanas.

A substituição das regiões constantes de anticorpo de origem murina por regiões constantes humanas dá origem a um anticorpo quimérico. Esta foi a primeira estratégia de engenharia genética no desenvolvimento de anticorpos, seguida pelo processo de humanização, em que apenas as regiões determinantes de complementaridade (CDRs) das regiões variáveis são de origem heteróloga (Harding et al., 2010). Entretanto, técnicas de humanização são altamente laboriosas e ainda dependem da utilização de modelo animal. Desta forma, a probabilidade de ocorrência de efeitos colaterais e sua magnitude são reduzidas, mas não excluídas (Maranhão et al., 2015).

## 1.8 Bibliotecas de anticorpos e *Phage Display*

A técnica de Phage Display para a apresentação de proteínas exógenas na superfície de bacteriófagos foi descrita pela primeira vez em 1985 por George P. Smith (Smith, 1985). Posteriormente, Greg Winter e colaboradores demonstraram a aplicação dessa tecnologia para a construção e seleção de fragmentos de anticorpos a partir de repertórios de genes das regiões variáveis, permitindo a obtenção de anticorpos com especificidade pré-determinada sem a necessidade de imunização ou do uso da tecnologia de hibridomas (Winter et al., 1994). Essas contribuições consolidaram o Phage Display como uma plataforma central para a engenharia e o desenvolvimento de anticorpos terapêuticos humanos, culminando na concessão do Prêmio Nobel de Química de 2018 a George P. Smith e Sir Gregory P. Winter pelo desenvolvimento do Phage Display de peptídeos e anticorpos (Nobel Prize, 2018).

Atualmente, o Phage Display é amplamente utilizado em diversas aplicações além do desenvolvimento de anticorpos, incluindo o desenvolvimento de biossensores, a identificação de substratos enzimáticos, bem como a descoberta de drogas e vacinas (Mimmi et al., 2019; Sioud, 2019). No contexto da engenharia de anticorpos, a construção de bibliotecas apresentadas em fagos permite um mapeamento abrangente de perfis funcionais do repertório humano de anticorpos, especialmente em termos de especificidade antigênica (Ledsgaard et al., 2018).

Bibliotecas de anticorpos apresentadas em fagos podem ter origem natural ou sintética. Em bibliotecas naturais, a partir de linfócitos B circulantes, isola-se o mRNA,

que é convertido em cDNA para amplificação das regiões variáveis de cadeia pesada (VH) e leve (VL) de anticorpo. Os segmentos gênicos de VH e VL são posteriormente clonados em um vetor fagomídeo (vetor que possui, além da origem de replicação bacteriana, uma origem de replicação de fago, permitindo a geração de DNA de fita simples pelo mecanismo do círculo rolante) para geração de uma biblioteca sintética de anticorpos apresentada na superfície de bacteriófagos (Barbas et al., 2001; Almagro et al., 2019; Liu, 2014; Zhang, 2023).

Uma vez expressas na superfície dos fagos, essas proteínas são submetidas ao processo de seleção denominado biopaning, em que são realizados 3 a 5 ciclos de seleção com sucessivas lavagens e posterior eluição de clones de maior especificidade contra um determinado antígeno (Alfaleh et al., 2020). No processo de biopanning, pode-se utilizar um antígeno imobilizado em uma placa de microtitulação ou até mesmo antígenos biotinilados que se ligam a beads magnéticas ou resinas revestidas por estreptoavidina (Zhang, 2023). Há ainda a possibilidade de usar a superfície de células, como no método BRASIL (Biopanning and Rapid Analysis of Selective and Interactive Ligands) (Giordano et al., 2001; Dantas-Barbosa et al., 2005), ou ainda in vivo (Pasqualini et al., 1996; Staquicini et al., 2021) ou a superfície de tecidos ou peças anatômicas (Silva et al., 2016). Por fim, as sequências de DNA codificadoras dos anticorpos eluídos no último ciclo são analisadas para identificação dos clones mais enriquecidos pelo biopanning. Estes terão seus genes sintetizados para expressão da proteína do anticorpo e validação de sua eficácia. A Figura 4 ilustra o processo de construção de uma biblioteca de Phage Display e seleção de anticorpos *in vitro* a partir de células B.

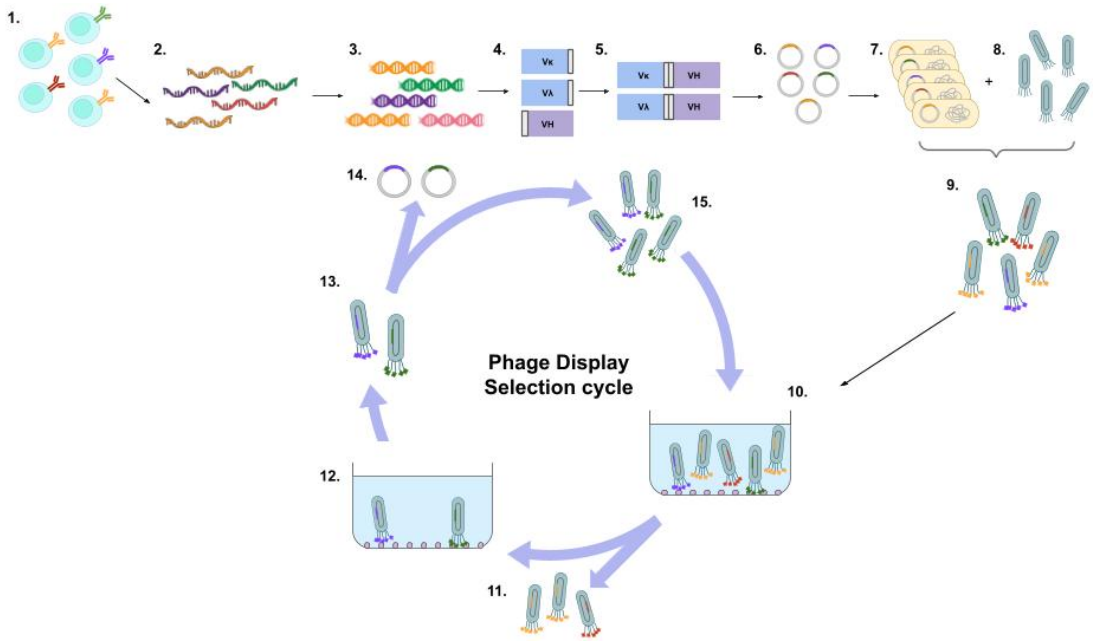


**Figura 4. Processo de Construção de uma biblioteca de Phage Display e seleção de anticorpos específicos.** Os genes que codificam um repertório contendo bilhões de anticorpos são clonados em um vetor de fagomídeo que carrega o gene que codifica a proteína pIII do bacteriófago. A biblioteca de fagos apresentando os anticorpos são obtidas por transformação de E. coli com o fagomídeo e infecção com um fago auxiliar, que contém todos os genes do bacteriófago filamentoso. O ssDNA originário dos fagomídeos, ao invés do ssDNA do fago auxiliar, é então revestido pelas proteínas estruturais. Isso ocorre porque os fagos auxiliares apresentam mutações em sua sequência que dificultam o empacotamento de seu próprio material genético. Os fagos resultantes são selecionados contra antígenos de interesse por várias rodadas de biopanning, que envolve a ligação ao antígeno, lavagens sucessivas, eluição dos fagos ligantes, reinfecção com os fagos eluídos e amplificação. Os fagos selecionados de maior potencial de ligação ao antígeno podem então ser identificados por ELISA e sequenciamento de DNA. Antonelli et al. 2025.

Os bacteriófagos filamentosos pertencem à família Inoviridae e possuem material genético de DNA fita simples (ssDNA). Diferentes fagos filamentosos já foram descritos para apresentação de proteínas heterólogas (M13, f1, fd), sendo o M13 o mais utilizado entre eles. O genoma do fago filamentoso codifica 11 proteínas, cinco das quais compõem o capsídeo viral (pIII, pVI, pVII, pVIII e pIX). PIII e PVIII são as proteínas mais utilizadas para apresentação de anticorpos, especialmente PIII, que pode ser fusionada a proteínas maiores sem comprometer sua função no processo de infecção (Ledsgaard et al., 2018). Fagos filamentosos infectam células bacterianas Gram negativas da família das Enterobacteriaceae, como E. coli, por meio de uma interação entre o pílus sexual das células hospedeiras e a proteína pIII do capsídeo viral. Os vírions gerados são liberados pela extrusão do ssDNA através do envelope bacteriano, sem lisar a célula ou impedir sua divisão. Após atravessar a membrana, o DNA viral passa a ser revestido pelas proteínas estruturais, completando assim a montagem da partícula viral (Smith; Scott, 1993).

A estratégia de construção da biblioteca de anticorpos pode variar e é essencial na seleção de anticorpos por Phage Display. As bibliotecas de anticorpos podem ser

derivadas de células de indivíduos não imunizados (biblioteca naïve) ou de indivíduos previamente expostos ao antígeno de interesse (biblioteca imune). Bibliotecas imunes apresentam como vantagem a geração de anticorpos de maior afinidade, uma vez que estes já passaram pelo processo de maturação de afinidade in vivo (Ledsgaard et al., 2018).

O phage display tem se consolidado como uma das principais plataformas para a descoberta de anticorpos antivirais. A tecnologia já foi empregada para isolar VHHs neutralizantes contra influenza A/H1N1 a partir de bibliotecas imunizadas, resultando em nanocorpos capazes de reconhecer hemaglutinina e bloquear a infecção viral in vitro (Páez-Hernández et al., 2024). De forma semelhante, estratégias de biopanning permitiram a obtenção de nanobodies com ampla reatividade contra diferentes variantes de SARS-CoV-2, incluindo moléculas capazes de neutralizar múltiplas linhagens ou mediar a eliminação de células infectadas por ADCC (Aripov et al., 2025; Moussa et al., 2024). Além disso, bibliotecas derivadas de pacientes cronicamente infectados por HCV facilitaram a identificação de Fabs de alta afinidade com neutralização ampla contra genótipos diversos do vírus (Soerensen et al., 2025).

No contexto dos ortoflavivírus, Throsby et al. (2006) selecionaram anticorpos humanos anti-WNV a partir de bibliotecas oriundas de pacientes infectados e identificaram mAbs neutralizantes direcionados majoritariamente ao domínio II da proteína E, alguns dos quais conferiram proteção in vivo. Para Zika vírus, bibliotecas naïve permitiram o isolamento de nanobodies com afinidade nanomolar e capacidade neutralizante contra o domínio III da proteína E (Hu et al., 2025). Para dengue, Dahiya et al. (2025) identificaram um sdAb derivado de uma biblioteca de VHH camelídea capaz de reconhecer o EDII da proteína E, exibindo potente neutralização in vitro e proteção in vivo com mínima indução de ADE. Além disso, Nilchan et al. (2024) selecionaram anticorpos anti-EDIII com atividade neutralizante contra DENV-2 e baixo potencial de ADE.

Em conjunto, esses estudos demonstram o potencial das bibliotecas apresentadas em fago para a identificação de anticorpos neutralizantes contra diferentes domínios da proteína E dos ortoflavivírus, incluindo os domínios II e III, bem como formatos alternativos de anticorpos, como nanobodies e VHHs. No entanto, a maior parte dessas abordagens tem se concentrado em epítopos conformacionais ou sorotipo-específicos, o que pode limitar a amplitude de neutralização. Nesse contexto, o *loop* de fusão, uma região altamente conservada do domínio II da proteína E e essencial para o processo de

entrada viral mediado por fusão de membranas, emerge como um alvo estratégico para o desenvolvimento de anticorpos com potencial de neutralização cruzada (Antonelli et al., 2025). Assim, a aplicação da tecnologia de Phage Display para a seleção de anticorpos monoclonais humanos direcionados ao *loop* de fusão a partir de bibliotecas derivadas de células B de memória representa uma abordagem metodológica promissora para a geração de candidatos terapêuticos contra ortoflavivírus, fundamentando o objetivo deste trabalho.

# 2 OBJETIVOS

## 2.1 Objetivo geral

Desenvolver anticorpos monoclonais humanos anti-*fusion loop* de ortoflavivírus por meio de Phage Display, visando aplicações terapêuticas.

## 2.2 Objetivos específicos

• Construir uma biblioteca de anticorpos scFv humanos a partir do repertório de células B de memória específicas para ortoflavivírus;

• Selecionar, por Phage Display, anticorpos scFv que reconheçam o loop de fusão dos ortoflavivírus;

• Expressar os domínios VH e VL selecionados em formato de FvFc e IgG1 em células de mamífero;

• Caracterizar os anticorpos desenvolvidos quanto a sua especificidade, afinidade e atividade neutralizante contra ortoflavivírus.

# 3 METODOLOGIA

## 3.1 Desenho experimental

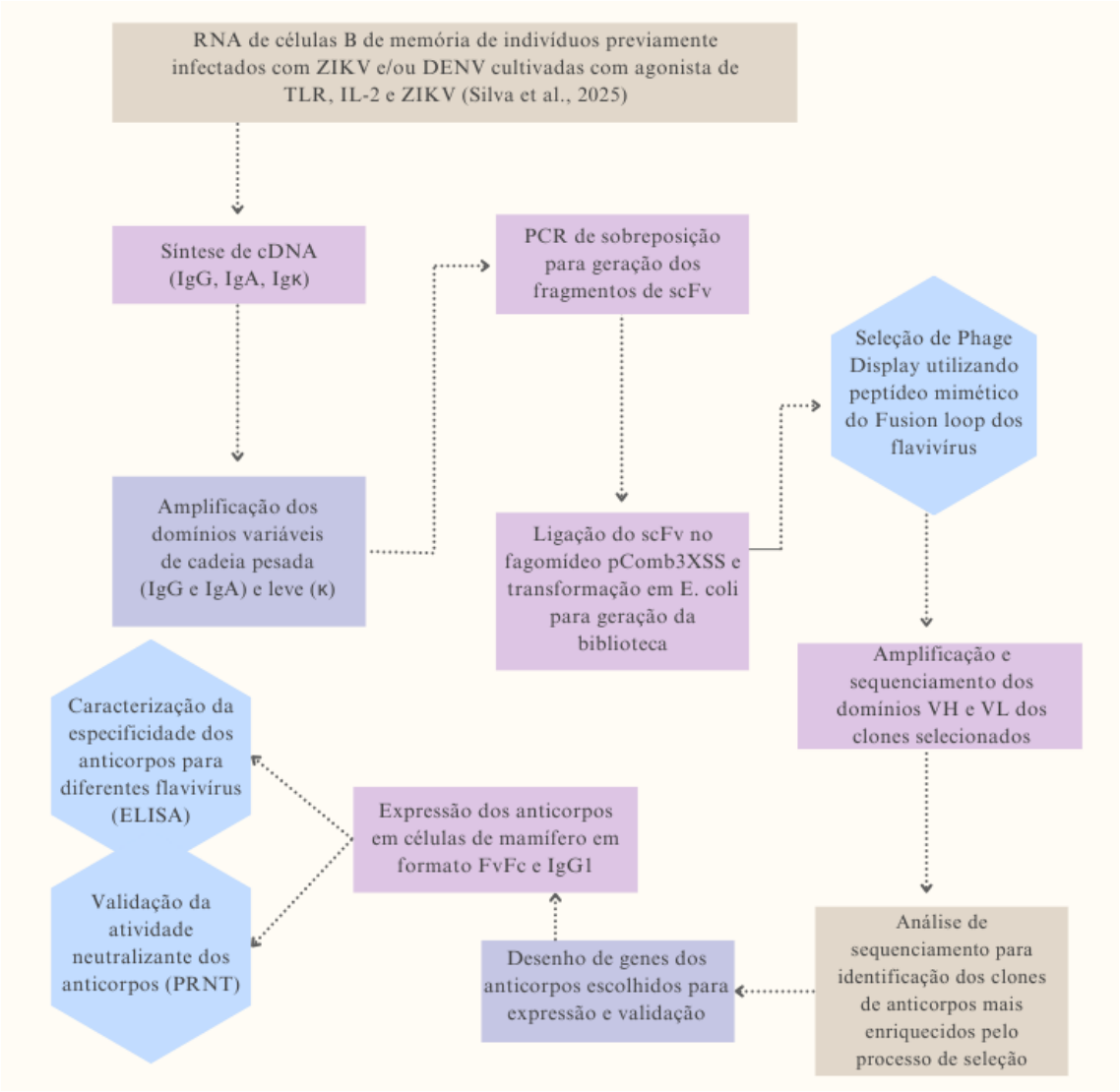


**Figura 5. Desenho Experimental contendo todas as etapas de realização do trabalho.**

## 3.2 Construção da Biblioteca de Anticorpos scFv a partir do Repertório de Células B de Memória Derivadas de Indivíduos Previamente Infectados por Ortoflavivírus

Os métodos da seção 4.2 descrevem as etapas de construção da biblioteca de scFv humana a partir de um repertório imune de células B de memória (CBM) ortoflavivírus-específicas gerado previamente pelo grupo (Silva et al., 2025). Brevemente, foi realizada a expansão *in vitro* de CBM a partir de células mononucleares de sangue periférico (PBMC) de indivíduos com resposta IgG positiva para ZIKV e indivíduos com IgG positiva tanto para ZIKV quanto DENV, visando a obtenção de um maior número de CBM específicas. As

células B de memória foram ativadas por IL-2 e R848, ligante de TLR7/8, e estimuladas com o ZIKV *in vitro*. Análises de citometria de fluxo mostraram um aumento significativo de até 33% de CBM viáveis. Além disso, foi observado através de Ensaios Imunoenzimáticos (ELISA) com os sobrenadantes do cultivo celular, que as CBM diferenciadas após estímulo produziam preferencialmente IgG específica para o ZIKV (SILVA, 2021). A Tabela 1 apresenta as características demográficas e sorológicas dos indivíduos incluídos no estudo, cujas amostras foram utilizadas para a geração da biblioteca de anticorpos scFv. O estudo foi conduzido de acordo com as diretrizes do Comitê de Ética em Pesquisa da Pontifícia Universidade Católica de Goiás, sob o número de CAAE 57.696.716.9.0000.0037, e todos os participantes assinaram o Termo de Consentimento Livre e Esclarecido. As amostras de sangue periférico foram coletadas de indivíduos de ambos os sexos, sendo o gênero definido por autodeclaração. A coleta de sangue e os procedimentos de cultivo celular foram realizados aproximadamente dois anos após o diagnóstico da fase aguda da infecção por ZIKV. Durante a fase aguda, a detecção do RNA viral em amostras de sangue e urina foi realizada por RT-qPCR, utilizando o kit BioGene Zika Virus PCR Kit (Bioclin®, Cat. #K203). Após a coleta, a sorologia para ZIKV e DENV (IgM e IgG) foi realizada por meio do teste imunocromatográfico TR DPP® Zika/Dengue IgM/IgG (Bio-Manguinhos, Rio de Janeiro, Brasil), garantindo a caracterização sorológica dos indivíduos incluídos no estudo.

**Tabela 1. Caracterização dos indivíduos do estudo.**

| Identificação | Idade | Sexo | Dias após sintomas | IgG anti-ZIKV | IgG anti-DENV |
|---|---|---|---|---|---|
| **Zika$^+$** | | | | | |
| PVZ-01 | 26 | F | 546 | Positivo | Negativo |
| PVZ-02 | 27 | F | 984 | Positivo | Negativo |
| PVZ-04 | 28 | M | - | Positivo | Negativo |
| PVZ-05 | 26 | F | 552 | Positivo | Negativo |
| **Vírus Zika$^+$/Dengue$^+$** | | | | | |
| PZD-01 | 55 | M | 1020 | Positivo | Positivo |
| PZD-03 | 26 | M | 1005 | Positivo | Positivo |
| PZD-04 | 36 | F | 1013 | Positivo | Positivo |
| PZD-05 | 21 | F | 983 | Positivo | Positivo |

PVZ = positivo para ZIKV; PZD = positivo para ZIKV e DENV; F = feminino; M = masculino.
Os valores de IgG anti-ZIKV e anti-DENV correspondem à leitura de testes imunocromatográficos. Para ZIKV, valores >27 foram considerados positivos; para DENV, valores ≥20 foram considerados positivos.
* Intervalo estimado com base em questionário clínico.

3.2.1 Síntese da primeira fita de cDNA a partir de RNA total de células B de memória purificadas

A síntese de DNA complementar (cDNA) foi realizada a partir do RNA previamente extraído das células B de memória ortoflavivírus-específicas. Três *pools* de cDNAs distintos foram gerados para os domínios variáveis de cadeia pesada (VH) de IgG e IgA e para os domínios variáveis de cadeia leve κ (Vκ). A fita de cDNA foi sintetizada a partir de 4 µg de RNA e 0,8 µM de iniciador específico para VH de IgG ou IgA, 8 µg de RNA utilizando primer específico para Vκ (Tabela 2), utilizando o *High Capacity cDNA Reverse Transcription (Applied Biosystems)* seguindo as instruções do fabricante.

**Tabela 2. Oligonucleotídeos utilizados no desenvolvimento do trabalho.**

| Nome | Sequência na orientação 5' – 3' |
|---|---|
| **Para gerar os cDNAs** | |
| HuIgG1 | GTC CAC CTT GGT GTT GCT GGG CTT |
| IgA rev externo | TGG GAA GTT TCT GGC GGT CAC G |
| HuGκF | AGA CTC TCC CCT GTT GAA GCT CTT |
| **Para a região variável da cadeia pesada (VH)** | |
| HSCVH1-F | GGT GGT TCC TCT AGA TCT TCC TCC TCT GGT GGC GGT GGC TCG GGC GGT GGT GGG CAG GTG CAG CTG GTG CAG TCT GG |
| HSCVH2-F | GGT GGT TCC TCT AGA TCT TCC TCC TCT GGT GGC GGT GGC TCG GG GGT GGT GGG CAG ATC ACC TTG AAG GAG TCT GG |
| HSCVH35-F | GGT GGT TCC TCT AGA TCT TCC TCC TCT G6GT GGC GGT GGC TCG GG GGT GGT GGG GAG GTG CAG CTG GTG SAG TCT GG |
| HSCVH3a-F | GGT GGT TCC TCT AGA TCT TCC TCC TCT GGT GGC G6GT GGC TCG GG GGT GGT GGG GAG GTG CAG CTG KTG GAG TCT G |
| HSCVH4-F | GGT GGT TCC TCT AGA TCT TCC TCC TCT GGT GGC GGT GGC TCG GG GGT GGT GGG CAG GTG CAG CTG CAG GAG TCG GG |
| HSCVH4a-F | GGT GGT TCC TCT AGA TCT TCC TCC TCT GGT GGC GGT GGC TCG GG GGT GGT GGG CAG GTG CAG CTA CAG CAG TGG GG |
| HSCG1234-B | CCT GGC CGG CCT GGC CAC TAG TGA CCG ATG GGC CCT TGG TGG ARG |
| HSCA-B | CCT GGC CGG CCT GGC CAC TAG TGA CCT TGG GGC TGG TCG GGG ATG |
| **Para a região variável da cadeia leve κ (Vκ)** | |
| HSCK1-F | GGG CCC AGG CGG CCG AGC TCC AGA TGA CCC AGT CTC C |
| HSCK24-F | GGG CCC AGG CGG CCG AGC TCG TGA TGA CYC AGT CTC C |

| | |
|---|---|
| HSCK3-F | GGG CCC AGG CGG CCG AGC TCG TGW TGA CRC AGT CTC C |
| HSCK5-F | GGG CCC AGG CGG CCG AGC TCA CAC TCA CGC AGT CTC C |
| HSCK14-B | GGA AGA TCT AGA GGA ACC ACC TTT GAT YTC CAC CTT GGT CCC |
| HSCK2-B | GGA AGA TCT AGA GGA ACC ACC TTT GAT CTC CAG CTT GGT CCC |
| HSCK3-B | GGA AGA TCT AGA GGA ACC ACC TTT GAT ATC CAC TIT GGT CCC |
| HCK5-B | GGA AGA TCT AGA GGA ACC ACC TTT AAT CTC CAG TCG TGT CCC |

**Primers para geração do fragmento d scFv**

| | |
|---|---|
| RSC-F | GAG GAG GAG GAG GAG GAG GCG GGG CCC AGG CGG CCG AGC TC |
| RSC-B | GAG GAG GAG GAG GAG GAG CCT GGC CGG CCT GGC CAC TAG TG |

**Primers para amplificação dos domínios VH e VL após seleção de *Phage Display* para sequenciamen**

| | |
|---|---|
| VHScFv_5' | TCGTCGGCAGCGTCAGATGTGTATAAGAGACAGGGTGGTTCCTCTAGATCTTCCTCCI |
| VHScFv_3' | GTCTCGTGGGCTCGGAGATGTGTATAAGAGACAGGGCCGGCCTGGCCACTAGTG |
| VLScFv_5' | TCGTCGGCAGCGTCAGATGTGTATAAGAGACAGGAGGAGGAGGAGGAGGAGGCGG |
| VLScFv_3' | GTCTCGTGGGCTCGGAGATGTGTATAAGAGACAGGAGGAGGAAGATCTAGAAACCACC |
| pCombScFv_5' | GTATGTTGTGTGGAATTGTGAGC |
| pCombScFv_3' | GCCACCACCCTCCTAAGAAG |

3.2.2 Amplificação das Cadeias VH e VL (1º ciclo de PCR) (Adaptado de Andris-Widhopf et al., 2000)

Os cDNAs gerados das cadeias pesadas de IgG e IgA e cadeia leve Kappa foram utilizados como molde para amplificação por reação em cadeia da polimerase (PCR) dos genes de VH e Vκ rearranjados. Para a amplificação dos rearranjos gênicos da região variável foram feitas 6 reações de amplificação para VH de IgG e 6 reações para amplificação de VH de IgA utilizando cada um dos oligonucleotídeos senso HSCVH1, HSCVH2, HSCVH35, HSCVH3a, HSCVH4 e HSCVH4a combinados com os oligonucleotídeos anti-senso HSCG1234-B ou HSCA-B. Para a obtenção da cadeia leve Kappa foram realizadas 16 reações de amplificação utilizando cada um dos oligonucleotídeos senso HSCK1-F, HSCK24-F, HSCK3-F e HSCK5-F combinados com cada um dos oligonucleotídeos anti-senso HSCK14-B, HSCK2-B, HSCK3-B e HSCK5-B. A sequência de todos os oligonucleotídeos utilizados está descrita na Tabela 2. As reações de amplificação foram realizadas utilizando-se o QuantiNova™ Probe RT-PCR Kit (Qiagen – Cat.: 208352) seguindo as recomendações do fabricante com algumas modificações. Cada reação consistiu de 0.5µg de cDNA, 0.6 uM dos primers 5' e 3' e Tampão de PCR Probe

RT-PCR Master Mix 1X. As condições de termociclagem foram: desnaturação inicial a 94 ºC por 5 min; 30 ciclos de desnaturação a 94 ºC por 15s, anelamento a 56 ºC por 90s, extensão a 60 ºC por 190s; extensão final a 60 ºC por 5 min. As replicatas de cada reação foram misturadas e precipitadas com 2V de etanol e 0,1V de acetato de sódio 3M (pH 5,0) e glicogênio a 50µg/mL Em seguida, os produtos de PCR foram submetidos à eletroforese em gel de agarose 1,5% e purificados com o *kit* QIAquick gel extraction.

### 3.2.3 Obtenção dos fragmentos de scFv por PCR de Sobreposição (2º ciclo de PCR) (Adaptado de Andris-Widhopf et al., 2000)

Os produtos de PCR das regiões VH e Vκ purificados foram misturados em quantidades iguais para gerar um produto final de sobreposição. Os primers utilizados no primeiro ciclo de PCR geraram sequências idênticas na região 3' da cadeia leve e na extremidade 5' da cadeia pesada que serviram para a sobreposição destas gerando um produto de extensão no segundo ciclo de PCR que corresponde ao scFv (~850pb). A PCR de sobreposição para geração do scFv foi realizada utilizando-se o QuantiNova™ Probe RT-PCR Kit (Qiagen – Cat.: 208352) seguindo as recomendações do fabricante com algumas modificações. Cada reação consistiu de 100ηg dos produtos de PCR purificados de VH e 100ηg dos produtos de PCR purificados de Vκ, 0.6 µM dos primers 5' e 3'(RSC-F e RSC-B) e Tampão de PCR Probe RT-PCR Master Mix 1X. As condições de termociclagem foram: desnaturação inicial a 94 ºC por 5 min; 25 ciclos de desnaturação a 94 ºC por 15s, anelamento a 56 ºC por 15s, extensão a 60 ºC por 2min; extensão final a 60 ºC por 5 min. As replicatas de cada reação foram misturadas e precipitadas com 2V de etanol e 0,1V de acetato de sódio 3M (pH 5,0) e glicoblue a 50µg/mL Em seguida, os produtos de PCR foram submetidos à eletroforese em gel de agarose 1,5% e purificados com o *kit* QIAquick gel extraction.

### 3.2.4 Digestão dos fragmentos de scFv e do Vetor pComb3XSS com a Enzima *Sfi*I (Adaptado de Andris-Widhopf et al., 2000)

A construção da biblioteca foi finalizada a partir da ligação dos fragmentos de scFv no vetor fagomídeo pComb3XSS (~5000pb) (Figura 4) e posterior transformação de células de *E.coli*. Para tornar possível a ligação inserto-vetor, os scFvs obtidos pela PCR de sobreposição e purificados e o vetor pComb3XSS foram inicialmente digeridos com a

enzima SfiI (20.000 U/mL) (New England Biolabs, catálogo R0123). O sistema de digestão dos fragmentos de scFv consistiu de 6µg de DNA, 120U de SfiI e tampão CutSmart 1X (New England Biolabs, catálogo B6004O) e foi incubado a 50ºC *overnight*. Os fragmentos digeridos (scFv, vetor e fragmento Fab excisado do vetor) foram submetidos a eletroforese em gel de agarose 1%. O DNA dos fragmentos excisados foi extraído utilizando-se o Agarose Gel Extraction Kit (Cellco, catálogo DPK-105) e em seguida purificados utilizando-se o QIAquick PCR Purification Kit (Qiagen).

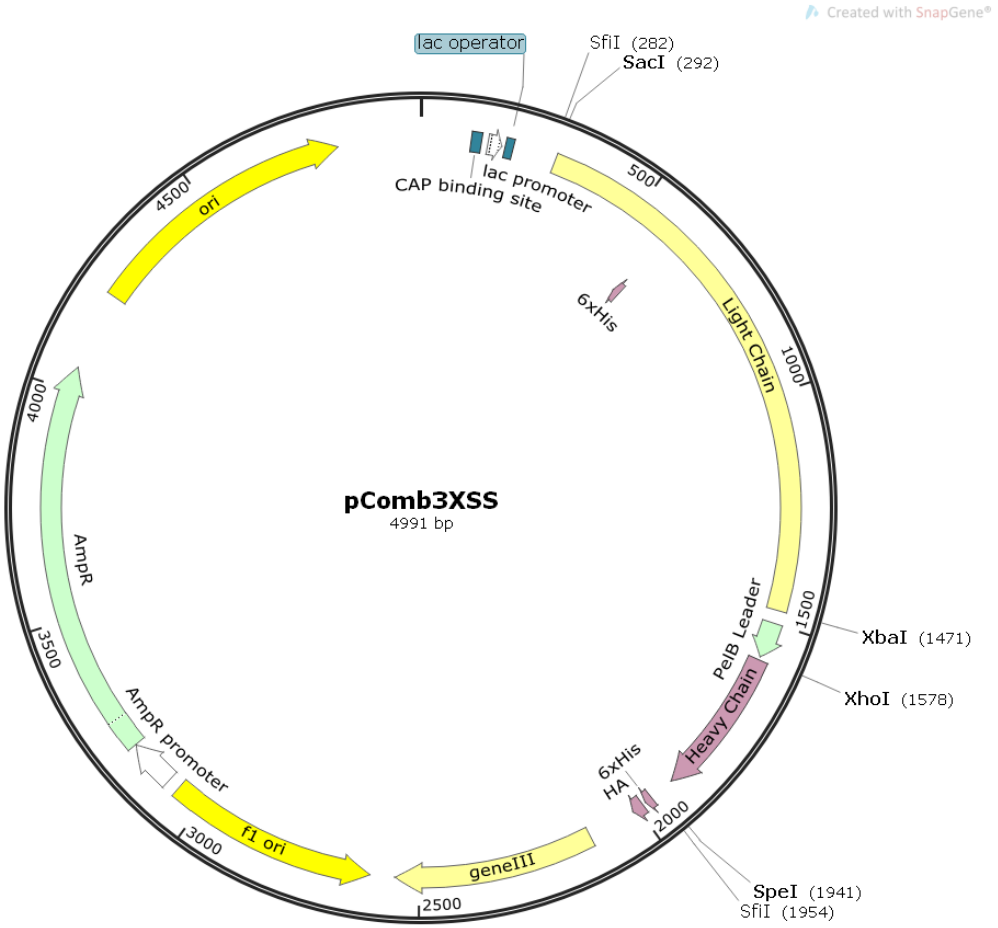


**Figura 6. Vetor fagomídeo pComb3xSS.** Os genes dos domínios variáveis de cadeia leve e pesada são delimitados por sítios de SfiI. O plasmídeo possui uma origem de replicação adicional em fago e o gene da proteína pIII, com a qual o anticorpo expresso é fusionado. As tags 6xHis e HA permitem purificação e detecção.

### 3.2.5 Testes de ligação do scFv com o Vetor pComb3XSS (Adaptado de Rader et al., 2000)

Inicialmente foram realizados testes de ligação em pequena escala. Para tanto foram feitos diversos sistemas de ligação, tanto a ligação do scFv com o vetor pComb3XSS, como também ligações controle negativa (sem inserto) e positiva (com o inserto Fab original do

vetor liberado após a digestão com SfiI). As ligações testes consistiram de 140ηg de vetor pComb3XSS, 70ηg de scFv ou 140ηg de Fab (com excessão da ligação de controle negativo), 1 U de T4 DNA ligase (Invitrogen, catálogo 15224017), 1X tampão de DNA ligase 5X (Invitrogen, catálogo 15224017) e água nuclease-free para completar o volume de 20uL final. As amostras foram incubadas a 25ºC *overnight* e em seguida a enzima T4 DNA Ligase foi inativada por incubação a 70°C por 10 minutos. 3µL de cada sistema foram utilizados para transformar alíquotas de células XL1-*Blue* eletrocompetentes. As placas foram incubadas *overnight* a 37°C. A ligação definitiva em maior escala só foi realizada quando os cálculos do número de colônias da transformação das ligações testes atingiram valor de 1 x $10^5$ transformantes/µg de DNA da ligação teste do scFv. O número de transformantes com o sistema de ligação controle negativo (teste de autoligação do vetor) deveria ser menor que 10% em comparação aos outros sistemas. Após a obtenção dos valores mencionados, prosseguiu-se para a realização da ligação definitiva do scFv no vetor pComb3XSS e transformação da biblioteca em células de *Escherichia coli* da linhagem XL1-blue MRF por eletroporação.

## 3.3 Preparação para a transformação da biblioteca e seleção de *Phage Display* (Adaptado de Rader et al., 2000)

### 3.3.1 Preparação de Células Eletrocompetentes

Uma colônia isolada de células de *E. coli,* linhagem XL1-BLUE MRF' foi inoculada em 5 mL de meio SB (Peptona bacteriológica 3%, Extrato de Levedura 2%, MOPS 1%, pH 7,0) com 10µg/mL tetraciclina. A cultura foi incubada durante a noite a 250 rpm e 37°C. Os 5mL de cultura foram adicionados em 500mL de meio SB contendo 2,5mL de solução estoque de glicose 2 M e 2,5mL de solução estoque de Mg 2 M (MgCl2 1 M e MgSO4 1 M). O inóculo foi incubado, a 250 rpm e 37 °C, até atingir uma densidade óptica (D.O.) a 600ηm entre 0,7 a 0,9. A cultura foi resfriada e as células foram centrifugadas a 3000 x g e 4°C por 20 minutos. Em seguida as células foram ressuspendidas em 100mL de glicerol 10% (v/v) gelado e centrifugadas novamente a 3000 x *g* e 4 °C por 20 min. O sobrenadante foi descartado e esse procedimento foi repetido mais duas vezes, uma segunda vez com 100mL de glicerol 10%, e uma terceira vez com 25mL de glicerol 10%. Por fim, as células foram ressuspendidas em glicerol 10% para uma densidade óptica a 600ηm de aproximadamente 280. Foram feitas

alíquotas de 120uL das células eletrocompetentes, que foram congeladas rapidamente em banho de álcool e gelo seco e armazenadas a -80 ℃.

### 3.3.2 Preparação do Fago Auxiliar

Foram inoculados 2µL de *E. coli* XL1-Blue eletrocompetentes em 2mL de meio SB contendo tetraciclina a uma concentração final de 10µg/mL e incubados a 37°C por 1 hora a 250rpm. Paralelamente, foram preparadas diluições do fago auxiliar VCSM13 da ordem de $10^{-6}$, $10^{-7}$ e $10^{-8}$. Em seguida 1µL de cada uma destas diluições foi utilizado para infectar alíquotas de 50µL da cultura de XL1-Blue. Após incubação por 15 minutos a temperatura ambiente adicionou-se os 50µL de células a 3mL de meio LB top ágar liquefeito (45-50°C), misturando em seguida o tubo por inversão e, posteriormente espalhando em placas pré-aquecidas de meio LB ágar. As placas foram incubadas a 37°C durante a noite. Após esse período foram observadas placas de retardo de crescimento (colônias de bactérias com retardo no crescimento devido à infecção pelo fago VCSM13). Em um tubo tipo Falcon de 50mL contendo 10mL de meio SB pré-aquecido a 37°C, acrescido 10µg/mL de tetraciclina foram inoculados 10µL de XL1-Blue eletrocompetente. A cultura foi incubada a 37°C por uma hora em agitador a 250 rpm. Com uma ponteira estéril, transferiu-se uma placa de lise para a cultura de XL1-Blue, seguido de incubação nas mesmas condições por 2 horas. Após este período a cultura infectada foi transferida para um Erlenmeyer de 1L contendo 500mL de meio SB pré-aquecido a 37°C, acrescido de 10µg/mL de tetraciclina e 70µg/mL de kanamicina. Após homogeneização metade da cultura foi transferida para outro Erlenmeyer de 1L e ambos os frascos foram incubados a 37°C durante a noite sob agitação de 250 rpm. Na manhã seguinte a cultura foi transferida para dez tubos de polipropileno de 50 mL e centrifugada a 2500 x *g* por 15 minutos. O sobrenadante foi transferido para novos tubos e incubados a 70°C por 20 minutos, com o objetivo de eliminar células ainda presentes na cultura. Em seguida, as amostras foram centrifugadas novamente a 2500 x *g* por 15 minutos e os sobrenadantes transferidos para novos tubos e estocados a 4°C. Os fagos auxiliares obtidos foram titulados em um procedimento de infecção de cultura de células XL1-*Blue* como descrito para a obtenção de placas de retardo de crescimento. Após a incubação durante a noite, o título foi determinado pela contagem do número de placas de lise presentes multiplicados pela diluição do fago.

### 3.4 Ligação da biblioteca de scFv no vetor pComb3XSS

A ligação definitiva dos fragmentos de scFv no vetor pComb3XSS foi consistiu de 700ηg de DNA de scFv, 1,4µg de DNA do vetor pCom3XSS digerido, 10 U de T4 DNA ligase (Invitrogen, catálogo 15224017), 1X tampão de DNA ligase 5X (Invitrogen, catálogo 15224017) e água nuclease-free para completar o volume de 200µL final. O sistema de ligação foi incubado a 25ºC *overnight* com posterior inativação da enzima T4 DNA Ligase a 70°C por 10 minutos. Em seguida, a ligação foi precipitada durante a noite com 2V de etanol, 0,1V de acetato de sódio 3M (pH 5,0) e glicoblue a 50µg/mL. A biblioteca precipitada foi centrifugada a 18.000 x *g* por 2 horas a 4°C. O sobrenadante foi descartado e ao *pellet* foi adicionado etanol 70% (v/v) gelado. Após centrifugação de 15 min a 4ºC e 18.000 x *g*, o *pellet* de DNA foi seco e ressuspenso em 10 µL de água.

### 3.5 Transformação da Biblioteca de scFv em Células de *Escherichia coli* por Eletroporação

Para a transformação do sistema de ligação (10µL), este foi dividido em 10 tubos com 1 µL cada para a realização de 10 choques elétricos com o objetivo de aumentar a eficiência de transformação. 10 alíquotas de 120µL de células XL1-Blue foram retiradas do *freezer* -80ºC aos poucos e à medida que se descongelaram foram transferidas cuidadosamente para os tubos contendo DNA da ligação e em seguida para cubetas de eletroporação, 0.2 cm (Biorad, catálogo 1652086) pré-resfriadas. O pulso elétrico foi realizado nas seguintes condições: voltagem de 2,5 kV, 25µF de capacitância e 200 Ω de resistência, gerando pulsos entre 4 e 5 mili segundos de duração. Imediatamente após o choque, a cubeta foi lavada 3 vezes com 1mL de meio SOC (Bactotriptona 2%, Extrato de levedura 0,5%, NaCl 0,06%, KCl 0,02%, MgCl2 10 mM, MgSO4 10 mM, pH 7,0). A cada um dos 10 choques elétricos o volume de células em meio SOC era adicionado a um mesmo Erlenmeyer estéril de 125mL, totalizando 30mL de células. Após os choques, as células foram transferidas para um Erlenmeyer de 500mL e o volume da cultura foi completado para 50mL com meio SB. As células foram recuperadas a 250 rpm e 37 ºC, por 1,5 h. Aos 50mL de células transformadas, foram adicionados 10µL de solução estoque de carbenicilina 100mg/mL, 100µL de solução estoque de tetraciclina 5mg/mL e 5mL de solução estoque de glicose 20%. A cultura foi incubada a 300 rpm e 37 ºC, por 1 h. Em seguida, 15µL de solução estoque de carbenicilina 100 mg/mL foram adicionados e a cultura foi incubada a 300 rpm e 37 ºC por mais 1 hora. O volume da cultura foi então completado para 200mL pela adição de meio SB pré-aquecido

contendo dois mL de fago helper VCSM13 ($10^{12}$ pfu/mL) e carbenicilina a 50mg/mL, tetraciclina a 10µg/mL e glicose a 1% (p/v). A cultura foi incubada, em seguida, a 300 rpm e 37 ℃, por 1,5 h, para a geração da biblioteca de anticorpos expressos na superfície de fagos. Posteriormente, 280uL de solução estoque de kanamicina 50mg/mL foram adicionados e a cultura foi incubada a 300 rpm e 37 ℃, durante a noite.

### 3.6 Seleção da Biblioteca de scFv contra µM Peptídeo Mimético do *loop* de Fusão de Ortoflavivírus

Duas alíquotas de 1mL da cultura de bactérias com fagos foram separadas e centrifugadas por 5 min a 5000 x *g* para armazenamento do *pellet* de células e do sobrenadante contendo os fagos. O volume total da cultura foi centrifugado em garrafas de 500mL por 15 min a 3000 x *g*, 4ºC. O sobrenadante contendo os fagos foi coletado e as células desprezadas. Ao sobrenadante, foram adicionados 6g de NaCl e 8g de PEG 8000 para precipitação dos fagos. A mistura foi homogeneizada por 5 min a 250rpm/ 37℃ e em seguida incubada por 30 min no gelo. Após centrifugação a 15000 x *g* por 15 min a 4ºC, os fagos foram precipitados formando um *pellet* difuso e o sobrenadante foi descartado. O pellet de fagos foi ressuspendido com 2mL de TBS contendo BSA a 1% gerando as alíquotas de fagos *input* (fagos obtidos após a amplificação *overnight* dos fagos eluídos pela seleção que serão utilizados no próximo ciclo), que foram centrifugadas brevemente para eliminação do residual de células.

Cinquenta microlitros de uma resina de agarose conjugada a streptoavidina (1mg/mL) (Sigma-Aldrich, catálogo S-1638) foi adicionada a um tubo de 2mL e incubada com 150µL de TBS contendo BSA a 3% (m/v) e com 10µM de um peptídeo mimético do *loop* de fusão do envelope do ZIKV biotinilado (antígeno escolhido para a seleção). Este sistema foi incubado por 1 hora em agitador orbital a 30rpm. Em seguida, o sistema foi centrifugado por 5min a 10000 x *g* e o sobrenadante retirado e descartado. Cem microlitros do fago input foram adicionados ao sistema, que foi incubado por mais 1 hora a temperatura ambiente em orbital a 30rpm. Após a incubação, foram realizadas lavagens sucessivas com 500µL de TBST (tween 20 a 0.1%) para eliminação dos fagos não ligantes (5 lavagens no ciclo 1 de seleção, 10 no ciclo 2 e 15 no ciclo 3). A cada lavagem a resina era ressuspensa em TBST, incubada por 1 min e centrifugada a 10.000 x *g* por 2 min para remoção e eliminação do sobrenadante contendo os fagos não ligantes. Após a última lavagem, 100uL do peptídeo mimético do *loop* de fusão do ZIKV não biotinilado

(100µM) foram adicionados ao sistema de seleção para realizar uma eluição por competição. O sistema foi incubado em orbital por 15 min a 30rpm e centrifugado por 5 min a 10.000 x *g*. Após a centrifugação, o sobrenadante contendo os fagos eluídos por competição foi adicionado a um novo tubo de 1,5mL e o *pellet* de resina contendo os fagos que permaneceram ligados ao antígeno biotinilado foi também armazenado. A partir deste momento, dois sistemas de seleção foram conduzidos paralelamente, sistema de seleção competitiva (a partir do sobrenadante de fagos ligantes ao antígeno não biotinilado) e sistema de seleção com antígeno adsorvido (a partir do *pellet* de resina contendo os fagos que permaneceram ligados ao antígeno biotinilado).

Uma cultura de células de XL1-Blue com OD de 1 em meio SB contendo glicose a 1% e tetraciclina a 10µg/mL foi utilizada para infecção com fagos oriundos da seleção com antígeno adsorvido e seleção competitiva. Dois mililitros da cultura de células foram adicionados a tubos cônicos de 50mL (um tubo para cada seleção- competitiva e antígeno adsorvido na resina). Ao tubo da seleção competitiva, foram adicionados 50µL do sobrenadante de fagos eluídos. Para infecção das células com os fagos provenientes da seleção com antígeno adsorvido, o pellet de resina foi ressuspendido com 500µL da cultura de células e adicionado ao tubo contendo o 1,5 mL restante. Para a infecção, os tubos foram incubados por 15 min a temperatura ambiente. Em seguida, alíquotas de 200µL foram separadas de cada um dos tubos gerando o *output* (título de saída) de cada uma das seleções. Doze mililitros de meio SB pré aquecido a 37ºC contendo 20µg/mL de carbenicilina, 10µg/mL de tetraciclina e 1% de glicose foram adicionados aos tubos de infecção, que foram então incubados a 37ºC por 1 hora sob agitação a 250rpm. Após a incubação, foi adicionado um reforço de carbenicilina às culturas para uma concentração final de 50µg/mL e realizada nova incubação por 1 hora, 250rpm, 37ºC. As culturas foram então transferidas para erlenmeyers de 1L contendo 92 mL de meio SB pré-aquecido a 37º (1% glicose, 50µg/mL carbenicilina e 10µg/mL tetraciclina) contendo 1mL de fago auxiliar VCSM13 ($10^{12}$ PFU) totalizando 100mL de volume. As culturas foram incubadas por 1 hora e meia a 37ºC, 250rpm, e em seguida foram adicionados às culturas 140µL de kanamicina para uma concentração final de 70µg/mL. As culturas foram incubadas durante a noite. Na manhã seguinte, todo o processo era iniciado novamente para realização de um novo ciclo de seleção, totalizando 3 ciclos de seleção.

### 3.7 Titulação de fagos

Para cada ciclo de seleção, 2 mL de células de XL1-BLUE MRF', a uma densidade óptica (D.O.) a 600 ηm de 1,0 foram infectados com 100µL de fagos eluídos à temperatura ambiente por 15 min. Após esse tempo, 100µL de diluições entre $10^{-1}$, e $10^{-5}$ das células infectadas foram plaqueadas em meio SB ágar contendo ampicilina e glicose para concentrações finais de 200 µg/mL e 1%, respectivamente, a fim de titular os fagos eluídos (*output*). As placas foram incubadas a 37 ℃, durante à noite. Para cada ciclo de seleção, 100 µL de células XL1-BLUE MRF' com D.O. a 600 ηm de 1,0 foram infectadas, à temperatura ambiente, por 15 min, com diluições de $10^{-7}$, a $10^{-11}$ de fagos amplificados e ressuspendidos (*input*, ou título de entrada). As células foram plaqueadas em meio SB ágar, nas mesmas condições anteriores, para titulação dos fagos amplificados. As placas foram incubadas a 37 ℃, durante à noite.

### 3.8 Extração de DNA plasmidial

Uma alíquota da biblioteca de scFvs recombinantes gerada anteriormente à adição fago helper foi utilizada para preparação de um inóculo em meio SB para extração de DNA plasmidial em média escala (midiprep). Para isso, foi utilizado o kit QIAprep Spin Midiprep (QIAGEN, Hilden, Alemanha, cat: 12145) de acordo com as instruções do fabricante. O DNA obtido foi ressuspenso em água nuclease-*free* e analisado por eletroforese em gel de agarose. A cada ciclo de seleção uma alíquota dos fagos reamplificados era armazenada para extração de DNA plasmidial por em pequena escala (miniprep), realizada com o kit QIAprep Spin Miniprep (QIAGEN, Hilden, Alemanha, cat:27106) de acordo com as especificações do fabricante.

### 3.9 Amplificação dos domínios variáveis

Usando como molde o DNA da biblioteca anterior ao processo de seleção (obtido por Midiprep) e o DNA de anticorpos provenientes do último ciclo de seleção (obtido por miniprep), os domínios variáveis da cadeia pesada (VH) e da cadeia leve (VL) foram amplificados, separadamente por PCR. Os oligonucleotídeos iniciadores utilizados (VHScFv_5', VHScFv_3', VLScFv_5', VLScFv_3', pCombScFv_5', pCombScFv_3') estão descritos na tabela 2. Para a amplificação de VL, foi necessário amplificar o fragmento de scFv com os primers pCombScFv_5', pCombScFv_3', e em seguida amplificar VL

utilizando o DNA do scFv como template. Para as reações foi utilizado o QuantiNova™ Probe RT-PCR Kit (Qiagen – Cat.: 208352) seguindo as recomendações do fabricante com algumas modificações. Cada reação consistiu de 20ng de DNA, 0.6 mM dos primers 5' e 3' e Tampão de PCR Probe RT-PCR Master Mix 1X. As condições de termociclagem foram: desnaturação inicial a 95 ℃ por 5 min; 30 ciclos de desnaturação a 95 ℃ por 30s, anelamento a 65 ℃ por 30s, extensão a 72 ℃ por 1 min; extensão final a 72 ℃ por 5 min. As replicatas de cada reação foram misturadas e precipitadas com 2V de etanol e 0,1V de acetato de sódio 3M (pH 5,0) e glicoblue a 50ug/mL Em seguida, os produtos de PCR foram submetidos à eletroforese em gel de agarose 1,5% e purificados com o Agarose Gel Extraction Kit (Cellco, catálogo DPK-105).

### 3.10 Sequenciamento de Nova Geração (NGS) pela plataforma Illumina

Os amplicons correspondentes à amplifificação dos domínios variáveis das cadeias pesada e leve dos anticorpos provenientes da biblioteca gerada previamente à seleção e das populações selecionadas após o último ciclo de *Phage Display* foram enviados para sequenciamento de nova geração. O sequenciamento foi realizado na empresa Macrogen (Seoul, Coreia do Sul), pelo sistema Miseq da plataforma Illumina, com tamanho de leitura de 2 x 300 pb e cobertura de 1 milhão de *reads*.

### 3.11 Análise do NGS pela plataforma ATTILA

Os dados de leituras provenientes do sequenciamento Illumina foram analisados com a ferramenta automatizada de análise de imunoglobulinas, ATTILA, previamente desenvolvida pelo grupo (Maranhão et al., 2020). Esse programa analisa as sequências dos domínios variáveis da cadeia pesada (VH) e leve (VL) com base nas definições de CDRs e frameworks. Além disso, é realizada uma análise de enriquecimento, que determina a frequência de cada sequência de domínio variável em cada ciclo de seleção avaliado. Assim, o programa gera um relatório contendo a variação da frequência de cada sequência (*fold-change*) entre o último ciclo de seleção e a biblioteca antes da seleção. Além disso é fornecido a sequência de aminoácidos de cada domínio, bem como sua classificação germline.

### 3.12 Desenho de genes para expressão dos anticorpos anti-ortoflavivírus

A partir dos resultados da análise do sequenciamento, foram selecionados os domínios VH e VL mais enriquecidos para desenho dos genes dos anticorpos anti-ortoflavivírus a serem expressos. Os domínios VH e VL selecionados foram combinados entre si e as sequências recombinantes foram otimizadas pela plataforma GenSmart™ Codon Optimization com o uso de códons preferenciais das linhagens de células HEK 293 e CHO. As sequências de DNA codificadoras dos anticorpos recombinantes desenhadas para expressão de FvFc no vetor pMIW e IgG1 e Igκ em vetores pcDNA3.4. Os plasmídeos foram sintetizados pela empresa GenScript (China).

### 3.13 Expressão dos anticorpos anti-ortoflavivírus em células de mamífero

A expressão dos anticorpos recombinantes do tipo FvFc e IgG foi realizada por transfeção transiente de células Expi293F™ (Thermo Fisher Scientific) utilizando o sistema Expi293™ Expression System e o reagente ExpiFectamine™ 293 Transfection Kit, de acordo com as recomendações do fabricante (MAN0019402, Thermo Fisher Scientific). As células Expi293F™, derivadas de HEK293 adaptadas para crescimento em suspensão, foram mantidas em meio de cultivo Expi293™ Expression. As culturas foram mantidas a 37 °C e 8% de $CO_2$, em agitação orbital de 125 rpm. As células foram subcultivadas a cada 3–4 dias e utilizadas para transfeção quando atingiram densidade de 3–5 × $10^6$ células/mL, com viabilidade superior a 95%. No dia anterior à transfeção (Dia −1), as células foram diluídas para 2,5–3 × $10^6$ células/mL e cultivadas durante a noite. No dia da transfeção (Dia 0), a cultura foi ajustada para uma densidade final de 3 × $10^6$ células/mL em um volume de 25 mL de meio Expi293 Expression Medium, previamente aquecido a 37 °C, em frascos Erlenmeyer estéreis e ventilados de 125 mL. O complexo DNA-ExpiFectamine foi preparado conforme o protocolo: para cada mL de cultura, foi utilizado 1 µg de DNA plasmidial purificado (totalizando 25 µg de DNA para 25 mL de cultura, sendo que para os anticorpos em formato de IgG, foram utilizados 12.5 µg de DNA IgG e 12.5 µg de DNA IgK). O DNA foi diluído em 1,5 mL de Opti-MEM™ I Reduced Serum Medium, enquanto 80 µL de ExpiFectamine™ 293 Reagent foram diluídos separadamente em 1,5 mL de Opti-MEM™ I. As duas soluções foram combinadas e incubadas à temperatura ambiente por 15–20 minutos para formação dos complexos lipídicos. Em seguida, a mistura foi adicionada lentamente à cultura de células sob leve agitação. Após 18–22 h, foram adicionados os reagentes de intensificação da transfeção: 150 µL de ExpiFectamine™ 293 Transfection Enhancer 1 e 1,5 mL de

ExpiFectamine™ 293 Transfection Enhancer 2, homogeneizando-se suavemente o frasco após cada adição. As culturas foram então incubadas a 37 °C e 8% de $CO_2$ com agitação contínua a 125rpm. A coleta do sobrenadante foi realizada entre 6 dias pós-transfeção, período correspondente ao pico de secreção da proteína recombinante. O meio foi centrifugado a 6000 × *g* por 20 minutos a 4 °C para remoção de células e detritos, e o sobrenadante clarificado foi filtrado em membrana de 0,22μm antes da etapa de purificação por afinidade em coluna de Proteína A.

### 3.14 Purificação dos anticorpos por afinidade à proteína A

A purificação dos anticorpos recombinantes do tipo FvFc e IgG foi realizada no sistema de cromatografia ÄKTA Pure (Cytiva) utilizando uma coluna HiTrap Protein A HP 5 mL (Cytiva, cat. nº 17040301). Essa coluna é preenchida com uma resina revestida com proteína A, que apresenta alta afinidade pela região Fc de imunoglobulinas humanas, permitindo a captura seletiva de anticorpos a partir do sobrenadante de cultura celular. Antes do início da purificação, a coluna foi equilibrada com 25 mL de tampão de ligação (20mM fosfato de sódio, pH 7,0) a um fluxo de 5mL/min. Em seguida, o sobrenadante de cultura contendo os anticorpos, previamente clarificado por centrifugação e filtração em membrana de 0,22 μm, foi aplicado à coluna utilizando o superloop, em um volume entre 25 e 50mL. O flow-through, correspondente à fração não ligada, foi coletado pela válvula de outlet para monitoramento da eficiência de ligação. Após a aplicação da amostra, a coluna foi lavada com 15mL do mesmo tampão de ligação para remoção de proteínas e impurezas não especificamente ligadas. A eluição dos anticorpos foi realizada utilizando 15mL de tampão ácido (0,1 M ácido cítrico, pH 3,0), em steps ou gradiente linear conforme o método programado no sistema. As frações eluídas foram coletadas automaticamente em alíquotas de 1mL por meio do coletor de frações. Cada fração eluída foi imediatamente neutralizada com 200μL de tampão Tris 1 M, pH 9,0, para evitar desnaturação induzida pelo pH ácido. As frações correspondentes ao pico de eluição foram analisadas por SDS-PAGE sob condições desnaturantes, a fim de avaliar pureza e integridade das amostras. Ao término da purificação, a coluna foi reequilibrada com 25mL do tampão de ligação e posteriormente lavada com 50mL de água Milli-Q. Para armazenamento, foi realizada uma lavagem com 25mL de etanol 20% (v/v), seguida de vedação das extremidades e conservação a 4 °C.

### 3.15 Eletroforese em gel desnaturante de poliacrilamida

A análise das proteínas foi realizada por eletroforese em gel desnaturante de poliacrilamida (SDS-PAGE) utilizando o sistema Mini-PROTEAN Tetra Cell, 4-Gel System (Bio-Rad). O gel separador (*running gel*) foi preparado a 12% (3mL de acrilamida/bisacrilamida 29:1; 2,5mL de Tris-HCl 1,5M pH 8,8; 100µL de SDS 10%; 5µL de TEMED (Invitrogen); 100µL de APS 10%; e água destilada até 10mL). Os catalisadores TEMED e APS foram adicionados por último, imediatamente antes do vertimento entre as placas de vidro. Após o enchimento, uma fina camada de isopropanol foi aplicada sobre o gel para nivelamento. Após a polimerização, o isopropanol foi removido e o gel lavado com água destilada. O gel concentrador (*stacking gel*) foi preparado a 5% (470µL de acrilamida/bisacrilamida 29:1; 472,5µL de Tris-HCl 1,0M pH 6,8; 37,5µL de SDS 10%; 4µL de TEMED; 37,5µL de APS 10%; e água destilada até 3,7 mL). Após adição dos catalisadores, o gel concentrador foi vertido sobre o separador e o pente inserido imediatamente. Após a polimerização, o sistema foi montado e preenchido com tampão de corrida 1X (Tris 25mM; glicina 0,192 M; SDS 0,1%; pH 8,3–8,4). As amostras foram preparadas com tampão de amostra 5X (Tris-HCl 200 mM pH 6,8; SDS 4%; β-mercaptoetanol 4%; glicerol 20%; azul de bromofenol 0,1%), diluídas para 1X e aquecidas a 95 °C por 10 minutos. Cerca de 20µL de cada amostra foram aplicados no gel, juntamente com 3,5µL do marcador de peso molecular TrueColor High Range Protein Marker (Sinapse Biotecnologia). A eletroforese foi conduzida a 100 V por aproximadamente 2 h e 15 min. A migração foi monitorada pela frente do corante azul de bromofenol. Ao término, o gel foi submetido à coloração com *Coomassie Blue* ou Prata, ou ainda à imunodetecção por western blot.

### 3.16 Coloração do gel com Coomassie Blue ou Prata

Após a corrida, o gel concentrador foi removido e descartado, e o gel separador submetido à coloração. Para coloração com Coomassie Blue, o gel foi imerso em Solução Corante (Azul Brilhante de Coomassie R-250 0,25%; metanol 30%; ácido acético glacial 7%) por 2 horas sob agitação suave. Em seguida, a solução corante foi descartada e o gel lavado com Solução Descorante (metanol 30%; ácido acético glacial 7%) até visualização nítida das bandas de proteína. Para coloração com prata, foi utilizado o kit Silver Stain (Invitrogen, Ref: 45-1001). Todas as etapas foram conduzidas sob agitação suave. O gel foi inicialmente fixado em 25mL de solução fixadora (etanol 40%; ácido acético 10%;

água destilada q.s.p. 25mL) por 20 minutos, seguidos de lavagem com etanol 30% por 10 minutos. Em seguida, foi realizada a sensibilização com 25mL de solução sensibilizadora (7,5 mL de etanol; 2,5 mL de solução sensibilizadora do kit; água destilada q.s.p. 25 mL) por 10 minutos, seguida de nova lavagem com etanol 30% (10 min) e duas lavagens com água destilada (10 min cada). Após as lavagens, o gel foi incubado por 15 minutos em 25 mL da solução de coloração (250µL do corante do kit em água destilada), lavado rapidamente (60 s) com água destilada e, em seguida, incubado na solução reveladora (2,5mL de revelador + 1 gota de amplificador de revelação) por 4–8 minutos, até o aparecimento das bandas. Quando atingida a intensidade desejada, a reação foi interrompida pela adição da solução Stopper fornecida no kit, e o gel mantido em água destilada até o registro da imagem.

### 3.17 Western Blot

Após a separação das proteínas por SDS-PAGE, estas foram transferidas para uma membrana de nitrocelulose utilizando o sistema TE 70PWR (Amersham Bioscciences). As membranas foram equilibradas em tampão de transferência (Tris 25 mM; glicina 192 mM; metanol 20%) por 10 minutos antes da montagem do sistema. A transferência foi realizada a 10V, 150mA por 1h. Após a transferência, as membranas foram bloqueadas por 1 hora à temperatura ambiente com Tampão PBS-T (Tween-20 0,1%) contendo 5% de leite desnatado. Em seguida, foram incubadas com o anticorpo produzido em cabra anti-Fc humano (diluição 1:1500) (Thermo Fisher Scientific, catálogo A18820) por 2 horas em temperatura ambiente ou overnight a 4 °C. Após três lavagens com PBS-T, a revelação foi realizada com o substrato NBT/BCIP - Nitro Blue Tetrazolium/5-Bromo-4-Chloro-3-Indolyl Phosphate (Thermo Fisher Scientific) até o aparecimento das bandas. A reação foi interrompida pela lavagem com água destilada e as membranas foram mantidas em condições secas e protegidas da luz até o registro da imagem.

### 3.18 ELISA contra os vírus ZIKV e DENV1-4 inativados

A análise da ligação dos anticorpos recombinantes aos vírus ZIKV e aos quatro sorotipos do DENV foi realizada por ELISA indireto, utilizando como antígenos partículas virais inativadas por exposição à luz ultravioleta por 1 h. Foram empregados o ZIKV inativado da cepa H/PF/2013, bem como os sorotipos DENV-1 (Hawaii), DENV-2 (N. Guinea C), DENV-3 (H87) e DENV-4 (BC 295/97), cedidos gentilmente pela

Professora Doutora Lucimeire Antonelli da Silveira da Universidade Federal de Goiás. Placas de 96 poços de poliestireno de alta adsorção *Polysorp* (Thermo Fisher Scientific) foram sensibilizadas com 100µL por poço da suspensão viral em PBS (diluição suficiente para adicionar cerca de 200 PFU por poço) e incubadas a 4 °C durante a noite. No dia seguinte, as placas foram mantidas a 37 °C por 1 hora para garantir completa adsorção do antígeno. Após o período de sensibilização, as placas foram lavadas três vezes com 200µL de PBST (PBS 1×, 0,05% Tween-20). Em seguida, foi realizada a etapa de bloqueio com 200µL de BSA 3% em PBST, previamente filtrada em membrana de 0,22µm, por 2 horas a 37 °C. Após o bloqueio, as placas foram novamente lavadas três vezes com PBST, e em seguida foram adicionados os anticorpos recombinantes (FvFc ou IgG) em diluições seriadas, partindo de uma concentração inicial de 1000 nM em PBS. Como controle negativo, foi utilizado o anticorpo monoclonal humano Rituximabe, que não apresenta especificidade para antígenos de ortoflavivírus, permitindo validar a especificidade da ligação observada para os anticorpos recombinantes testados. O volume final em cada poço foi de 100µL, e a incubação foi realizada por 1 hora e meia a 37 °C. Após três lavagens com PBST, foi adicionado o anticorpo goat anti-human Fc conjugado à fosfatase alcalina (AP) (Sigma-Aldrich), diluído 1:1000 em PBST, com 100µL por poço, seguido de incubação por 1 hora a 37 °C. As placas foram novamente lavadas três vezes com PBST. A revelação foi realizada com 100µL por poço da solução de substrato p-nitrofenil fosfato (PNPP, 1 mg/mL - Thermo Scientific, catálogo 34045) preparada em tampão APB (Tris-HCl 100 mM, NaCl 100 mM, $MgCl_2$ 5 mM, pH 9,5). A reação foi conduzida por 5 a 10 minutos em temperatura ambiente e protegida da luz. A leitura foi realizada em leitor de placa SpectraMax M2e (Molecular Devices) a 405ηm. Os valores de absorbância foram utilizados para plotagem das curvas de ligação, nas quais foi aplicada análise por regressão não linear no programa Graphpad.

### 3.19 Ensaio de Neutralização PRNT (*Plaque Reduction Neutralization Test*) contra os vírus ZIKV e DENV-2

A capacidade neutralizante dos anticorpos recombinantes foi avaliada por meio do ensaio de neutralização por redução de placas (PRNT), utilizando o vírus Zika (ZIKV) e o vírus da dengue sorotipo 2 (DENV-2) em células Vero (ATCC® CCL-81™). As células Vero foram cultivadas em meio MEM (Minimum Essential Medium) suplementado com 10% de soro fetal bovino (SFB) e 1% de antibiótico-antimicótico

(Gibco, catálogo 15240-062), sendo mantidas a 37 °C em atmosfera de 5% de $CO_2$. Para o ensaio, $1,5 \times 10^5$ células foram semeadas por poço em placas de 24 poços, atingindo 90–100% de confluência após aproximadamente 24 horas de incubação. As amostras virais de ZIKV e DENV-2 foram previamente tituladas por contagem de placas, a fim de determinar a concentração necessária para produzir aproximadamente 50 a 100 unidades formadoras de placa (PFU) por poço. Para o teste de neutralização, os anticorpos recombinantes (FvFc ou IgG) foram diluídos serialmente, a partir de uma concentração inicial de 12 μM, em meio MEM sem soro, sendo aplicados 100 μL por poço. Um volume igual de suspensão viral contendo a quantidade previamente determinada de PFUs foi adicionado a cada diluição do anticorpo, resultando em uma proporção 1:1 (v/v) entre vírus e anticorpo. As misturas foram incubadas a 37 °C por 1 hora, para permitir a interação entre os anticorpos e as partículas virais. Após a incubação, o meio de cultura foi cuidadosamente removido das células Vero, deixando apenas uma pequena quantidade para evitar o ressecamento do poço. Em seguida, foram adicionadas as misturas vírus-anticorpo (100μL por poço). As placas foram incubadas a 37 °C com 5% de $CO_2$ por 1 hora, com agitação leve a cada 20 minutos para favorecer a adsorção viral. Decorrido o período de adsorção, cada poço recebeu 500μL de meio de sobreposição semissólido, composto por MEM 10× contendo carboximetilcelulose (CMC) 3%, 2% de SFB e 1% de antibiótico-antimicótico. As placas foram incubadas a 37 °C e 5% de $CO_2$ por 7 dias para DENV-2 e 4 dias para ZIKV, até o desenvolvimento das placas de lise celular. Ao término da incubação, o meio de sobreposição foi removido, e as células foram fixadas com formaldeído 4% (v/v) à temperatura ambiente, overnight. Após a fixação, as placas foram lavadas com água corrente e coradas com cristal violeta 1% (p/v) em etanol 20% (v/v) por 30 minutos. O excesso de corante foi removido com água, e as placas foram deixadas para secar à temperatura ambiente. As placas de lise foram visualizadas e contadas manualmente. O número médio de placas em cada condição foi comparado ao controle viral (vírus sem anticorpo), permitindo o cálculo do percentual de neutralização. A porcentagem de redução de placas (PRNT%) foi calculada de acordo com a fórmula: % Neutralização = 100 × [1 - (número de placas incubadas com mAb ÷ número de placas sem mAb)].

O título neutralizante ($PRNT_{50}$) foi determinado por análise de regressão não linear utilizando o software GraphPad Prism, representando a concentração de anticorpo capaz de reduzir em 50% o número de placas em relação ao controle. Como controle negativo, foram utilizados o anticorpo monoclonal humano Rituximabe e um anticorpo

scFv anti-SARS-CoV-2, que não reconhecem antígenos de ortoflavivírus, garantindo a especificidade da resposta neutralizante observada.

# 4 RESULTADOS

O período de doutorado resultou, até o momento, em dois manuscritos científicos. O primeiro corresponde a um artigo de revisão intitulado “Therapeutic Antibodies for Mosquito-Borne Orthoorthoflavivirus Infections: Discovery, Engineering Approaches, and Advances in mRNA-Based Delivery Systems”, publicado na revista Advanced Therapeutics. Essa revisão possibilitou um aprofundamento teórico sobre a estrutura e os mecanismos de evasão dos ortoflavivírus, bem como sobre as principais estratégias empregadas no desenvolvimento de anticorpos monoclonais terapêuticos, incluindo abordagens de engenharia e plataformas emergentes baseadas em mRNA. O manuscrito foi publicado na revista Advanced Therapeutics (Antonelli et al., 2025). O texto completo da revisão encontra-se apresentado no Anexo 1.

O segundo manuscrito, intitulado “Phage Display Selection from Human Memory B Cells Reveals Cross-Neutralizing Monoclonal Antibodies Targeting the Orthoflavivirus Fusion Loop”, encontra-se em fase de preparação e apresenta os resultados experimentais obtidos ao longo do doutorado. O trabalho descreve a construção de uma biblioteca de células B de memória humanas e a seleção de anticorpos monoclonais contra o *fusion loop* do envelope viral, destacando a obtenção de anticorpos humanos com afinidade elevada e neutralização cruzada entre ZIKV e DENV. Esse manuscrito é apresentado a seguir e ainda não foi submetido para publicação, pois está sendo complementado com experimentos adicionais que visam ampliar e consolidar os resultados obtidos.

# Phage Display Selection from Human Memory B Cells Reveals Cross-Neutralizing Monoclonal Antibodies Targeting the Orthoflavivirus Fusion Loop

Ana Clara Barbosa Antonelli[1,2], Lucas Silva Rodrigues[1,3], Pedro Henrique Aragão Barros[1,3], Renato Kaylan Alves de Oliveira França[1,2], Maria Clara Moura Pinheiro[1], Jacyelle Medeiros Silva[1,3], Matheus de Oliveira Souza[6,7], Ahmed S. Fahad[6,7], Lucimeire Antonelli da Silveira[5], Brandon J. DeKosky[6,7], Marcelo de Macedo Brígido[1,2,3,4], Andréa Queiroz Maranhão[1,2,3,4*]

[1]Department of Cell Biology, University of Brasilia, Brasilia, Brazil
[2]Molecular Pathology Graduation Program, University of Brasilia, Brasilia, Brazil
[3] Molecular Biology Graduation Program, University of Brasilia, Brasilia, Brazil
[4]Institute for Investigation in Immunology (iii) INCT, Brazil.
[5]Institute of Tropical Pathology and Public Health, Federal University of Goiás, Brazil
[6]Ragon Institute of Massachusetts General Hospital (MGH), Massachusetts Institute of Technology (MIT), and Harvard, Cambridge, MA, United States.
[7]Department of Chemical Engineering, Massachusetts Institute of Technology, Cambridge, MA, United States
[*]Correspondent author: andreaqm@unb.br

## ABSTRACT

Orthoflaviviruses such as Zika (ZIKV) and dengue (DENV) viruses continue to pose major public health challenges, and there are no approved antiviral therapies. Broadly neutralizing monoclonal antibodies (mAbs) represent a promising strategy for therapeutic development; however, most antibodies targeting conserved epitopes, such as the envelope (E) protein fusion loop, have been considered weakly neutralizing or prone to antibody-dependent enhancement (ADE). Here, we used a human memory B-cell–derived phage display library, obtained from previously ZIKV and DENV infected individuals to isolate fully human antibodies recognizing the fusion loop, ais conserved region among all orthoflaviviruses. Biopanning was performed using a conformationally constrained peptide mimicking the orthoflavivirus fusion loop, followed by next-generation sequencing to track repertoire enrichment along the selection. Among the selected clones, two IgG1 antibodies (FH2 and FH4) were successfully expressed and purified. Both antibodies displayed strong, dose-dependent binding to UV-inactivated ZIKV and all four DENV serotypes, confirming recognition of a structurally conserved epitope. FH2 and FH4 neutralized ZIKV infection by >95% and 84%, respectively, at micromolar concentrations, and FH2 also cross-neutralized DENV-2 by 78%. These findings demonstrate that the orthoflavivirus fusion loop can serve as a functional target for potent and cross-neutralizing human antibodies and that phage display libraries built from antigen-experienced memory B cells are particularly suited to recover such antibodies. This approach therefore provides a practical framework for discovering broadly reactive mAbs against viral infections.

**Keywords:** Broadly neutralizing antibodies; Orthoflaviviruses; Fusion loop epitope; Memory B-cell library; Monoclonal antibodies; Phage display

## Introduction

Orthoflaviviruses comprise a large group of mosquito- and tick-borne RNA viruses that include major human pathogens such as dengue virus (DENV), Zika virus (ZIKV), yellow fever virus (YFV), West Nile virus (WNV), Japanese encephalitis virus (JEV), and tick-borne encephalitis virus (TBEV) (Lindenbach & Rice, 2003; Ts et al., 2023). These viruses are responsible for widespread outbreaks worldwide, particularly in tropical and subtropical regions. Despite the widespread impact of these pathogens, no specific antiviral therapy is currently approved (Casadevall et al., 2021), and existing vaccines, when available, are limited by their use of live-attenuated formulations, which restrict administration in immunocompromised individuals and pregnant women (Fuertes Marraco et al., 2015; Rivera et al., 2022; Silva et al., 2018). The growing incidence and geographic expansion of orthoflaviviruses highlight the urgent need for the development of safe and effective therapeutic strategies.

Monoclonal antibodies (mAbs) have emerged as promising candidates for the treatment and prevention of viral infections, including orthoflavivirus diseases (Akaishi & Nakashima, 2017). Several potent neutralizing antibodies targeting the viral envelope (E) protein have been identified, demonstrating protective efficacy in preclinical models of DENV and ZIKV infection (Zhao et al., 2016; Oliphant et al., 2006; Sharma et al., 2021; Rouvinski et al., 2015; Zhang et al., 2017; Sankhala et al., 2023; Magnani et al., 2017; Robbiani et al., 2017; Niu et al., 2019; Zhao et al., 2020; Keeffe et al., 2018; Dussupt et al., 2020; Remmel et al., 2021; Ledsgaard et al., 2018; Ramadhany et al., 2015; Fibriansah et al., 2015; Gunale et al., 2024). Notable examples include antibodies recognizing the E dimer epitope (EDE) (Dejnirattisai et al., 2015; Rouvinski et al., 2015; Ledsgaard et al., 2018; Ramadhany et al., 2015) or the domain III of the envelope protein (EDIII) (Zhao et al., 2016; Oliphant et al., 2006; Zhang et al., 2017; Sankhala et al., 2023; Low et al., 2020), which can block viral attachment. However, antibody-based interventions face two major challenges: viral escape due to epitope variability and the potential for antibody-dependent enhancement (ADE) of infection (Dejnirattisai et al., 2015; Barba-Spaeth et al., 2016; Halstead, 2019; Gallichotte et al., 2019). Viral escape due to epitope variability underscores the importance of identifying antibodies directed against conserved epitopes, such as the fusion loop of the E protein, which mediates the low-pH-triggered fusion of viral and endosomal membranes. Although the fusion loop is an attractive target for broadly neutralizing antibodies across orthoflaviviruses, its

therapeutic potential has been historically underexploited due to concerns about antibody-dependent enhancement (ADE) (Halstead, 2019). However, recent evidence demonstrates that ADE associated with FL-directed antibodies can be effectively eliminated through simple Fc-engineering strategies, such as LALA mutation, without compromising neutralization potency (Kotaki et al., 2021).

Traditional hybridoma or humanization approaches for antibody generation are time-consuming and may yield immunogenic antibodies (Köhler and Milstein, 1975; Morrison et al., 1984). In contrast, phage display technology provides a powerful in vitro platform for the discovery of fully human antibodies with high affinity and specificity (Ledsgaard et al., 2018; Smith, 1985; Mimmi et al., 2019; Sioud, 2019; França et al., 2023). This method allows the screening of large combinatorial libraries of antibody fragments under controlled conditions, bypassing the need for immunization. Libraries derived from memory B cells (MBCs) of previously infected individuals are particularly valuable, as they capture naturally affinity-matured repertoires enriched in antigen-experienced clones (Ledsgaard et al., 2018; Ditzel, 2009). Combined with next-generation sequencing (NGS), phage display enables high-resolution mapping of immune repertoires and identification of enriched antibody clones with desirable binding and neutralizing profiles (Ledsgaard et al., 2018; França et al., 2023).

Here, we constructed a human scFv phage display library from the memory B cell repertoire of individuals previously exposed to orthoflaviviruses, aiming to recover naturally matured antibodies targeting conserved regions of the viral envelope. The library was subjected to three rounds of biopanning against a biotinylated peptide mimicking the fusion loop of the ZIKV envelope protein previously described (França et al., 2022). Enriched clones were identified by NGS sequencing and analysis. Selected variable regions were then expressed as recombinant FvFc and/or full-length IgG1 antibodies in mammalian cells. The binding and neutralization profiles of these antibodies were assessed against inactivated ZIKV and DENV1–4 antigens by ELISA and plaque reduction neutralization tests (PRNT).

By leveraging a memory B-cell–derived phage display library together with a structurally conserved fusion-loop antigen, we were able to isolate fully human antibodies that are cross-reactive and with broadly neutralizing potential against different orthoflaviviruses.

## Results

*Construction of a Human Memory B Cell–Derived scFv Library*

Peripheral blood memory B cells (MBCs) were isolated from eight donors previously exposed to orthoflaviviruses (four with confirmed ZIKV infection and four with both ZIKV and DENV seropositivity). Total RNA from pooled MBC samples was used to generate cDNA libraries corresponding to the variable heavy (VH) and light κ (Vκ) chain repertoires of IgG and IgA isotypes.

Amplification of the rearranged variable regions successfully recovered all major human immunoglobulin families. Twelve distinct PCR reactions were performed for VH amplification, six from IgG- and six from IgA-derived cDNA, yielding products of approximately 550 bp, consistent with the expected size of VH fragments (Fig. 1A,B). Similarly, sixteen reactions targeting κ light-chain families (Vκ1–Vκ5) generated fragments of ~450 bp (Fig. 1C).

All amplified products exhibited specific bands, confirming efficient coverage of the VH and Vκ repertoires within the MBC-derived pool. The differential amplification intensities observed among families were consistent with their variable abundance in the human antibody repertoire. These results validated the successful recovery of diverse VH and Vκ sequences suitable for subsequent assembly into single-chain variable fragments (scFv) for library construction.

PCR-amplified VH and Vκ products from all immunoglobulin families were pooled into two separate mixes and used in equimolar amounts as templates for overlap extension PCR to assemble single-chain variable fragments (scFv: VL-linker-VH). The primers used in the first amplification introduced short complementary sequences at the 3′ end of Vκ and 5′ end of VH, enabling seamless joining of both fragments into a continuous scFv gene.

Agarose gel electrophoresis confirmed the generation of a distinct band of approximately 850 bp, corresponding to the expected size of the assembled scFv (Fig. 1D). The scFv bands were excised and purified, yielding clean products suitable for downstream cloning (Fig. 1E).

Purified scFv fragments (~850 bp) were digested with Sfi I and ligated into the pComb3XSS phagemid vector pre-digested with the same enzyme. Small-scale test ligations were performed to assess transformation efficiency and library complexity. The optimized large-scale ligation and electroporation into E. coli XL1-Blue cells yielded

approximately $7.8 \times 10^6$ independent transformants, confirming successful generation of a diverse human memory B cell–derived scFv library.

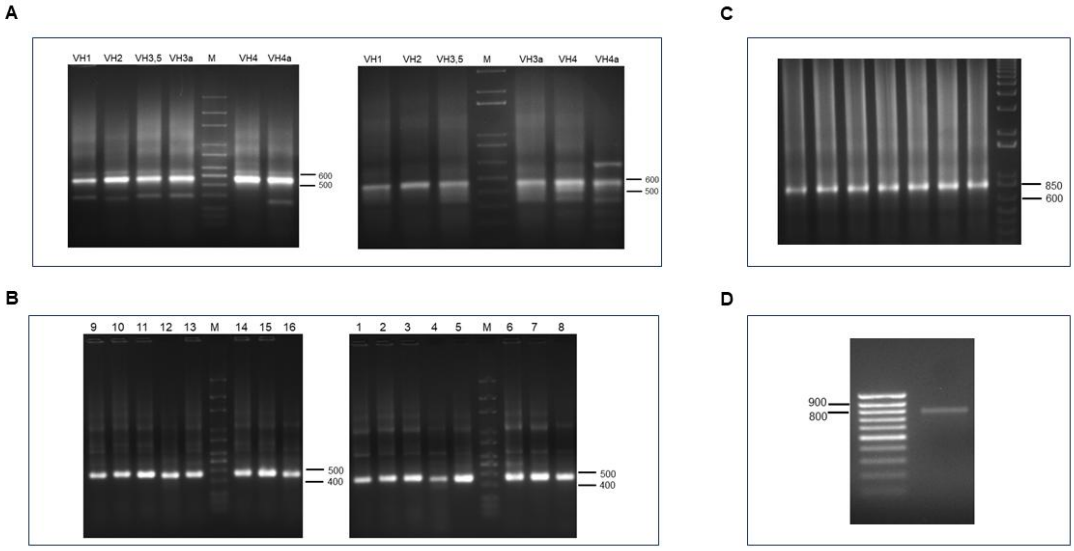


**Figure 1. Amplification of variable immunoglobulin regions from memory B-cell cDNA.** ~550 bp VH regions amplified from IgG (A) and IgA (B) derived cDNA. (C) ~450 bp κ light-chain (Vκ) families 1–5. 1, 5, 9, and 13: Vκ1 family; 2, 6, 10, and 14: Vκ2 and Vκ4 families; 3, 7, 11, and 15: Vκ3 family; wells 4, 8, 12, and 16: Vκ5 family. (D) Overlap extension PCR showing the ~850 bp scFv product. (E) Purified scFv fragment after agarose gel extraction. M, molecular-weight marker.

*Selection of the scFv Phage Display Library Against the Orthoflavivirus Fusion Loop*

Phage particles displaying scFv-pIII fusion proteins were rescued using the M13 helper phage, generating a recombinant phage library subsequently used for biopanning against a orthoflavivirus-derived antigen. The selection target consisted of a biotinylated synthetic peptide mimicking the fusion loop region of the ZIKV E protein, a highly conserved and functionally critical epitope shared among orthoflaviviruses (França et al., 2022).

Three rounds of panning were performed, progressively increasing washing stringency (5, 10, and 15 washes, respectively). Two parallel selection schemes were conducted: adsorbed-antigen selection, in which bound phages were directly eluted from biotinylated peptide-coated streptavidin-agarose beads, and competitive selection, using a 10-fold molar excess of the non-biotinylated peptide to competitively elute phages displaying higher-affinity binders.

Phage titration across selection rounds reflected the impact of increasing stringency on library complexity rather than a simple increase in absolute output titers.

For the adsorbed-antigen system, absolute output titers decreased from $5.8 \times 10^7$ to $3.4 \times 10^6$ PFU across three rounds; however, the input/output ratio improved by ~2 logs from $4.1 \times 10^5$ in round 1 to $1.8 \times 10^3$ in round 2, indicating efficient enrichment of fusion loop–binding phage clones (Table 1). A similar pattern was observed in the competitive selection, with output titers decreasing from $4 \times 10^7$ to $1.6 \times 10^6$ PFU, while the input/output ratio dropped from $6 \times 10^5$ to $1.6 \times 10^3$ between rounds 1 and 2 (Table 2). The subsequent slight reduction in enrichment in round 3 likely reflects amplification constraints, and the titers obtained were sufficient to enable downstream monoclonal screening and NGS analyses.

**Table 1. Phage titration during biopanning against the adsorbed fusion loop peptide.**

| Selection Cycle | Input (PFU) | Output (PFU) | Input/Output (PFU |
|---|---|---|---|
| 1 | $2.4 \times 10^{13}$ | $5.84 \times 10^7$ | $4.1 \times 10^5$ |
| 2 | $2.06 \times 10^{10}$ | $1.15 \times 10^7$ | $1.79 \times 10^3$ |
| 3 | $1.37 \times 10^{11}$ | $3.37 \times 10^6$ | $4 \times 10^4$ |

**Table 2. Phage titration during biopanning with competitive elution.**

| Selection Cycle | Input (PFU) | Output (PFU) | Input/Output (PFU) |
|---|---|---|---|
| 1 | $2.4 \times 10^{13}$ | $4 \times 10^7$ | $6 \times 10^5$ |
| 2 | $2.46 \times 10^{10}$ | $1.52 \times 10^7$ | $1.62 \times 10^3$ |
| 3 | $5.6 \times 10^{10}$ | $1.62 \times 10^6$ | $3.46 \times 10^4$ |

*Next-Generation Sequencing Analysis of the scFv Phage Library Before and After Selection*

To assess repertoire enrichment throughout the phage display selection process, the variable heavy (VH) and light (VL) chain domains of the scFv library were amplified from plasmid DNA obtained both before selection and after the third biopanning round (Supplementary Fig. S1). Amplicons were sequenced on the Illumina MiSeq platform ($2 \times 300$ bp paired-end reads, $\sim 1 \times 10^6$ reads per sample).

Sequencing data were analyzed using ATTILA, an bioinformatic pipeline developed for antibody repertoire profiling (Maranhão et al., 2020). The software annotated framework and complementarity-determining regions (CDRs), assigned germline gene usage, and calculated the fold-change enrichment of individual VH and VL sequences between the initial (cycle 0) and final (cycle 3) phage populations.

A pronounced reduction in repertoire diversity was observed after selection, together with strong enrichment of dominant clones (Supplementary Tables S2–S5). The VH2-5 gene family accounted for the majority of the most enriched heavy chains, followed by VH4-34, while the light-chain repertoires were dominated by Vκ2 and Vκ1 families (Fig. 2A–B). Seven VH CDR3 sequences were shared between the adsorbed and competitive selections, suggesting convergent selection toward similar structural motifs within the fusion loop epitope. In contrast, no overlap was observed among the top-enriched VLs, consistent with greater diversity in light-chain pairing.

The competitive selection produced higher fold-change values for both VH and VL clones compared with the adsorbed selection, indicating stronger selection pressure for high-affinity binders capable of recognizing soluble antigen (Fig. 2C). Collectively, these results demonstrate that the phage display strategy efficiently refined the human memory B-cell repertoire, enriching for fusion loop-reactive antibodies with potential cross-neutralizing activity against multiple orthoflaviviruses. Supplementary Figure S1 shows the PCR amplification of VH and VL fragments prior to NGS, and Supplementary Tables S2–S5 list the 15 most enriched sequences per chain and selection condition.

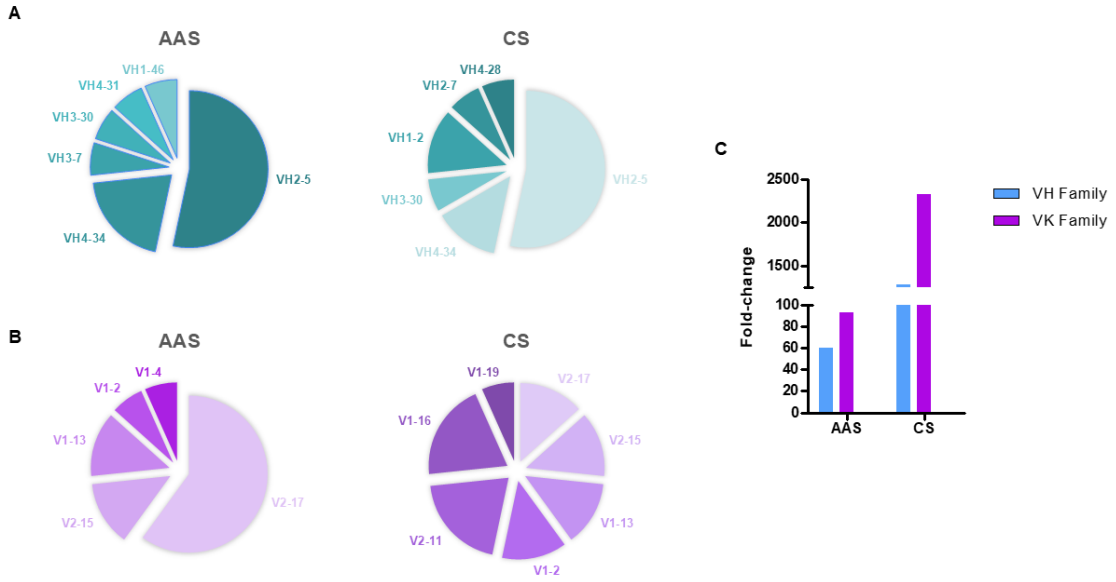


**Figure 2. Germline family distribution and enrichment of antibody variable domains after phage display selection.** (A) Frequency of VH germline families among the top-15 enriched heavy-chain sequences after adsorbed and competitive selections. (B) Frequency of VL germline families among the top-15 enriched light-chain sequences for each selection. (C) Comparison of fold-change values of VH and VL domains obtained from the adsorbed antigen (AAS) and competitive (CS) selections.

*Selection of VH and VL Domains for Recombinant Antibody Design and Expression*

Based on the NGS enrichment profiles, five antibody candidates were designed by combining the most enriched VH and VL domains identified after phage display selection. The selection criteria included (i) high fold-change enrichment across biopanning rounds, (ii) recurrence of identical or homologous CDR3 motifs in both selection strategies (adsorbed and competitive), and (iii) representation of distinct VH and VL germline families to preserve diversity among the constructs.

The selected VH and VL domains were paired to generate five recombinant antibodies, designed for expression in both FvFc and IgG1 formats for comparative functional evaluation. A schematic representation of the VH–VL pairings used for antibody design and the complete sequence information are provided in Supplementary Figures S2–S3.

Recombinant antibodies were transiently expressed in mammalian cells using the Expi293™ system. Among the designed constructs, three antibodies yielded detectable expression levels suitable for downstream characterization: FH4 FvFc, FH4 IgG, and FH2 IgG. All expressed antibodies were purified by Protein A affinity chromatography, with chromatographic profiles and Coomassie-stained SDS-PAGE gels confirming recovery of the expected antibody species (Fig. 3).

Notably, expression yields varied markedly among constructs. FH2 IgG exhibited the highest production levels, followed by FH4 IgG, whereas FH4 FvFc was expressed at very low concentrations and showed evidence of partial degradation in SDS-PAGE and Western blot analyses. Due to the limited recovery and reduced integrity of FH4 FvFc, this construct was only evaluated in antigen-binding assays (ELISA), while neutralization analyses were performed using the two IgG1 antibodies.

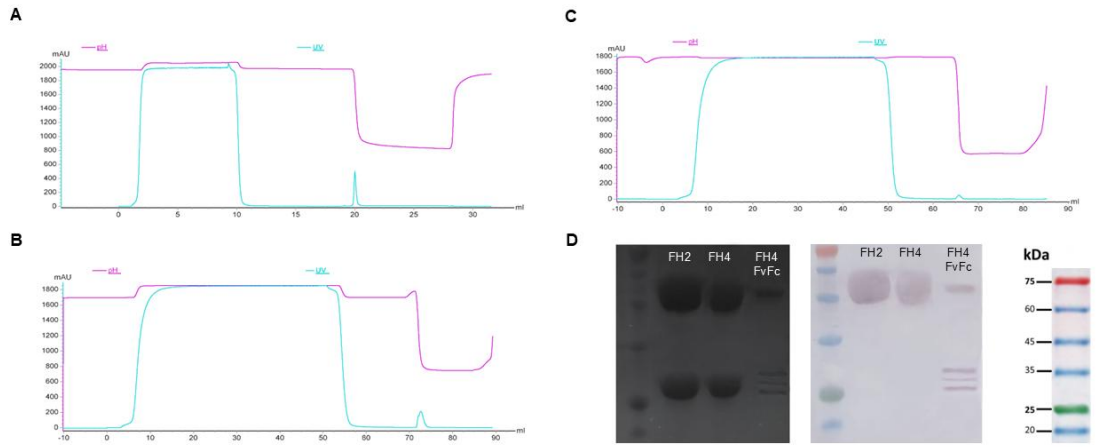

**Figure 3. Expression and purification of recombinant anti-orthoflavivirus antibodies.** (A) Protein A affinity purification chromatogram of FH2 IgG (A), FH4 IgG (B), and FH4 FvFc. (D) SDS-PAGE and Western blot analyses of purified antibodies expressed in Expi293 cells. Purified IgGs displayed the expected molecular weights for heavy (~50 kDa) and light (~25 kDa) chains, whereas the FH4 FvFc construct showed lower yield and evidence of partial degradation.

*Antigen-binding profiles of recombinant antibodies against orthoflaviviruses*

The binding activity of the recombinant antibodies to ZIKV and DENV serotypes 1–4 was assessed by ELISA using inactivated virions as antigens. Both FH2 IgG and FH4 IgG displayed strong and dose-dependent binding to all tested orthoflaviviruses, confirming recognition of a conserved epitope within the fusion loop region of the viral E protein (Fig. 4A–E).

The apparent binding affinities, determined from $EC_{50}$ values, revealed distinct binding patterns between the two antibodies. FH4 IgG exhibited the strongest binding overall, particularly against DENV-1 (39.6 nM), DENV-3 (23.3 nM), and DENV-4 (96.3 nM), whereas FH2 IgG showed higher affinity for ZIKV (286.4 nM) and DENV-4 (30.9 nM) (Table 3). These differences suggest that both antibodies target the conserved fusion loop region but may rely on partially distinct structural determinants within this epitope, likely reflecting subtle conformational or sequence variations among orthoflavivirus serotypes.

In contrast, the FH4 FvFc construct showed weak and incomplete binding curves, yielding non-convergent $EC_{50}$ estimates ($>10^{10}$ nM). This poor performance is consistent with the low expression yield and partial degradation observed during purification, indicating that structural instability rather than loss of epitope recognition likely impaired antigen binding.

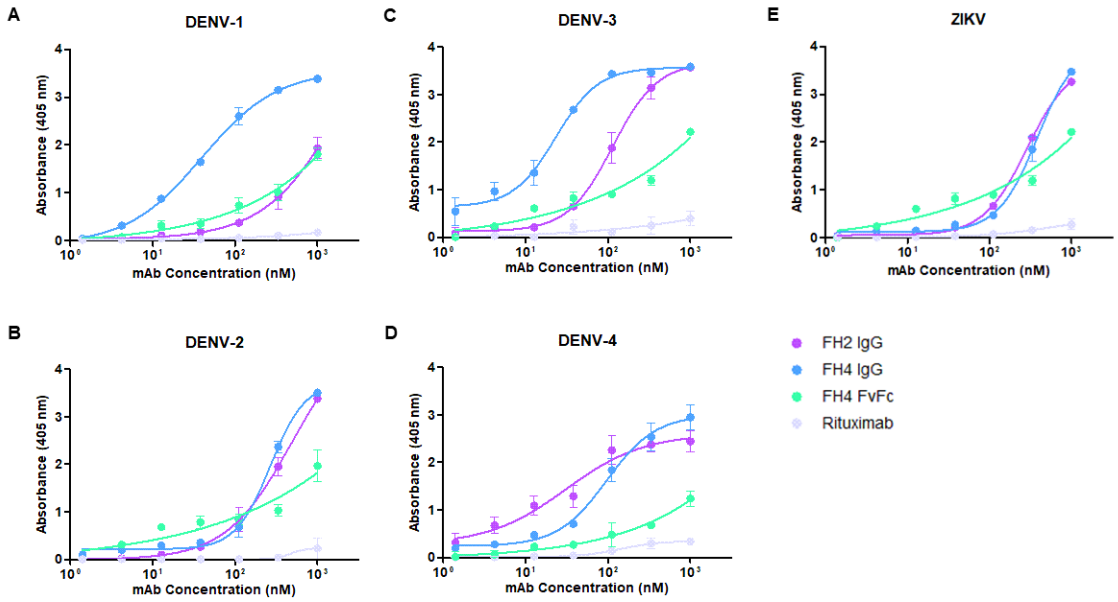


**Figure 4. Binding of recombinant antibodies to inactivated orthoflaviviruses measured by indirect ELISA.** Serial 3-fold dilutions of antibodies (starting from 1000 nM) were tested for binding to UV-inactivated DENV-1 (A), DENV-2 (B), DENV-3 (C), DENV-4 (D), and ZIKV (E). Rituximab was used as an isotype control. Data represent mean ± SD of at least two independent experiments performed in triplicate. Absorbance values at 405 nm are plotted against antibody concentration (nM). Apparent $EC_{50}$ values were determined by nonlinear regression in GraphPad Prism (Table 3).

**Table 3. Apparent $EC_{50}$ values (nM) for binding of recombinant antibodies to ZIKV and DENV serotypes determined by ELISA.**

| Antibody | ZIKV | DENV-1 | DENV-2 | DENV-3 | DENV-4 |
|---|---|---|---|---|---|
| **FH2 IgG** | **286.4** | **2534** | **493.6** | **113.4** | **30.85** |
| **FH4 IgG** | **385.1** | **39.6** | **268.0** | **23.3** | **96.3** |
| **FH4 FvFc** | **ND** | **ND** | **ND** | **ND** | **ND** |

**ND - Non-determinable (binding curves did not reach saturation; $EC_{50} > 10^{10}$ nM)**

*Comparative Neutralization Analysis*

Neutralization assays confirmed that both FH2 and FH4 IgG antibodies effectively inhibit ZIKV infection in a concentration-dependent manner, consistent with their binding profiles observed in ELISA (Fig. 4A–B). FH2 IgG displayed the strongest neutralizing activity, achieving nearly complete inhibition (> 95%) at 7 µM, whereas FH4 IgG reached approximately 84% under the same conditions. Despite the slightly lower

potency of FH4 IgG, both antibodies maintained > 70% neutralization at micromolar concentrations, confirming robust antiviral activity.

Cross-neutralization analysis revealed that FH2 IgG also inhibited DENV-2, reaching 78% neutralization at 2.16 µM, although with apparently lower potency than against ZIKV (Fig. 4C). However, because the maximum concentration tested for DENV-2 was lower than that used in the ZIKV assay, this difference likely reflects the limited concentration range, rather than a true reduction in neutralizing capacity. Indeed, when compared to the equivalent ZIKV concentration (2.33 µM), neutralization levels were comparable, suggesting that higher antibody concentrations could further enhance DENV-2 inhibition.

Together, these results demonstrate that antibodies derived from fusion-loop-directed phage display selection can effectively neutralize ZIKV and, to a lesser extent, DENV-2, supporting the potential of this strategy for isolating broadly reactive human anti-orthoflavivirus antibodies.

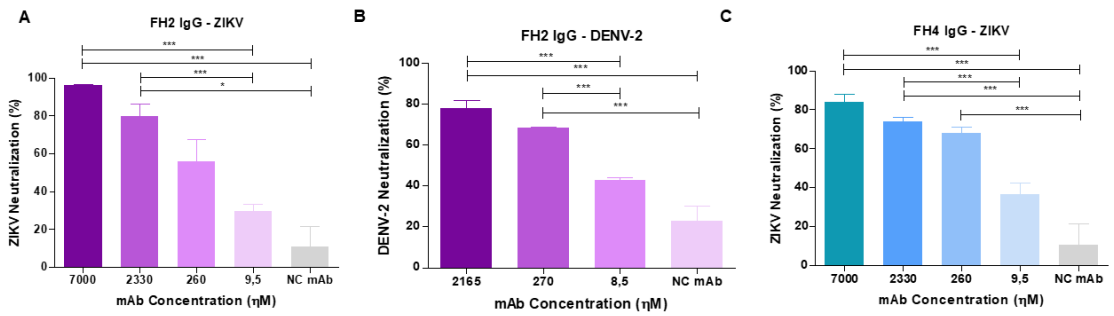


**Figure 5. Neutralization activity of recombinant anti-orthoflavivirus antibodies.** (A) ZIKV neutralization by FH2 IgG. (B) DENV-2 neutralization by FH2 IgG. (C) ZIKV neutralization by FH4 IgG. Neutralization percentages were determined by plaque reduction assays using different antibody concentrations. Bars represent mean ± SD of two independent experiments performed in triplicate. Statistical significance was assessed by one-way ANOVA followed by Tukey's post hoc test (*$p < 0.05$; **$p < 0.01$).

## Discussion

Over the past few decades, the pharmaceutical landscape has undergone a significant shift with the growing use of biologics, particularly monoclonal antibodies (mAbs). Their combination of high antigen specificity and effector functions has expanded the range of immunotherapeutic possibilities. In this context, we aimed to generate a human antibody library derived from memory B cells (MBCs) of individuals

previously exposed to orthoflaviviruses and to select antibodies targeting a conserved region within the viral envelope protein. This strategy was designed to identify human mAbs with potential cross-neutralizing activity, underscoring how antigen selection and library origin influence antibody discovery.

Immune libraries derived from antigen-experienced donors offer significant advantages over naïve or synthetic libraries because their repertoires are already shaped by affinity maturation and somatic hypermutation. As a result, immune libraries often yield antibodies of higher specificity and affinity toward the target antigen (Ditzel, 2009). Nonetheless, the number of circulating antigen-specific memory B cells is low, typically around 1–2% of total peripheral B cells (Morbach et al., 2010), which may restrict the diversity of such libraries. To enhance the representation of antigen-specific clones, we adopted a previously validated protocol (Silva et al., 2025) in which PBMCs from convalescent ZIKV- or DENV-infected individuals were stimulated in vitro with IL-2, a TLR7/8 agonist (R848), and UV-inactivated ZIKV antigen. This approach significantly increased the proportion of viable MBCs and the production of ZIKV-specific IgG in culture supernatants, confirming the expansion of antigen-experienced B cells before library construction. The resulting scFv library thus represents a focused yet naturally diversified repertoire, capturing the outcome of prior immune exposure while maintaining polyclonality.

To maximize immunoglobulin gene diversity, we amplified VH segments from both IgG and IgA isotypes, as recent studies have shown that IgA antibodies can also contribute to orthoflavivirus neutralization (Waickman et al., 2020). Amplified genes from human VH families (VH1–VH5) and Vκ families (Vκ1–Vκ5) were assembled into scFv fragments and cloned into the pComb3XSS phagemid vector, generating a library of $7.8 \times 10^6$ transformants. Although smaller than large naïve libraries ($10^9$–$10^{10}$), this size is consistent with high-quality immune libraries derived from antigen-specific repertoires (Dantas-Barbosa et al., 2005; Bertoglio et al., 2021). Given the restricted frequency of circulating memory B cells, the generated library represents an authentic reflection of the human immune response to natural infection.

The choice of antigen is a key determinant of successful antibody discovery. Selection was performed using a peptide mimetic of the orthoflavivirus fusion loop (FL), a highly conserved motif in domain II of the envelope (E) protein (França et al., 2022). The FL mediates low-pH–triggered conformational rearrangements essential for membrane fusion (Heinz and Stiasny, 2017; Zhang et al., 2017). Previous studies showed

that anti-FL antibodies can block the membrane fusion process or interfere with virion maturation (Volkova et al., 1999; Oliphant et al., 2006). However, the fusion loop is often partially buried in the mature virion. To address this, we used a structurally constrained peptide mimetic stabilized by a disulfide bridge linking the FL to an adjacent segment of domain II (França et al., 2022), designed to preserve native conformation and enrich for antibodies recognizing authentic structural features.

Two complementary biopanning strategies were employed: one using antigen adsorbed onto streptavidin-agarose beads and another using competitive elution with excess soluble, non-biotinylated antigen. The latter approach yielded greater enrichment of VH and VL sequences, indicating the selection of higher-affinity binders (Barbas et al., 2001). Next-generation sequencing (NGS) revealed strong fold-change enrichment, particularly among VL domains (up to 2300-fold), suggesting asymmetric selection pressure and the preferential recovery of specific germline families (VH2-5 and VH4-34), consistent with previous findings (Cook and Tomlinson, 1995; Kohsaka et al., 1996). The absence of overlap in top VL CDR3 sequences between strategies suggests multiple structural solutions for recognizing this conserved but partially cryptic epitope.

One inherent limitation of scFv-based library sequencing is the loss of the VH–VL pairing information. Here, we prioritized VH–VL combinations that displayed strong enrichment in both strategies and represented distinct germline families, leading to the design of five recombinant antibodies expressed in FvFc and IgG1 formats. The FvFc configuration was chosen to explore potential advantages of a smaller bivalent construct with a silenced Fc (LALA mutation), thereby avoiding further antibody-dependent enhancement (ADE) (Schlothauer et al., 2016).

Although not all constructs were expressed efficiently, two IgG1 antibodies (FH2 and FH4) were successfully produced. The FvFc version of FH4 exhibited degradation and poor recovery, explaining its reduced ELISA signal compared to the IgG form. Expression bottlenecks in other constructs indicate suboptimal folding and codon optimization for scFv-derived antibodies (Wurm, 2004; Maranhão et al., 2015; Bujak et al., 2014).

Although selection was performed using a peptide, FH2 and FH4 IgGs bound strongly and dose-dependently to UV-inactivated ZIKV and all four DENV serotypes, indicating recognition of the epitope in its native quaternary context. The apparent $EC_{50}$ values revealed complementary binding patterns: FH4 IgG bound more strongly to DENV-1 (39.6 nM), DENV-3 (23.3 nM), and DENV-4 (96.3 nM), while FH2 IgG

showed enhanced affinity for ZIKV (286.4 nM) and DENV-4 (30.9 nM). These differences may suggest that both antibodies target overlapping but non-identical determinants within the fusion loop, shaped by serotype-specific conformational variations. The EC50 values observed are within the same order of magnitude as those reported for other fusion loop–directed antibodies. For example, the murine IgG E60, known for cross-neutralizing WNV and DENV, exhibited $EC_{50}$ values ranging from 17 to 612 ng/mL depending on virus and assay conditions (Pierson et al., 2006), which corresponds to approximately 113 to 4080 nM when assuming a molecular weight of 150 kDa for IgGs. Similarly, the human IgG 1C19, which binds a region adjacent to the fusion loop, showed $EC_{50}$ values of ≤60 ng/mL (Smith et al., 2013), approximately ≤400 nM.

Neutralization assays confirmed that both antibodies effectively inhibit ZIKV infection in a concentration-dependent manner. FH2 IgG achieved >95% inhibition at 7 μM, whereas FH4 reached ~84% under the same conditions. Although only FH2 was tested against DENV-2, it reached ~78% neutralization at 2.16 μM. Given that this concentration was below the top dose used for ZIKV (7 μM), FH2 might achieve similar inhibition at higher doses. Interestingly, FH4 bound DENV-2 more strongly than FH2, suggesting potentially greater neutralizing capacity.

Dowd et al. (2011) demonstrated that the structural dynamics ("breathing") of orthoflavivirus particles can transiently expose otherwise inaccessible epitopes, including the fusion loop. This dynamic exposure enables antibodies to achieve neutralization even when targeting partially buried epitopes. Thus, differences in neutralization potency between FH2 and FH4 may reflect not only intrinsic affinity but also time-dependent epitope exposure and binding stoichiometry.

Despite being traditionally regarded as a suboptimal or ADE-associated target (Dowd et al., 2015; Oliphant et al., 2006; Kotaki et al., 2021), our findings reinforce the potential of the orthoflavivirus fusion loop as a neutralizing epitope. Multiple studies also support this notion. Costin et al. (2013) identified human mAbs (4.8A, D11C, 1.6D) that neutralized all four DENV serotypes by binding residues W101, L107, and G109 within the fusion loop, blocking viral fusion rather than attachment. Similarly, Deng et al. (2011) described the broadly cross-reactive mAb 2A10G6, which recognizes the conserved 98DRXW101 motif and neutralizes DENV 1–4, YFV, and WNV, protecting mice from lethal infection. Sultana et al. (2009) identified a human mAb (mAb11) against the West Nile virus fusion loop that also cross-reacted with all four DENV serotypes and conferred protection against lethal infection in mice. Consistent with these results, Fan et al. (2024)

demonstrated that mutations in the Japanese encephalitis virus fusion loop (W101G, G106K, L107D) drastically reduced neutralizing titers and survival in mice, confirming the functional importance of this region.

Previous structural studies provide further context. Oliphant et al. (2006) showed that antibodies recognizing domains I–II, including the fusion loop, can neutralize by blocking fusion, while Cherrier et al. (2009) demonstrated that the exposure of the loop varies between mature and immature virions, influencing accessibility. These structural dynamics likely account for the distinct binding and neutralization profiles observed for FH2 and FH4.

The use of memory B-cell–derived libraries likely contributed to the isolation of antibodies with broad cross-orthoflavivirus reactivity. Secondary DENV infection preferentially expands cross-reactive B-cell clones capable of recognizing conserved epitopes (Mathew et al., 2011; Zompi et al., 2012). In our system, memory B cells were re-stimulated with inactivated ZIKV prior to library construction, mimicking secondary exposure and promoting the expansion of cross-reactive clones targeting conserved epitopes such as the fusion loop. Consistent with this, Chaudhury et al. (2017) showed that secondary DENV infections elicit a focused recall of memory B cells targeting conserved epitopes, including the fusion loop and E-dimer interface.

A previous study from our group (França et al., 2022) demonstrated that antibodies selected from a naïve human library using the same fusion loop peptide exhibited strong cross-reactivity among orthoflaviviruses and effectively neutralized ZIKV. Here, we confirmed that this cross-reactivity can translate into cross-neutralization, demonstrating that the fusion loop can elicit functionally protective antibodies. Although the best clone from the naïve library (AZ1p, $EC_{50}$ = 14.7 nM for ZIKV) displayed higher affinity for ZIKV, the IgG antibodies generated here showed comparable or superior binding to DENV serotypes ($EC_{50}$ = 23–268 nM). In the previous work, scFv clones exhibited cross-reactivity to DENV ($EC_{50}$ = 545–1094 nM), whereas FH2 and FH4 demonstrated markedly improved affinities across all four serotypes. This suggests that the memory B cell–derived library may have favored the recovery of affinity-matured antibodies capable of accommodating subtle structural variations within the fusion loop among different orthoflaviviruses. Importantly, despite their larger molecular size, the IgG antibodies achieved binding and neutralization efficiencies comparable to those of the scFv fragments, indicating that the fusion loop remains accessible even to full-length antibodies. Nevertheless, smaller derivatives such as FvFc

could potentially further improve epitope accessibility and enhance neutralization potency.

Given that fusion loop–directed antibodies have been implicated in ADE, future therapeutic applications should carefully assess Fc-mediated effector functions. One strategy is to develop Fc-silenced variants (e.g., LALA mutants), which retain binding and neutralization capacity while preventing FcγR engagement. Testing both wild-type and Fc-silenced versions of FH2 and FH4 will be essential to determine their protective potential. Notably, Vogt et al. (2011) showed that fusion loop–specific antibodies against West Nile virus, although weakly neutralizing in vitro, provided protection in vivo via FcγR- and complement-dependent mechanisms. These findings emphasize that Fc engineering can optimize the balance between efficacy and safety for fusion loop–targeting therapeutics.

Together, we showed that using Phage Display with a memory B cell–derived library with and a fusion loop antigen engineered to preserve key structural features, we were able to generate fully human IgG antibodies capable of cross-binding and neutralizing orthoflaviviruses. The differential reactivity of FH2 and FH4 underscores the structural and functional versatility of the fusion loop epitope, highlighting its potential as a target for broad-spectrum antiviral strategies. Overall, the antibodies identified here represent promising starting points for further evaluation, including testing against additional orthoflaviviruses, *in vivo* assessment of protective activity, and exploration of alternative formats such as Fc-engineered variants or scFv-Fc fusions.

## Materials and Methods

### *Construction of a Human scFv Phage Display Library from the Memory B Cell Repertoire of Orthoflavivirus-Exposed Individuals (Adapted from Andris-Widhopf et al., 2000)*

A human single-chain variable fragment (scFv) antibody library was generated from the memory B cell (MBC) repertoire of individuals who had been previously exposed to orthoflaviviruses. Peripheral blood mononuclear cells (PBMCs) from donors with confirmed IgG seropositivity for Zika virus (ZIKV) or both ZIKV and dengue virus (DENV) were used as the source of B cells (Silva et al., 2025). Human PBMC samples were obtained from orthoflavivirus-exposed donors under informed consent. The study

was conducted in accordance with the guidelines of the Research Ethics Committee of the Pontifical Catholic University of Goiás (CAAE reference no. 57.696.716.9.0000.0037), and all participants provided written informed consent. Peripheral blood samples were collected from male and female individuals, with gender defined by self-report. Blood collection and cell culture procedures were performed approximately two years after the diagnosis of the acute phase of ZIKV infection. During the acute phase, viral RNA detection in blood and urine samples was carried out by RT-qPCR using the BioGene Zika Virus PCR Kit (Bioclin®, Cat. #K203). Following blood collection, serological testing for ZIKV and DENV (IgM and IgG) was performed using the TR DPP® Zika/Dengue IgM/IgG immunochromatographic assay (Bio-Manguinhos, Rio de Janeiro, Brazil), ensuring the serological characterization of the individuals included in the study. MBCs were expanded in vitro with IL-2 and the TLR7/8 agonist R848, followed by stimulation with ZIKV antigen to enrich orthoflavivirus-specific clones. Flow cytometry analysis confirmed a marked increase in viable MBCs (up to 33%) after stimulation, and ELISA of culture supernatants revealed predominant production of ZIKV-specific IgG antibodies. Samples from eight donors were selected for library construction.

Total RNA extracted from purified orthoflavivirus-specific MBCs was used for cDNA synthesis targeting the variable domains of immunoglobulin heavy (VH, IgG and IgA) and light (Vκ) chains using the High-Capacity cDNA Reverse Transcription Kit (Applied Biosystems). Variable domains were amplified by PCR with family-specific primers using the QuantiNova™ RT-PCR Kit (Qiagen). Purified VH and Vκ products were assembled into scFv fragments (~850 bp) by overlap extension PCR. The resulting scFv inserts were digested with SfiI and cloned into the pComb3XSS phagemid vector, which enables display of scFvs as pIII fusion proteins on M13 phage particles, via T4 DNA ligase. Ligation mixtures were electroporated into E. coli XL1-Blue competent cells, and transformed bacteria were infected with helper phage VCSM13 to generate the human scFv phage display library. The library was amplified in SB medium under antibiotic selection and analyzed by colony PCR and phage titration to estimate its diversity and size.

*Selection of the scFv Library Against a Mimetic Peptide of the Orthoflavivirus Fusion Loop (Adapted from Rader et al., 2000)*

Phage-displayed scFv libraries were subjected to three rounds of biopanning against a biotinylated mimetic peptide of the orthoflavivirus fusion loop region previously designed by our group (França et al., 2022). Phage particles were precipitated from overnight culture supernatants with 6 g of NaCl and 8 g of PEG 8000 per 100 mL, incubated on ice for 30 min, and pelleted by centrifugation at 15,000 × g for 15 min at 4 °C. The resulting phage pellets were resuspended in TBS containing 1% BSA, generating the input phage pool for selection.

For target coating, streptavidin-conjugated agarose beads (1 mg/mL; Sigma-Aldrich) were incubated with 10 µM of the biotinylated ZIKV fusion loop peptide in TBS containing 3% BSA for 1 h at room temperature. After washing, 100 µL of input phage were added to the peptide-coated beads and incubated for 1 h at room temperature with gentle agitation. Unbound phages were removed by successive washes with TBST (TBS + 0.1% Tween-20) — 5, 10, and 15 washes for the first, second, and third selection rounds, respectively.

Bound phages were eluted competitively with 100 µM of the non-biotinylated fusion loop peptide, incubated for 15 min under agitation, and recovered by centrifugation. Both the competitively eluted fraction and the bead-bound fraction were used as independent inputs for subsequent amplification steps.

E. coli XL1-Blue cultures ($OD_{600} \approx 1.0$) grown in SB medium containing 1% glucose and 10 µg/mL tetracycline were infected with phages from each selection pathway (competitive and adsorptive). After 15 min at room temperature, infected cells were cultured in SB medium supplemented with carbenicillin (50 µg/mL), tetracycline (10 µg/mL), and 1% glucose, and superinfected with helper phage VCSM13 ($10^{12}$ pfu/mL). Cultures were incubated at 37 °C, 250 rpm for 1.5 h, followed by the addition of kanamycin (final 70 µg/mL) and overnight incubation at 37 °C, 300 rpm.

Phage particles were harvested and used as input for the next biopanning cycle, totaling three consecutive rounds of selection. Input and output titers were determined by plating serial dilutions on E. coli XL1-Blue MRF′.

*Plasmid DNA Extraction and Amplification of Variable Domains*

Plasmid DNA from the recombinant scFv library, collected both before selection (midiprep) and after the final biopanning round (miniprep), was extracted using the QIAprep Spin Midiprep Kit and QIAprep Spin Miniprep Kit (Qiagen), following the manufacturer's protocols. Purified DNA was resuspended in nuclease-free water and verified by agarose gel electrophoresis.

The variable heavy (VH) and light (VL) chain domains were amplified separately by PCR using specific primer sets (listed in Supplementary Table S2). Reactions were performed with the QuantiNova™ Probe RT-PCR Kit (Qiagen) according to the manufacturer's instructions, with 20 ng of template DNA, 0.6 μM of each primer, and 1× PCR Master Mix. The thermocycling profile was as follows: 95 °C for 5 min, followed by 30 cycles of 95 °C for 30 s, 65 °C for 30 s, and 72 °C for 1 min, and a final extension at 72 °C for 5 min. Amplified products were resolved on 1.5% agarose gels and purified using the Agarose Gel Extraction Kit (Cellco).

*Next-Generation Sequencing and Bioinformatic Analysis*

The variable heavy (VH) and light (VL) chain domains from both the pre-selection scFv library and the final round of selected phage populations were subjected to next-generation sequencing (NGS). Sequencing was performed by Macrogen Inc. (Seoul, South Korea) using the Illumina MiSeq platform, with 2 × 250 bp paired-end reads and a depth of approximately 1 million reads per sample.

Raw sequence data were processed and analyzed using ATTILA, an in-house bioinformatic pipeline for immunoglobulin repertoire analysis (Maranhão et al., 2020). The software identifies CDR and framework regions, assigns germline gene usage, and calculates the enrichment frequency of each variable domain across selection rounds. Fold-change values were determined by comparing the relative abundance of each sequence between the final biopanning output and the original library, to identify enriched clones and monitor selection dynamics across biopanning rounds.

*Expression and Purification of Recombinant Anti-Orthoflavivirus Antibodies*

Based on the NGS analysis, the most enriched VH and VL sequences were selected and codon-optimized for mammalian expression using the GenSmart™ Codon

Optimization platform (GenScript), with codon usage adapted to HEK293 and CHO cells. Optimized genes were synthesized and cloned into the pMIW vector for FvFc constructs and into pcDNA3.4 vectors for full-length IgG1 and Igκ expression.

Recombinant antibodies were produced by transient transfection of Expi293F™ cells (Thermo Fisher Scientific) using the Expi293™ Expression System and ExpiFectamine™ 293 Transfection Kit, following the manufacturer's protocol. Cells were cultured in Expi293™ Expression Medium at 37 °C, 8% $CO_2$, and 125 rpm agitation. Supernatants were harvested 6 days post-transfection, clarified by centrifugation, and filtered through 0.22 μm membranes.

Purification of FvFc and IgG antibodies was performed by Protein A affinity chromatography using an ÄKTA Pure system (Cytiva) equipped with a HiTrap Protein A HP 5 mL column (Cytiva). Antibodies were eluted with 0.1 M citric acid, pH 3.0, and immediately neutralized with 1 M Tris-HCl, pH 9.0. Elution fractions were analyzed by SDS-PAGE under denaturing conditions to confirm purity and integrity.

Protein integrity was assessed by SDS-PAGE under reducing conditions and visualized by Coomassie blue or silver staining, and analyzed by Western blotting, with detection using a goat anti-human Fc antibody followed by development with NBT/BCIP substrate (Thermo Fisher Scientific).

*ELISA Binding Assay Against Inactivated ZIKV and DENV1–4*

The binding of recombinant antibodies to UV-inactivated ZIKV (H/PF/2013 strain) and all four DENV serotypes, DENV-1 (Hawaii strain), DENV-2 (N. Guinea C strain), DENV-3 (H 87 strain), and DENV-4 (BC 295/97 strain) was assessed by indirect ELISA. Viral antigens (200 PFU/well, UV-inactivated for 1 h) were immobilized overnight at 4 °C on high-binding 96-well polystyrene plates (Thermo Fisher Scientific). Plates were blocked with 3% BSA in PBST for 2 h at 37 °C and incubated with recombinant antibodies in serial 3-fold dilutions (starting from 1000 nM).

Binding was detected using a goat anti-human Fc–alkaline phosphatase (AP) conjugate (Sigma-Aldrich), followed by incubation with p-nitrophenyl phosphate (pNPP) substrate prepared in alkaline phosphatase buffer (100 mM Tris-HCl, 100 mM NaCl, 5 mM $MgCl_2$, pH 9.5). Absorbance was measured at 405 nm using a SpectraMax M2e plate reader (Molecular Devices). Rituximab, an unrelated human monoclonal antibody, was included as a negative control. All experiments were performed in triplicate and repeated

at least twice. Data were analyzed by nonlinear regression using GraphPad Prism, with results expressed as mean ± SD.

*Plaque Reduction Neutralization Test (PRNT) Against ZIKV and DENV-2*

The neutralizing activity of recombinant antibodies was evaluated by plaque reduction neutralization test (PRNT) using Zika virus (ZIKV) and Dengue virus serotype 2 (DENV-2) in Vero cells (ATCC® CCL-81™). Cells were cultured in MEM supplemented with 10% fetal bovine serum (FBS) and 1% Antibiotic Antimycotic Solution (Sigma Aldrich), and seeded in 24-well plates to reach full confluence after 24h.

Serial 3-fold dilutions of antibodies starting at 7 uM were mixed 1:1 (v/v) with viral suspensions containing approximately 50–100 PFU per well and incubated for 1 h at 37 °C to allow antibody–virus interaction. The mixtures were then applied to Vero cell monolayers and incubated for 1 h at 37 °C to permit viral adsorption. Subsequently, cells were overlaid with MEM containing 1.5% carboxymethylcellulose and incubated until plaque formation (4 days for ZIKV and 7 days for DENV-2).

After fixation with 4% formaldehyde, monolayers were stained with 1% crystal violet, and plaques were counted manually. The percentage of plaque reduction (PRNT%) was calculated relative to virus-only controls as follows: Inhibition percentage = 100 × [1- (plaque number incubated with mAb/plaque number without mAb)]. The neutralization titer ($PRNT_{50}$) was determined by nonlinear regression analysis using GraphPad Prism. All experiments were performed in triplicate and repeated at least twice. Rituximab and an anti-SARS-CoV-2 scFv were included as negative controls to confirm assay specificity.

## References

AKAISHI, T.; NAKASHIMA, I. Efficiency of antibody therapy in demyelinating diseases. International Immunology, v. 29, n. 7, p. 327–335, 2017.

ANDRIS-WIDHOPF, J.; STEINBERGER, P.; FÜLLER, R.; RADER, C.; BARBAS III, C. F. Generation of antibodies libraries: PCR amplification and assembly of light- and heavy-chain coding region. In: BARBAS III, C. F. et al. *Phage Display: a Laboratory Manual*. 1. ed. Cold Spring Harbor, NY: CSHL Press, 2000. p. 9.1–9.113.

BARBAS, C. F. Phage Display: A Laboratory Manual. Cold Spring Harbor: Cold Spring Harbor Laboratory Press, 2001.

BARBA-SPAETH, G. et al. Structural basis of potent Zika–dengue virus antibody cross-neutralization. Nature, v. 536, n. 7614, p. 48–53, 2016.

BERTOGLIO, Federico et al. A SARS-CoV-2 neutralizing antibody selected from COVID-19 patients binds to the ACE2-RBD interface and is tolerant to most known RBD mutations. Cell Reports, v. 36, n. 4, 2021.

BUJAK, Emil et al. Chapter 20: Reformatting of scFv antibodies into the scFv-Fc format and their downstream purification. In: Methods in Molecular Biology, v. 1131, p. 315–334, 2014.

CASADEVALL, A.; PIROFSKI, L.; JOYNER, M. J. The principles of antibody therapy for infectious diseases with relevance for COVID-19. mBio, v. 12, n. 2, e03372-20, 2021.

CHAUDHURY, S.; GROMOWSKI, G. D.; RIPOLL, D. R.; KHAVRUTSKII, I. V.; DESAI, V.; WALLQVIST, A. Dengue virus antibody database: systematically linking serotype-specificity with epitope mapping in dengue virus. PLoS Neglected Tropical Diseases, v. 11, n. 2, e0005395, 2017. DOI: 10.1371/journal.pntd.0005395.

CHERRIER, M. V. et al. Structural basis for the preferential recognition of immature orthoflaviviruses by a fusion-loop antibody. The EMBO Journal, v. 28, n. 20, p. 3269–3276, 2009. DOI: 10.1038/emboj.2009.245.

COOK, Graham P.; TOMLINSON, Ian M. The human immunoglobulin VH repertoire. Immunology Today, v. 16, n. 5, p. 237–242, 1995.

COSTIN, J. M. et al. Mechanistic study of broadly neutralizing human monoclonal antibodies against dengue virus that target the fusion loop. Journal of Virology, v. 87, n. 1, p. 52–66, 2013. DOI: 10.1128/JVI.02273-12.

DANTAS-BARBOSA, C.; BRÍGIDO, M. M.; MARANHÃO, A. Q. Construction of a human Fab phage display library from antibody repertoires of osteosarcoma patients. Genetics and Molecular Research, v. 4, n. 2, p. 126–140, 2005.

DEJNIRATTISAI, W. et al. A new class of highly potent, broadly neutralizing antibodies isolated from viremic patients infected with dengue virus. Nature Immunology, v. 16, n. 2, p. 170–177, 2015.

DITZEL, H. J. Affinity isolation of antigen-specific circulating B cells for generation of phage display-derived human monoclonal antibodies. In: AITKEN, R. (ed.). Antibody Phage Display. Methods in Molecular Biology, v. 562. Totowa: Humana Press, 2009. p. 37–43.

DOWD, K. A.; DeMASO, C. R.; PIERSON, T. C. Genotypic differences in dengue virus neutralization are explained by a single amino acid mutation that modulates virus breathing. mBio, v. 6, n. 6, e01559-15, 2015.

DOWD, K. A.; JOST, C. A.; DURBIN, A. P.; WHITEHEAD, S. S.; PIERSON, T. C. A dynamic landscape for antibody binding modulates antibody-mediated neutralization of West Nile virus. PLoS Pathogens, v. 7, n. 6, e1002111, 2011. DOI: 10.1371/journal.ppat.1002111.

DUSSUPT, V.; MODJARRAD, K.; KREBS, S. J. Landscape of monoclonal antibodies targeting Zika and dengue: therapeutic solutions and critical insights for vaccine development. Frontiers in Immunology, v. 11, p. 621043, 2020.

FAN, Y.-C.; CHEN, J.-M.; CHEN, Y.-Y.; KE, Y.-D.; CHANG, G.-J. J.; CHIOU, S.-S. Epitope(s) involving amino acids of the fusion loop of Japanese encephalitis virus envelope protein is(are) important to elicit protective immunity. Journal of Virology, v. 98, n. 4, e0177323, 2024. DOI: 10.1128/jvi.01773-23.

FIBRIANSAH, G. et al. A highly potent human antibody neutralizes dengue virus serotype 3 by binding across three surface proteins. Nature Communications, v. 6, p. 6341, 2015.

FRANÇA, R. K. A. et al. Progress on phage display technology: tailoring antibodies for cancer immunotherapy. Viruses, v. 15, n. 9, p. 1903, 2023.

FRANÇA, R. K. A. O. et al. New anti-orthoflavivirus fusion loop human antibodies with Zika virus-neutralizing potential. International Journal of Molecular Sciences, v. 23, n. 14, p. 7805, 2022.

FUERTES MARRACO, S. A. et al. Long-lasting stem cell-like memory $CD8^+$ T cells with a naïve-like profile upon yellow fever vaccination. Science Translational Medicine, v. 7, n. 282, 2015.

GALLICHOTTE, E. N. et al. Role of Zika virus envelope protein domain III as a target of human neutralizing antibodies. mBio, v. 10, n. 5, e01485-19, 2019.

GUNALE, B. et al. An observer-blind, randomized, placebo-controlled, phase 1 study of dengue monoclonal antibody in healthy adults in Australia. The Lancet Infectious Diseases, v. 24, n. 6, p. 639–649, 2024.

HALSTEAD, S. Recent advances in understanding dengue. F1000Research, v. 8, p. 1279, 2019.

HEINZ, F. X.; STIASNY, K.; REY, F. A. Orthoflavivirus structural heterogeneity: implications for cell entry. Current Opinion in Virology, v. 24, p. 132–139, 2017.

KEEFFE, J. R. et al. A combination of two human monoclonal antibodies prevents Zika virus escape mutations in non-human primates. Cell Reports, v. 25, n. 6, p. 1385–1394.e7, 2018.

KÖHLER, G.; MILSTEIN, C. Continuous cultures of fused cells secreting antibody of predefined specificity. Nature, v. 256, p. 495–497, 1975.

KOHSAKA, Hitoshi et al. The human immunoglobulin VH gene repertoire is genetically controlled and unaltered by chronic autoimmune stimulation. Journal of Clinical Investigation, v. 98, n. 12, p. 2794–2800, 1996.

KOTAKI, T. et al. An affinity-matured human monoclonal antibody targeting fusion loop epitope of dengue virus with in vivo therapeutic potency. Scientific Reports, v. 11, p. 12987, 2021.

LEDSGAARD, L. et al. Basics of antibody phage display technology. Toxins, v. 10, n. 6, p. 236, 2018.

LINDENBACH, B. D.; RICE, C. M. Molecular biology of orthoflaviviruses. In: Advances in Virus Research, v. 59. Amsterdam: Elsevier, 2003. p. 23–61.

LOW, J. G. et al. Phase 1 trial of a therapeutic anti-yellow fever virus human antibody. New England Journal of Medicine, v. 383, n. 5, p. 452–459, 2020.

MAGNANI, D. M. et al. Neutralizing human monoclonal antibodies prevent Zika virus infection in macaques. Science Translational Medicine, v. 9, n. 410, eaan8184, 2017.

MATHEW, A. et al. B-cell responses during primary and secondary dengue virus infections in humans. Journal of Infectious Diseases, v. 204, n. 10, p. 1514–1522, 2011. DOI: 10.1093/infdis/jir607.

MIMMI, S.; MAISANO, D.; QUINTO, I.; IACCINO, E. Phage display: an overview in context to drug discovery. Trends in Pharmacological Sciences, v. 40, n. 2, p. 87–91, 2019.

MORBACH, H.; EICHHORN, E. M.; LIESE, J. G.; GIRSCHICK, H. J. Reference values for B cell subpopulations from infancy to adulthood. *Clinical and Experimental Immunology*, v. 162, n. 2, p. 271–279, 2010.

MORRISON, S. L. et al. Chimeric human antibody molecules: mouse antigen-binding domains with human constant region domains. Proceedings of the National Academy of Sciences USA, v. 81, n. 21, p. 6851–6855, 1984.

NIU, X. et al. Convalescent patient-derived monoclonal antibodies targeting different epitopes of E protein confer protection against Zika virus in a neonatal mouse model. Emerging Microbes & Infections, v. 8, n. 1, p. 749–759, 2019.

OLIPHANT, T. et al. Antibody recognition and neutralization determinants on domains I and II of West Nile virus envelope protein. Journal of Virology, v. 80, n. 24, p. 12149–12159, 2006.

RADER, C.; STEINBERGER, P.; BARBAS III, C. F. Selection from antibody libraries. In: BARBAS III, C. F. et al. *Phage Display: a Laboratory Manual*. 1. ed. Cold Spring Harbor, NY: Cold Spring Harbor Laboratory Press, 2000. p. 10.2–10.20.

RAMADHANY, R. et al. Antibody with an engineered Fc region as a therapeutic agent against dengue virus infection. Antiviral Research, v. 124, p. 61–68, 2015.

REMMEL, J. L. et al. Diverse contributions of avidity to the broad neutralization of dengue virus by antibodies targeting the E dimer epitope. Virology, v. 559, p. 57–64, 2021.

RIVERA, L. et al. Three-year efficacy and safety of Takeda's dengue vaccine candidate (TAK-003). Clinical Infectious Diseases, v. 75, n. 1, p. 107–117, 2022.

ROBBIANI, D. F. et al. Recurrent potent human neutralizing antibodies to Zika virus in Brazil and Mexico. Cell, v. 169, n. 4, p. 597–609.e11, 2017.

ROUVINSKI, A. et al. Recognition determinants of broadly neutralizing human antibodies against dengue viruses. Nature, v. 520, n. 7545, p. 109–113, 2015.

SANKHALA, R. S. et al. Zika-specific neutralizing antibodies targeting inter-dimer envelope epitopes. Cell Reports, v. 42, n. 8, p. 112942, 2023.

SCHLOTHAUER, T. et al. Novel human IgG1 and IgG4 Fc-engineered antibodies with completely abolished immune effector functions. mAbs, v. 8, n. 8, p. 480–497, 2016.

SCHLOTHAUER, Tilman et al. Novel human IgG1 and IgG4 Fc-engineered antibodies with completely abolished immune effector functions. mAbs, v. 29, n. 10, p. 457–466, 2016.

SHARMA, A. et al. The epitope arrangement on orthoflavivirus particles contributes to Mab C10's extraordinary neutralization breadth across Zika and dengue viruses. Cell, v. 184, n. 25, p. 6052–6066.e18, 2021.

SILVA, J. V. J. et al. Current status, challenges and perspectives in the development of vaccines against yellow fever, dengue, Zika and chikungunya viruses. Acta Tropica, v. 182, p. 257–263, 2018.

SILVA, Jacyelle Medeiros et al. Rescuing pathogen-specific memory B cells from PBMC of prior Zika virus-infected individuals. Immunology Letters, v. 271, p. 106944, 2025.

SIOUD, M. Phage display libraries: from binders to targeted drug delivery and human therapeutics. Molecular Biotechnology, v. 61, n. 4, p. 286–303, 2019.

SMITH, G. P. Filamentous fusion phage: novel expression vectors that display cloned antigens on the virion surface. Science, v. 228, n. 4705, p. 1315–1317, 1985.

SMITH, S. A. et al. The potent and broadly neutralizing human dengue virus-specific monoclonal antibody 1C19 reveals a unique cross-reactive epitope on the bc loop of domain II of the envelope protein. mBio, v. 4, n. 6, e00873-13, 2013. doi: 10.1128/mBio.00873-13.

SULTANA, H. et al. Fusion loop peptide of the West Nile virus envelope protein is essential for pathogenesis and is recognized by a therapeutic cross-reactive human monoclonal antibody. Journal of Immunology, v. 183, n. 1, p. 650–660, 2009. DOI: 10.4049/jimmunol.0900093.

TS, P. et al. Renaming of the genus Orthoflavivirus to Orthoorthoflavivirus. Archives of Virology, v. 168, n. 9, 2023.

VOGT, M. R. et al. Poorly neutralizing cross-reactive antibodies against the fusion loop of West Nile virus envelope protein protect in vivo via Fc gamma receptor and complement-dependent effector mechanisms. Journal of Virology, v. 85, n. 22, p. 11567–11580, 2011. DOI: 10.1128/JVI.05859-11.

VOLKOVA, T. D. et al. A monoclonal antibody that recognizes the predicted tick-borne encephalitis virus E protein fusion sequence blocks fusion. Archives of Virology, v. 144, n. 5, p. 1035–1039, 1999.

WAICKMAN, Adam T. et al. Transcriptional and clonal characterization of B cell plasmablast diversity following primary and secondary natural DENV infection. EBioMedicine, v. 54, p. 102733, 2020. Disponível em: https://doi.org/10.1016/j.ebiom.2020.102733

WURM, Florian M. Production of recombinant protein therapeutics in cultivated mammalian cells. Nature Biotechnology, v. 22, n. 11, p. 1393–1398, 2004.

ZHANG, X. et al. Structures and functions of the envelope glycoprotein in orthoflavivirus infections. Viruses, v. 9, n. 11, p. 338, 2017.

ZHAO, H. et al. Mechanism of differential Zika and dengue virus neutralization by a public antibody lineage. Journal of Experimental Medicine, v. 217, n. 2, e20191792, 2020.PIERSON, T. C. et al. The stoichiometry of antibody-mediated neutralization and enhancement of West Nile virus infection. Cell Host & Microbe, v. 8, n. 2, p. 139–146, 2006.

ZHAO, H. et al. Structural basis of Zika virus-specific antibody protection. Cell, v. 166, n. 4, p. 1016–1027, 2016.

ZOMPI, S.; MONTOYA, M.; POHL, M. O.; BALMASEDA, A.; HARRIS, E. Dominant cross-reactive B cell response during secondary acute dengue virus infection in humans. PLoS Neglected Tropical Diseases, v. 6, n. 3, e1568, 2012. DOI: 10.1371/journal.pntd.0001568.

## Supplementary Material

## Figures

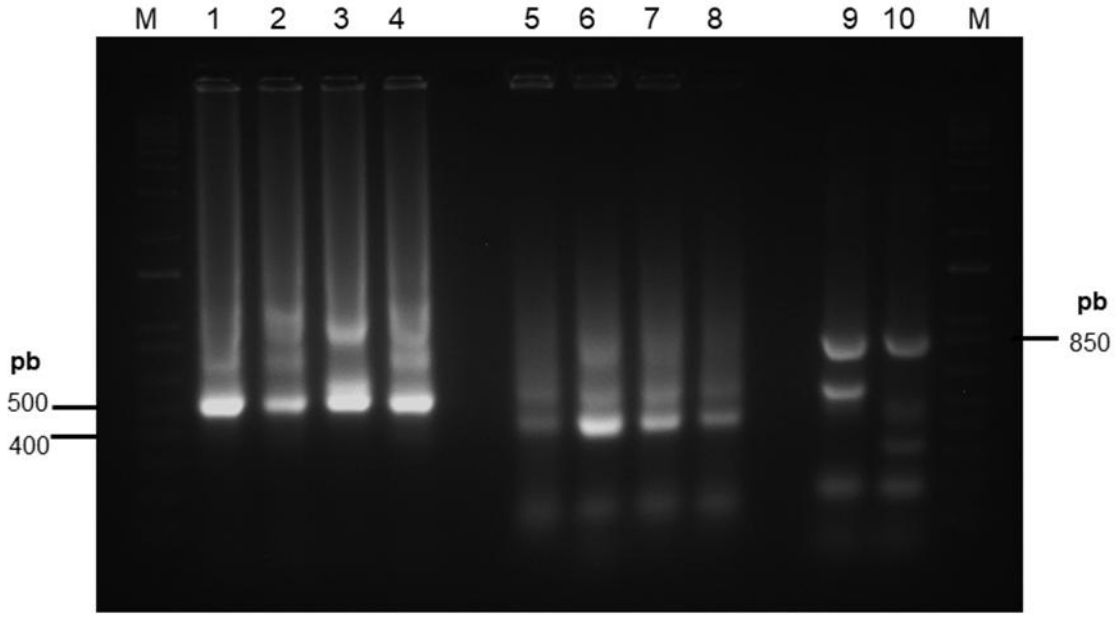


Supplementary Figure S1. Amplification of VH and VL domains of scFvs for sequencing analysis. Plasmid DNA (pComb3XSS-scFv) from the library before selection and after the final round of biopanning was used as a template for amplification of antibody VH and VL domains, aimed at sequencing and identification of the most enriched variable regions. Wells 1–4: VH; wells 5–8: VL; wells 9–10: scFv. M corresponds to the 1 kb Plus DNA ladder marker.

## Tables

**Supplementary Table S2. Heavy-chain variable (VH) domains most enriched during selection with adsorbed antigen.** List of the 15 VH sequences most enriched throughout the selection process using adsorbed antigen. The Fold-Change value represents the number of times a given sequence increased in frequency from selection round 0 to round 3. The immunoglobulin gene family to which each VH sequence belongs, as well as the corresponding CDR3 amino acid sequence, are shown.

| Sequence | Fold-Change | Family | CDR3 |
|---|---|---|---|
| VHA1 | 60.28 | VH2-5 | ILGYSYSTAWYDW |
| VHA2 | 59.48 | VH2-5 | RVYYDDVFDI |
| VHA3 | 57.10 | VH2-5 | RDTIRYTFAF |
| VHA4 | 53.14 | VH2-5 | SEQRLLWGFDF |
| VHA5 | 53.14 | VH2-5 | RRADAFDI |
| VHA6 | 51.55 | VH2-5 | RYSSSSGEVY |
| VHA7 | 47.59 | VH4-34 | MEGFGELQNWYFDL |
| VHA8 | 46.00 | VH3-7 | SSGFYLGEY |
| VHA9 | 46.00 | VH4-34 | QVYFGDGMDV |
| VHA10 | 46.00 | VH2-5 | SAVVRRYAFHV |
| VHA11 | 45.21 | VH1-46 | RCGRDCYG |
| VHA12 | 45.21 | VH4-34 | VRFLYFES |
| VHA13 | 44.41 | VH3-30 | VDEY |
| VHA14 | 44.41 | VH4-31 | GDYYGRADF |
| VHA15 | 43.62 | VH2-5 | TNSNGDGMDL |

**Supplementary Table S3. Heavy-chain variable (VH) domains most enriched during competitive selection.** List of the 15 VH sequences most enriched throughout the competitive selection process. The Fold-Change value represents the number of times a given sequence increased in frequency from selection round 0 to round 3. The immunoglobulin gene family to which each VH sequence belongs, as well as the corresponding CDR3 amino acid sequence, are shown.

| Sequence | Fold-Change | Family | CDR3 |
|---|---|---|---|
| VHC1 | 93.04 | VH3-30 | VDEY |
| VHC2 | 90.31 | VH2-5 | RRADAFDI |
| VHC3 | 87.57 | VH2-5 | ILGYSYSTAWYDW |
| VHC4 | 82.10 | VH2-5 | RYSSSSGEVY |
| VHC5 | 76.62 | VH2-70 | MRTDASGLFDS |
| VHC6 | 69.33 | VH2-5 | RDTIRYTFAF |
| VHC7 | 67.50 | VH4-34 | VRFLYFES |
| VHC8 | 67.50 | VH1-2 | EQPDDGMDV |
| VHC9 | 66.59 | VH4-28 | RKAREAFDI |
| VHC10 | 65.68 | VH2-5 | TNSNGDGMDL |
| VHC11 | 61.12 | VH2-5 | DIRVYDGSGYYLFDY |
| VHC12 | 61.12 | VH4-34 | CSGWLGDAYDVW |
| VHC13 | 61.12 | VH1-2 | GRETVTPYVDY |
| VHC14 | 60.20 | VH2-5 | NRVVVATAFDP |
| VHC15 | 59.29 | VH2-5 | VNQHYYGMDV |

**Supplementary Table S4. Light-chain variable (VL) domains most enriched during selection with adsorbed antigen.** List of the 15 VL sequences most enriched throughout the selection process using adsorbed antigen. The Fold-Change value represents the number of times a given sequence increased in frequency from selection round 0 to round 3. The immunoglobulin gene family to which each VL sequence belongs, as well as the corresponding CDR3 amino acid sequence, are shown.

| Sequence | Fold-Change | Family | CDR3 |
|---|---|---|---|
| VLA1 | 1275.77 | V2-15 | LQHDNFPYT |
| VLA2 | 507.30 | V2-17 | QQYNHYPVT |
| VLA3 | 471.48 | V2-17 | QQSYDAPVT |
| VLA4 | 397.52 | V2-17 | QQLNT |
| VLA5 | 361.70 | V2-17 | QQYNHYPVT |
| VLA6 | 313.16 | V1-2 | QQYNHYPVT |
| VLA7 | 300.45 | V2-17 | QQYNHYPVT |
| VLA8 | 294.68 | V2-17 | QQYNHYPVT |
| VLA9 | 283.12 | V1-13 | QQSYSSPPVT |
| VLA10 | 273.87 | V2-17 | QQSYSSPPVT |
| VLA11 | 265.79 | V2-17 | QQLNT |
| VLA12 | 255.39 | V2-15 | LQHDNFPYT |
| VLA13 | 253.07 | V1-13 | QHYDNLPLG |
| VLA14 | 248.45 | V2-17 | QQYNHYPVT |
| VLA15 | 247.68 | V1-4 | QQSYSSPFT |

**Supplementary Table S5. Light-chain variable (VL) domains most enriched during competitive selection.** List of the 15 VL sequences most enriched throughout the competitive selection process. The Fold-Change value represents the number of times a given sequence increased in frequency from selection round 0 to round 3. The immunoglobulin gene family to which each VL sequence belongs, as well as the corresponding CDR3 amino acid sequence, are shown.

| Sequence | Fold-Change | Family | CDR3 |
|---|---|---|---|
| VLC1 | 2319.90 | V2-15 | LQHDDFART |
| VLC2 | 2063.35 | V2-11 | LQHDNFPLT |
| VLC3 | 1894.77 | V1-2 | MQTVQVPGT |
| VLC4 | 1700.53 | V1-19 | QQRGNWPLT |
| VLC5 | 1638.22 | V1-16 | LQHDDFART |
| VLC6 | 1194.77 | V2-11 | LQHDNFPLT |
| VLC7 | 1084.82 | V2-15 | LQHDDFART |
| VLC8 | 1070.16 | V2-17 | QQYYNWPPIT |
| VLC9 | 1029.84 | V1-13 | QQRGNWPLT |
| VLC10 | 1018.85 | V1-16 | LQHDDFART |
| VLC11 | 1004.19 | V1-13 | QQYGSSLLT |
| VLC12 | 1000.53 | V2-11 | LQHDDFART |
| VLC13 | 912.57 | V2-17 | QCNDWPT |
| VLC14 | 906.46 | V1-16 | LQHDDFART |
| VLC15 | 905.24 | V1-2 | MQTVQVPGT |

## 5 Discussão

O presente trabalho descreveu a construção e aplicação de uma biblioteca de phage display derivada de células B de memória humanas, voltada à seleção de anticorpos monoclonais contra o fusion loop, uma região altamente conservada do envelope de ortoflavivírus (Pierson & Diamond, 2020). A partir dessa biblioteca, foram obtidos e caracterizados anticorpos recombinantes com capacidade de ligação e neutralização cruzada entre diferentes ortoflavivírus, validando a estratégia de seleção empregada.

Enquanto o artigo resultante deste projeto apresenta e discute detalhadamente os achados experimentais, esta seção amplia a análise sob uma perspectiva técnica e conceitual, abordando os desafios e decisões estratégicas que nortearam o desenvolvimento da plataforma. São discutidos aspectos da construção da primeira biblioteca de B de memória do laboratório, da expressão e purificação dos anticorpos em diferentes formatos, e das implicações dessas escolhas metodológicas sobre a eficiência e estabilidade dos produtos obtidos. Além disso, são consideradas a evolução da linha de pesquisa do grupo em anticorpos monoclonais anti-ortoflavivírus e as perspectivas de aprimoramento da tecnologia desenvolvida.

A biblioteca construída neste trabalho representa um avanço importante na plataforma de seleção de anticorpos do grupo. Historicamente, o laboratório utilizava uma biblioteca do tipo Fab, construída inicialmente a partir de células de pacientes com osteossarcoma (Dantas-Barbosa et al., 2005) e, posteriormente, empregada como biblioteca naïve em diversas seleções, incluindo para ortoflavivírus (França et al., 2022). A biblioteca atual difere da anterior em dois aspectos principais: é a primeira derivada de células B de memória humanas e a primeira construída no formato single-chain variable fragment (scFv).

O uso de células B de memória de indivíduos previamente expostos a ortoflavivírus permitiu gerar um repertório enriquecido em clones já submetidos à maturação de afinidade e seleção natural (Tiller et al., 2008). O tamanho obtido da biblioteca ($7{,}8 \times 10^6$ transformantes), reflete um repertório funcionalmente relevante, contendo imunoglobulinas de alta especificidade. O vetor pComb3XSS foi empregado para montagem das construções scFv (Barbas et al., 2001), com um long linker flexível entre as regiões VH e VL, favorecendo a orientação correta e o reconhecimento antigênico.

A adoção do formato scFv foi motivada por sua simplicidade de construção e compatibilidade com expressão bacteriana, reduzindo etapas de amplificação e

facilitando a seleção dos anticorpos. Além disso, o formato compacto pode favorecer o acesso a epítopos parcialmente ocultos, como o fusion loop (Saphire et al., 2001). Ainda assim, a transição de formato trouxe desafios, principalmente no desenho de primers para sequenciamento por NGS, etapa essencial para o monitoramento da diversidade e enriquecimento da biblioteca. Essa experiência contribuiu para aprimorar o pipeline de análise molecular no grupo.

Um desafio persistente nas bibliotecas de phage display é a perda da informação natural de pareamento VH–VL. Para contornar essa limitação, o grupo tem explorado novas abordagens, como o sequenciamento completo de plasmídeos via tecnologia de nanoporo (MinION, Oxford Nanopore), que permite a leitura de moléculas longas e identificação simultânea das regiões variáveis das cadeias pesada e leve (Wick et al., 2019). Essa estratégia pode fornecer uma visão mais completa da diversidade funcional das bibliotecas e das combinações naturais envolvidas no reconhecimento antigênico.

A expressão dos anticorpos recombinantes foi conduzida nos formatos IgG1 e FvFc, com vetores e abordagens distintas. Para as IgG1, utilizou-se o vetor pcDNA3.4, amplamente validado em sistemas de expressão em células de mamíferos. Embora o projeto inicial previsse produção bacteriana de scFv, a oportunidade de estágio no Ragon Institute (Harvard/MIT/MGH), sob orientação do Prof. Brandon DeKosky, levou à adoção da pipeline local baseado em células Expi293 e no vetor pcDNA3.4. Essa estratégia garantiu compatibilidade metodológica e resultou em anticorpos FH2 e FH4 expressos e purificados com bons rendimentos e estabilidade, possibilitando sua caracterização funcional e ensaios de neutralização.

Em paralelo, o formato FvFc foi testado no vetor pMIW, derivado do pMIRES desenvolvido no laboratório. O pMIW contém promotor CMV, cassete IRES–Neo para expressão bicistrônica, e o elemento WPRE para aumento da estabilidade e exportação do mRNA, além de mutações LALA no domínio Fc para reduzir atividade efetora (Lazar et al., 2006). Embora o vetor tenha apresentado bom desempenho em anticorpos FvFc anti-CD3 previamente produzidos no laboratório, a expressão do FvFc anti-ortoflavivírus resultou em baixo rendimento e degradação significativa em Expi293. Essa diferença pode refletir tanto a maior sensibilidade do formato FvFc ao dobramento correto quanto a menor compatibilidade do vetor otimizado para CHO-K1 (Kunert & Reinhart, 2006).

De modo geral, os resultados indicam que o gargalo experimental ocorreu nas etapas de transição de formato e expressão, e não na seleção dos clones. O formato IgG mostrou desempenho mais estável e reprodutível para o alvo conformacional do fusion

loop. Futuras otimizações podem incluir testar a expressão do FH4 FvFc em CHO-K1 com pressão seletiva, buscando melhorar o rendimento de expressão. O fato de FH2 e FH4 em formato IgG1 apresentarem alta afinidade e neutralização robusta indica que, apesar de críptico, o fusion loop é acessível a anticorpos de tamanho completo, possivelmente devido às flutuações estruturais do envelope viral descritas como viral breathing (Dowd et al., 2011).

O presente trabalho representa um avanço importante na consolidação da plataforma de phage display do grupo, construída ao longo de mais de uma década de experiência com anticorpos monoclonais humanos. A biblioteca derivada de células B de memória contribui para a expansão das abordagens metodológicas do laboratório e indica o estabelecimento de um pipeline apto a gerar, expressar e caracterizar anticorpos humanos funcionais de forma independente.

Essa consolidação amplia as possibilidades de aplicação da plataforma, incluindo o desenvolvimento de anticorpos contra vírus emergentes, como o Oropouche (Naveca et al., 2019), e o desenho de anticorpos bispecíficos que combinem alvos complementares, como o fusion loop e o domínio III do envelope, para ampliar a amplitude de neutralização. O uso de ferramentas de modelagem estrutural também surge como caminho promissor para refinar a engenharia e otimizar estabilidade, afinidade e segurança.

Em linhas gerais, este estudo oferece contribuições para o entendimento de anticorpos anti-ortoflavivírus e para iniciativas nacionais associadas ao desenvolvimento de biofármacos baseados em anticorpos, integrando aspectos conceituais e técnicos do laboratório.

## 6 Conclusão e perspectivas

Este trabalho apresentou a construção da primeira biblioteca de células B de memória humanas do laboratório e a seleção de anticorpos monoclonais contra o fusion loop do envelope de ortoflavivírus. Foram isolados dois anticorpos, FH2 e FH4, com alta afinidade e capacidade de neutralização cruzada para ZIKV e DENV, comprovando que essa região conservada pode ser explorada como alvo funcional.

A biblioteca derivada de B de memória favoreceu a obtenção de clones com maior maturação de afinidade e melhor desempenho funcional em relação aos obtidos de repertórios naïve. O formato IgG mostrou-se mais estável e eficiente que o FvFc, indicando que ajustes no vetor e no sistema de expressão podem aprimorar futuras produções.

Os achados indicam que os anticorpos gerados apresentam potencial neutralizante contra diferentes ortoflavivírus. Ensaios complementares, como testes de especificidade e neutralização com outros ortoflavivírus como YFV e WNV, experimentos *in vivo* e a análise de configurações moleculares distintas, poderão aprofundar a avaliação de sua atividade e ampliar sua aplicabilidade.

**REFERÊNCIAS**

AGUIAR, Renato S. et al. Molecular alterations in the extracellular matrix in the brains of newborns with congenital Zika syndrome. *Nature Communications*, v. 6736, n. June, p. 1–14, 2020.

AGUIAR, Renato S. et al. Molecular alterations in the extracellular matrix in the brains and molecular biology reviews. *Microbiology and Molecular Biology Reviews*, v. 81, n. 1, p. 1–27, 2017.

AKAISHI, Tetsuya; NAKASHIMA, Ichiro. Efficiency of antibody therapy in demyelinating diseases. *Neurology and Clinical Neuroscience*, v. 29, n. 7, p. 327–335, 2017.

ALFALEH, Mohamed A. et al. Phage display-derived monoclonal antibodies: from bench to bedside. *Frontiers in Immunology*, v. 11, Aug. 2020.

ALMAGRO, Juan C. et al. Phage display libraries for antibody therapeutic discovery and development. *Antibodies*, v. 8, n. 3, p. 44, 2019.

ARIPOV, V. S. et al. The use of heterologous antigens for biopanning enables the selection of broadly neutralizing nanobodies against SARS-CoV-2. *Antibodies*, v. 14, n. 1, p. 23, 2025. doi: 10.3390/antib14010023.

AVIRUTNAN, Panisadee et al. Antagonism of the complement component C4 by orthoflavivirus nonstructural protein NS1. *Journal of Experimental Medicine*, v. 207, n. 4, p. 793–806, 2010.

Barbas et al., 2001. Phage Display: A Laboratory Manual. Cold Spring Harbor Laboratory Press.

BARBAS, Carlos F. et al. *Phage Display: A Laboratory Manual*. Cold Spring Harbor Laboratory Press, 2001.

BARDINA, Susana et al. Enhancement of Zika virus pathogenesis by preexisting antiorthoflavivirus immunity. *Science*, v. 356, n. 6334, p. 175–180, 2017.

BARJAS-CASTRO, Maria L. et al. Probable transfusion-transmitted Zika virus in Brazil. *Transfusion*, v. 56, n. 7, p. 1684–1688, 2016.

BERTOGLIO, Federico et al. A SARS-CoV-2 neutralizing antibody selected from COVID-19 patients binds to the ACE2-RBD interface and is tolerant to most known RBD mutations. *Cell Reports*, v. 36, n. 4, 2021.

BHATT, Samir et al. The global distribution and burden of dengue. *Nature*, v. 496, n. 7446, p. 504–507, 2013. Disponível em: http://dx.doi.org/10.1038/nature12060.

BOONAK, K. et al. Cell type specificity and host genetic polymorphisms influence antibody-dependent enhancement of dengue virus infection. *Journal of Virology*, v. 85, p. 1671–1683, 2011.

BOWEN, James R. et al. Zika virus antagonizes type I interferon responses during infection of human dendritic cells. *PLoS Pathogens*, v. 13, n. 2, p. 1–30, 2017.

BRASIL, P. et al. Zika virus infection in pregnant women in Rio de Janeiro. *Current Medicine Research and Practice*, v. 6, n. 2, p. 95, 2016.

BRASIL. Agência Nacional de Vigilância Sanitária – ANVISA. Anvisa publica registro da vacina contra a dengue do Instituto Butantan. *Agência Brasil*, 08 dez. 2025. Disponível em: https://agenciabrasil.ebc.com.br/saude/noticia/2025-12/anvisa-publica-registro-da-vacina-contra-dengue-do-butantan. Acesso em: 19 jan. 2026.

BRASIL. Ministério da Saúde. *Boletim Epidemiológico* n. 22.

BRASIL. Ministério da Saúde. *Boletim Epidemiológico* n. 47.

BRASIL. Ministério da Saúde. Monitoramento das arboviroses: dengue, zika e chikungunya. Brasília: Ministério da Saúde, 2025. Disponível em: <https://www.gov.br/saude/pt-br/assuntos/saude-de-a-a-z/a/aedes-aegypti/monitoramento-das-arboviroses>. Acesso em: 19 jan. 2026.

BROWN, Julia A. et al. Dengue virus immunity increases Zika virus-induced damage during pregnancy. *Immunity*, v. 50, n. 3, p. 751–762.e5, 2019.

BUJAK, Emil et al. Chapter 20: Reformatting of scFv antibodies into the scFv-Fc format and their downstream purification. In: *Methods in Molecular Biology*, v. 1131, p. 315–334, 2014.

CALVET, Guilherme et al. Detection and sequencing of Zika virus from amniotic fluid of fetuses with microcephaly in Brazil: a case study. *The Lancet Infectious Diseases*, v. 16, n. 6, p. 653–660, 2016.

CASADEVALL, Arturo; PIROFSKI, Liise Anne; JOYNER, Michael J. The principles of antibody therapy for infectious diseases with relevance for COVID-19. *mBio*, v. 12, n. 2, p. 1–13, 2021.

CASADEVALL, Arturo; SCHARFF, Matthew D. Serum therapy revisited: animal models of infection and development of passive antibody therapy. *Antimicrobial Agents and Chemotherapy*, v. 38, n. 8, p. 1695–1702, 1994.

CENTER FOR DISEASE CONTROL AND PREVENTION. *Facts about microcephaly*.

CENTER FOR DISEASE CONTROL AND PREVENTION. *Zika virus: microcephaly and other birth defects*. 2019. Disponível em:

https://www.cdc.gov/zika/healtheffects/birth_defects.html. Acesso em: 29 maio 2023.

CENTERS FOR DISEASE CONTROL AND PREVENTION (CDC). *Zika Travel Information*. Atlanta, GA, 2022. Disponível em: https://wwwnc.cdc.gov/travel/page/zika-information.

CHEN, Hsuan-ying et al. Long-term neurological and healthcare burden of adults with Japanese encephalitis: a nationwide study 2000–2015. *PLoS Neglected Tropical Diseases*, p. 1–17, 2021. Disponível em: http://dx.doi.org/10.1371/journal.pntd.0009703.

CHIPPAUX, Jean-Philippe; CHIPPAUX, Alain. Yellow fever in Africa and the Americas: a historical and epidemiological perspective. *Journal of Venomous Animals and Toxins including Tropical Diseases*, v. 24, 2018.

CHONG, Hui Ying et al. Orthoflavivirus infection: a review of immunopathogenesis, immunological response, and immunodiagnosis. *Virus Research*, v. 274, p. 197770, 2019. Disponível em: https://doi.org/10.1016/j.virusres.2019.197770.

CHUNG, K. M.; THOMPSON, B. S.; FREMONT, D. H.; DIAMOND, M. S. Antibody recognition of cell surface-associated NS1 triggers Fc-gamma receptor-mediated phagocytosis and clearance of West Nile virus-infected cells. *Journal of Virology*, v. 81, n. 17, p. 9551–9555, 2007. DOI: 10.1128/JVI.00879-07.

COOK, Graham P.; TOMLINSON, Ian M. The human immunoglobulin VH repertoire. *Immunology Today*, v. 16, n. 5, p. 237–242, 1995.

CRÉANGE, A. Guillain-Barré syndrome: 100 years on. *Revue Neurologique*, v. 172, n. 12, p. 770–774, 2016.

DAHIYA, S.; SINGH, S.; BHATI, G. K.; SEHRAWAT, S. In vitro and in vivo neutralization of dengue virus by a single domain antibody. *ImmunoHorizons*, v. 9, n. 5, p. vlaf012, 2025. doi: 10.1093/immhor/vlaf012.

DANTAS-BARBOSA, C.; BRÍGIDO, M. M.; MARANHÃO, A. Q. Construction of a human Fab phage display library from antibody repertoires of osteosarcoma patients. *Genetics and Molecular Research*, v. 4, n. 2, p. 126–140, 2005.

DANTAS-BARBOSA, Carmela et al. Isolation of osteosarcoma-associated human antibodies from a combinatorial Fab phage display library. *Journal of Immunology Research*, v. 2009, 2009.

DANTAS-BARBOSA, Carmela; BRÍGIDO, Marcelo M.; MARANHÃO, Andréa Q. Construction of a human Fab phage display library from antibody repertoires of osteosarcoma patients. *mAbs*, v. 4, n. 2, p. 126–140, [ano não informado].

DE ABREU, Ariane de Jesus Lopes et al. A systematic review and a meta-analysis of the

yellow fever vaccine in the elderly population. *Vaccines*, v. 10, n. 5, 2022.

DE ARAÚJO, Thalia Velho Barreto et al. Association between Zika virus infection and microcephaly in Brazil, January to May 2016: preliminary report of a case-control study. *The Lancet Infectious Diseases*, v. 16, n. 12, p. 1356–1363, 2016.

DE BARROS MIRANDA-FILHO, Demócrito et al. Initial description of the presumed congenital Zika syndrome. *American Journal of Public Health*, v. 106, n. 4, p. 598–600, 2016.

DE OLIVEIRA FIGUEIREDO, Poliana et al. Re-emergence of yellow fever in Brazil during 2016–2019: challenges, lessons learned, and perspectives. *Viruses*, v. 12, n. 11, p. 1233, 2020.

DEY, Debajit et al. Structural and biochemical insights into orthoflavivirus proteins. *Virus Research*, v. 296, p. 198343, 2021. Disponível em: https://doi.org/10.1016/j.virusres.2021.198343

DICK, G. W. A.; KITCHEN, S. F.; HADDOW, A. J. Zika virus. *Transactions of the Royal Society of Tropical Medicine and Hygiene*, v. 46, n. 5, 1952.

DOWD, K. A.; DeMASO, C. R.; PIERSON, T. C. Broadly neutralizing activity of dengue virus antibodies against Zika virus. *mBio*, v. 6, e01559, 2015.

FELL, H. P.; TUCKER, P. W. Immunoglobulin genes. *Immunology Series*, v. 43, n. 116, p. 181–202, 1989.

FERDOUS, Saba et al. B-cell epitopes: discontinuity and conformational analysis. *Molecular Immunology*, v. 114, Nov. 2018, p. 643–650, 2019.

FERNANDEZ, Estefania et al. Human antibodies to the dengue virus E-dimer epitope have therapeutic activity against Zika virus infection. *Nature Immunology*, v. 18, n. 11, p. 1261–1269, 2017.

FERRARIS, Pauline; YSSEL, Hans; MISSÉ, Dorothée. Zika virus infection: an update. *Microbes and Infection*, 2019.

FRANÇA, Renato Kaylan Alves de Oliveira et al. New anti-orthoflavivirus fusion loop human antibodies with Zika virus-neutralizing potential. *International Journal of Molecular Sciences*, v. 23, n. 14, 2022.

FUERTES MARRACO, Silvia A. et al. Long-lasting stem cell-like memory $CD8^+$ T cells with a naïve-like profile upon yellow fever vaccination. *Science Translational Medicine*, v. 7, n. 282, 2015.

GAUCHER, Denis et al. Yellow fever vaccine induces integrated multilineage and polyfunctional immune responses. *Journal of Experimental Medicine*, v. 205, n. 13, p.

3119–3131, 2008.

GEORGE, Jeffy et al. Prior exposure to Zika virus significantly enhances peak dengue-2 viremia in Rhesus macaques. *PLoS Pathogens*, n. August, p. 1–10, 2017.

GIANCHECCHI, Elena et al. Yellow fever: origin, epidemiology, preventive strategies and future prospects. *Vaccines*, v. 10, n. 3, p. 372, 2022.

Giordano, R.; Cardó-Vila, M.; Lahdenranta, J.; et al. Biopanning and rapid analysis of selective interactive ligands. Nature Medicine, New York, v. 7, p. 1249–1253, 2001. DOI: 10.1038/nm1101-1249.

GOTUZZO, Eduardo; YACTAYO, Sergio; CÓRDOVA, Erika. Efficacy and duration of immunity after yellow fever vaccination: systematic review on the need for a booster every 10 years. *American Journal of Tropical Medicine and Hygiene*, v. 89, n. 3, p. 434–444, 2013.

GRANT, Alesha et al. Zika virus targets human STAT2 to inhibit type I interferon signaling. *Cell Host and Microbe*, v. 19, n. 6, p. 882–890, 2016.

GUARNER, Jeannette; HALE, Gillian L. Four human diseases with significant public health impact caused by mosquito-borne orthoflaviviruses: West Nile, Zika, dengue and yellow fever. *Seminars in Diagnostic Pathology*, v. 36, n. 3, p. 170–176, 2019. Disponível em: https://doi.org/10.1053/j.semdp.2019.04.009.

GUZMAN, Maria G.; HARRIS, Eva. Dengue. *The Lancet*, v. 385, n. 9966, p. 453–465, 2015.

HALSTEAD, S. B.; NIMMANNITYA, S.; COHEN, S. N. Observations related to pathogenesis of dengue hemorrhagic fever. IV. Relation of disease severity to antibody response and virus recovered. *Yale Journal of Biology and Medicine*, v. 42, n. 5, p. 311, 1970.

HALSTEAD, Scott. Recent advances in understanding dengue. *F1000Research*, v. 8, p. 1279, 2019.

HARDING, Fiona A. et al. The immunogenicity of humanized and fully human antibodies: residual immunogenicity resides in the CDR regions. *mAbs*, v. 2, n. 3, p. 256–265, 2010.

HART, John et al. West Nile virus neuroinvasive disease: neurological manifestations and prospective longitudinal outcomes. *BMC Infectious Diseases*, v. 14, n. 1, p. 1–10, 2014.

HEINZ, Franz X.; ALLISON, Steven L. The machinery for orthoflavivirus fusion with host cell membranes. *Current Opinion in Microbiology*, v. 4, n. 4, p. 450–455, 2001.

HEINZ, Franz X.; STIASNY, Karin. The antigenic structure of Zika virus and its relation to other orthoflaviviruses: implications for infection and immunoprophylaxis. *Microbiology and Molecular Biology Reviews*, v. 81, n. 1, p. 1–27, 2017.

HIGUERA, Adriana; RAMÍREZ, Juan David. Molecular epidemiology of dengue, yellow fever, Zika and Chikungunya arboviruses: an update. *Acta Tropica*, v. 190, p. 99–111, 2019. Disponível em: https://doi.org/10.1016/j.actatropica.2018.11.010.

HOOGENBOOM, Hennie R. et al. Antibody phage display technology and its applications. *Immunotechnology*, v. 4, p. 1–20, 1998.

HOTTA, Susumu. Experimental studies on dengue: I. Isolation, identification and modification of the virus. *The Journal of Infectious Diseases*, p. 1–9, 1952.

HU, H.; DENG, Q.; GUO, C.; WU, Q.; LI, Q. A high-affinity and potently neutralizing nanobody against Zika virus. *ACS Infectious Diseases*, v. 11, n. 7, p. 1975–1982, 2025. doi: 10.1021/acsinfecdis.5c00205.

HUANG, Zhiwei et al. Vaccine development for mosquito-borne viral diseases. *Frontiers in Immunology*, v. 14, May, p. 1–14, 2023.

HURTADO-MONZÓN, Arianna Mahely et al. The role of anti-orthoflavivirus humoral immune response in protection and pathogenesis. *Reviews in Medical Virology*, v. 30, n. 4, p. 1–12, 2020.

INOUE, Takeshi; SHINNAKASU, Ryo; KUROSAKI, Tomohiro. Generation of high-quality memory B cells. *Frontiers in Immunology*, v. 12, p. 1–10, 2022.

INOUE, Takeshi; TOMOHIRO, Kurosaki. Memory B cells. *Nature Reviews Immunology*, 2023.

JOHNSON, T. P. *et al.* Chronic dengue virus panencephalitis in a patient with progressive dementia with extrapyramidal features. *Annals of Neurology*, Hoboken, v. 86, n. 5, p. 695–703, nov. 2019. DOI: 10.1002/ana.25588.

KALLÁS, Esper G. et al. Live, attenuated, tetravalent Butantan–dengue vaccine in children and adults. New England Journal of Medicine, Boston, v. 390, n. 5, p. 397–408, 2024. DOI: 10.1056/NEJMoa2301790.

KIPPS, Thomas J.; GHIA, Emanuela M.; RASSENTI, Laura Z. Immunoglobulin genes. In: *Manual of Molecular and Clinical Laboratory Immunology*. p. 51–64, 2016.

KNYAZHANSKAYA, Ekaterina; MORAIS, Marc C.; CHOI, Kyung H. Orthoflavivirus enzymes and their inhibitors. *The Enzymes*, v. 49, p. 265–303, 2021.

KOHSAKA, Hitoshi et al. The human immunoglobulin VH gene repertoire is genetically controlled and unaltered by chronic autoimmune stimulation. *Journal of Clinical*

*Investigation*, v. 98, n. 12, p. 2794–2800, 1996.

KOTAKI, T. et al. A virus-like particle–based therapeutic dengue vaccine candidate inducing strong neutralizing antibody responses. *Scientific Reports*, v. 11, p. 12987, 2021. doi: 10.1038/s41598-021-92354-x.

KRAMER, Laura D.; STYER, Linda M.; EBEL, Gregory D. A global perspective on the epidemiology of West Nile virus. *Annual Review of Entomology*, v. 53, p. 61–81, 2008.

KROEMER, Guido et al. Evolutionary relationship between human and mouse immunoglobulin kappa light chain variable region genes. *Immunogenetics*, v. 33, p. 42–49, 1991.

KUNERT, R.; REINHART, D. Advances in recombinant antibody manufacturing. *Applied Microbiology and Biotechnology*, v. 100, n. 8, p. 3451–3461, 2016. doi: 10.1007/s00253-016-7388-9.

KURTH, J. H.; MOUNTAIN, J. L.; CAVALLI-SFORZA, L. L. Subclustering of human immunoglobulin kappa light chain variable region genes. *Genomics*, v. 1, p. 69–77, 1993.

KYLE, Jennifer L.; HARRIS, Eva. Global spread and persistence of dengue. *Annual Review of Microbiology*, v. 62, p. 71–92, 2008.

LAZAR, G. A. et al. Engineered antibody Fc variants with enhanced effector function. *Proceedings of the National Academy of Sciences of the USA*, v. 103, n. 11, p. 4005–4010, 2006. doi: 10.1073/pnas.0508123103.

LEACH, Sarah et al. Requirement for memory B-cell activation in protection from heterologous influenza virus reinfection. *Journal of Virology*, v. 31, n. 12, p. 771–779, 2019.

LEDSGAARD, Line et al. Basics of antibody phage display technology. *Toxins*, v. 10, n. 6, 2018.

LEOWATTANA, Wattana; LEOWATTANA, Tawithep. Dengue hemorrhagic fever and the liver. *Journal of Medical Case Reports*, v. 13, n. 12, p. 1968–1976, 2021.

LETA, Samson et al. Global risk mapping for major diseases transmitted by *Aedes aegypti* and *Aedes albopictus*. *International Journal of Infectious Diseases*, v. 67, p. 25–35, 2018. Disponível em: http://dx.doi.org/10.1016/j.ijid.2017.11.026.

LIM, Jean K. et al. Genetic deficiency of chemokine receptor CCR5 is a strong risk factor for symptomatic West Nile virus infection: a meta-analysis of 4 cohorts in the US epidemic. *Journal of Infectious Diseases*, v. 197, 2008.

LIN, Hsiao Han et al. Zika virus structural biology and progress in vaccine development. *Biotechnology Advances*, v. 36, n. 1, p. 47–53, 2018. Disponível em:

https://doi.org/10.1016/j.biotechadv.2017.09.004.

LINDENBACH, Brett D.; RICE, Charles M. Molecular biology of orthoflaviviruses. In: *Advances in Virus Research*. v. 59, 2003.

LIU, Justin K. H. The history of monoclonal antibody development: progress, remaining challenges and future innovations. *Annals of Medicine and Surgery*, v. 3, n. 4, p. 113–116, 2014. Disponível em: http://dx.doi.org/10.1016/j.amsu.2014.09.001.

LIU, Wen Jun et al. A single amino acid substitution in the West Nile virus nonstructural protein NS2A disables its ability to inhibit alpha/beta interferon induction and attenuates virus virulence in mice. *Journal of Virology*, v. 80, n. 5, p. 2396–2404, 2006.

LOKE, Hsin et al. Susceptibility to dengue hemorrhagic fever in Vietnam: evidence of an association with variation in the vitamin D receptor and Fc gamma receptor IIa genes. *American Journal of Tropical Medicine and Hygiene*, v. 67, n. 1, p. 102–106, 2002.

LU, Guoliang; GONG, Peng. A structural view of the RNA-dependent RNA polymerases from the Orthoflavivirus genus. *Virus Research*, v. 234, p. 34–43, 2017. Disponível em: http://dx.doi.org/10.1016/j.virusres.2017.01.020.

MARCHETTE, N. J. et al. Isolation of Zika virus from *Aedes aegypti* mosquitoes in Malaysia. *American Journal of Tropical Medicine and Hygiene*, v. 18, n. 3, 1969.

MAUL, Robert W.; GEARHART, Patricia J. AID and somatic hypermutation. *Advances in Immunology*, v. 105, p. 159–191, 2010.

MESSINA, Jane P. et al. Global spread of dengue virus types: mapping the 70-year history. *Trends in Microbiology*, v. 22, n. 3, p. 138–146, 2014. Disponível em: http://dx.doi.org/10.1016/j.tim.2013.12.011.

MIMMI, Selena et al. Phage display: an overview in context to drug discovery. *Trends in Pharmacological Sciences*, Disponível em: https://doi.org/10.1016/j.tips.2018.12.005.

MONATH, Thomas P.; BARRETT, Alan D. T. Pathogenesis and pathophysiology of yellow fever. *Advances in Virus Research*, v. 60, p. 343–395, 2003.

MONATH, Thomas P.; VASCONCELOS, Pedro F. C. Yellow fever. *Journal of Clinical Virology*, v. 64, p. 160–173, 2015. Disponível em: http://dx.doi.org/10.1016/j.jcv.2014.08.030.

MONNIER, Philippe P.; VIGOUROUX, Robin J.; TASSEW, Nardos G. In vivo applications of single chain Fv (variable domain) (scFv) fragments. *Antibodies*, v. 2, n. 2, p. 193–208, 2013.

MOUSSA, D. A. et al. Discovery of a pan anti-SARS-CoV-2 monoclonal antibody with highly efficient infected cell killing capacity for novel immunotherapeutic approaches.

*Emerging Microbes & Infections*, v. 14, n. 1, p. 2432345, 2025. doi: 10.1080/22221751.2024.2432345.

MURRAY, K. et al. Risk factors for encephalitis and death from West Nile virus infection. *Epidemiology & Infection*, v. 134, n. 6, p. 1325–1332, 2006.

MUSSO, D.; NILLES, E. J.; CAO-LORMEAU, V. M. Rapid spread of emerging Zika virus in the Pacific area. *Clinical Microbiology and Infection*, v. 20, n. 10, p. O595–O596, 2014. Disponível em: http://dx.doi.org/10.1111/1469-0691.12707.

MWALE, Pharaoh Fellow et al. Expression, purification and characterization of anti-Zika virus envelope protein: polyclonal and chicken-derived single chain variable fragment antibodies. *International Journal of Molecular Sciences*, v. 21, n. 2, p. 1–21, 2020.

NAVECA, F. G. et al. Phylogeography of Zika virus in the Americas. *PLoS Neglected Tropical Diseases*, v. 13, n. 3, e0007103, 2019. doi: 10.1371/journal.pntd.0007103.

NGONO, Annie Elong; SHRESTA, Sujan. Immune response to dengue and Zika. *Annual Review of Immunology*, v. 36, n. 1, 2018.

NILCHAN, N. et al. An engineered N-glycosylated dengue envelope protein domain III facilitates epitope-directed selection of potently neutralizing and minimally enhancing antibodies. *ACS Infectious Diseases*, v. 10, n. 8, p. 2690–2704, 2024. doi: 10.1021/acsinfecdis.4c00058.

Nobel Prize. The Nobel Prize in Chemistry 2018. Stockholm: Nobel Foundation, 2018. Disponível em: <https://www.nobelprize.org/prizes/chemistry/2018/summary/>

NYBAKKEN, Grant E. et al. Structural basis of West Nile virus neutralization by a therapeutic antibody. *Nature*, v. 437, n. 7059, p. 764–769, 2005.

OLIPHANT, T. et al. Antibody recognition and neutralization determinants on domains I and II of West Nile virus envelope protein. *Journal of Virology*, v. 80, p. 12149–12158, 2006. doi: 10.1128/JVI.00879-07.

OLIPHANT, Theodore et al. Antibody recognition and neutralization determinants on domains I and II of West Nile virus envelope protein. *Journal of Virology*, v. 80, n. 24, p. 12149–12159, 2006.

OLIVEIRA MELO, A. S. et al. Zika virus intrauterine infection causes fetal brain abnormality and microcephaly: tip of the iceberg? *Ultrasound in Obstetrics and Gynecology*, v. 47, n. 1, p. 6–7, 2016.

PÁEZ-HERNÁNDEZ, Z. Y. et al. Neutralization of the pandemic influenza A/H1N1 virus with Lama glama humanized nanobodies (VHH). *Antibodies*, v. 14, n. 2, p. 42, 2025. doi: 10.3390/antib14020042.

PANG, Xiaojing; ZHANG, Rudian; CHENG, Gong. Progress towards understanding the pathogenesis of dengue hemorrhagic fever. *Virologica Sinica*, v. 32, n. 1, p. 16–22, 2017.

PANTOJA, Petraleigh et al. Zika virus pathogenesis in rhesus macaques is unaffected by pre-existing immunity to dengue virus. *Nature Communications*, v. 8, 2017.

PARDY, Ryan D.; RICHER, Martin J. Protective to a T: the role of T cells during Zika virus infection. *Cells*, v. 8, n. 8, p. 820, 2019.

PASQUALINI, R.; RUOSLAHTI, E. Organ targeting in vivo using phage display peptide libraries. *Nature*, v. 380, p. 364–366, 1996. doi: 10.1038/380364a0.

PERERA-LECOIN, Manuel et al. Orthoflavivirus entry receptors: an update. *Viruses*, v. 6, n. 1, p. 69–88, 2013.

PETERSEN, Lyle R.; MARFIN, Anthony A. Shifting epidemiology of Flaviviridae. *Journal of Travel Medicine*, v. 12, p. S3–S11, 2008.

PIERSON, T. C. et al. The stoichiometry of antibody-mediated neutralization and enhancement of West Nile virus infection. *Cell Host & Microbe*, v. 8, n. 2, p. 139–146, 2006. doi: 10.1016/j.chom.2006.07.002.

PIERSON, T. C.; DIAMOND, M. S. The continued threat of emerging orthoflaviviruses. *Nature Microbiology*, v. 5, n. 6, p. 796–812, 2020. doi: 10.1038/s41564-020-0714-0.

PIERSON, Theodore C. et al. Structural insights into the mechanisms of antibody-mediated neutralization of orthoflavivirus infection: implications for vaccine development. *Current Opinion in Virology*, p. 229–238, 2008.

PIERSON, Theodore C.; DIAMOND, Michael S. The continued threat of emerging orthoflaviviruses. *Nature Microbiology*, v. 5, n. 6, p. 796–812, 2020. Disponível em: http://dx.doi.org/10.1038/s41564-020-0714-0.

PRIYAMVADA, Lalita et al. Human antibody responses after dengue virus infection are highly cross-reactive to Zika virus. *Proceedings of the National Academy of Sciences*, v. 113, n. 28, 2016.

PURTHA, Whitney E. et al. Memory B cells, but not long-lived plasma cells, possess antigen specificities for viral escape mutants. *Journal of Experimental Medicine*, v. 208, n. 13, p. 2599–2606, 2011.

QIAN, Xijing; QI, Zhongtian. Mosquito-borne orthoflaviviruses and current therapeutic advances. *Viruses*, v. 14, n. 6, 2022.

QUARESMA, Juarez A. S. et al. Immunity and immune response, pathology and pathologic changes: progress and challenges in the immunopathology of yellow fever. *Reviews in Medical Virology*, v. 23, n. 5, p. 305–318, 2013.

QUARESMA, Juarez A. S.; DUARTE, Maria I. S.; VASCONCELOS, Pedro F. C. Midzonal lesions in yellow fever: a specific pattern of liver injury caused by direct virus action and in situ inflammatory response. *Medical Hypotheses*, v. 67, n. 3, p. 618–621, 2006.

RIVERA, Luis et al. Three-year efficacy and safety of Takeda's dengue vaccine candidate (TAK-003). *Clinical Infectious Diseases*, v. 75, n. 1, p. 107–117, 2022.

ROBBIANI, Davide F. et al. Recurrent potent human neutralizing antibodies to Zika virus in Brazil and Mexico. *Cell*, v. 169, n. 4, p. 597–609.e11, 2017. Disponível em: http://dx.doi.org/10.1016/j.cell.2017.04.024.

ROBERTSON, Miranda. Immunoglobulin genes and the immune response. *Nature*, v. 269, n. 5630, p. 648–650, 1977.

ROBINSON, Luke N. et al. Structure-guided design of an anti-dengue antibody directed to a non-immunodominant epitope. *Cell*, v. 162, n. 3, p. 493–504, 2015.

SALAZAR, Georgina et al. Antibody therapies for the prevention and treatment of viral infections. *npj Vaccines*, v. 2, n. 1, p. 1–12, 2017. Disponível em: http://dx.doi.org/10.1038/s41541-017-0019-3.

SAPHIRE, E. O. et al. Crystal structure of a neutralizing human IgG against HIV-1: definition of a new epitope on gp120. *Science*, v. 293, n. 5536, p. 1155–1159, 2001. doi: 10.1126/science.1060956.

SCHLOTHAUER, Tilman et al. Novel human IgG1 and IgG4 Fc-engineered antibodies with completely abolished immune effector functions. *mAbs*, v. 29, n. 10, p. 457–466, 2016.

SCHROEDER, Harry W. Jr.; CAVACINI, Lisa. Structure and function of immunoglobulins. *Journal of Allergy and Clinical Immunology*, v. 125, n. 2, p. S41–S52, 2010.

SEIFERT, M.; KÜPPERS, R. Human memory B cells. *Leukemia*, v. 30, n. 12, p. 2283–2292, 2016.

SERMAN, Taryn M.; GACK, Michaela U. Evasion of innate and intrinsic antiviral pathways by the Zika virus. *Viruses*, v. 11, n. 10, 2019. Disponível em: http://www.ncbi.nlm.nih.gov/pubmed/31652496.

SILVA, Jacyelle Medeiros et al. Rescuing pathogen-specific memory B cells from PBMC of prior Zika virus-infected individuals. *Immunology Letters*, v. 271, p. 106944, 2025.

SILVA, José V. J. et al. Current status, challenges and perspectives in the development of vaccines against yellow fever, dengue, Zika and chikungunya viruses. *Acta Tropica*,

v. 182, p. 257–263, 2018. Disponível em: https://doi.org/10.1016/j.actatropica.2018.03.009.

SILVA, Rosemeire et al. CTHRSSVVC peptide as a possible early molecular imaging target for atherosclerosis. *International Journal of Molecular Sciences*, v. 17, p. 1383, 2016.

SIMPSON, D. I. H. Zika virus infection in man. *Transactions of the Royal Society of Tropical Medicine and Hygiene*, v. 58, n. 4, p. 335–338, 1964.

SIOUD, Mouldy. Phage display libraries: from binders to targeted drug delivery and human therapeutics. *Molecular Biotechnology*, v. 0, n. 0, p. 0, 2019. Disponível em: http://dx.doi.org/10.1007/s12033-019-00156-8.

SIROHI, Devika; KUHN, Richard J. Zika virus structure, maturation, and receptors. *Journal of Infectious Diseases*, v. 216, supl. 10, p. S935–S944, 2017.

SITNIKOVA, Tatyana; NEI, Masatoshi. Evolution of immunoglobulin kappa chain variable region genes in vertebrates. *Molecular Biology and Evolution*, v. 15, n. 1, p. 50–60, 1998.

SLON CAMPOS, Jose Luis; MONGKOLSAPAYA, Juthathip; SCREATON, Gavin R. The immune response against orthoflaviviruses. *Nature Immunology*, v. 19, n. 11, p. 1189–1198, 2018. Disponível em: http://dx.doi.org/10.1038/s41590-018-0210-3.

SMITH, George P. Filamentous fusion phage: novel expression vectors that display cloned antigens on the virion surface. *Science*, v. 228, n. 4705, p. 1315–1317, 1985.

SMITH, George P.; SCOTT, Jamie K. Libraries of peptides and proteins displayed on filamentous phage. *Methods in Enzymology*, v. 217, p. 228–257, 1993.

SMITH, S. A. et al. The potent and broadly neutralizing human dengue virus-specific monoclonal antibody 1C19 reveals a unique cross-reactive epitope on the bc loop of domain II of the envelope protein. *mBio*, v. 4, n. 6, e00873-13, 2013. doi: 10.1128/mBio.00873-13.

SOERENSEN, A. et al. Selection and characterization of a broadly neutralizing class of HCV anti-E2 VH1-69 antibodies. *PLoS Pathogens*, v. 21, n. 3, e1012428, 2025. doi: 10.1371/journal.ppat.1012428.

SOLOMON, A.; WEISS, D. T. Structural and functional properties of human λ-light-chain variable-region subgroups. *Clinical and Diagnostic Laboratory Immunology*, v. 2, n. 4, p. 387–394, 1995.

STAQUICINI, D. I. et al. Targeted phage display-based pulmonary vaccination in mice and non-human primates. *Med*, v. 2, n. 3, p. 321–342, 2021. doi:

10.1016/j.medj.2020.10.005.

STETTLER, Karin et al. Specificity, cross-reactivity, and function of antibodies elicited by Zika virus infection. *Science*, v. 353, n. 6301, p. 823–826, 2016.

SUN, Haiyan; CHEN, Qiang; LAI, Huafang. Development of antibody therapeutics against orthoflaviviruses. *International Journal of Molecular Sciences*, v. 19, n. 1, 2018.

SWANSTROM, J. A. et al. Dengue virus envelope dimer epitope monoclonal antibodies isolated from dengue patients are protective against Zika virus. *mBio*, v. 7, n. 4, p. 1–8, 2016.

TAYAL, Anshula; KUMAR, Sushil; RAKESH, Kabra. Management of dengue: an updated review. *Indian Journal of Pediatrics*, v. 90, p. 168–177, 2023.

TEILLAUD, Jean-Luc. From whole monoclonal antibodies to single domain antibodies: think small. In: *Methods in Molecular Biology*. v. 911, p. 3–13.

THE SER TRANSTUMAB; ERBB; ITOH, K. Molecular suppressive system structural and functional characterization of tumor monoclonal antibody by phage display. *Journal*, v. 133, n. 2, p. 239–245, 2003.

TILLER, T. et al. Efficient generation of monoclonal antibodies from single human B cells by single cell RT-PCR and expression cloning. *Journal of Immunological Methods*, v. 329, n. 1–2, p. 112–124, 2008. doi: 10.1016/j.jim.2007.09.017.

TRIVEDI, Sweety; CHAKRAVARTY, Ambar. Neurological complications of dengue fever. *Current Neurology and Neuroscience Reports*, p. 515–529, 2022. Disponível em: https://doi.org/10.1007/s11910-022-01213-7.

VAN DEN HURK, Andrew F.; RITCHIE, Scott A.; MACKENZIE, John S. Ecology and geographical expansion of Japanese encephalitis virus. *Annual Review of Entomology*, v. 54, p. 17–35, 2009.

VAN LEUR, Sophie Wilhelmina et al. Pathogenesis and virulence of orthoflavivirus infections. *Virulence*, v. 12, n. 1, p. 2814–2838, 2021. Disponível em: https://doi.org/10.1080/21505594.2021.1996059.

VOLKOVA, T. D. et al. A monoclonal antibody that recognizes the predicted tick-borne encephalitis virus E protein fusion sequence blocks fusion. *Archives of Virology*, v. 144, n. 5, p. 1035–1039, 1999.

WAHAAB, Abdul et al. Potential role of orthoflavivirus NS2B-NS3 proteases in viral pathogenesis and anti-orthoflavivirus drug discovery employing animal cells and models: a review. *Viruses*, v. 14, n. 1, p. 44, 2021.

WAICKMAN, Adam T. et al. Transcriptional and clonal characterization of B cell plasmablast diversity following primary and secondary natural DENV infection. *EBioMedicine*, v. 54, p. 102733, 2020. Disponível em: https://doi.org/10.1016/j.ebiom.2020.102733.

WESSEL, A. W. et al. Antibodies targeting epitopes on the cell-surface form of NS1 protect against Zika virus infection during pregnancy. *Nature Communications*, v. 11, p. 5278, 2020. DOI: 10.1038/s41467-020-19096-y.

WICK, R. R. et al. Deepbinner: demultiplexing barcoded Oxford Nanopore reads with deep convolutional neural networks. *Nature Biotechnology*, v. 37, p. 27–29, 2019. doi: 10.1038/nbt.4223.

WICK, R. R.; JUDD, L. M.; HOLT, K. E. Performance of neural network basecalling tools for Oxford Nanopore sequencing. *Genome Biology*, v. 20, p. 129, 2019. doi: 10.1186/s13059-019-1727-y.

WILSON, Patrick C.; ANDREWS, Sarah F. Tools to therapeutically harness the human antibody response. *Nature Reviews Immunology*, v. 12, n. 10, p. 709–719, 2012.

Winter, G.; Griffiths, A. D.; Hawkins, R. E.; Hoogenboom, H. R. Making antibodies by phage display technology. Annual Review of Immunology, Palo Alto, v. 12, p. 433–455, 1994. DOI: 10.1146/annurev.iy.12.040194.002245.

WONG, Rachel et al. Affinity-restricted memory B cells dominate recall responses to heterologous orthoflaviviruses. *Immunity*, v. 53, n. 5, p. 1078–1094.e7, 2020. Disponível em: https://doi.org/10.1016/j.immuni.2020.09.001.

WORLD HEALTH ORGANIZATION. Yellow fever – African Region (AFRO). *Disease Outbreak News*, 2023.

WU, Bingan; QI, Zhongtian; QIAN, Xijing. Recent advancements in mosquito-borne orthoflavivirus vaccine development. *Viruses*, v. 15, n. 4, 2023.

WURM, Florian M. Production of recombinant protein therapeutics in cultivated mammalian cells. *Nature Biotechnology*, v. 22, n. 11, p. 1393–1398, 2004.

XIA, Hongjie et al. An evolutionary NS1 mutation enhances Zika virus evasion of host interferon induction. *Nature Communications*, v. 9, n. 1, 2018. Disponível em: http://dx.doi.org/10.1038/s41467-017-02816-2.

XIE, Xuping et al. Targeting dengue virus NS4B protein for drug discovery. *Antiviral Research*, v. 118, p. 39–45, 2015.

YE, Qing et al. Genomic characterization and phylogenetic analysis of Zika virus circulating in the Americas. *Infection, Genetics and Evolution*, v. 43, p. 43–49, 2016. Disponível em: http://dx.doi.org/10.1016/j.meegid.2016.05.004.

YU, L. et al. Monoclonal antibodies against Zika virus NS1 protein confer protection via Fcγ receptor-dependent and -independent pathways. *mBio*, v. 12, n. 1, p. e03179-20, 2021. DOI: 10.1128/mBio.03179-20.

ZHANG, Xingcui et al. Structures and functions of the envelope glycoprotein in orthoflavivirus infections. *Viruses*, p. 1–14, 2017.

ZHANG, Yang. Evolution of phage display libraries for therapeutic antibody discovery. *mAbs*, v. 15, n. 1, 2023. Disponível em: https://doi.org/10.1080/19420862.2023.2213793.

ZHAO, Baoyu et al. Structure and function of the Zika virus full-length NS5 protein. *Nature Communications*, v. 8, n. 1, p. 14762, 2017.

## Anexo 1 – Artigo de revisão publicado em periódico científico



REVIEW

ADVANCED THERAPEUTICS
www.advtherap.com

# Therapeutic Antibodies for Mosquito-Borne Orthoflavivirus Infections: Discovery, Engineering Approaches, and Advances in mRNA-Based Delivery Systems

*Ana Clara Barbosa Antonelli, Lucas Silva Rodrigues, Maria Clara Moura Pinheiro, Sylvia Barbosa Pinhate, Marcelo de Macedo Brígido, and Andréa Queiroz Maranhão**

**Mosquito-borne orthoflaviviruses such as Zika virus (ZIKV), dengue (DENV), yellow fever (YFV), West Nile (WNV), and Japanese encephalitis virus (JEV) are major public health concerns worldwide due to their epidemic potential, immune evasion mechanisms, and the absence of specific antiviral treatments. While vaccines exist for JEV, DENV, and Yellow Fever, their use is limited by safety concerns in vulnerable populations. In this context, monoclonal antibodies (mAbs) gain attention as potent and specific therapeutic tools. A central focus of recent research is the orthoflavivirus envelope (E) protein, particularly the fusion loop (FL), which is a highly conserved region within domain II that plays a critical role in viral membrane fusion and entry. The FL is a structural conservation across orthoflavivirus species, making it a target for the development of neutralizing antibodies (NAbs). This review highlights the key mechanisms of mAb-mediated neutralization, with a focus on FL-targeting strategies, and discusses how rational antigen design and antibody engineering are overcoming challenges related to epitope accessibility and antibody-dependent enhancement. Strategies for antibody discovery, such as phage display and Fc engineering are explored. Finally, mRNA-based platforms for in vivo antibody expression, offering an approach to rapid antibody expression to combat orthoflavivirus infections are discussed.**

## 1. Introduction

The *Orthoflavivirus* genus is the largest within the *Flaviviridae* family. It comprises single-stranded, positive-sense RNA (ssRNA$^+$) viruses that are primarily transmitted by arthropod vectors such as mosquitoes and ticks.[1] In 2023, the International Committee on Taxonomy of Viruses (ICTV) officially renamed the genus Orthoflavivirus to Orthoorthoflavivirus.[2] Accordingly, this review uses the updated terminology and focuses specifically on mosquito-borne orthoflaviviruses, excluding tick-borne species such as tick-borne encephalitis virus (TBEV). Among mosquito-borne orthoflaviviruses, several represent major global public health threats, including dengue virus (DENV), yellow fever virus (YFV), Zika virus (ZIKV), West Nile virus (WNV), and Japanese encephalitis virus (JEV). These viruses are predominantly transmitted by mosquitoes of the *Aedes* genus (DENV, YFV, ZIKV) and the *Culex* genus (WNV, JEV). Notably, ZIKV can also be transmitted via sexual contact, vertical transmission, and blood transfusion.[3–7]

The *Orthoflavivirus* genome consists of an ≈11 kb positive-sense single-stranded RNA (ssRNA$^+$) molecule containing a single open reading frame (ORF) flanked by untranslated regions (UTRs),[1,8] This ORF encodes a polyprotein that is proteolytically cleaved into three structural proteins: capsid (C), precursor membrane (prM), and envelope (E); and seven non-structural proteins: NS1, NS2A, NS2B, NS3, NS4A,

A. C. B. Antonelli, L. S. Rodrigues, M. C. M. Pinheiro, S. B. Pinhate, M. de M. Brígido, A. Q. Maranhão
Department of Cell Biology
University of Brasilia
Brasilia 70910-900, Brazil
E-mail: andreaqm@unb.br

The ORCID identification number(s) for the author(s) of this article can be found under https://doi.org/10.1002/adtp.202500422



**DOI: 10.1002/adtp.202500422**

A. C. B. Antonelli, M. de M. Brígido, A. Q. Maranhão
Molecular Pathology Graduation Program
University of Brasilia
Brasilia 70910-900, Brazil

L. S. Rodrigues, S. B. Pinhate, M. de M. Brígido, A. Q. Maranhão
Molecular Biology Graduation Program
University of Brasilia
Brasilia 70910-900, Brazil

M. de M. Brígido, A. Q. Maranhão
Institute for Investigation in Immunology (iii) INCT
Brasilia 05403-900, Brazil

NS4B, and NS5, all of which are essential for viral replication and immune evasion.[1,8]

Orthoflavivirus infections are asymptomatic or cause mild symptoms in ≈50–80% of cases.[9] Symptomatic infections are generally self-limiting and are characterized by fever, headache, myalgia, and arthralgia.[10,11] However, disease severity varies depending on viral factors, such as strain, virulence, and immune evasion strategies, as well as host factors including comorbidities, age, immune status, and genetic predisposition.[12–14] Certain orthoflaviviruses, such as DENV and YFV, are viscerotropic, primarily targeting visceral organs such as the liver and kidneys, potentially causing visceral organ failure.[15,16]

Others, including ZIKV, WNV, and JEV, are neurotropic and can cross the blood–brain barrier, leading to neurological complications.[10,17–19] ZIKV infection has been associated with Guillain–Barré syndrome and congenital Zika syndrome (CZS), the latter encompassing neurological, auditory, and ocular abnormalities in infants.[20–22] Severe dengue can lead to thrombocytopenia, increased capillary permeability, hypovolemic shock, multi-organ failure, and hemorrhagic manifestations.[23,24] Although not classically neurotropic, DENV has been linked to encephalopathy, particularly in DENV-2 and DENV-3 infections.[25] Both dengue and yellow fever can result in immune-mediated kidney injury, hepatic dysfunction, and acute liver failure.[26,27] Severe yellow fever is further characterized by jaundice, coagulopathy, cardiovascular instability, and multi-organ failure, frequently involving the liver.[28,29]

Currently, there are licensed vaccines available for DENV, YFV, and JEV.[30–32] The live-attenuated YFV-17D vaccine is the most extensively studied, eliciting long-lasting immunity through the induction of neutralizing antibodies and memory T cell responses.[31,33] The TAK-003 DENV vaccine has also demonstrated efficacy and received regulatory approval.[32] However, both these vaccines rely on live-attenuated virus platforms and are contraindicated in populations at higher risk, such as immunocompromised individuals and pregnant women.[34] As for JEV, several vaccine platforms, ranging from inactivated and live-attenuated to recombinant chimeric formulations, have been licensed (e.g., IXIARO, SA14-14-2, IMOJEV), however, long-term protection across diverse viral strains has not been fully achieved.[30] It is worth noting that there is also a licensed vaccine for TBEV[35] which belongs to the Orthoflavivirus genus but is transmitted by ticks rather than mosquitoes.

Despite the availability of vaccines, no FDA-approved antiviral treatments exist for orthoflavivirus infections, underscoring the need for alternative therapeutic strategies such as neutralizing monoclonal antibodies (mAbs). The introduction of mAbs in the 1980s revolutionized the treatment of cancer and autoimmune diseases, firmly establishing these biopharmaceuticals in modern medicine.[36] Since the development of hybridoma technology,[37] advances in genetic engineering and other protocols, such as phage display and transgenic mice generation, have enabled the production of chimeric, humanized, and fully human antibodies with enhanced efficacy and reduced immunogenicity.[38] However, the use of mAbs for infectious disease treatment remained limited until the SARS-CoV-2 pandemic, which catalyzed the rapid development and emergency use authorization of several mAbs for mild to moderate COVID-19 cases.[39] Prior to this, only a few mAbs had been approved for infectious diseases, including palivizumab for respiratory syncytial virus (RSV), ibalizumab for HIV,[40] and Twinrab and Rabshield licensed in India for treatment of rabies virus exposure.[41]

These developments have renewed interest in mAbs as viable countermeasures against emerging viral pathogens, including orthoflaviviruses. Nevertheless, challenges remain: no mAbs targeting orthoflavivirus infections have received FDA approval to date. Advances in screening methodologies, including single B-cell isolation and phage display, have facilitated the discovery of high-affinity mAbs, while Fc engineering and novel antibody formats, such as bispecific antibodies, offer promise for enhancing therapeutic efficacy. In light of these developments, this review examines the key mechanisms of mAb-mediated neutralization and the role of rational antigen design in improving the selection of broadly neutralizing, cross-reactive epitopes. We also discuss evolving screening strategies for mAb discovery, ranging from classical phage display to emerging technologies such as droplet microfluidics-based mammalian display. Finally, we explore mRNA-based antibody platforms, representing a scalable and innovative strategy for in vivo delivery of therapeutic antibodies.

## 2. Basic Mechanisms of Action of Therapeutic Antibodies in Infection

### 2.1. Neutralization, Opsonization, and Fc-mediated Effector Functions

Therapeutic antibodies represent a promising strategy for the treatment of cancer, autoimmune, and infectious diseases due to their high specificity, prolonged half-life, and capacity to engage immune effector functions such as neutralization, opsonization, antibody-dependent cellular cytotoxicity (ADCC), antibody-dependent cellular phagocytosis (ADCP), and complement-dependent cytotoxicity (CDC).[42] Among these mechanisms, neutralization plays a central role in antiviral defense. Neutralizing antibodies recognize viral epitopes (or their cell receptors) that are critical for infection and pathogenesis, typically those involved in receptor binding, membrane fusion, viral entry, or egress.[43] Monoclonal antibodies (mAbs) have emerged as a promising approach to treat infections caused by viruses for which no effective vaccines currently exist.

In orthoflavivirus infections, the envelope (E) protein is the main target of neutralizing antibodies (nAb) due to its essential role in viral entry. Domain II mediates membrane fusion, while Domain III facilitates host receptor binding, making both regions attractive targets for antibody targeting.[44] One notable example is E16, a broadly neutralizing mAb that binds a conserved epitope in Domain III of the WNV E protein, demonstrating potent neutralization activity in preclinical models.[45]

Beyond neutralization, antibody effector functions also rely on interactions with immune cells, primarily mediated through the Fc region of the antibody. In opsonization, antibodies act as opsonins, tagging pathogens for recognition by phagocytes, which subsequently engulf and destroy them, thereby preventing the spread of infection. While the Fab region mediates antigen recognition and neutralization, the Fc region is essential for opsonization, as it engages Fc receptors on the surface of

 

phagocytes. Fc receptor (FcR) binding overcomes repulsive membrane forces, facilitating internalization and degradation of the opsonized target.[46,47]

Another critical Fc-mediated mechanism is ADCC, in which antibodies promote the elimination of infected or malignant cells by engaging Fc receptors on phagocytes, granulocytes, and natural killer (NK) cells. These effector cells express three main types of Fc$\gamma$ receptors, Fc$\gamma$RI (CD64), Fc$\gamma$RII (CD32), and Fc$\gamma$RIIIA (CD16), and contain cytotoxic granules capable of inducing cell death. Upon antigen binding, antibodies undergo conformational changes that enhance Fc–FcR affinity, triggering signaling cascades that culminate in the destruction of the target cell via perforin/granzyme, FAS-L, or reactive oxygen species (ROS)/reactive oxygen intermediates (ROI) pathways.[48] Notably, monoclonal antibodies 3G2 and 4B8 have demonstrated ADCC activity against the NS1 protein of ZIKV, providing additional antiviral effects beyond direct neutralization.[49]

In addition to ADCC, Fc–FcR interactions also drive ADCP, in which macrophages and dendritic cells internalize antibody-opsonized virions or infected cells through Fc$\gamma$R engagement, leading to lysosomal degradation and enhanced antigen presentation.[50,51] This mechanism contributes to viral clearance and the stimulation of adaptive immune responses. Supporting this, a previous study demonstrated that monoclonal antibodies targeting the nonstructural protein 1 (NS1) of WNV protect mice through Fc-receptor-dependent pathways.[52] Specifically, only antibodies recognizing cell surface–associated NS1 were able to trigger Fc$\gamma$RI- and/or Fc$\gamma$RIV-mediated phagocytosis and clearance of WNV-infected cells, highlighting ADCP as a key protective mechanism in vivo.[52] Furthermore, studies with anti-NS1 monoclonal antibodies against ZIKV revealed robust C3b deposition on NS1-coated particles, indicating activation of the classical complement pathway, along with efficient internalization of these opsonized targets by monocytes and neutrophils.[53] Collectively, these observations highlight that Fc-mediated effector mechanisms, including ADCC, ADCP, and complement engagement, cooperate to enhance antibody-mediated protection against orthoflavivirus infection.

Conversely, antibodies may facilitate viral entry and replication through a phenomenon known as antibody-dependent enhancement (ADE). This process was first described in the context of DENV infection.[54,55] ADE occurs when viral neutralization is incomplete-either due to subneutralizing antibody concentrations or to the inability of antibodies to fully block infection. In such cases, virus–antibody complexes bind to Fc or complement receptors on host cells and are internalized. Rather than preventing infection, this interaction enhances viral replication, increases viral load, and triggers pro-inflammatory signaling, thereby exacerbating pathogenesis and disease severity.[56]

Although ADE is well-documented in secondary DENV infections, its relevance to other orthoflavivirus infections remains controversial. In vitro studies have shown that ZIKV infection can be enhanced by cross-reactive DENV antibodies, suggesting that prior exposure to one orthoflavivirus may exacerbate infection with another.[57–60] However, these data contrast with other in vivo findings. For example, Pantoja et al. (2017) observed a reduction in ZIKV viremia duration and protection for up to 6 months in rhesus macaques with pre-existing DENV immunity.[61] Moreover, clinical studies have found no evidence of ADE-associated disease exacerbation in patients with prior DENV (1-4) infection who were subsequently infected with either ZIKV or DENV-2.[62,63]

### 2.2. Neutralizing and Broadly Neutralizing Antibodies (bNAbs)

A defining characteristic of antibodies is their ability to bind specifically to their cognate epitopes. When the targeted epitope is highly variable, a corresponding neutralizing antibody often exerts its effector function in a strain-specific manner. In contrast, some antibodies can recognize conserved epitopes shared across multiple viral strains or species, enabling them to neutralize a broader spectrum of pathogens—these are known as broadly neutralizing antibodies (bNAbs).[64] For instance, Doyle et al. (2022) identified two monoclonal antibodies, YFV-121 and YFV-136, from memory B cells from YFV vaccinated individuals. These mAbs specifically neutralized the YFV-17D vaccine strain in mouse and hamster models by targeting Domain II of the envelope (E) protein.[65] Notably, residue H67, on domain II, was shown to be critical for YFV-136-mediated neutralization, as substitutions such as H67Y in YFV-17D and H67N in YFV ES-504 enabled the virus to escape neutralization and remain infectious.[66]

bNAbs are of particular interest in antiviral therapeutics because they can neutralize a wide range of viral strains, often at low concentrations.[67] Their discovery has facilitated the identification of conserved epitopes, which are critical for the rational design of vaccines and antiviral therapies. However, bNAbs tend to occur naturally at low l titers and often exhibit structural complexity, which can hinder their development. These features include frequent insertions and deletions at the genetic level, extensive somatic hypermutation in both framework and complementarity-determining regions (CDRs), and variable post-translational modifications.[64]

In the case of orthoflaviviruses, the structural and functional diversity of neutralizing antibodies has been comprehensively described,[68,69] and antibody responses according to the targeted domains of the E protein (DI–DIII), the fusion loop (FL) within Domain II, and complex quaternary epitopes spanning E-dimer interfaces have been previously reviewed.[68] These studies established that antibodies against Domain III often mediate potent, type-specific neutralization by blocking receptor engagement. A well-characterized example is E16, a humanized bNAb against WNV that binds to Domain III of the E protein, thereby blocking viral entry by preventing receptor engagement.[45] Those targeting the fusion loop or quaternary E-dimer epitopes can display broad cross-reactivity but may vary in neutralization potency and susceptibility to ADE. bNAbs with broader reactivity include MZ20, which targets Domain II, and MZ54/56, which binds the highly conserved fusion loop. These antibodies have demonstrated cross-neutralization across all four serotypes of DENV as well as ZIKV, JEV, and WNV.[70]

Many cross-reactive antibodies recognize conformational epitopes exposed only in immature or mosaic virions, adding complexity to the understanding of protective versus enhancing responses,[68,69] Although such antibodies may display broad binding activity, their interaction does not always translate into effective neutralization,[68,69,71] In orthoflavivirus infections, par-

ticularly dengue, some cross-reactive antibodies recognize conserved but poorly accessible epitopes, such as the pre-membrane (prM) protein or the fusion loop on immature or partially mature virions. These antibodies can form non-neutralizing immune complexes that promote viral uptake into Fcγ receptor–bearing cells, a process known as ADE. For example, Dejnirattisai et al. isolated prM-specific monoclonal antibodies from human memory B cells that enhanced DENV infection in vitro, highlighting that the specificity and accessibility of the targeted epitope are key determinants of whether an antibody will neutralize or exacerbate infection.[72]

## 3. Orthoflaviviruses Immune Evasion Mechanisms

Orthoflaviviruses employ multiple strategies to evade host immune responses, facilitating viral replication and persistence. A central mechanism involves antagonism of the type I interferon (IFN) pathway, a critical component of innate antiviral defense. For instance, orthoflavivirus NS5 mediates the degradation of STAT2, thereby blocking the activation of IFN-stimulated genes.[73,74] Similarly, WNV NS4B inhibits JAK–STAT signaling by preventing JAK1 and TYK2 phosphorylation.[75] To avoid detection by pattern recognition receptors (PRRs), orthoflaviviruses sequester viral double-stranded RNA within intracellular membrane vesicles, effectively shielding it from sensors such as RIG-I and TLR3.[76] ZIKV further disrupts innate immunity by cleaving FAM134B, a reticulophagy receptor, thereby impairing degradation of viral replication complexes.[77] ZIKV also upregulates MHC class I molecules on infected cells, reducing their susceptibility to natural killer (NK) cell-mediated lysis.[78] The secreted non-structural protein NS1 contributes to immune evasion by binding mannose-binding lectin (MBL) and C4b, inhibiting activation of the lectin complement pathway and diminishing viral clearance.[79] In addition, orthoflaviviruses manipulate host stress responses by disrupting stress granules and activating endoplasmic reticulum (ER) stress pathways, which collectively enhance viral replication while dampening antiviral signaling.[80]

In addition to suppressing innate immune pathways, orthoflaviviruses have evolved diverse mechanisms to evade recognition by the adaptive immune system, particularly by antibodies. While monoclonal antibodies provide powerful antiviral defense, orthoflaviviruses can subvert their function through several evasion strategies. These include antigenic variability, dynamic conformational changes in viral surface proteins-referred to as "viral breathing",[81,82] and the exploitation of ADE. These mechanisms underscore the complexity of orthoflavivirus pathogenesis and pose substantial challenges for the development of effective antibody-based therapeutics.

### 3.1. Structural Flexibility and Viral Breathing

The E protein, the major surface glycoprotein of orthoflaviviruses and a key mediator of viral entry, undergoes extensive structural rearrangements throughout the viral life cycle. These conformational changes are influenced by variations in pH within intracellular compartments, interactions with the precursor membrane (prM) protein in immature virions, and the transition to the extracellular environment.[9,83] This intrinsic structural flexibility enables oligomeric rearrangements and domain repositioning that are essential for viral maturation, membrane fusion, and host cell entry. In addition to these large-scale shifts, the E protein exhibits subtle, transient conformational dynamics, collectively referred to as "viral breathing", which expose otherwise cryptic epitopes on the virion surface.[84] Growing evidence suggests that these dynamic oscillations not only regulate key stages of the orthoflavivirus life cycle but also contribute to immune evasion by modulating epitope accessibility and antibody binding.[81,82,85]

### 3.2. Antigenic Variation and Escape Mutations

Orthoflaviviruses have evolved multiple strategies to evade neutralizing antibodies, including antigenic variation driven by genetic mutations. While structural breathing transiently exposes cryptic epitopes enabling antibody access, escape mutations can result in permanent alterations to the antigenic landscape. A notable example is TBEV, which evades neutralization by monoclonal antibodies through specific amino acid substitutions in the E protein. In particular, the K311N and E230K mutations act synergistically to confer complete resistance to the monoclonal antibody T025.[86] These substitutions destabilize the quaternary structure of the virion, disrupting electrostatic interactions between neighboring E proteins and preventing effective antibody binding, without great interference with virus replication. This case exemplifies a broader mechanism by which orthoflaviviruses escape immune recognition without significantly compromising viral fitness.

Other orthoflaviviruses, such as DENV and ZIKV, also undergo antigenic drift in response to selective pressure from neutralizing antibodies. Key mutations have been identified in the lateral ridge and fusion loop epitopes of the E protein, both of which are major targets of the humoral response.[85,87] These mutations often reduce susceptibility to neutralization while preserving infectivity, enabling continued viral circulation in populations with pre-existing immunity. Such antigenic variation presents significant challenges for vaccine development, as immunity against one strain may not confer cross-protection against emerging variants.

### 3.3. Maturation State and Immune Evasion

Orthoflavivirus maturation is a tightly regulated process that governs the structural conformation and epitope accessibility of E proteins on the virion surface. During maturation, virions transition from non-infectious, prM-covered particles to fully mature infectious forms via furin-mediated cleavage of prM in the trans-Golgi network.[88] However, this process is often incomplete, resulting in the secretion of partially mature, "mosaic" virions that contain a mixture of mature and immature structural features.[89] These mosaic particles present a significant challenge for antibody recognition, as they can mask or occlude key neutralizing epitopes—particularly those targeted by fusion loop-directed antibodies.[90]

In addition to reducing antibody binding, incomplete maturation allows orthoflaviviruses to modulate immune recognition through population heterogeneity. Certain antibodies exhibit preferential binding to either mature or immature virions, and

 

the coexistence of structurally diverse viral particles may permit immune escape even in the presence of strong neutralizing antibody responses.[91] This maturation-dependent evasion mechanism complicates vaccine development, as effective immunogens must elicit protective responses against both fully mature and partially mature forms of the virus.

### 3.4. Antibody-Enhanced Infection

The structural dynamics of the envelope (E) protein modulate not only viral neutralization but also mechanisms of antibody-mediated enhancement of infection. In TBEV, a recently characterized enhancement pathway has been described that operates independently of Fc$\gamma$ receptor (Fc$\gamma$R) engagement, distinguishing it from classical ADE mechanisms.[86] In this Fc$\gamma$R-independent pathway, certain antibodies, such as monoclonal antibody A5, which targets Domain II at the E protein dimer interface, shift the conformational equilibrium toward monomeric E protein states. This structural transition exposes the otherwise hidden fusion loop, promoting its direct interaction with the host cell plasma membrane and thereby facilitating viral attachment and entry.[86]

A similar Fc$\gamma$R-independent enhancement phenomenon was reported for WNV, where mAb E100 increased infection by targeting a structurally analogous site in Domain II.[92] These findings indicate that orthoflavivirus immune evasion strategies extend beyond escape from antibody neutralization to include mechanisms that exploit antibody binding to promote viral entry. These phenomena pose a substantial obstacle to the development of vaccines and therapeutic antibodies, as some antibody responses may unintentionally promote viral entry and infection instead of conferring protective immunity.

### 3.5. Implications for Vaccine and Antiviral Strategies

A comprehensive understanding of orthoflavivirus antigenic variability and immune evasion mechanisms is critical for the development of effective vaccines and antiviral therapies. Broadly neutralizing antibodies that target conserved quaternary epitopes have demonstrated potential in overcoming viral escape.[93] However, successful vaccine candidates must also address challenges posed by viral breathing, incomplete maturation, and escape mutations to achieve durable and cross-protective immunity. Emerging strategies, such as stabilizing E protein dimers to reduce conformational flexibility,[94] or designing small-molecule inhibitors that block the structural rearrangements required for membrane fusion, offer promising therapeutic avenues.[95]

The diversity of orthoflavivirus evasion strategies underscores the intricate interplay between viral architecture, immune recognition, and host adaptation. These insights are essential for the rational design of therapeutic antibodies and immunogens, particularly when targeting viral elements that remain both accessible and conserved despite ongoing viral evolution.

## 4. Antibody Target Design for Orthoflavivirus Therapy

The success of therapeutic antibody development against orthoflaviviruses critically depends on the rational selection of viral targets. These viruses pose unique challenges due to high genetic variability, overlapping antigenic structures, and diverse immune evasion strategies.[96,97]

### 4.1. Envelope Protein (E)

The E protein, the major surface glycoprotein of orthoflaviviruses, plays a central role in viral entry by mediating receptor binding and membrane fusion. In ZIKV, E proteins form 90 dimers arranged with icosahedral symmetry, producing a smooth viral surface. The E protein is composed of three distinct domains—DI, DII, and DIII, each presenting unique opportunities for antibody targeting. EDIII mediates host cell receptor binding and is a major target for type-specific neutralizing antibodies, particularly in ZIKV. In contrast, the fusion loop (FL) within EDII represents a highly conserved epitope across orthoflaviviruses (**Figure 1**) and enables the generation of broadly neutralizing antibodies.[72,98] In mature DENV and other orthoflaviviruses, E proteins form a herringbone pattern across the virion surface, further influencing epitope accessibility and antibody interactions.[99]

Despite these advantages, the E protein presents several challenges as an antigenic target. Antigenic variability, particularly in EDIII, limits cross-reactivity and increases the potential for escape mutations. Additionally, structural shielding and dynamic conformational changes, such as "viral breathing", can obscure epitope access. Moreover, antibodies targeting the E protein must contend with the risk of ADE, in which non-neutralizing antibodies facilitate viral entry into Fc receptor-bearing cells, potentially worsening disease severity.[100] These characteristics highlight the need for rational antigen design strategies that exploit conserved epitopes, such as the fusion loop and E dimer epitope (EDE), while minimizing the risks associated with antigenic variability and ADE.[93]

#### *4.1.1. Domain III (EDIII)*

Domain III of the envelope protein (EDIII) plays a central role in receptor engagement and is a prominent target of potently neutralizing monoclonal antibodies. In ZIKV, EDIII is highly immunogenic and structurally distinct, making it amenable to monoclonal antibody targeting. Prototypical mAbs such as ZKA190 and ZV-67, which bind the lateral ridge of EDIII, exhibit potent and specific neutralizing activity.[103,104] However, this specificity is driven by substantial sequence variation across orthoflavivirus species and serotypes, which limits cross-reactivity and facilitates viral escape.[72,93,105]

Although multiple EDIII-targeting antibodies have been isolated from ZIKV-infected individuals,[106–111] they are generally elicited at later stages of infection and comprise a minor fraction of the polyclonal neutralizing response, in contrast to the immunodominance observed in murine models (Gallichotte et al., 2019). Moreover, EDIII-directed monoclonal antibodies, when used individually, can rapidly select for resistant viral variants, underscoring their limited robustness in therapeutic applications.[103]

Functionally, while EDIII has been implicated in receptor binding, orthoflaviviruses do not rely on a single, conserved entry

the coexistence of structurally diverse viral particles may permit immune escape even in the presence of strong neutralizing antibody responses.[91] This maturation-dependent evasion mechanism complicates vaccine development, as effective immunogens must elicit protective responses against both fully mature and partially mature forms of the virus.

### 3.4. Antibody-Enhanced Infection

The structural dynamics of the envelope (E) protein modulate not only viral neutralization but also mechanisms of antibody-mediated enhancement of infection. In TBEV, a recently characterized enhancement pathway has been described that operates independently of Fc$\gamma$ receptor (Fc$\gamma$R) engagement, distinguishing it from classical ADE mechanisms.[86] In this Fc$\gamma$R-independent pathway, certain antibodies, such as monoclonal antibody A5, which targets Domain II at the E protein dimer interface, shift the conformational equilibrium toward monomeric E protein states. This structural transition exposes the otherwise hidden fusion loop, promoting its direct interaction with the host cell plasma membrane and thereby facilitating viral attachment and entry.[86]

A similar Fc$\gamma$R-independent enhancement phenomenon was reported for WNV, where mAb E100 increased infection by targeting a structurally analogous site in Domain II.[92] These findings indicate that orthoflavivirus immune evasion strategies extend beyond escape from antibody neutralization to include mechanisms that exploit antibody binding to promote viral entry. These phenomena pose a substantial obstacle to the development of vaccines and therapeutic antibodies, as some antibody responses may unintentionally promote viral entry and infection instead of conferring protective immunity.

### 3.5. Implications for Vaccine and Antiviral Strategies

A comprehensive understanding of orthoflavivirus antigenic variability and immune evasion mechanisms is critical for the development of effective vaccines and antiviral therapies. Broadly neutralizing antibodies that target conserved quaternary epitopes have demonstrated potential in overcoming viral escape.[93] However, successful vaccine candidates must also address challenges posed by viral breathing, incomplete maturation, and escape mutations to achieve durable and cross-protective immunity. Emerging strategies, such as stabilizing E protein dimers to reduce conformational flexibility,[94] or designing small-molecule inhibitors that block the structural rearrangements required for membrane fusion, offer promising therapeutic avenues.[95]

The diversity of orthoflavivirus evasion strategies underscores the intricate interplay between viral architecture, immune recognition, and host adaptation. These insights are essential for the rational design of therapeutic antibodies and immunogens, particularly when targeting viral elements that remain both accessible and conserved despite ongoing viral evolution.

## 4. Antibody Target Design for Orthoflavivirus Therapy

The success of therapeutic antibody development against orthoflaviviruses critically depends on the rational selection of viral targets. These viruses pose unique challenges due to high genetic variability, overlapping antigenic structures, and diverse immune evasion strategies.[96,97]

### 4.1. Envelope Protein (E)

The E protein, the major surface glycoprotein of orthoflaviviruses, plays a central role in viral entry by mediating receptor binding and membrane fusion. In ZIKV, E proteins form 90 dimers arranged with icosahedral symmetry, producing a smooth viral surface. The E protein is composed of three distinct domains—DI, DII, and DIII, each presenting unique opportunities for antibody targeting. EDIII mediates host cell receptor binding and is a major target for type-specific neutralizing antibodies, particularly in ZIKV. In contrast, the fusion loop (FL) within EDII represents a highly conserved epitope across orthoflaviviruses (**Figure 1**) and enables the generation of broadly neutralizing antibodies.[72,98] In mature DENV and other orthoflaviviruses, E proteins form a herringbone pattern across the virion surface, further influencing epitope accessibility and antibody interactions.[99]

Despite these advantages, the E protein presents several challenges as an antigenic target. Antigenic variability, particularly in EDIII, limits cross-reactivity and increases the potential for escape mutations. Additionally, structural shielding and dynamic conformational changes, such as "viral breathing", can obscure epitope access. Moreover, antibodies targeting the E protein must contend with the risk of ADE, in which non-neutralizing antibodies facilitate viral entry into Fc receptor-bearing cells, potentially worsening disease severity.[100] These characteristics highlight the need for rational antigen design strategies that exploit conserved epitopes, such as the fusion loop and E dimer epitope (EDE), while minimizing the risks associated with antigenic variability and ADE.[93]

#### *4.1.1. Domain III (EDIII)*

Domain III of the envelope protein (EDIII) plays a central role in receptor engagement and is a prominent target of potently neutralizing monoclonal antibodies. In ZIKV, EDIII is highly immunogenic and structurally distinct, making it amenable to monoclonal antibody targeting. Prototypical mAbs such as ZKA190 and ZV-67, which bind the lateral ridge of EDIII, exhibit potent and specific neutralizing activity.[103,104] However, this specificity is driven by substantial sequence variation across orthoflavivirus species and serotypes, which limits cross-reactivity and facilitates viral escape.[72,93,105]

Although multiple EDIII-targeting antibodies have been isolated from ZIKV-infected individuals,[106–111] they are generally elicited at later stages of infection and comprise a minor fraction of the polyclonal neutralizing response, in contrast to the immunodominance observed in murine models (Gallichotte et al., 2019). Moreover, EDIII-directed monoclonal antibodies, when used individually, can rapidly select for resistant viral variants, underscoring their limited robustness in therapeutic applications.[103]

Functionally, while EDIII has been implicated in receptor binding, orthoflaviviruses do not rely on a single, conserved entry

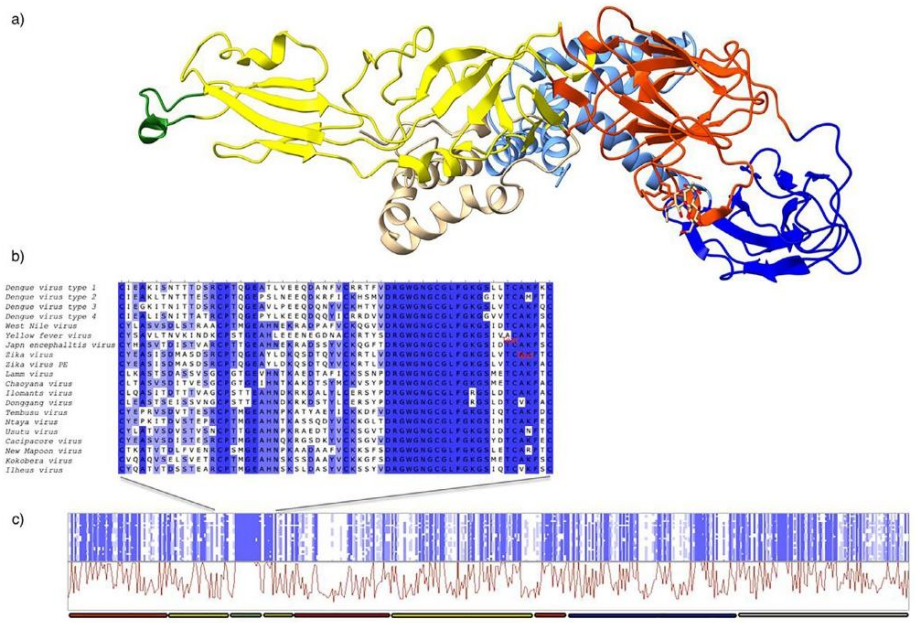


**Figure 1.** The Protein E of Orthoflaviviruses is a surface protein and major antigenic target. a) The structure of Protein E and M is depicted as a ribbon representation based on the PDB file 5IRE. Coloring distinct the domains: red, Domain I; yellow, Domain II; green, Fusion loop; blue, Domain III; salmon, Transmembrane Domain; light blue, the M Protein. b) Multi-sequence Alignment of representative orthoflavivirus in the conserved region of the E protein, the fusion loop. c) Overview of the multi-sequence Alignment and conservation plot of the whole E protein, detaching the fusion loop as observed in b. Below, a bar representation of the domain system of Protein E, following the color code in a. Structural domains I and II are not continuous in the primary sequence. ChimeraX[101] was used to generate structural illustration, and Ugene[102] was used for Alignment.

factor. Instead, they exploit a broad array of attachment receptors, including glycosaminoglycans, DC-SIGN, and tight junction proteins like claudin-1, whose expression varies with host species, cell type, and viral glycosylation patterns.[112,113] This receptor redundancy helps explain why antibodies targeting EDIII often display reduced efficacy in vivo despite potent in vitro neutralization. Supporting this, epitope transplant and mapping studies have shown that EDIII-specific antibodies account for less than 10% of serum neutralizing activity in naturally infected individuals.[105]

Furthermore, recombinant antigen-based assays tend to overrepresent the role of EDIII by failing to preserve the native quaternary structure of the virion, which may obscure the contribution of more conserved and functionally essential epitopes.[105] These insights have spurred efforts to design bispecific or combinatorial antibody therapies that co-target EDIII and more conserved domains, such as the fusion loop (FL) or envelope dimer epitope (EDE), aiming to enhance breadth and reduce the likelihood of immune escape.[93,110] Advances in epitope mapping technologies, including HDX-MS, are further enabling precise therapeutic design by revealing key neutralizing determinants.[114]

#### *4.1.2. Fusion Loop (FL)*

The fusion loop (FL), located in domain II of the envelope (E) protein, is the most conserved region across orthoflaviviruses (Figure 1B,C), making it an ideal target for broadly neutralizing antibodies. During viral entry, acidic pH in endosomal compartments triggers the transition of E protein dimers into trimers, exposing the fusion loop, which is essential for membrane fusion[115,116] (**Figure 2**). This structural shift results in the transient exposure of the fusion loop located at the tip of domain II (EDII), which anchors into the host cell membrane to initiate the fusion process[83] (Figure 2). FL-specific neutralization antibodies are able to block the interaction of the exposed FL or interfere with trimer formation.[117] Studies have demonstrated that such antibodies can disrupt the transition from immature to mature viral particles in WNV[92] and stabilize pre-fusion structures in YFV, preventing conformational changes necessary for membrane fusion.[118]

Despite these advantages, targeting the FL is challenging due to its cryptic nature. On mature virions, the FL is buried within the E protein dimer interface, limiting antibody accessibility. However, under certain physiological conditions, such as during

ADVANCED SCIENCE NEWS
www.advancedsciencenews.com

ADVANCED THERAPEUTICS
www.advtherap.com

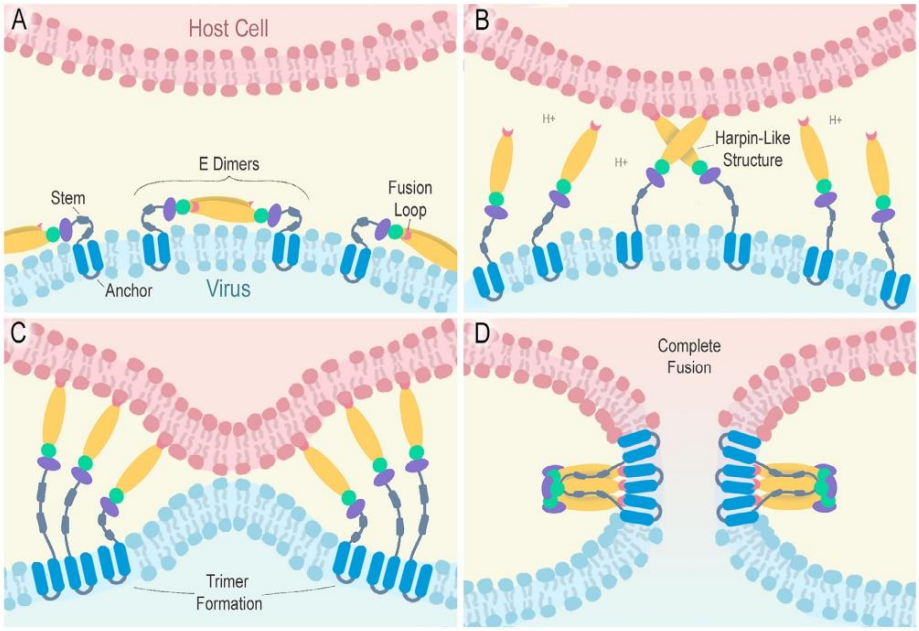


**Figure 2.** Mechanism of orthoflavivirus envelope protein (E)-mediated membrane fusion with the host cell. Schematic representation of the sequential steps of membrane fusion between the orthoflavivirus and host cell, mediated by the envelope glycoprotein. A) On the mature virion, E proteins form antiparallel dimers laying flat on the viral surface, with the fusion loop (pink) buried at the dimer interface to prevent premature interaction with the host membrane. B) Endosomal acidification ($H^+$ influx) triggers conformational changes that dissociate the dimers, exposing the fusion loop, which inserts into the host cell membrane. The E proteins extend into a hairpin-like intermediate conformation. C) Subsequent trimerization of E proteins brings the viral and host membranes into close proximity by anchoring both via the inserted fusion loop and transmembrane domains (TM1/TM2, blue). D) The E proteins rearrange into a stable trimer, positioning the fusion loops and membrane anchors side by side, which facilitates the formation of a fusion pore through which the viral genome is delivered into the host cytoplasm. The structural domains of the E protein are color-coded: Domain I (EDI) in green, Domain II (EDII) in yellow, with the fusion loop at its tip in pink, Domain III (EDIII) in purple, the stem region in grey, and transmembrane segments TM1 and TM2 in blue.

"viral breathing" or in immature particles, the FL becomes transiently or partially exposed, providing an opportunity for antibody binding.[81,92]

To overcome these structural barriers, rational antigen design is essential. Recent advances have focused on mimicking the natural conformation of the FL to elicit effective immune responses. Our group developed a novel FL-based antigen in which the fusion loop was stabilized via a disulfide bond to an adjacent peptide from EDII, preserving its native conformation. This strategy enabled the selection of single-chain variable fragment (scFv) antibodies that demonstrated neutralizing activity against ZIKV and cross-reactivity with DENV and YFV.[95]

Kotaki et al. (2021) generated a panel of human monoclonal antibodies from an Indonesian dengue patient using human hybridoma technology and identified 3G9, which showed exceptional neutralization potency (NT50 < 0.1 μg $mL^{-1}$) against all four DENV serotypes and also cross-neutralized ZIKV, JEV, and WNV. Epitope mapping revealed that 3G9 binds critical conserved residues (W101, L107, F108) in the fusion loop. Although wild-type 3G9 induced strong ADE in vitro, introduction of Fc mutations (LALA, D265A, N297A) abolished ADE without compromising neutralization. In murine models, both wild-type and Fc-modified 3G9 significantly improved survival following lethal DENV challenge, with Fc-modified variants showing superior protection and reduced viremia.[119]

Together, these findings underscore the potential of the FL as a structurally conserved and functionally critical epitope for the development of pan-orthoflavivirus antibody therapies. With regard to ADE, although wild-type antibodies targeting this region are prone to mediating enhancement, Fc-engineered variants consistently abolish ADE while preserving neutralization capacity. While challenges related to epitope accessibility remain, advances in antigen engineering and antibody discovery platforms continue to improve the feasibility of targeting this conserved region.

This rationale is further supported by our structural and bioinformatic analyses presented in Figure 1. Panel A illustrates the spatial positioning of the fusion loop (green) within domain II (yellow) of the E protein trimer, highlighting its key role in the viral fusion process and the conformational rearrangements that expose it. As shown in Panel B, multi-sequence alignment of 20 representative orthoflaviviruses reveals the high sequence conservation of the FL, which remains nearly invariant across dengue, Zika, West Nile, and YFVs. Panel C provides a conservation plot across the full E protein, emphasizing the FL as one of the most conserved surface-accessible regions. This contrasts with domain III (in blue), which exhibits greater variability across orthoflaviviruses and is often associated with serotype-specific responses and escape mutations. While DIII-targeting antibodies may offer strong neutralization within a given serotype, FL-targeting antibodies hold greater potential for cross-reactivity, making them better suited for pan-orthoflavivirus therapeutic strategies. Thus, the fusion loop stands out not only for its functional indispensability, but also for its structural conservation, a rare combination that elevates its value as a target for broad-spectrum antiviral antibody development.

#### *4.1.3. E-Dimer Interface (EDE)*

The envelope dimer epitope (EDE), located at the interface of E protein dimers, is a conserved quaternary structure targeted by broadly neutralizing antibodies (bnAbs) capable of cross-serotype neutralization in DENV and cross-reactivity with ZIKV. Antibodies such as EDE1-C10 and EDE2-A11 exemplify this category, binding to the conserved dimer interface to stabilize the pre-fusion conformation of the E protein, thereby inhibiting the conformational rearrangements required for viral fusion and entry.[72,98]

The EDE epitopes are accessible due to the "breathing" dynamics of DENV's surface proteins, where transient movements expose the dimer interface. This structural behavior allows EDE antibodies to bind mature virions and partially mature particles containing precursor membrane (prM) proteins, enhancing their therapeutic potential.[120] The bivalent binding of EDE1-C10 under acidic conditions further stabilizes E dimers and prevents trimerization, essential for viral fusion, making it particularly effective at neutralizing DENV without promoting ADE.[98]

Structural studies, including cryo-electron microscopy (cryo-EM) and X-ray crystallography, have provided detailed insights into the interactions of EDE bnAbs with the E dimer. These antibodies primarily recognize quaternary epitopes formed at the interface of two E monomers, bridging domains I and II of adjacent subunits. A hallmark of anti-EDE antibodies is their ability to bind across the E dimer without requiring rearrangement, targeting a structurally conserved region involved in viral fusion and maturation.[83,93] This conserved quaternary epitope includes residues from the fusion loop of domain II and adjacent surfaces of domain I, contributing to high cross-reactivity across DENV serotypes. Advanced mass spectrometry methods have also contributed to epitope mapping, supporting the development of antigen designs that mimic natural E dimer conformations and maximize epitope exposure.[114]

The conserved nature of EDE across orthoflaviviruses, combined with its critical role in viral entry, makes it an attractive target for therapeutic antibodies and vaccine design. Strategies that scaffold or engineer immunogens to replicate the natural quaternary structure of E dimers could elicit robust bnAb responses, addressing challenges posed by variability in other epitopes like EDIII.[98,93]

### 4.2. Non-Structural Protein 1 (NS1)

Beyond the E protein, nonstructural proteins such as NS1 are gaining attention as alternative antibody targets. The orthoflavivirus non-structural protein 1 (NS1) is a highly conserved glycoprotein essential for viral pathogenesis and can be a promising antigenic target for therapeutics and vaccines. NS1 is expressed in three forms: monomeric, dimeric, and hexameric. It is synthesized as a monomer in the endoplasmic reticulum (ER) and is later assembled into membrane-associated dimers or secreted as lipid-associated hexamers.[121,122] These forms interact with host cells, contributing to immune evasion, vascular leakage, and complement inhibition.[121–123]

NS1-specific antibodies play dual roles, offering protection or contributing to immunopathogenesis. Protective antibodies inhibit NS1-induced endothelial hyperpermeability, reduce apoptosis, and mediate ADCC, promoting clearance of infected cells.[124,125] Structural studies have identified critical epitopes on the $\beta$-ladder and wing domains of NS1, where antibodies, such as 2B7 and 1G5.3, block interactions with endothelial cells and hinder hexamer formation.[126,127]

Pathogenic anti-NS1 antibodies, however, may cross-react with host proteins due to molecular mimicry, targeting endothelial cells, fibrinogen, and platelets, and contributing to plasma leakage, coagulopathy, and tissue damage. For example, anti-NS1 antibodies recognizing Lysine-Rich CEACAM1 co-isolated protein (LYRIC), a tight junction-associated protein, in endothelial cells enhance apoptosis and nitric oxide production.[128] They also impair platelet function by targeting protein disulfide isomerase and inducing plasminogen activation.[129,130]

NS1's absence on virions eliminates the risk of ADE, making it a safer target for antibody therapy. Cross-reactive epitopes conserved across orthoflaviviruses highlight NS1's potential for universal therapeutic applications. Studies demonstrate that anti-NS1 antibodies can protect against severe disease by reducing viral loads, inhibiting NS1-induced vascular damage, and disrupting pathogenic interactions with host cells in preclinical models.[131,132] Leveraging structural and functional insights into NS1 and its interactions with antibodies holds significant promise for developing effective antibody-based therapies against orthoflaviviruses.

## 5. Discovery and Selection of Antibodies against Orthoflaviviruses

Once suitable antigenic targets have been identified, the next critical step involves selecting or engineering antibodies capable of recognizing these epitopes with high affinity and specificity. Hybridoma technology, introduced in 1975, was the first method

developed for monoclonal antibody (mAb) production.[37] This method produced murine antibodies, which elicited strong immune responses in humans, imposing further modifications to reduce immunogenicity. Genetic engineering enabled the development of less immunogenic antibodies by chimerization[133] or humanization. In the latter, only the murine CDRs were retained within a human antibody framework, improving compatibility and half-life.[38] The development of fully human antibodies became possible through single B-cell screening, and display technologies such as phage and yeast display, which allowed faster selection of high-affinity human antibodies compared to traditional methods.

### 5.1. Single B Cell Screening

The global emergence of novel pandemics has highlighted the critical necessity for accelerated discovery of monoclonal antibodies (mAbs) targeting infectious pathogens, thereby driving significant progress in single B cell screening associated with high-throughput sequencing methodologies. This approach enables the direct isolation of antigen-specific B cells while preserving the native pairing of antibody heavy and light chains, which is critical for maintaining natural specificity.[134] Traditional screening methods rely on fluorescence-activated cell sorting (FACS) or magnetic-activated cell sorting (MACS) to isolate antigen-binding B cells, followed by reverse transcription–polymerase chain reaction (RT-PCR) and next-generation sequencing (NGS) to retrieve and clone antibody variable genes.[135,136] These methods have led to the discovery of some neutralizing antibodies against orthoflavivirus.[132,137]

To improve scalability, droplet microfluidics-based platforms have been integrated into high-throughput single-cell screening. Technologies such as CelliGO compartmentalize single IgG-secreting cells into droplets, allowing real-time bioassays to evaluate IgG activity before sorting and sequencing.[138] Another droplet-based system, developed by Shembekar et al. (2018), co-encapsulates antibody-secreting hybridoma cells with target cells, employing fluorescence-based binding assays and dielectrophoretic sorting to isolate antigen-specific clones.[139] These platforms enable the simultaneous screening of tens of thousands of antibody candidates, significantly increasing throughput and efficiency. Microfluidic approaches have successfully identified broadly neutralizing antibodies against infectious diseases such as HIV, Ebola, and COVID-19.[140,141] Additionally, LIBRA-seq, a high-throughput sequencing method that links B cell receptors to antigen specificity via DNA barcoding, has facilitated the discovery of cross-reactive antibodies against SARS-CoV-2, HIV, and hepatitis C virus.[142,143]

Hybridoma technology has also been integrated with single B-cell screening to improve mAb discovery against orthoflaviviruses. Sapparapu et al. (2016) identified ZIKV-specific mAbs by culturing peripheral blood mononuclear cells (PBMCs) from ZIKV-infected individuals, selecting antigen-reactive B cells via FACS, and fusing them with myeloma cells to generate hybridomas.[144] The resulting clones were expanded, purified, and sequenced using RT-PCR to characterize their variable regions. Their multi-step approach successfully identified potent neutralizing mAbs against ZIKV, highlighting the potential of hybrid screening strategies for orthoflavivirus antibody discovery.

### 5.2. Display Technologies

#### *5.2.1. Phage Display*

Display technologies have facilitated antibody discovery by enabling high-throughput selection of molecules with desired binding properties while maintaining the genotype–phenotype linkage.[145] Various platforms, including phage display, ribosome display, yeast surface display, and mammalian cell display, offer distinct advantages in antibody screening. The phage display technique for presenting exogenous proteins on bacteriophage surfaces was first described in 1985.[146] Since then, it has been applied in various fields beyond antibody development, including biosensor design, enzyme substrate identification, drug discovery, and vaccine development.[147–149] In antibody research, phage-displayed libraries enable a detailed mapping of the human antibody repertoire, particularly in relation to antigen specificity.[145,149]

Phage-displayed antibody libraries can be either natural or synthetic. The strategy used to construct antibody libraries influences the selection of antibodies through phage display. Natural libraries can be derived from naïve donors (naïve libraries) or individuals previously exposed to the target antigen (immune libraries). Immune libraries offer an advantage by containing a repertoire of antibodies with higher affinity and specificity for the antigen of interest. This specificity arises from natural processes such as B cell activation, affinity maturation, somatic hypermutation, and memory B cell (MBC) generation. However, a limitation of immune libraries is the relatively low number of circulating antigen-specific B cells, which may restrict the diversity of antibodies represented in the library.[145,150]

For generating a human antibody library, the mRNA derived from the donors' B cells is converted into cDNA and used to amplify the variable heavy (VH) and light (VL) chain regions of antibodies. These gene segments are then cloned into a phagemid vector containing both a bacterial origin of replication and a filamentous phage origin, generating a synthetic antibody library expressed on bacteriophage surfaces.[151–154] Once expressed, antibodies undergo selection through biopanning, a process involving multiple rounds of antigen binding, washing, and elution to enrich clones with higher specificity.[155] Biopanning can be performed using antigens immobilized on microtiter plates or biotinylated antigens bound to magnetic beads or streptavidin-coated resins.[154] Antibody sequences from the final selection round are analyzed, synthesized, and expressed to evaluate their binding and functional properties. A schematic overview of this workflow, from antibody gene amplification to phage display selection rounds, is illustrated in **Figure 3**.

Filamentous bacteriophages, members of the *Inoviridae* family, contain single-stranded DNA (ssDNA) as their genetic material. Various filamentous phages, including M13, f1, and fd, have been used for protein display, with M13 being the most commonly employed. The M13 genome encodes 11 proteins, five of which form the viral capsid (pIII, pVI, pVII, pVIII, and pIX). Among these, pIII and pVIII are widely used for antibody presen-

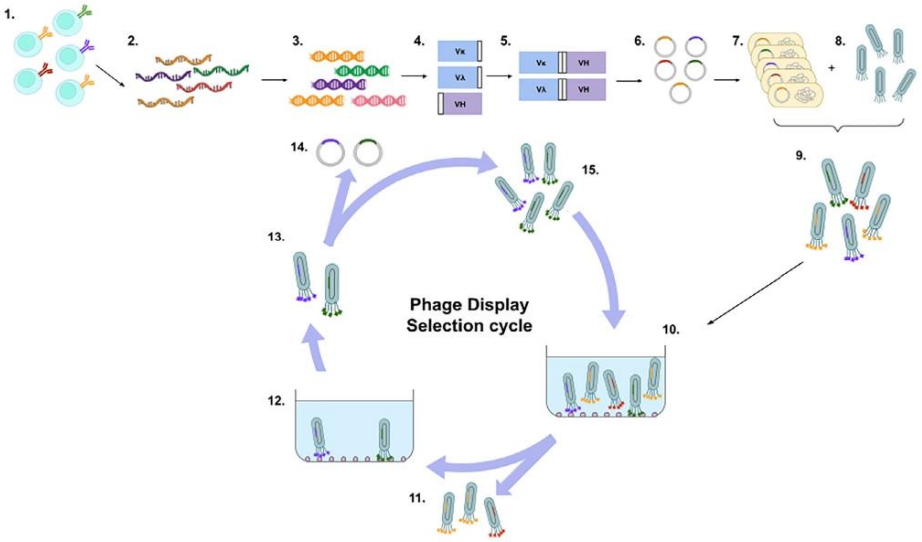


**Figure 3.** Schematic representation of the generation of a human antibody library in the scFv format from B cells and the subsequent selection of specific binders through phage display. B cells, isolated from immunized or naïve donors, are used as the source of total RNA (1–2), which is then reverse transcribed into cDNA (3). The variable regions of the immunoglobulin light (VL) and heavy (VH) chains are amplified by PCR (4) and assembled into single-chain variable fragments (scFv) through the insertion of a flexible linker between them (5). These constructs are cloned into phagemid vectors, generating a diverse recombinant combinatorial library (6), which is subsequently transformed into *E. coli* (7). The transformed bacteria are infected with a helper phage to enable the production of recombinant phage particles displaying the scFv fragments on their surface (8–9). The resulting phage display library is incubated with the immobilized target antigen (10), and non-binding phages are removed through washing steps (11), while specific binders remain attached to the target (12). Bound phages are then eluted (13), and their encoding plasmid DNA is recovered from infected bacteria to allow amplification of the selected VH and VL sequences (14). The selected phages are propagated overnight in bacterial culture (15) to initiate a new round of selection. This biopanning process is typically repeated for 3 to 5 rounds to progressively enrich high-affinity scFv binders. RNA and DNA icons were retrieved from NIH Bioart Image Repository.[247,248]

tation, particularly pIII, as it can accommodate larger fusion proteins without disrupting its function in phage infection.[145] Filamentous phages infect gram-negative bacteria such as *Escherichia coli* by interacting with the host cell's sex pilus via the pIII protein. During infection, newly synthesized viral ssDNA is extruded through the bacterial envelope without lysing the cell, allowing continuous replication and phage production. As viral particles are released, their ssDNA is coated with structural proteins, completing phage assembly.[156]

Phage display is a powerful tool for isolating monoclonal antibodies (mAbs) with high specificity and has been extensively used in the selection of antibodies against orthoflaviviruses. Throsby et al. (2006) constructed phage display libraries from WNV-infected patients and screened 480 monoclonal scFv phages for WNV-specific binding.[157] Among the 138 identified mAbs, 12 exhibited neutralizing activity, with two providing in vivo protection. The majority of antibodies targeted domain II of the viral envelope (E) protein, whereas potent neutralizers against domain III were less frequent.

A recent study from our group further exemplifies the utility of phage display for the identification of cross-reactive and potentially therapeutic antibodies against orthoflaviviruses.[95] França et al. (2022) employed phage display to select human monoclonal antibodies targeting a synthetic mimetic peptide derived from the highly conserved fusion loop (FL) region of the ZIKV envelope protein. Using two distinct panning strategies, acidic and competitive elution. Three distinct scFv antibodies were identified after NGS analysis. These antibodies bound specifically to ZIKV and exhibited cross-reactivity with yellow fever and DENVs, consistent with the conserved nature of the FL epitope. Notably, two antibodies (AZ1p and AZ6m) demonstrated in vitro neutralization of ZIKV, highlighting the therapeutic potential of targeting conserved structural elements for the development of broadly reactive anti-orthoflavivirus antibodies.[95]

### 5.2.2. Yeast Display

Yeast display, like phage display, is a powerful tool for epitope mapping, affinity maturation, and antibody repertoire analysis. Unlike phage-based systems, yeast display occurs in a eukaryotic environment, allowing for proper protein folding, post-

translational modifications, and the selection of high-affinity antibodies. Oliphant et al. (2005) employed yeast display to map the binding site of E16, a humanized monoclonal antibody (mAb) targeting domain III of the WNV envelope (E) protein.[92] The study identified 14 mAbs, with E16 exhibiting broad neutralization across 10 WNV strains and significant in vivo protection. Yeast display enabled precise epitope mapping, revealing a dominant neutralizing site recognized by antibodies from WNV-infected individuals, providing a foundation for E16's therapeutic optimization.

Further advancing yeast display applications, Fahad et al. (2021) used this approach to analyze antibody repertoires from ZIKV-infected individuals, integrating NGS and yeast surface display to construct renewable B cell-derived antibody libraries.[158] These libraries were screened against ZIKV and YFV virus-like particles (VLPs) using FACS, enriching antigen-binding clones. This strategy enabled the identification of maturation-state-specific, ZIKV-specific, and cross-reactive antibodies, demonstrating the precision and scalability of yeast display in therapeutic antibody discovery.

#### 5.2.3. Mammalian Display

Mammalian display provides a physiologically relevant platform for antibody selection, preserving native folding, post-translational modifications, and authentic antigen interactions. Zhang et al. (2014) developed a mammalian display system using HEK293T cells to screen scFv antibodies from a non-immune library of healthy donors and cancer patients.[159] Using FACS, they identified three ErbB3-specific scFv candidates with nanomolar binding affinities, demonstrating that mammalian display enables the selection of high-affinity therapeutic antibodies while preserving biologically relevant structural features.

Recent advancements in mammalian display technology have led to functional screening platforms, such as the Droplet Reporter Cell Testing for Neutralization (DrReCT-Neutralization), a platform which integrates microfluidics, NGS, and droplet-based single-cell encapsulation to identify neutralizing antibodies based on their functional activity rather than just binding affinity.[160] Unlike traditional affinity-based display methods, which select antibodies based solely on antigen binding, DrReCT-Neutralization directly assesses neutralization capacity against infectious agents, which the authors demonstrated against SARS-CoV-2 and HIV pseudoviruses. In this system, antibody-secreting reporter cells are encapsulated in microdroplets, allowing secreted antibodies to accumulate before a pseudovirus challenge. If infection occurs, a fluorescent reporter gene is activated, enabling FACS-based sorting of neutralizing clones. NGS then identifies enriched sequences with high-affinity mutations. By integrating functional screening directly into the discovery process, this system provides the direct selection of potent neutralizing antibodies.

## 6. Antibody Engineering and Optimization

### 6.1. Antibody Formats

To further enhance the efficacy, safety, and pharmacokinetics of selected antibodies, advances in engineering and optimization strategies of mAbs have been instrumental.[161,162] Antibody formats refer to structural variations that influence their functional properties, stability, and therapeutic applicability. The most widely utilized format is the full-length immunoglobulin G (IgG).[161] Full-length IgG combines antigen-binding capacity with Fc-mediated effector functions, such as ADCC and CDC.[163] Smaller antibody fragments, including Fab (fragment antigen-binding) and scFv, have been engineered to address the limitations of full-length antibodies.[161,164] Nanobodies, derived from the single-domain antibodies of camelids, represent another innovative format with unique structural and functional advantages.[165] Moreover, emerging hybrid formats, such as bispecific antibodies, further expand the scope of therapeutic antibody design by enabling simultaneous targeting of multiple epitopes or antigens.[166,167]

#### 6.1.1. Full-Length IgG

Full-length IgG antibodies remain the gold standard for therapeutic applications due to their prolonged serum half-life, conferred by interactions with neonatal Fc receptors (FcRn), and their ability to recruit immune effector functions through their Fc domains.[161] These properties render IgG highly effective in neutralizing viral infections and clearing infected cells.[163] However, their large molecular size (≈150 kDa) can limit tissue penetration, particularly in dense or protected tissues such as the brain, and limit access to cryptic epitopes.[161,168] Additionally, in the context of orthoflavivirus infections, IgG antibodies face challenges such as the risk of ADE. Engineering efforts have focused on mitigating these limitations. For instance, EDE1-C10, a broadly neutralizing antibody targeting conserved epitopes on the DENV envelope protein, demonstrates cross-serotype neutralization.[169] Furthermore, Sharma and colleagues showed that a highly cross-reactive antibody, C10, increases its binding and neutralization capacity to ZIKV and the four types of DENV when it changes from a Fab format to a complete IgG. Similarly, ZIKV-117, an IgG targeting the ZIKV envelope protein, has shown potent neutralization in preclinical and clinical studies.[144] Despite the risk of ADE when using full-length antibodies, Nilchan et al. (2024) developed a full-length human IgG targeting the DENV envelope protein domain III (EDIII) that maintained strong neutralization capabilities across dengue serotypes without promoting ADE.[170] The authors discussed that careful selection of target epitopes can mitigate ADE risks and subtle differences in the binding epitopes and topology can influence the occurrence of ADE.

#### 6.1.2. Antibody Fragments (Fab, scFv)

Smaller antibody fragments, such as Fab (≈50 kDa) and scFv (≈25 kDa), offer some advantages over full-length IgG. Their reduced size facilitates superior tissue penetration and enables access to cryptic or sterically hindered epitopes that are less accessible to larger IgG molecules.[161,168,171] França et al. 2022 generated scFv mAbs targeting the orthoflavivirus fusion loop, which is a cryptic antigen, that neutralized ZIKV in vitro and cross-recognized Yellow Fever and DENVs.[95] Fab and scFv fragments

are also amenable to production in bacterial expression systems, reducing manufacturing complexity and cost. However, these fragments lack Fc domains, which preclude effector functions such as ADCC and CDC. Furthermore, they have shorter serum half-lives and low stability. However, since they are easier to produce, they are often used as a first molecule in screening experiments, and then further expressed in a full-length format for in vivo validation.[171]

#### 6.1.3. Nanobodies

Nanobodies, the smallest antibody format (≈15 kDa), represent an advancement in the therapeutic arsenal against infectious diseases. Their compact single-domain structure enables them to bind cryptic epitopes that are inaccessible to conventional antibody formats, making them particularly effective against structurally complex viral proteins, such as the envelope protein of orthoflaviviruses.[165,168] Nanobodies directed against conserved epitopes on viral capsid proteins, as exemplified by Chaudhuri et al. (2023) in the context of DENV, demonstrate their broad applicability for targeting a range of viral pathogens.[172] These nanobodies, developed using computational affinity maturation, exhibited high specificity and binding stability in vitro. Delfin-Riela et al. (2020) demonstrated that nanobodies against the NS1 protein of ZIKV effectively interfered with NS1-mediated pathogenic mechanisms in vitro, showcasing their therapeutic potential.[173] Similarly, nanobodies targeting domain III of the WNV envelope protein, as described by Hruškovicová et al. (2022), exhibited strong neutralization potential and structural stability.[168] The study also assessed hemocompatibility using sheep erythrocytes, showing that these nanobodies did not cause hemolysis, which supports their safety for therapeutic applications. Cytotoxicity testing with endothelial cells further confirmed their non-toxic profile. Nanobodies also exhibit exceptional thermal and conformational stability and can be efficiently produced in prokaryotic systems, making them attractive and scalable candidates for therapeutic use in global health settings.[174] Despite their benefits, nanobodies, like scFvs, face challenges such as short circulation half-life, imposing additional engineering to improve pharmacokinetics. Their modularity, however, allows for the creation of multivalent constructs, significantly enhancing avidity and neutralization potency, and broadening their applicability in antiviral therapies. An illustrative example of a nanobody successfully translated into clinical use is caplacizumab (Cablivi), the first nanobody-based therapy approved by the FDA for the treatment of acquired thrombotic thrombocytopenic purpura (aTTP).[175–177] This humanized, bivalent, variable domain-only immunoglobulin fragment specifically targets the A1 domain of von Willebrand factor (VWF), preventing its interaction with the platelet glycoprotein Ib-IX-V receptor and thereby inhibiting the formation of microvascular thrombi. Structurally, caplacizumab is composed of two identical VHH anti-VWF-binding domains (PMP12A2h1) joined by a three-alanine linker and is efficiently produced in *E. coli*.[175,176] This therapeutic format highlights how nanobody engineering can be leveraged to produce effective, targeted biologics.

#### 6.1.4. Multi-Targeting Strategies: Antibody Cocktails and Bispecific mAbs

Targeting multiple epitopes is a well-established strategy to enhance the efficacy and durability of antibody-based therapies, especially in contexts of resistance or antigenic variability. A clinically validated approach is the use of monoclonal antibody (mAb) cocktails, which combine two or more antibodies targeting distinct epitopes to increase therapeutic breadth and reduce the likelihood of viral escape.[178–180] For example, *Inmazeb*, approved for Ebola virus disease, comprises three mAbs that bind non-overlapping regions of the viral glycoprotein, synergizing to neutralize the virus and engage Fc-mediated effector functions.[181] Similar strategies have been employed for rabies (*Twinrab*) and SARS-CoV-2 (*Casirivimab/Imdevimab, Amubarvimab/Romlusevimab*), demonstrating the effectiveness of multi-targeted therapies in infectious diseases.[41,182,183]

Building on this rationale, bispecific antibodies (bsAbs) offer an alternative multi-targeting format, capable of binding two distinct antigens or epitopes within a single molecule. This design simplifies dosing and production while enabling mechanisms of action not easily achieved with separate mAbs, such as dual epitope engagement, improved avidity, and reduced potential for viral escape.[166,167,178,184] Although no bsAbs have been approved yet for infectious diseases, their success in oncology and autoimmune disorders provides a strong foundation for antiviral applications.[166,167,184]

In viral infections, bsAbs present an innovative solution to challenges such as antigenic diversity, rapid mutation, and immune evasion. For instance, bsAbs have been engineered to counter SARS-CoV-2 variants that escape traditional neutralizing antibodies. Constructs combining antibodies from different receptor-binding domains (RBD) classes showed enhanced breadth and potency against Alpha, Beta, Gamma, and Delta variants.[185] Notable examples include CoV-X2[186](De Gasparo et al., 2021) and 14-H-06,[187] which pair broadly neutralizing or cryptic epitope-targeting arms to overcome variant resistance.

In the orthoflavivirus context, Wang et al. (2017) developed FIT-1, a bsAb targeting domains II and III of the ZIKV E protein, achieving enhanced neutralization and resistance to viral escape.[188] Similarly, Khandia et al. (2018) engineered bsAbs to minimize ADE while maintaining strong neutralization in DENV and ZIKV.[189] Other strategies include bsAbs that simultaneously bind conserved epitopes across DENV serotypes or recognize both Zika and DENVs, a key advantage in co-endemic regions. Moreover, some constructs have been designed to interfere with distinct stages of the viral lifecycle, such as entry and membrane fusion.[190]

These studies highlight that bispecific antibodies can not only match the efficacy of mAb cocktails but, in some cases, surpass their parental mAbs in neutralization and functional versatility, supporting their potential for future antiviral therapies.

### 6.2. Fc Engineering Strategies

The optimization of therapeutic antibodies is a critical step in developing safe and effective treatments for orthoflavivirus infections, which are complicated by genetic variability, immune

 

evasion, and the risk of ADE.[189,191] One widely used strategy to mitigate ADE is the introduction of the LALA mutation into the Fc region of antibodies.[163,189,191] By substituting leucine residues at positions 234 and 235 with alanine in the human IgG1 Fc, the LALA mutation silences FcγR binding.[192] However, this approach comes at a cost: it also eliminates Fc-mediated effector functions such as ADCC and CDC, which are important for clearing infected cells.[193] This trade-off highlights the challenge of balancing safety with therapeutic efficacy. The engineering of the ZIKV-117 monoclonal antibody demonstrates this strategy in action.[144,194] In addition to the LALA mutation, ZIKV-117 incorporates the YTE mutation to enhance neonatal Fc receptor (FcRn) binding, extending its serum half-life. Despite the loss of effector functions, this engineered antibody provided complete protection in rhesus macaques at remarkably low doses, demonstrating its potential as a potent therapeutic.[194]

Swapping the Fc domain of human IgG1 antibodies with that of human IgG2 or IgG4, which exhibit lower affinity for activating Fc gamma receptors (FcγRs), has been shown to significantly reduce ADE in cells co-expressing FcγRI and FcγRII. For example, D23-1G7C2 antibodies engineered with IgG2 or IgG4 Fc regions exhibited substantially lower ADE activity by eight and fourfold, respectively, compared to the IgG1 variant, which showed a 256-fold increase in DENV-2 infection in THP-1 cells.[195] Furthermore, the N297A mutation that disrupts FcγR binding further minimized enhancement.[195] However, the effect is cell type-dependent; in K562 cells, which only express FcγRII, the IgG2 variant paradoxically increased ADE, underscoring the importance of cellular context. Complementary findings by Goncalvez et al. (2007) demonstrated that Fc engineering through IgG2/IgG4 subclass replacement reduced ADE, though not entirely.[196] Notably, they identified a nine–amino acid deletion in the CH2 domain that completely abrogated enhancement, suggesting that precise structural alterations may be required for optimal safety. Collectively, these studies highlight that while subclass switching to IgG2 or IgG4 can attenuate ADE, additional fine-tuning, such as point mutations or domain deletions, may be necessary to fully eliminate enhancement risk.

Glycosylation is a post-translational modification that influences antibody stability, functionality, and interactions with immune components.[161] The Fc region of IgG antibodies contains N-linked glycans at Asn297 that modulate interactions with Fc gamma receptors (FcγRs) and complement proteins, thereby regulating immune effector mechanisms such as ADCC and CDC.[161] For orthoflavivirus-targeting antibodies, glycoengineering can enhance effector functions critical for clearing infected cells. For instance, afucosylation of Fc glycans increases binding affinity to activating FcγRIIIa receptors on natural killer (NK) cells, leading to enhanced ADCC.[197–199] Moreover, pH-sensitive Fc modifications allow antibodies to bind antigens tightly at acidic endosomal pH but release them at neutral pH, facilitating more efficient antigen clearance through FcRn-mediated recycling.[161,197]

Targeted mutations in the Fc region also improve antibody pharmacokinetics by enhancing binding to the neonatal Fc receptor (FcRn), which facilitates recycling and extends serum half-life.[161] Half-life extension is particularly critical for smaller antibody formats, such as Fab fragments and nanobodies, which naturally lack Fc regions. In such cases, fusion to albumin-binding domains or PEGylation can dramatically prolong circulation time, reducing the frequency of dosing.[161]

Mutational engineering is also valuable for enhancing stability under physiological and storage conditions. Stabilizing mutations in the antibody framework reduce aggregation and denaturation, ensuring robustness during transport and deployment in resource-limited regions.[200,201] For example, the introduction of engineered disulfide bonds can reinforce antibody structural integrity.[201,202]

An alternative approach to address ADE while maintaining Fc-mediated effector functions is glycoengineering, as exemplified in the optimization of the anti-Zika monoclonal antibody ZV54.[193] Instead of silencing the Fc region, glycoengineering modifies the glycan profile of the Fc to prevent cross-reactivity with DENV, thereby avoiding ADE without compromising effector functions like ADCC and CDC. ZV54 variants were produced with tailored glycan profiles using plant-based expression systems, such as *Nicotiana benthamiana*, which enabled precise glycovariant control. These modifications allowed ZV54 to retain its Fc-mediated immune clearance capabilities while achieving specific neutralization of ZIKV. Moreover, the antibody was engineered to target a unique epitope on the envelope domain III (EDIII) of the ZIKV, further enhancing its specificity and minimizing off-target effects. This dual optimization, epitope targeting combined with glycoengineering, ensures both safety and efficacy, avoiding the trade-offs associated with LALA mutations.[193]

To better contextualize the therapeutic potential of monoclonal antibodies (mAbs) against orthoflaviviruses, **Table 1** summarizes key characteristics of some antibodies described in the literature and those currently or previously under clinical investigation. The table includes information on the targeted orthoflavivirus, epitope specificity, screening method used for discovery, antibody format, Fc engineering strategies, and clinical status, when available.

## 7. mRNA-Encoded Antibodies: A Novel Therapeutic Approach

The delivery of antibody genes via viral vectors, DNA, or mRNA is an emerging approach that expands the possibilities for exploring monoclonal antibodies. This strategy enables direct in vivo expression, offering a promising alternative to traditional passive transfer, which can be labor-intensive and costly. mRNA vaccine technology represented a revolutionary innovation and played a fundamental role in controlling the SARS-CoV-2 pandemic.[207,208] The success in developing mRNA and RNA-based therapies results from years of research since 1961 when the mRNA molecule was described. Krieg and colleagues (1984) successfully synthesized mRNA in vitro using RNA polymerase SP6, providing the basis for future in vitro studies on mRNA. Naked mRNA exhibits extremely low transfection efficiency because of its inherent negative charge and susceptibility to degradation.[209] Malone and colleagues (1989) overcame this limitation by encapsulating mRNA in cationic lipid vectors, achieving successful in vitro expression in mammalian cells.[210] Subsequently, Wolff and collaborators (1990) demonstrated in vivo protein expression following direct administration

ADVANCED SCIENCE NEWS
www.advancedsciencenews.com

ADVANCED THERAPEUTICS
www.advtherap.com

**Table 1.** Overview of therapeutic antibodies against orthoflaviviruses: discovery methodologies, targets, formats, ade potential and development status.

| Antibody name | Virus | Discovery method | Format | Fc modifications | Target epitope | ADE potential | Development stage | Clinical trial ID/reference |
|---|---|---|---|---|---|---|---|---|
| ZIKV-117 | ZIKV | EBV-transformed B cells + hybridoma | IgG1 | LALA + YTE | DII E-dimer interface (EDE) | No cross-reactivity with DENV or WNV | Preclinical (protected macaques) | [144, 194] |
| C10 | DENV1–4 ZIKV | EBV-transformed B cells + hybridoma | IgG1 | None reported | E-dimer interface (EDE) | No cross-reactivity with ZIKV or WNV | Mouse model | [87, 98, 169] |
| ZV54 | ZIKV | EBV-transformed B cells + hybridoma | IgG1 | None reported | DIII | Minimal cross-reactivity to DENV | Mouse model | [71] |
| E16 | WNV | Hybridoma from immunized mice | IgG1 (murine) | None reported | DIII | Showed ADE at low concentrations | Mouse model | [92] |
| ZV-67 | ZIKV | EBV-transformed B cells + hybridoma | IgG1 | None reported | DIII (lateral ridge) | Minimal cross-reactivity to DENV | Mouse model | [71] |
| MZ4 | ZIKV/DENV2 | Single B cell sorting | IgG1 | LALA | DIII/DI linker region | ADE at low concentrations was eliminated by adding LALA | Mouse model | [111] |
| 2D22 | DENV2 | EBV-transformed B cells + hybridoma | IgG1 | LALA | Quaternary epitope spanning DI (glycan loop), DII (fusion loop), and DIII across E dimers | LALA abolished ADE | Mouse model | [203, 204] |
| 3G9 | DENV1–4, ZIKV, WNV, JEV | B cells from DENV patient (acute secondary infection) → SPYMEG hybridoma technology | IgG1 | LALA (L234A/L235A), D265A, N297A | Fusion Loop | High ADE in vitro with wild-type IgG1; Fc-modified variants abolished ADE while retaining neutralization | Mouse model | [119] |
| VIS513 | DENV1–4 | Structure-guided engineering | Humanized IgG1 | None | DIII A-strand | No ADE | Phase 1 (completed); Phase 2 (ongoing) | [205]; NCT03883620; NCT06551844 |
| AV-1 | DENV3 | Not stated | Not reported | Not stated | Not disclosed | Not reported | Phase 1 (completed); Phase 2 (recruiting) | NCT04273217; NCT06799741 |
| TY014 | Yellow Fever | Not stated | Full IgG | Not stated | Not disclosed | Not reported | Phase 1 (completed) | [206]; NCT03776786 |
| ZKT-001 (Tyzivumab) | Zika | Not stated | Full IgG | Not stated | Not disclosed | Not reported | Phase 1 (completed) | NCT03443830 |

ADVANCED SCIENCE NEWS
www.advancedsciencenews.com

ADVANCED THERAPEUTICS
www.advtherap.com

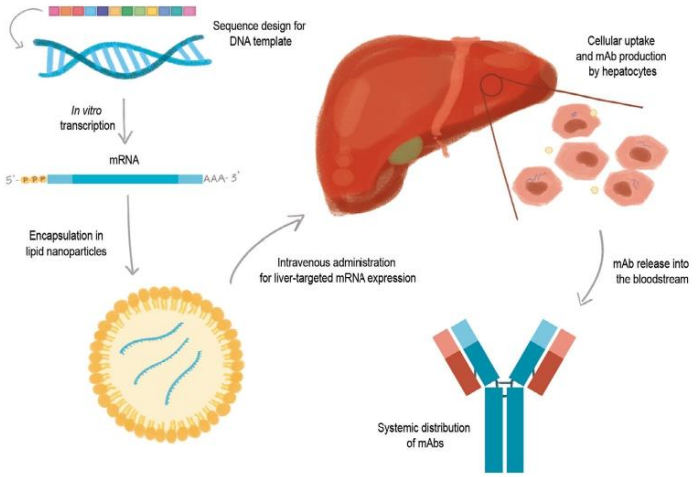


**Figure 4.** Process overview of mRNA-based delivery of monoclonal antibodies (mAbs). First, the DNA template sequence is designed and optimized to be used as a template for in vitro transcription into mRNA. The mRNA contains the mAb coding sequence, the cap structure, and the poly-A tail. Then, mRNA is encapsulated in lipid nanoparticles (LNPs) and administered intravenously. The LNPs target hepatocytes and are internalized via endocytosis. Afterward, the mRNA is translated by ribosomes, and the resulting mAb is post-translationally modified in the endoplasmic reticulum (ER) and the Golgi apparatus. This mechanism results in the secretion and systemic distribution of a fully processed mAb capable of producing therapeutic effects.

of in vitro-transcribed (IVT) mRNA.[211] Later, Karikó and colleagues found that mRNA synthesized using modified uridine could avoid recognition and degradation by the immune system, which greatly improved mRNA stability and immunogenicity in vivo.[212]

The discovery of RNA interference (RNAi) and short interfering RNA (siRNA), and their potential as a treatment for diseases, boosted the study of the composition of lipid nanoparticles (LNP) for RNA delivery.[213] To induce gene silencing, siRNA must be present in the cytosol of cells to form a complex with RNAi and then induce gene silencing in target cells. Certain physicochemical characteristics of the RNA molecule make it unfavorable for in vivo therapies, whether to induce gene silencing, gene expression, or even editing.[214] Characteristics such as its negative charge and size make it difficult for the target cell to capture it. In addition, nucleic acids are subject to degradation by nucleases and can induce immunological responses triggered by PRRs, such as TLR 3, TLR7, and TLR8, RIG-1, and NOD2.[215,216] Therefore, delivery technologies have been investigated to improve cellular internalization of nucleic acids.[213,214,217]

Although naked mRNA can be taken up by different cells, it is generally degraded in the endosomal acidic environment. LNPs have been the most explored strategy for delivering nucleic acids.[218–221] In 2018, Onppattro, an siRNA-based encapsulated drug, was approved by the FDA for the treatment of hereditary transthyretin (hATTR) amyloidosis.[134,220] Onppattro is a siRNA designed to bind to mRNA encoded by the transthyretin (TTR), and the siRNA is delivered by LNPs. Because Onpattro needs to reach the hepatocytes, the size of the LNPs is a relevant factor in their distribution in the liver. Therefore, mRNA-based technologies for in vivo therapies, whether for gene silencing, expression, or editing, have become highly viable, including their use for monoclonal antibody expression.

The mechanism of in vivo antibody expression relies on delivering mRNA encoding the antibody gene to target cells in the liver, requiring intravenous administration (**Figure 4**). However, this route presents a major limitation, as it is both time-consuming and costly.[222] Studies are already underway to make the intramuscular route viable.[223] LNP-encapsulated mRNA enters in the cells by endocytosis. After the endosome is formed, the lipid composition of LNP assists in the evasion of mRNA from the endosome, preventing its lysosomal degradation. When mRNA escapes from the endosome, it becomes available in the cytoplasm, where it can be translated into antibodies by the ribosomes.[222,224]

mRNA-based gene delivery offers an advantage over DNA delivery because it does not require access to the cell nucleus, eliminating the risk of genomic integration.[225] As a transient carrier of genetic information for protein synthesis, mRNA enables rapid expression, with detectable protein production occurring within hours after administration.[218,219]

### 7.1. In Vitro Transcription

To achieve biological functionality, an mRNA molecule must possess several critical elements: a 5′ UTR, a 3′ UTR, an ORF, a 5′ cap structure, and a 3′ poly(A) tail. The 5′ cap and poly(A) tail synergistically regulate both translational efficiency and mRNA stability.[226,227]

Currently, mRNA can be synthesized in vitro using T7 RNA polymerase. For transcription, the template DNA must contain a T7 promoter region.[209] The mRNA generation standard protocol involves using a linearized plasmid as the DNA template. Transcription will occur from the T7 promoter region up to the point where the plasmid has been linearized. The cap can be added enzymatically after transcription or simultaneously. There are two widely used technologies to add the Cap during transcription: CleanCap (TriLink Biotechnologies, San Diego, CA, USA) and ARCA.[228–230] CleanCap is a trinucleotide (GAG) that binds to the T7 promoter region through base complementarity, with guanosine methylated at position 7 (7-methyl-guanosine). The cap undergoes a second methylation on the ribose of the first nucleotide at the 2′ position, called CAP-1. CAP-1 is important in evading the cellular innate immune response in vivo.[231] Another method for capping mRNA during in vitro transcription is the use of anti-reverse cap analog (ARCA).[228] ARCA is a modified cap analog that enables the addition of Cap-0, which lacks a methyl group at the 2′ position of the first nucleotide. In ARCA, the 3′-OH group closest to 7-methylguanosine is replaced by a methyl group, forcing T7 RNA polymerase to incorporate the cap in the correct orientation using the 5′-hydroxyl group. Cap-0 can then be enzymatically converted into Cap-1 using 2′-O-methyltransferase (2′-O-MTase), improving mRNA stability and translational efficiency.[228–230]

### 7.2. Modifications to mRNA

In vitro-transcribed mRNA can trigger an innate immune response as it can be recognized as pathogen-associated molecular patterns (PAMPs). This activation can be beneficial in vaccination by acting as an adjuvant.[232] However, for therapeutic purposes, it also reduces protein expression, potentially lowering antibody levels.[233] Kariko showed that incorporating chemically modified nucleosides can prevent innate immune activation.[234] Modified nucleosides such as pseudouridine, thiouridine (s2U), and 5-methylcytidine (m5C) have been shown to reduce mRNA immunogenicity, while also enhancing its stability and translation efficiency.[234,235] Notably, N1-methylpseudouridine was used in the mRNA-1273 and BNT162b2 COVID-19 vaccines.

### 7.3. Lipid Nanoparticles (LNPs)

Various delivery technologies have been explored to enhance cellular uptake, protect RNA from degradation, and minimize immune activation, thereby improving its therapeutic potential. Therefore, LNPs have demonstrated great utility in the delivery of mRNA therapies. One of the most important factors regarding LNPs, besides lipid composition, is particle size. The particle size could affect the biodistribution and uptake.[236] For intravenous administration, several studies have shown that LNPs tend to accumulate in the liver and spleen cells.[237,238] The size of LNPs is a relevant factor in their distribution in the liver, and particles larger than 100 nm are not able to access hepatocytes as they are close in size to the liver fenestrae. For subcutaneous administration, smaller particles have shown better results because they are able to be absorbed by the lymphatic vessels and capillaries.[214]

Lipid formulations for nucleic acid encapsulation consist of four key components: ionizable lipids, PEGylated lipids, helper phospholipids, and cholesterol.[239,240] Ionizable lipids are composed of three main elements: an ionizable head group, a linker region, and hydrocarbon chains. The ionizable head group, typically containing tertiary amines, remains uncharged at neutral pH but becomes protonated in acidic environments, facilitating endosomal escape. The linker region connects the head group to the lipid tail, which enhances the molecule's hydrophobicity and promotes efficient incorporation into nanoparticles during formulation. Protonated lipids form structures that enhance membrane fusion within acidified endosomes, promoting efficient mRNA release after cellular uptake. LNPs are formulated in acidic buffers to ensure protonation of tertiary amines, which facilitates interaction with anionic nucleic acids and endosomal escape by the mRNA.[241]

Polyethylene glycol (PEG) is primarily located on the surface of LNPs, where its concentration plays a key role in controlling particle size. Additionally, PEG enhances storage stability by preventing particle aggregation and extending circulation time in vivo.[242] Helper phospholipids, which are amphiphilic in nature, contribute to maintaining the integrity of the lipid bilayer. Both phospholipids and cholesterol are essential for stabilizing the formulation, with cholesterol further facilitating fusion with endosomal membranes, thereby improving the efficiency of intracellular delivery.[239]

### 7.4. mRNA-Encoded Antibodies against Infections Caused by Viruses

Following the advent of scalable IVT mRNA production, numerous studies have demonstrated successful in vivo antibody expression via LNP-encapsulated mRNA delivery. Pardi et al. (2017) showed the expression of the antibody VRC01, a neutralizing anti-HIV-1 antibody.[218] A single dose from mRNA-LNPs encoding the heavy and light chains of the VRC01 mAb was administered in BALB/c. A peak of expression of VRC01 was detected 24 h after the injection, and the antibody remained detectable for 11 days after injection. The delivery of mRNA-LNPs encoding VRC01 was able to protect animals from HIV-1 viral challenge. Two weeks after the challenge with the SF162 HIV-1, the viral levels in the plasma of mice were measured by qRT–PCR. Viral RNA was detected only in the groups that received the lowest dose of mRNA and in the control, showing the protection of intravenous administration of VRC01 encoded mRNA.

Kose et al. (2019) showed the expression of a human mAb (CHKV-24 mAb) against chikungunya virus (CHIKV) after intravenous administration of its mRNA encapsulated in LNPs.[219] They showed that delivery of mRNA-LNPs encoding CHKV-24 mAb could protect animals from CHIKV viral challenge. AG129 mice were treated by the intravenous route with a single administration of CHKV-24–encoding mRNA. Complete survival of mice was observed after treatment with the highest dose of CHKV-24 mRNA. They also showed the expression of the CHKV-24 mAb in cynomolgus macaques. The intravenous administration of CHKV-24 mRNA in macaques achieved a maximal mAb concentration of 10.1 to 35.9 μg $mL^{-1}$ and a half-life of 23 days. August et al. (2021) conducted a phase 1 clin-

ical trial (NCT03829384) which was a randomized, placebo-controlled, dose-escalation study in healthy adults.[243] This was the first clinical trial of an mRNA-encoded antibody.[224,244] The clinical trial showed that CHKV-24 IgG expression reached therapeutically relevant serum concentrations with a half-life of 69 days.

In the context of orthoflavivirus infections, Erasmus et al. (2020) developed a self-amplifying mRNA (SAM) platform encoding ZIKV-117, a potent neutralizing monoclonal antibody (mAb) against ZIKV.[223] The SAM construct was engineered by inserting the replicon machinery of Venezuelan equine encephalitis virus (VEEV) downstream of the antibody sequence, generating a replicon RNA (RepRNA). This RepRNA platform demonstrated significantly higher serum antibody titers compared to conventional non-replicating mRNA. To evaluate the protective efficacy of ZIKV-117 RepRNA, the researchers employed a lethal ZIKV challenge model in C57BL/6 mice, where viral lethality was induced through the combined administration of a ZIKV strain and anti-IFNAR1 blocking antibody. Serum analysis 24 h post-challenge with ZIKV revealed complete protection against detectable viremia (quantified by qRT-PCR) and 100% survival in the ZIKV-117 RepRNA group. This study establishes a novel mRNA-based approach for in vivo mAb delivery through intramuscular administration.

These findings highlight the promising therapeutic potential of this platform for infectious diseases, particularly orthoflavivirus infections such as ZIKV. ZIKV is associated with severe clinical outcomes, including congenital Zika syndrome (CZS) and Guillain–Barré syndrome (GBS). Notably, the rapid expression of protective antibodies, within 24 h, supports the use of this approach for early intervention and treatment in infected individuals.

## 8. Conclusions and Future Perspectives

The development of antibody therapies against orthoflaviviruses has advanced significantly with the refinement of technologies for antibody discovery and selection. Platforms such as phage display, yeast and mammalian cell display, and single B cell screening have enabled the isolation of human monoclonal antibodies with high specificity, cross-reactivity, and neutralizing potential. These methods have been particularly valuable in identifying antibodies that target conserved epitopes and in guiding the design of molecules less susceptible to escape and enhancement. The availability of such tools now allows for a more rational and targeted approach to therapeutic antibody generation, even in the face of viral diversity and immune evasion.

Among the antigenic targets explored, both domain III and the fusion loop of the envelope protein offer relevant possibilities. DIII is a well-defined epitope associated with potent, often type-specific neutralization, but its variability and susceptibility to escape mutations pose challenges for broad application. The FL, on the other hand, is highly conserved and functionally essential across orthoflaviviruses, making it a promising target for cross-neutralizing antibodies. However, its limited surface accessibility on mature virions and the potential association with ADE require careful validation. Rather than focusing on a single epitope, current strategies favor combining antibodies that target multiple regions, such as the FL, DIII, and quaternary structures like the envelope dimer epitope (EDE), to improve breadth and reduce the risk of viral escape.

In addition to epitope selection, engineering approaches are essential for improving antibody performance and safety. Fc modifications, including LALA and YTE mutations, glycoengineering, and modulation of glycosylation profiles, can regulate effector functions, extend half-life, and help prevent ADE. The use of IgG2 or IgG4 subclasses has also shown potential to reduce Fc$\gamma$R-mediated enhancement while preserving therapeutic activity. These tools allow fine-tuning of antibody properties for the specific context of orthoflavivirus infection.

mRNA-based antibody delivery is an emerging strategy that offers a promising alternative to conventional passive immunization. By enabling in vivo expression of therapeutic antibodies, this platform bypasses the need for large-scale protein production. In the context of orthoflaviviruses, this approach holds particular appeal for rapid deployment during outbreaks. Future research must address the optimization of expression kinetics, tissue targeting, and formulation strategies that minimize immunogenicity and maximize bioavailability. As delivery systems evolve and regulatory experience with mRNA-based therapies expands, this platform may become a central component in the next generation of antibody interventions against emerging arboviruses.

Reducing the cost of antibody-based therapeutics remains a key challenge for their widespread use, particularly in endemic regions with limited manufacturing capacity. Several emerging strategies may help overcome this limitation. Microbial expression platforms have emerged as transformative alternatives, offering cost-effectiveness, rapid cultivation cycles, and high genetic tractability for large-scale monoclonal antibody production.[245] Recent advances in CRISPR/Cas9-mediated gene editing now enable precise metabolic engineering of microbial hosts to enhance protein folding, secretion efficiency, and translational accuracy. Synthetic biology approaches further allow the reconstruction of mammalian glycosylation pathways in microbial systems, yielding antibodies with near-native structural integrity.[245] Notably, the successful development of Caplacizumab (Cablivi), a nanobody for aTTP treatment produced in *E. coli*, demonstrates the clinical feasibility of these systems and highlights the potential of rational host engineering for biopharmaceutical production.[246] In parallel, Fc-engineering approaches that extend antibody half-life can decrease both the dose and frequency required for therapeutic efficacy. Notably, mRNA-encoded antibody delivery, discussed in Section 7, represents a transformative alternative by enabling in vivo antibody synthesis without the need for conventional bioreactor production or cold-chain logistics. Together, these advances represent a shift toward more accessible, scalable, and costless antibody therapeutics, with the potential to democratize orthoflavivirus treatment and prevention in resource-limited settings.

Altogether, the development of antibody therapies against orthoflaviviruses increasingly relies on integrating strategies that combine antigenic precision, functional optimization, and adaptable delivery platforms. Future advances will likely depend not on a single solution, but on the thoughtful combination of these complementary approaches to produce safe and broadly effective interventions.

## Acknowledgements

The authors would like to acknowledge the Coordenação de Aperfeiçoamento de Pessoal de Nível Superior – Brasil (CAPES) for financial support (Finance Code 001) and the Fundação de Apoio à Pesquisa do Distrito Federal (FAP-DF) for additional funding (grant number 00193-00001263/2021-12).

The Article Processing Charge for the publication of this research was funded by the Coordenacao de Aperfeicoamento de Pessoal de Nivel Superior - Brasil (CAPES) (ROR identifier: 00x0ma614).

## Conflict of Interest

The authors declare no conflict of interest.

## Author Contributions

A.C.B.A., L.S.R., M.C.M.P.—reviewed the literature and wrote the original draft. A.C.B.A., S.B.P., and M.M.B. dealt with data analysis and figure constructions. A.C.B.A. and A.Q.M. dealt with editing. A.Q.M. and M.M.B. dealt with reviewing. All authors have read and agreed to the published version of the manuscript.

## Data Availability Statement

This review did not generate new data. Sequence alignments were based on publicly available flavivirus reference sequences.

## Keywords

display technologies, Fc engineering, fusion loops, monoclonal antibodies, mRNA, orthoflaviviruses

Received: August 25, 2025
Revised: October 21, 2025
Published online:

[1] B. D. Lindenbach, C. M. Rice, *Adv. Virus Res.* **2003**, *59*, 23.
[2] P. Ts, M. Beer, B. J. Blitvich, J. Bukh, X. Lamballerie, J. F. Drexler, A. Imrie, A. Kapoor, G. G. Karganova, P. Lemey, V. Lohmann, P. Simmonds, D. B. Smith, J. T. Stapleton, J. H. Kuhn, *Arch. Virol.* **2023**, *168*, 224.
[3] M. L. Barjas-Castro, R. N. Angerami, M. S. Cunha, A. Suzuki, J. S. Nogueira, I. M. Rocco, A. Y. Maeda, F. G. S. Vasami, G. Katz, I. F. S. F. Boin, R. S. B. Stucchi, M. R. Resende, D. L. A. Esposito, R. P. de Souza, B. A. da Fonseca, M. Addas-Carvalho, *Transfusion* **2016**, *56*, 1684.
[4] G. Calvet, R. S. Aguiar, A. S. O. Melo, S. A. Sampaio, I. de Filippis, A. Fabri, E. S. M. Araujo, P. C. de Sequeira, M. C. L. de Mendonça, L. de Oliveira, D. A. Tschoeke, C. G. Schrago, F. L. Thompson, P. Brasil, F. B. dos Santos, R. M. R. Nogueira, A. Tanuri, A. M. B. de Filippis, *Lancet Infect. Dis.* **2016**, *16*, 653.
[5] L. D. Kramer, L. M. Styer, G. D. Ebel, *Annu. Rev. Entomol.* **2008**, *53*, 61.
[6] L. R. Petersen, A. A. Marfin, *J. Travel Med.* **2005**, *12*, S3.
[7] A. F. van den Hurk, S. A. Ritchie, J. S. Mackenzie, *Annu. Rev. Entomol.* **2009**, *54*, 17.
[8] D. Dey, S. Poudyal, A. Rehman, S. S. Hasan, *Virus Res.* **2021**, *296*, 198343.
[9] T. C. Pierson, M. S. Diamond, *Nat. Microbiol.* **2020**, *5*, 796.
[10] J. Guarner, G. L. Hale, *Semin. Diagn. Pathol.* **2019**, *36*, 170.
[11] A. Higuera, J. D. Ramírez, *Acta Trop.* **2019**, *190*, 99.
[12] J. K. Lim, C. Y. Louie, C. Glaser, C. Jean, B. Johnson, H. Johnson, D. H. McDermott, P. M. Murphy, *J. Infect. Dis.* **2008**, *197*, 262.
[13] H. Loke, D. Bethell, C. X. T. Phuong, N. Day, N. White, J. Farrar, A. Hill, *Am. J. Trop. Med. Hyg.* **2002**, *67*, 102.
[14] K. Murray, S. Baraniuk, M. Resnick, R. Arafat, C. Kilborn, K. Cain, R. Shallenberger, T. L. York, D. Martinez, J. S. Hellums, D. Hellums, M. Malkoff, N. Elgawley, W. McNeely, S. A. Khuwaja, R. B. Tesh, *Epidemiol. Infect.* **2006**, *134*, 1325.
[15] T. P. Monath, P. F. C. Vasconcelos, *J. Clin. Virol.* **2015**, *64*, 160.
[16] X. Pang, R. Zhang, G. Cheng, *Virol. Sin.* **2017**, *32*, 16.
[17] H.-Y. Chen, C.-Y. Yang, C.-Y. Hsieh, C.-Y. Yeh, C.-C. Chen, Y.-C. Chen, C.-C. Lai, R. C. Harris, H.-T. Ou, N.-Y. Ko, W.-C. Ko, *PLoS Negl. Trop. Dis.* **2021**, *15*, 0009703.
[18] A. S. Oliveira Melo, G. Malinger, R. Ximenes, P. O. Szejnfeld, S. A. Sampaio, A. M. Bispo de Filippis, *Ultrasound Obstet. Gynecol.* **2016**, *47*, 6.
[19] J. Hart, G. Tillman, M. A. Kraut, H.-S. Chiang, J. F. Strain, Y. Li, A. G. Agrawal, P. Jester, J. W. Gnann, R. J. Whitley, the NIAID Collaborative Antiviral Study Group West Nile Virus 210 Protocol Team, *BMC Infect. Dis.* **2014**, *14*, 248.
[20] D. Musso, E. J. Nilles, V.-M. Cao-Lormeau, *Clin. Microbiol. Infect.* **2014**, *20*, O595.
[21] *Centers for Disease Control and Prevention*, https://www.cdc.gov/zika/healtheffects/birth_defects.html, **2019**,(accessed: April, 2025).
[22] A. Créange, *Rev. Neurol.* **2016**, *172*, 770.
[23] M. G. Guzman, E. Harris, *Lancet* **2015**, *385*, 453.
[24] A. Tayal, S. K. Kabra, R. Lodha, *Indian J. Pediatr.* **2023**, *90*, 168.
[25] S. Trivedi, A. Chakravarty, *Curr. Neurol. Neurosci. Rep.* **2022**, *22*, 515.
[26] W. Leowattana, T. Leowattana, *World J. Hepatol.* **1968**, *13*, 1968.
[27] T. P. Monath, A. D. Barrett, *Adv. Virus Res.* **2003**, *60*, 343.
[28] J. A. S. Quaresma, C. Pagliari, D. B. A. Medeiros, M. I. S. Duarte, P. F. C. Vasconcelos, *Rev. Med. Virol.* **2013**, *23*, 305.
[29] J. A. S. Quaresma, M. I. S. Duarte, P. F. C. Vasconcelos, *Med. Hypotheses* **2006**, *67*, 618.
[30] P. Chugh, S. Soni, N. Ghanghas, S. Kumar, H. Mohan, *Antiviral Res.* **2025**, *243*, 106268.
[31] S. A. Fuertes Marraco, C. Soneson, L. Cagnon, P. O. Gannon, M. Allard, S. A. Maillard, N. Montandon, N. Rufer, S. Waldvogel, M. Delorenzi, D. E. Speiser, *Sci. Transl. Med.* **2015**, *7*.
[32] L. Rivera, S. Biswal, X. Sáez-Llorens, H. Reynales, E. López-Medina, C. Borja-Tabora, L. Bravo, C. Sirivichayakul, P. Kosalaraksa, L. Martinez Vargas, D. Yu, V. Watanaveeradej, F. Espinoza, R. Dietze, L. Fernando, P. Wickramasinghe, E. Duarte MoreiraJr, A. D. Fernando, D. Gunasekera, K. Luz, R. Venâncioda Cunha, M. Rauscher, O. Zent, M. Liu, E. Hoffman, I. LeFevre, V. Tricou, D. Wallace, M. Alera, A. Borkowski, *Clin. Infect. Dis.* **2022**, *75*, 107.
[33] D. Gaucher, R. ?. Therrien, N. Kettaf, B. R. Angermann, G.'V. Boucher, A. Filali-Mouhim, J. M. Moser, R. S. Mehta, D. R. Drake, E. Castro, R. Akondy, A. Rinfret, B. Yassine-Diab, E. A. Said, Y. Chouikh, M. J. Cameron, R. Clum, D. Kelvin, R. Somogyi, L. D. Greller, R. S. Balderas, P. Wilkinson, G. Pantaleo, J. Tartaglia, E. K. Haddad, R.-P. Sékaly, *J. Exp. Med.* **2008**, *205*, 3119.
[34] J. V. J. Silva, T. R. R. Lopes, E. F. D. Oliveira-Filho, R. A. S. Oliveira, R. Durães-Carvalho, L. H. V. G. Gil, *Acta Trop.* **2018**, *182*, 257.
[35] H. H. Askling, D. Zavadska, *Acta Paediatr.* **2025**, *16*, https://doi.org/10.1111/apa.70280.
[36] T. Akaishi, I. Nakashima, *Int. Immunol.* **2017**, *29*, 327.
[37] G. Köhler, C. Milstein, *Nature* **1975**, *256*, 495.
[38] F. A. Harding, M. M. Stickler, J. Razo, R. DuBridge, *mAbs* **2010**, *2*, 256.
[39] A. Casadevall, L. Pirofski, M. J. Joyner, *mBio* **2021**, *12*, 03372.

[40] G. Salazar, N. Zhang, T.-M. Fu, Z. An, *Npj Vaccines* **2017**, *2*, 19.
[41] K. Kansagra, D. Parmar, S. K. Mendiratta, J. Patel, S. Joshi, N. Sharma, A. Parihar, S. Bhoge, H. Patel, P. Kalita, R. Munshi, P. Kurmi, R. Shah, A. Gupta, H. Bhalla, H. Bekkalele, R. Verma, D. Agarwal, S. Sharma, A. Gawande, G. Chhaya, *Clin. Infect. Dis.* **2021**, *73*, 2722.
[42] A. C. Chan, P. J. Carter, *Nat. Rev. Immunol.* **2010**, *10*, 301.
[43] W. D. Crill, G.-J. J. Chang, *J. Virol.* **2004**, *78*, 13975.
[44] T. C. Pierson, D. H. Fremont, R. J. Kuhn, M. S. Diamond, *Cell Host Microbe* **2008**, *4*, 229.
[45] G. E. Nybakken, T. Oliphant, S. Johnson, S. Burke, M. S. Diamond, D. H. Fremont, *Nature* **2005**, *437*, 764.
[46] J. A. Winkelstein, *J. Pediatr.* **1973**, *82*, 747.
[47] "Physiology, Opsonization," in StatPearls, Treasure Island (FL): StatPearls Publishing, 2025, http://www.ncbi.nlm.nih.gov/books/NBK534215/, Accessed: Aug. 18, **2025**.
[48] D. N. Forthal, A. Finzi, *AIDS* **2018**, *32*, 2439.
[49] L. Yu, X. Liu, X. Ye, W. Su, X. Zhang, W. Deng, J. Luo, M. Xiang, W. Guo, S. Zhang, W. Xu, Q. Yan, Q. Wang, Y. Cui, C. Wu, W. Guo, X. Niu, F. Zhang, C. Lei, L. Qu, L. Chen, L. Feng, *mBio* **2021**, *12*, 03179.
[50] R. Kraivong, *Viruses* **2025**, *17*, 1226.
[51] F. R. Brennan, J. R. Polli, J. Sathish, M. Ramones, B. Wolf, T. Schlothauer, S. J. Peters, C. C. Maier, C. Ji, D. L. Wensel, D. Witcher, P. C. Ryan, T. S. Manetz, A. Flora, B. Soper, B. Fogal, L. Dzielak, X. Wang, P. N. Shastri, K. Price, M. Doyle, N. Sharda, M. Struthers, M. Brinkhaus, B. Balbino, E. Stefanich, M. Honda, J. T. Andersen, S. Mitchell-Ryan, D. P. Humphreys, *mAbs* **2025**, *17*, 2505092.
[52] K. M. Chung, B. S. Thompson, D. H. Fremont, M. S. Diamond, *J. Virol.* **2007**, *81*, 9551.
[53] A. W. Wessel, N. Kose, R. G. Bombardi, V. Roy, W. Chantima, J. Mongkolsapaya, M. A. Edeling, C. A. Nelson, I. Bosch, G. Alter, G. R. Screaton, D. H. Fremont, J. E. Crowe, M. S. Diamond, *Nat. Commun.* **2020**, *11*, 5278.
[54] S. B. Halstead, H. Shotwell, J. Casals, *J. Infect. Dis.* **1973**, *128*, 15.
[55] M. G. Guzman, M. Alvarez, S. B. Halstead, *Arch. Virol.* **2013**, *158*, 1445.
[56] R. Kulkarni, in *Dynamics of Immune Activation in Viral Diseases*, Springer Singapure, **2020**, pp. 9–41.
[57] S. V. Bardina, P. Bunduc, S. Tripathi, J. Duehr, J. J. Frere, J. A. Brown, R. Nachbagauer, G. A. Foster, D. Krysztof, D. Tortorella, S. L. Stramer, A. García-Sastre, F. Krammer, J. K. Lim, *Science* **2017**, *356*, 175.
[58] P. M. Castanha, E. J. M. Nascimento, C. Braga, M. T. Cordeiro, O. V. Carvalho, L. R. Mendonca, E. A. N. Azevedo, R. F. O. França, R. Dhalia, E. T. A. Marques, *J. Infect. Dis.* **2017**, *215*, 781.
[59] J. George, W. G. Valiant, M. J. Mattapallil, M. Walker, Y.-J. S. Huang, D. L. Vanlandingham, J. Misamore, J. Greenhouse, D. E. Weiss, D. Verthelyi, S. Higgs, H. Andersen, M. G. Lewis, J. J. Mattapallil, *Sci. Rep.* **2017**, *7*, 10498.
[60] L. Priyamvada, K. M. Quicke, W. H. Hudson, N. Onlamoon, J. Sewatanon, S. Edupuganti, K. Pattanapanyasat, K. Chokephaibulkit, M. J. Mulligan, P. C. Wilson, R. Ahmed, M. S. Suthar, J. Wrammert, *Proc. Natl. Acad. Sci. U. S. A.* **2016**, *113*, 7852.
[61] P. Pantoja, E. X. Pérez-Guzmán, I. V. Rodríguez, L. J. White, O. González, C. Serrano, L. Giavedoni, V. Hodara, L. Cruz, T. Arana, M. I. Martínez, M. A. Hassert, J. D. Brien, A. K. Pinto, A. de Silva, C. A. Sariol, *Nat. Commun.* **2017**, *8*, 15674.
[62] C. A. Sariol, M. L. Nogueira, N. Vasilakis, *Trends Microbiol.* **2018**, *26*, 186.
[63] A. C. B. Terzian, A. S. Schanoski, M. T. D. O. Mota, R. A. da Silva, C. F. Estofolete, T. E. Colombo, P. Rahal, K. A. Hanley, N. Vasilakis, J. Kalil, M. L. Nogueira, *Clin. Infect. Dis.* **2017**, *65*, 1260.
[64] D. Corti, A. Lanzavecchia, *Annu. Rev. Immunol.* **2013**, *31*, 705.
[65] M. P. Doyle, J. R. Genualdi, A. L. Bailey, N. Kose, C. Gainza, J. Rodriguez, K. M. Reeder, C. A. Nelson, P. N. Jethva, R. E. Sutton, R. G. Bombardi, M. L. Gross, J. G. Julander, D. H. Fremont, M. S. Diamond, J. E. Crowe, *mBio* **2022**, *13*, 0051222.
[66] D. Haslwanter, M. E. Dieterle, A. Z. Wec, C. M. O'Brien, M. Sakharkar, C. Florez, K. Tong, C. G. Rappazzo, G. Lasso, O. Vergnolle, A. S. Wirchnianski, R. H. Bortz, E. Laudermilch, J. M. Fels, A. Mengotto, R. J. Malonis, G. I. Georgiev, J. A. Quiroz, D. Wrapp, N. Wang, K. E. Dye, J. Barnhill, J. M. Dye, J. S. McLellan, J. P. Daily, J. R. Lai, A. S. Herbert, L. M. Walker, K. Chandran, R. K. Jangra, *mBio* **2021**, *12*, 02473.
[67] L. M. Walker, M. Huber, K. J. Doores, E. Falkowska, R. Pejchal, J.-P. Julien, S.-K. Wang, A. Ramos, P.-Y. Chan-Hui, M. Moyle, J. L. Mitcham, P. W. Hammond, O. A. Olsen, P. Phung, S. Fling, C.-H. Wong, S. Phogat, T. Wrin, M. D. Simek, P. G. Principal Investigators, W. C. Koff, I. A. Wilson, D. R. Burton, P. Poignard, *Nature* **2011**, *477*, 466.
[68] M. Sevvana, T. F. Rogers, A. S. Miller, F. Long, T. Klose, N. Beutler, Y.-C. Lai, M. Parren, L. M. Walker, G. Buda, D. R. Burton, M. G. Rossmann, R. J. Kuhn, *Viruses* **2020**, *12*, 1346.
[69] R. J. Kuhn, A. D. T. Barrett, A. M. Desilva, E. Harris, L. D. Kramer, R. R. Montgomery, T. C. Pierson, A. Sette, M. S. Diamond, *J. Infect. Dis.* **2023**, *228*, S398.
[70] V. Dussupt, K. Modjarrad, S. J. Krebs, *Front. Immunol.* **2020**, *11*, 621043.
[71] H. Zhao, E. Fernandez, K. A. Dowd, S. D. Speer, D. J. Platt, M. J. Gorman, J. Govero, C. A. Nelson, T. C. Pierson, M. S. Diamond, D. H. Fremont, *Cell* **2016**, *166*, 1016.
[72] W. Dejnirattisai, W. Wongwiwat, S. Supasa, X. Zhang, X. Dai, A. Rouvinski, A. Jumnainsong, C. Edwards, N. T. H. Quyen, T. Duangchinda, J. M. Grimes, W.-Y. Tsai, C.-Y. Lai, W.-K. Wang, P. Malasit, J. Farrar, C. P. Simmons, Z. H. Zhou, F. A. Rey, J. Mongkolsapaya, G. R. Screaton, *Nat. Immunol.* **2015**, *16*, 170.
[73] J. Ye, Z. Chen, Y. Li, Z. Zhao, W. He, A. Zohaib, Y. Song, C. Deng, B. Zhang, H. Chen, S. Cao, *J. Virol.* **2017**, *91*, 00039.
[74] M. U. Gack, M. S. Diamond, *Curr. Opin. Virol.* **2016**, *20*, 119.
[75] L. Miorin, A. M. Maestre, A. Fernandez-Sesma, A. García-Sastre, *Biochem. Biophys. Res. Commun.* **2017**, *492*, 587.
[76] L. Uchida, L. A. Espada-Murao, Y. Takamatsu, K. Okamoto, D. Hayasaka, F. Yu, T. Nabeshima, C. C. Buerano, K. Morita, *Sci. Rep.* **2014**, *4*, 7395.
[77] L. J. Lee, T. V. Komarasamy, N. A. A. Adnan, W. James, V. R. Balasubramaniam, *Front. Immunol.* **2021**, *12*, 750365.
[78] A. Glasner, E. Oiknine-Djian, Y. Weisblum, M. Diab, A. Panet, D. G. Wolf, O. Mandelboim, *J. Virol.* **2017**, *91*, 00785.
[79] R. Kraivong, N. Punyadee, M. K. Liszewski, J. P. Atkinson, P. Avirutnan, *Viruses* **2021**, *13*, 1219.
[80] A. L. C. Valadão, R. S. Aguiar, L. B. de Arruda, *Front. Microbiol.* **2016**, *7*, 1233.
[81] K. A. Dowd, C. R. DeMaso, T. C. Pierson, *mBio* **2015**, *6*, 01559.
[82] R. J. Kuhn, K. A. Dowd, C. B. Post, T. C. Pierson, *Virology* **2015**, *479–480*, 508.
[83] F. A. Rey, K. Stiasny, F. X. Heinz, *Curr. Opin. Virol.* **2017**, *24*, 132.
[84] K. A. Dowd, T. C. Pierson, *Annu. Rev. Virol.* **2018**, *5*, 185.
[85] L. Goo, L. A. VanBlargan, K. A. Dowd, M. S. Diamond, T. C. Pierson, *PLoS Pathog.* **2017**, *13*, 1006178.
[86] D. Haslwanter, D. Blaas, F. X. Heinz, K. Stiasny, *PLoS Pathog.* **2017**, *13*, 1006643.
[87] A. Sharma, X. Zhang, W. Dejnirattisai, X. Dai, D. Gong, W. Wongwiwat, S. Duquerroy, A. Rouvinski, M.-C. Vaney, P. Guardado-Calvo, A. Haouz, P. England, R. Sun, Z. H. Zhou, J. Mongkolsapaya, G. R. Screaton, F. A. Rey, *Cell* **2021**, *184*, 6052 .
[88] K. Stadler, S. L. Allison, J. Schalich, F. X. Heinz, *J. Virol.* **1997**, *71*, 8475.

[89] T. C. Pierson, M. S. Diamond, *Curr. Opin. Virol.* **2012**, *2*, 168.
[90] Combined Effects of the Structural Heterogeneity and Dynamics of Flaviviruses on Antibody Recognition-PMC, https://pmc.ncbi.nlm.nih.gov/articles/PMC4178732/, Accessed: Aug. 18, **2025**.
[91] I. A. Rodenhuis-Zybert, H. M. van der Schaar, J. M. da Silva Voorham, H. van der Ende-Metselaar, H.-Y. Lei, J. Wilschut, J. M. Smit, *PLoS Pathog.* **2010**, *6*, 1000718.
[92] T. Oliphant, G. E. Nybakken, M. Engle, Q. Xu, C. A. Nelson, S. Sukupolvi-Petty, A. Marri, B.-E. Lachmi, U. Olshevsky, D. H. Fremont, T. C. Pierson, M. S. Diamond, *J. Virol.* **2006**, *80*, 12149.
[93] G. Barba-Spaeth, W. Dejnirattisai, A. Rouvinski, M.-C. Vaney, I. Medits, A. Sharma, E. Simon-Lorière, A. Sakuntabhai, V.-M. Cao-Lormeau, A. Haouz, P. England, K. Stiasny, J. Mongkolsapaya, F. X. Heinz, G. R. Screaton, F. A. Rey, *Nature* **2016**, *536*, 48.
[94] A. Rouvinski, W. Dejnirattisai, P. Guardado-Calvo, M.-C. Vaney, A. Sharma, S. Duquerroy, P. Supasa, W. Wongwiwat, A. Haouz, G. Barba-Spaeth, J. Mongkolsapaya, F. A. Rey, G. R. Screaton, *Nat. Commun.* **2017**, *8*, 15411.
[95] R. K. A. D. O. França, J. M. Silva, L. S. Rodrigues, D. Sokolowskei, M. M. Brigido, A. Q. Maranhão, *Int. J. Mol. Sci.* **2022**, *23*, 7805.
[96] A. E. Ngono, S. Shresta, *Annu. Rev. Immunol.* **2018**, *36*, 279.
[97] J. L. Slon Campos, J. Mongkolsapaya, G. R. Screaton, *Nat. Immunol.* **2018**, *19*, 1189.
[98] A. Rouvinski, P. Guardado-Calvo, G. Barba-Spaeth, S. Duquerroy, M.-C. Vaney, C. M. Kikuti, M. E. Navarro Sanchez, W. Dejnirattisai, W. Wongwiwat, A. Haouz, C. Girard-Blanc, S. Petres, W. E. Shepard, P. Desprès, F. Arenzana-Seisdedos, P. Dussart, J. Mongkolsapaya, G. R. Screaton, F. A. Rey, *Nature* **2015**, *520*, 109.
[99] R. J. Kuhn, W. Zhang, M. G. Rossmann, S. V. Pletnev, J. Corver, E. Lenches, C. T. Jones, S. Mukhopadhyay, P. R. Chipman, E. G. Strauss, T. S. Baker, J. H. Strauss, *Cell* **2002**, *108*, 717.
[100] S. Halstead, *F1000Research* **2019**, *8*, 1279.
[101] E. C. Meng, T. D. Goddard, E. F. Pettersen, G. S. Couch, Z. J. Pearson, J. H. Morris, T. E. Ferrin, *Protein Sci. Publ. Protein Soc.* **2023**, *32*, 4792.
[102] K. Okonechnikov, O. Golosova, M. Fursov, U. G. E. N. E. team, *Bioinformatics* **2012**, *28*, 1166.
[103] X. Zhang, R. Jia, H. Shen, M. Wang, Z. Yin, A. Cheng, *Viruses* **2017**, *9*, 338.
[104] R. S. Sankhala, V. Dussupt, G. Donofrio, G. D. Gromowski, R. A. De La Barrera, R. A. Larocca, L. Mendez-Rivera, A. Lee, M. Choe, W. Zaky, G. Mantus, J. L. Jensen, W.-H. Chen, N. Gohain, H. Bai, M. K. McCracken, R. D. Mason, D. Leggat, B. M. Slike, U. Tran, N. Jian, P. Abbink, R. Peterson, E. A. Mendes, R. Freitas de Oliveira Franca, G. A. Calvet, A. M. Bispo de Filippis, A. McDermott, M. Roederer, M. Hernandez, et al., *Cell Rep.* **2023**, *42*, 112942.
[105] E. N. Gallichotte, E. F. Young, T. J. Baric, B. L. Yount, S. W. Metz, M. C. Begley, A. M. de Silva, R. S. Baric, *mBio* **2019**, *10*, 01485.
[106] D. M. Magnani, T. F. Rogers, N. Beutler, M. J. Ricciardi, V. K. Bailey, L. Gonzalez-Nieto, B. Briney, D. Sok, K. Le, A. Strubel, M. J. Gutman, N. Pedreño-Lopez, N. D. Grubaugh, C. G. T. Silveira, H. S. Maxwell, A. Domingues, M. A. Martins, D. E. Lee, E. E. Okwuazi, S. Jean, E. A. Strobert, A. Chahroudi, G. Silvestri, T. H. Vanderford, E. G. Kallas, R. C. Desrosiers, M. C. Bonaldo, S. S. Whitehead, D. R. Burton, D. I. Watkins, *Sci. Transl. Med.* **2017**, *9*, aan8184.
[107] D. F. Robbiani, L. Bozzacco, J. R. Keeffe, R. Khouri, P. C. Olsen, A. Gazumyan, D. Schaefer-Babajew, S. Avila-Rios, L. Nogueira, R. Patel, S. A. Azzopardi, L. F. K. Uhl, M. Saeed, E. E. Sevilla-Reyes, M. Agudelo, K.-H. Yao, J. Golijanin, H. B. Gristick, Y. E. Lee, A. Hurley, M. Caskey, J. Pai, T. Oliveira, E. A. Wunder, G. Sacramento, N. Nery, C. Orge, F. Costa, M. G. Reis, N. M. Thomas, et al., *Cell* **2017**, *169*, 597.
[108] X. Niu, L. Zhao, L. Qu, Z. Yao, F. Zhang, Q. Yan, S. Zhang, R. Liang, P. Chen, J. Luo, W. Xu, H. Lv, X. Liu, H. Lei, C. Yi, P. Li, Q. Wang, Y. Wang, L. Yu, X. Zhang, L. A. Bryan, E. Davidson, J. B. Doranz, L. Feng, W. Pan, F. Zhang, L. Chen, *Emerg. Microbes Infect.* **2019**, *8*, 749.
[109] H. Zhao, L. Xu, R. Bombardi, R. Nargi, Z. Deng, J. M. Errico, C. A. Nelson, K. A. Dowd, T. C. Pierson, J. E. Crowe, M. S. Diamond, D. H. Fremont, *J. Exp. Med.* **2020**, *217*, 20191792.
[110] J. R. Keeffe, K. K. A. Van Rompay, P. C. Olsen, Q. Wang, A. Gazumyan, S. A. Azzopardi, D. Schaefer-Babajew, Y. E. Lee, J. B. Stuart, A. Singapuri, J. Watanabe, J. Usachenko, A. Ardeshir, M. Saeed, M. Agudelo, T. Eisenreich, S. Bournazos, T. Y. Oliveira, C. M. Rice, L. L. Coffey, M. R. MacDonald, P. J. Bjorkman, M. C. Nussenzweig, D. F. Robbiani, *Cell Rep.* **2018**, *25*, 1385.
[111] V. Dussupt, R. S. Sankhala, G. D. Gromowski, G. Donofrio, R. A. De La Barrera, R. A. Larocca, W. Zaky, L. Mendez-Rivera, M. Choe, E. Davidson, M. K. McCracken, J. D. Brien, P. Abbink, H. Bai, A. L. Bryan, C. H. Bias, I. M. Berry, N. Botero, T. Cook, N. A. Doria-Rose, A. G. I. Escuer, J. A. Frimpong, A. Geretz, M. Hernandez, B. S. Hollidge, N. Jian, K. Kabra, D. J. Leggat, J. Liu, A. K. Pinto, et al., *Nat. Med.* **2020**, *26*, 228.
[112] C. Cruz-Oliveira, J. M. Freire, T. M. Conceição, L. M. Higa, M. A. R. B. Castanho, A. T. Da Poian, *FEMS Microbiol. Rev.* **2015**, *39*, 155.
[113] K. I. P. J. Hidari, T. Suzuki, *Trop. Med. Health* **2011**, *39*, S37.
[114] J. Adhikari, J. Heffernan, M. Edeling, E. Fernandez, P. N. Jethva, M. S. Diamond, D. H. Fremont, M. L. Gross, *Biomolecules* **2024**, *14*, 374.
[115] S. Mukhopadhyay, R. J. Kuhn, M. G. Rossmann, *Nat. Rev. Microbiol.* **2005**, *3*, 13.
[116] Y. Modis, S. Ogata, D. Clements, S. C. Harrison, *Nature* **2004**, *427*, 313.
[117] X. Zhang, J. Sheng, S. K. Austin, T. E. Hoornweg, J. M. Smit, R. J. Kuhn, M. S. Diamond, M. G. Rossmann, *J. Virol.* **2015**, *89*, 743.
[118] X. Lu, H. Xiao, S. Li, X. Pang, J. Song, S. Liu, H. Cheng, Y. Li, X. Wang, C. Huang, T. Guo, J. ter Meulen, S. Daffis, J. Yan, L. Dai, Z. Rao, H.-D. Klenk, J. Qi, Y. Shi, G. F. Gao, *Cell Rep.* **2019**, *26*, 438.
[119] T. Kotaki, T. Kurosu, A. Grinyo-Escuer, E. Davidson, S. Churrotin, T. Okabayashi, O. Puiprom, K. C. Mulyatno, T. H. Sucipto, B. J. Doranz, K.-I. Ono, S. Soegijanto, M. Kameoka, *Sci. Rep.* **2021**, *11*, 12987.
[120] J. L. Remmel, J. C. Frei, S. E. Butler, J. R. Lai, M. E. Ackerman, *Virology* **2021**, *559*, 57.
[121] D. L. Akey, W. C. Brown, S. Dutta, J. Konwerski, J. Jose, T. J. Jurkiw, J. DelProposto, C. M. Ogata, G. Skiniotis, R. J. Kuhn, J. L. Smith, *Science* **2014**, *343*, 881.
[122] I. Gutsche, F. Coulibaly, J. E. Voss, J. Salmon, J. d'Alayer, M. Ermonval, E. Larquet, P. Charneau, T. Krey, F. Mégret, E. Guittet, F. A. Rey, M. Flamand, *Proc. Natl. Acad. Sci. U. S. A.* **2011**, *108*, 8003.
[123] A. Reyes-Sandoval, J. E. Ludert, *Front. Immunol.* **2019**, *10*, 1651.
[124] S. B. Biering, D. L. Akey, M. P. Wong, W. C. Brown, N. T. N. Lo, H. Puerta-Guardo, F. Tramontini Gomes de Sousa, C. Wang, J. R. Konwerski, D. A. Espinosa, N. J. Bockhaus, D. R. Glasner, J. Li, S. F. Blanc, E. Y. Juan, S. J. Elledge, M. J. Mina, P. R. Beatty, J. L. Smith, E. Harris, *Science* **2021**, *371*, 194.
[125] L. A. Sanchez-Vargas, A. Mathew, H. Salje, D. Sousa, N. A. Casale, A. Farmer, D. Buddhari, K. Anderson, S. Iamsirithaworn, S. Kaewhiran, H. Friberg, J. R. Currier, A. L. Rothman, *J. Infect. Dis.* **2024**, *230*, 1147.
[126] J. S. G. Ooi, S.-M. Lok, *Trends Biochem. Sci.* **2021**, *46*, 519.
[127] N. Modhiran, H. Song, L. Liu, C. Bletchly, L. Brillault, A. A. Amarilla, X. Xu, J. Qi, Y. Chai, S. T. M. Cheung, R. Traves, Y. X. Setoh, S. Bibby, C. A. P. Scott, M. E. Freney, N. D. Newton, A. A. Khromykh, K. J. Chappell, D. A. Muller, K. J. Stacey, M. J. Landsberg, Y. Shi, G. F. Gao, P. R. Young, D. Watterson, *Science* **2021**, *371*, 190.
[128] I.-J. Liu, C.-Y. Chiu, Y.-C. Chen, H.-C. Wu, *J. Biol. Chem.* **2011**, *286*, 9726.
[129] H.-J. Cheng, H.-Y. Lei, C.-F. Lin, Y.-H. Luo, S.-W. Wan, H.-S. Liu, T.-M. Yeh, Y.-S. Lin, *Mol. Immunol.* **2009**, *47*, 398.
[130] Y.-C. Chuang, J. Lin, Y.-S. Lin, S. Wang, T.-M. Yeh, *J. Immunol.* **1950**, *196*, 1218.

[131] Y.-C. Lai, Y.-C. Chuang, C.-C. Liu, T.-S. Ho, Y.-S. Lin, R. Anderson, T.-M. Yeh, *Sci. Rep.* **2017**, *7*, 6975.
[132] M. J. Bailey, J. Duehr, H. Dulin, F. Broecker, J. A. Brown, F. O. Arumemi, M. C. Bermúdez González, V. H. Leyva-Grado, M. J. Evans, V. Simon, J. K. Lim, F. Krammer, R. Hai, P. Palese, G. S. Tan, *Nat. Commun.* **2018**, *9*, 4560.
[133] S. L. Morrison, M. J. Johnson, L. A. Herzenberg, V. T. Oi, *Proc. Natl. Acad. Sci. U. S. A.* **1984**, *81*, 6851.
[134] A. S. Adler, D. Bedinger, M. S. Adams, M. A. Asensio, R. C. Edgar, R. Leong, J. Leong, R. A. Mizrahi, M. J. Spindler, S. R. Bandi, H. Huang, P. Tawde, P. Brams, D. S. Johnson, *mAbs* **2018**, *10*, 431.
[135] L. D. Goldstein, Y.-J. J. Chen, J. Wu, S. Chaudhuri, Y.-C. Hsiao, K. Schneider, K. H. Hoi, Z. Lin, S. Guerrero, B. S. Jaiswal, J. Stinson, A. Antony, K. B. Pahuja, D. Seshasayee, Z. Modrusan, I. Hötzel, S. Seshagiri, *Commun. Biol.* **2019**, *2*, 304.
[136] M. Singh, G. Al-Eryani, S. Carswell, J. M. Ferguson, J. Blackburn, K. Barton, D. Roden, F. Luciani, T. Giang Phan, S. Junankar, K. Jackson, C. C. Goodnow, M. A. Smith, A. Swarbrick, *Nat. Commun.* **2019**, *10*, 3120.
[137] K. S. Cox, A. Tang, Z. Chen, M. S. Horton, H. Yan, X.-M. Wang, S. A. Dubey, D. J. DiStefano, A. Ettenger, R. H. Fong, B. J. Doranz, D. R. Casimiro, K. A. Vora, *mAbs* **2016**, *8*, 129.
[138] A. Gérard, A. Woolfe, G. Mottet, M. Reichen, C. Castrillon, V. Menrath, S. Ellouze,A. Poitou, R. Doineau, L. Briseno-Roa, P. Canales-Herrerias, P. Mary, G. Rose, C. Ortega, M. Delincé, S. Essono, B. Jia, B. Iannascoli, O. Richard-Le Goff, R. Kumar, S. N. Stewart, Y. Pousse, B. Shen, K. Grosselin, B. Saudemont, A. Sautel-Caillé, A. Godina, S. McNamara, K. Eyer, G. A. Millot, J. Baudry, P. England, C. Nizak, A. Jensen, A. D. Griffiths, P. Bruhns, C. Brenan, *Nat. Biotechnol.* **2020**, *38*, 715.
[139] N. Shembekar, H. Hu, D. Eustace, C. A. Merten, *Cell Rep.* **2018**, *22*, 2206.
[140] B. Wang, B. J. DeKosky, M. R. Timm, J. Lee, E. Normandin, J. Misasi, R. Kong, J. R. McDaniel, G. Delidakis, K. E. Leigh, T. Niezold, C. W. Choi, E. G. Viox, A. Fahad, A. Cagigi, A. Ploquin, K. Leung, E. S. Yang, W.-P. Kong, W. N. Voss, A. G. Schmidt, M. A. Moody, D. R. Ambrozak, A. R. Henry, F. Laboune, J. E. Ledgerwood, B. S. Graham, M. Connors, D. C. Douek, N. J. Sullivan *Nat. Biotechnol.* **2018**, *36*, 152.
[141] J. A. Wippold, H. Wang, J. Tingling, J. L. Leibowitz, P. De Figueiredo, A. Han, *Lab Chip* **2020**, *20*, 1628.
[142] I. Setliff, A. R. Shiakolas, K. A. Pilewski, A. A. Murji, R. E. Mapengo, K. Janowska, S. Richardson, C. Oosthuysen, N. Raju, L. Ronsard, M. Kanekiyo, J. S. Qin, K. J. Kramer, A. R. Greenplate, W. J. McDonnell, B. S. Graham, M. Connors, D. Lingwood, P. Acharya, L. Morris, I. S. Georgiev, *Cell* **2019**, *179*, 1636.
[143] K. A. Pilewski, S. Wall, S. I. Richardson, N. P. Manamela, K. Clark, T. Hermanus, E. Binshtein, R. Venkat, G. A. Sautto, K. J. Kramer, A. R. Shiakolas, I. Setliff, J. Salas, R. E. Mapengo, N. Suryadevara, J. R. Brannon, C. J. Beebout, R. Parks, N. Raju, N. Frumento, L. M. Walker, E. F. Fechter, J. S. Qin, A. A. Murji, K. Janowska, B. Thakur, J. Lindenberger, A. J. May, X. Huang, S. Sammour, et al., *Cell Rep.* **2023**, *42*, 112044.
[144] G. Sapparapu, E. Fernandez, N. Kose, Bin Cao, J. M. Fox, R. G. Bombardi, H. Zhao, C. A. Nelson, A. L. Bryan, T. Barnes, E. Davidson, I. U. Mysorekar, D. H. Fremont, B. J. Doranz, M. S. Diamond, J. E. Crowe, *Nature* **2016**, *540*, 443.
[145] L. Ledsgaard, M. Kilstrup, A. Karatt-Vellatt, J. McCafferty, A. H. Laustsen, *Toxins* **2018**, *10*, 236.
[146] G. P. Smith, *Science* **1985**, *228*, 1315.
[147] S. Mimmi, D. Maisano, I. Quinto, E. Iaccino, *Trends Pharmacol. Sci.* **2019**, *40*, 87.
[148] M. Sioud, *Mol. Biotechnol.* **2019**, *61*, 286.
[149] R. K. A. França, I. C. Studart, M. R. L. Bezerra, L. Q. Pontes, A. M. A. Barbosa, M. M. Brigido, G. P. Furtado, A. Q. Maranhão, *Viruses* **2023**, *15*, 1903.
[150] H. J. Ditzel, in *Antibody Phage Display* (Ed: R. Aitken), Humana Press, Totowa, NJ, USA **2009**, pp. 37–43.
[151] C. F. Barbas, *Phage Display : A Laboratory Manual*, Cold Spring Harbor Laboratory Press, Woodbury, NY, USA **2001**.
[152] J. C. Almagro, M. Pedraza-Escalona, H. I. Arrieta, S. M. Pérez-Tapia, *Antibodies* **2019**, *8*, 44.
[153] J. K. H. Liu, *Ann. Med. Surg.* **2014**, *3*, 113.
[154] Y. Zhang, *mAbs* **2023**, *15*, 2213793.
[155] M. A. Alfaleh, H. O. Alsaab, A. B. Mahmoud, A. A Alkayyal, M. L. Jones, S. M. Mahler, A. M. Hashem, *Front. Immunol.* **1986**, *11*, 1986.
[156] G. P. Smith, J. K. Scott, *Methods Enzymol.* **1993**, *217*, 228.
[157] M. Throsby, C. Geuijen, J. Goudsmit, A. Q. Bakker, J. Korimbocus, R. A. Kramer, M. Clijsters-van der Horst, M. de Jong, M. Jongeneelen, S. Thijsse, R. Smit, T. J. Visser, N. Bijl, W. E. Marissen, M. Loeb, D. J. Kelvin, W. Preiser, J. ter Meulen, J. de Kruif, *J. Virol.* **2006**, *80*, 6982.
[158] A. S. Fahad, M. R. Timm, B. Madan, K. E. Burgomaster, K. A. Dowd, E. Normandin, M. F. Gutiérrez-González, J. M. Pennington, M. O. De Souza, A. R. Henry, F. Laboune, L. Wang, D. R. Ambrozak, I. J. Gordon, D. C. Douek, J. E. Ledgerwood, B. S. Graham, L. R. Castilho, T. C. Pierson, J. R. Mascola, B. J. DeKosky, *Front. Immunol.* **2021**, *12*, 615102.
[159] J. Zhang, X. '. Zhang, Q. Liu, M. Li, L. Gao, X. Gao, S. Xiang, L. Wu, J. Fu, H. Song, *Acta Biochim. Biophys. Sin.* **2014**, *46*, 859.
[160] M. Gutierrez-Gonzalez, A. S. Fahad, C. L. Delley, C.-Y. Chung, S. Jin, N. Boyle, M. O. de Souza, A. Pirhanov, N. M. S. Galvez, C. T. França, S. Marglous, E. Bhagat, D. Vincent, D. Neumeier, Y. Cao, N. Doria-Rose, S. T. Reddy, A. G. Schmidt, A. B. Balazs, A. R. Abate, B. J. DeKosky, bioRxiv [Preprint] **2025**, https://doi.org/10.1101/2025.01.31.635965.
[161] D. R. Goulet, W. M. Atkins, *J. Pharm. Sci.* **2020**, *109*, 74.
[162] S. Ahangarzadeh, Z. Payandeh, R. Arezumand, K. Shahzamani, F. Yarian, A. Alibakhshi, *Int. Immunopharmacol.* **2020**, *86*, 106760.
[163] G. Pantaleo, B. Correia, C. Fenwick, V. S. Joo, L. Perez, *Nat. Rev. Drug Discovery* **2022**, *21*, 676.
[164] S. Oksanen, R. Saarinen, A. Korkiakoski, U. Lamminmäki, T. Huovinen, *Sci. Rep.* **2023**, *13*, 13107.
[165] Y. Mei, Y. Chen, J. P. Sivaccumar, Z. An, N. Xia, W. Luo, *Front. Pharmacol.* **2022**, *13*, 963978.
[166] A. F. Labrijn, M. L. Janmaat, J. M. Reichert, P. W. H. I. Parren, *Nat. Rev. Drug Discovery* **2019**, *18*, 585.
[167] A. V. Madsen, L. E. Pedersen, P. Kristensen, S. Goletz, *Front. Bioeng. Biotechnol.* **2024**, *12*, 1352014.
[168] J. Hruškovicová,K. Bhide, P. Petroušková, Z. Tkáčová, E. Mochnáčová,J. Čurlík, M. Bhide, A. Kulkarni, *Front. Microbiol.* **2022**, *13*, 801466.
[169] J. A. Swanstrom, J. A. Plante, K. S. Plante, E. F. Young, E. McGowan, E. N. Gallichotte, D. G. Widman, M. T. Heise, A. M. de Silva, R. S. Baric, *mBio* **2016**, *7*, 01123.
[170] N. Nilchan, R. Kraivong, P. Luangaram, A. Phungsom, M. Tantiwatcharakunthon, S. Traewachiwiphak, T. Prommool, N. Punyadee, P. Avirutnan, T. Duangchinda, P. Malasit, C. Puttikhunt, *ACS Infect. Dis.* **2024**, *10*, 2690.
[171] A. L. Nelson, J. M. Reichert, *Nat. Biotechnol.* **2009**, *27*, 331.
[172] D. Chaudhuri, S. Majumder, J. Datta, K. Giri, *J. Biomol. Struct. Dyn.* **2023**, *41*, 2289.
[173] T. Delfin-Riela, M. A. Rossotti, G. Mattiuzzo, C. Echaides, G. González-Sapienza, *Trop. Med. Infect. Dis.* **2023**, *8*, 55.
[174] L. Wang, R. Luo, W. Zhang, H. Jiang, Y. Yu, W. Zhou, F. Zhang,J. Ma, L. Mei, *Smart Mater. Med.* **2024**, *5*, 501.

[175] F. Callewaert, J. Roodt, H. Ulrichts, T. Stohr, W. Janse van Rensburg, S. Lamprecht, S. Rossenu, S. Priem,W. Willems, J.-B. Holz, *Blood* **2012**, *120*, 3603.
[176] M. Scully, S. R. Cataland, F. Peyvandi, P. Coppo, P. Knöbl, J. A. Kremer Hovinga, A. Metjian, J. de la Rubia, K. Pavenski, F. Callewaert, D. Biswas, H. De Winter, R. K. Zeldin, *N. Engl. J. Med.* **2019**, *380*, 335.
[177] FDA Approves First Therapy for the Treatment of Adult Patients with a Rare Blood Clotting Disorder, https://www.fda.gov/news-events/press-announcements/fda-approves-first-therapy-treatment-adult-patients-rare-blood-clotting-disorder, Feb. 2019. Accessed: May 24, **2025**.
[178] D. Focosi, S. McConnell, A. Casadevall, E. Cappello, G. Valdiserra, M. Tuccori, *Lancet Infect. Dis.* **2022**, *22*, 311.
[179] D. Kumar, S. Gauthami, J. Bayry, S. V. Kaveri, N. R. Hegde, *Monoclonal Antibodies Immunodiagn. Immunother.* **2021**, *40*, 36.
[180] S. R. Walsh, M. S. Seaman, *Front. Immunol.* **2021**, *12*, 712122.
[181] A. Markham, *Drugs* **2021**, *81*, 175.
[182] E. D. Deeks, *Drugs* **2021**, *81*, 2047.
[183] S. M. Hoy, *Drugs* **2022**, *82*, 1327.
[184] S. M. Choi, J.-H. Lee, S. Ko, S.-S. Hong, H.-E. Jin, *Biomol. Ther.* **2024**, *32*, 708.
[185] T. Li, M. Niu, J. Zhou, K. Wu, M. Yi, *Cell Commun. Signaling* **2024**, *22*, 179.
[186] R. De Gasparo, M. Pedotti, L. Simonelli, P. Nickl, F. Muecksch, I. Cassaniti, E. Percivalle, J. C. C. Lorenzi, F. Mazzola, D. Magrì, T. Michalcikova, J. Haviernik, V. Honig, B. Mrazkova, N. Polakova, A. Fortova, J. Tureckova, V. Iatsiuk, S. Di Girolamo, M. Palus, D. Zudova, P. Bednar, I. Bukova, F. Bianchini, D. Mehn, R. Nencka, P. Strakova, O. Pavlis, J. Rozman, S. Gioria, et al., *Nature* **2021**, *593*, 424.
[187] Z. Ku, X. Xie, J. Lin, P. Gao, B. Wu, A. El Sahili, H. Su, Y. Liu, X. Ye, E. Y. Tan, X. Li, X. Fan, B. C. Goh, W. Xiong, H. Boyd, A. E. Muruato, H. Deng, H. Xia, J. Zou, B. K. Kalveram, V. D. Menachery, N. Zhang, J. Lescar, P.-Y. Shi, Z. An, *Nat. Commun.* **2022**, *13*, 5552.
[188] J. Wang, M. Bardelli, D. A. Espinosa, M. Pedotti, T.-S. Ng, S. Bianchi, L. Simonelli, E. X. Y. Lim, M. Foglierini, F. Zatta, S. Jaconi, M. Beltramello, E. Cameroni, G. Fibriansah, J. Shi, T. Barca, I. Pagani, A. Rubio, V. Broccoli, E. Vicenzi, V. Graham, S. Pullan, S. Dowall, R. Hewson, S. Jurt, O. Zerbe, K. Stettler, A. Lanzavecchia, F. Sallusto, A. Cavalli, et al., *Cell* **2017**, *171*, 229.
[189] R. Khandia, A. Munjal, K. Dhama, K. Karthik, R. Tiwari, Y. S. Malik, R. K. Singh, W. Chaicumpa, *Front. Immunol.* **2018**, *9*, 597.
[190] X. Shi, Y. Deng, H. Wang, G. Ji, W. Tan, T. Jiang, X. Li, H. Zhao, T. Xia, Y. Meng, C. Wang, X. Yu, Y. Yang, B. Li, E.-D. Qin, J. Dai, C.-F. Qin, Y. Guo, *mAbs* **2016**, *8*, 574.
[191] L. F. Ormundo, C. T. Barreto, L. R. Tsuruta, *Viruses* **2023**, *15*, 2177.
[192] K. L. Armour, M. R. Clark, A. G. Hadley, L. M. Williamson, *Eur. J. Immunol.* **1999**, *29*, 2613.
[193] H. Sun, M. Yang, H. Lai, B. Neupane, A. Y.-H. Teh, C. Jugler, J. K.-C. Ma, H. Steinkellner, F. Bai, Q. Chen, *Viruses* **2023**, *15*, 1156.
[194] J. P. Nkolola, D. Hope, R. Guan, A. Colarusso, M. Aid, D. Weiss, J. Misamore, H. Andersen, M. G. Lewis, L. Williamson, R. H. Carnahan,J. E. Crowe Jr, D. H. Barouch, *J. Virol.* **2024**, *98*, 0142924.
[195] R. Ramadhany, I. Hirai, T. Sasaki, K.-i. Ono, P. Ramasoota, K. Ikuta, T. Kurosu, *Antiviral Res.* **2015**, *124*, 61.
[196] A. P. Goncalvez, R. E. Engle, M. St. Claire, R. H. Purcell, C.-J. Lai, *Proc. Natl. Acad. Sci. U. S. A.* **2007**, *104*, 9422.
[197] A. Gupta, K. S. Kao, R. Yamin, D. A. Oren, Y. Goldgur, J. Du, P. Lollar, E. J. Sundberg, J. V. Ravetch, *Nat. Commun.* **2023**, *14*, 2853.
[198] C. Ferrara, S. Grau, C. Jäger, P. Sondermann, P. Brünker, I. Waldhauer, M. Hennig, A. Ruf, A. C. Rufer, M. Stihle,P. Umaña, J. Benz, *Proc. Natl. Acad. Sci. U. S. A.* **2011**, *108*, 12669.
[199] R. L. Shields, J. Lai, R. Keck, L. Y. O'Connell, K. Hong, Y. G. Meng, S. H. A. Weikert, L. G. Presta, *J. Biol. Chem.* **2002**, *277*, 26733.
[200] J. M. Perchiacca, P. M. Tessier, *Annu. Rev. Chem. Biomol. Eng.* **2012**, *3*, 263.
[201] D. Y. Kim, H. Kandalaft, W. Ding, S. Ryan, H. van Faassen, T. Hirama, S. J. Foote, R. MacKenzie, J. Tanha, *Protein Eng. Des. Sel.* **2012**, *25*, 581.
[202] P. A. Barthelemy, H. Raab, B. A. Appleton, C. J. Bond, P. Wu, C. Wiesmann, S. S.*J. Biol. Chem.* **2008**, *283*, 3639.
[203] R. de Alwis, S. A. Smith, N. P. Olivarez, W. B. Messer, J. P. Huynh, W. M. P. B. Wahala, L. J. White, M. S. Diamond, R. S. Baric, J. E. Crowe Jr., A. M. de Silva, *Proc. Natl. Acad. Sci. U. S. A.* **2012**, *109*, 7439.
[204] G. Fibriansah, J. L. Tan, S. A. Smith, R. de Alwis, T.-S. Ng, V. A. Kostyuchenko, R. S. Jadi, P. Kukkaro, A. M. de Silva, J. E. Crowe, S.-M. Lok, *Nat. Commun.* **2015**, *6*, 6341.
[205] B. Gunale, N. Farinola, C. D. Kamat, C. S. Poonawalla, S. S. Pisal, R. M. Dhere, C. Miller, P. S. Kulkarni, *Lancet Infect. Dis.* **2024**, *24*, 639.
[206] J. G. Low, J. H. J. Ng, E. Z. Ong, S. Kalimuddin, L. Wijaya, Y. F. Z. Chan, D. H. L. Ng, H.-C. Tan, A. Baglody, Y.-H. Chionh, D. C. P. Lee, Y. Budigi, R. Sasisekharan, E.-E. Ooi, *N. Engl. J. Med.* **2020**, *383*, 452.
[207] L. A. Jackson, E. J. Anderson, N. G. Rouphael, P. C. Roberts, M. Makhene, R. N. Coler, M. P. McCullough, J. D. Chappell, M. R. Denison, L. J. Stevens, A. J. Pruijssers, A. McDermott, B. Flach, N. A. Doria-Rose, K. S. Corbett, K. M. Morabito, S. O'Dell, S. D. Schmidt, P. A. Swanson 2nd, M. Padilla, J. R. Mascola, K. M. Neuzil, H. Bennett, W. Sun, E. Peters, M. Makowski, J. Albert, K. Cross, W. Buchanan, R. Pikaart-Tautges, *N. Engl. J. Med.* **2020**, *383*, 1920.
[208] World Health Organization, "*Background Document on the mRNA Vaccine BNT162b2 (Pfizer-BioNTech) against COVID-19: Background Document to the WHO Interim Recommendations for Use of the Pfizer–BioNTech COVID-19 Vaccine, BNT162b2, under Emergency Use Listing, 14 January 2021*," World Health Organization, Geneva, Switzerland **2021**.
[209] P. A. Krieg, D. A. Melton, *Nucleic Acids Res.* **1984**, *12*, 7057.
[210] R. W. Malone, P. L. Felgner, I. M. Verma, *Proc. Natl. Acad. Sci. U. S. A.* **1989**, *86*, 6077.
[211] J. A. Wolff, R. W. Malone, P. Williams, W. Chong, G. Acsadi, A. Jani, P. L. Felgner, *Science* **1990**, *247*, 1465.
[212] K. Karikó, M. Buckstein, H. Ni, D. Weissman, *Immunity* **2005**, *23*, 165.
[213] A. Akinc, M. A. Maier, M. Manoharan, K. Fitzgerald, M. Jayaraman, S. Barros, S. Ansell, X. Du, M. J. Hope, T. D. Madden, B. L. Mui, S. C. Semple, Y. K. Tam, M. Ciufolini, D. Witzigmann, J. A. Kulkarni, R. van der Meel, P. R. Cullis, *Nat. Nanotechnol.* **2019**, *14*, 1084.
[214] Y. Sato, H. Hatakeyama, M. Hyodo, H. Harashima, *Mol. Ther.* **2016**, *24*, 788.
[215] S. S. Diebold, T. Kaisho, H. Hemmi, S. Akira, C. Reis E Sousa, *Science* **2004**, *303*, 1529.
[216] F. Heil, H. Hemmi, H. Hochrein, F. Ampenberger, C. Kirschning, S. Akira, G. Lipford, H. Wagner, S. Bauer, *Science* **2004**, *303*, 1526.
[217] R. H. Müller, K. Mäder, S. Gohla, *Eur. J. Pharm.* **2000**, *50*, 161.
[218] N. Pardi, A. J. Secreto, X. Shan, F. Debonera, J. Glover, Y. Yi, H. Muramatsu, H. Ni, B. L. Mui, Y. K. Tam, F. Shaheen, R. G. Collman, K. Karikó, G. A. Danet-Desnoyers, T. D. Madden, M. J. Hope, D. Weissman, *Nat. Commun.* **2017**, *8*, 14630.
[219] N. Kose, J. M. Fox, G. Sapparapu, R. Bombardi, R. N. Tennekoon, A. D. de Silva, S. M. Elbashir, M. A. Theisen, E. Humphris-Narayanan, G. Ciaramella, S. Himansu, M. S. Diamond, J. E. Crowe Jr., *Sci. Immunol.* **2019**, *4*, aaw6647.
[220] T. Kalita, S. A. Dezfouli, L. M. Pandey, H. Uludag, *Pharmaceutics* **2022**, *14*, 2520.
[221] F. Wang, R. M. Kream, G. B. Stefano, *Med. Sci. Monit.* **2020**, *26*, 924700.
[222] C. Chung, S. B. Kudchodkar, C. N. Chung, Y. K. Park, Z. Xu, N. Pardi, M. Abdel-Mohsen, K. Muthumani, *Antibodies* **2023**, *12*, 46.

[223] J. H. Erasmus,J. Archer, J. Fuerte-Stone, A. P. Khandhar, E. Voigt, B. Granger, R. G. Bombardi, J. Govero, Q. Tan, L. A. Durnell, R. N. Coler, M. S. Diamond, J. E. Crowe Jr, S. G. Reed, L. B. Thackray, R. H. Carnahan, N. Van Hoeven, *Mol. Ther.–Methods Clin. Dev.* **2020**, *18*, 402.
[224] C. E. Deal, A. Carfi, O. J. Plante, *Vaccines* **2021**, *9*, 108.
[225] Z. Wang, P. J. Troilo, X. Wang, T. G. Griffiths, S. J. Pacchione, A. B. Barnum, L. B. Harper, C. J. Pauley, Z. Niu, L. Denisova, T. T. Follmer, G. Rizzuto, G. Ciliberto, E. Fattori, N. L. Monica, S. Manam, B. J. Ledwith, *Gene Ther.* **2004**, *11*, 711.
[226] K. Leppek, R. Das, M. Barna, *Nat. Rev. Mol. Cell Biol.* **2018**, *19*, 158.
[227] A. Ramanathan, G. B. Robb, S.-H. Chan, *Nucleic Acids Res.* **2016**, *44*, 7511.
[228] J. Stepinski, C. Waddell, R. Stolarski, E. Darzynkiewicz, R. E. Rhoads, *RNA* **2001**, *7*, 1486.
[229] M. Mockey, C. Gonçalves, F. P. Dupuy, F. M. Lemoine, C. Pichon, P. Midoux, *Biochem. Biophys. Res. Commun.* **2006**, *340*, 1062.
[230] I. Kocmik, K. Piecyk, M. Rudzinska, A. Niedzwiecka, E. Darzynkiewicz, R. Grzela, M. Jankowska-Anyszka, *Cell Cycle* **2018**, *17*, 1624.
[231] M. S. Diamond, *Cytokine Growth Factor Rev.* **2014**, *25*, 543.
[232] S. Xu, K. Yang, R. Li, L. Zhang, *Int. J. Mol. Sci.* **2020**, *21*, 6582.
[233] C. S. Nelson, J. A. Jenks, N. Pardi, M. Goodwin, H. Roark, W. Edwards, J. S. McLellan, J. Pollara, D. Weissman, S. R. Permar, *J. Virol.* **2020**, *94*, 00186.
[234] K. Karikó, H. Muramatsu, J. Ludwig, D. Weissman, *Nucleic Acids Res.* **2011**, *39*, 142.
[235] D. Weissman, *Expert Rev. Vaccines* **2015**, *14*, 265.
[236] S. A. Dilliard, D. J. Siegwart, *Nat. Rev. Mater.* **2023**, *8*, 282.
[237] S. A. Dilliard, Q. Cheng, D. J. Siegwart, *Proc. Natl. Acad. Sci. U. S. A.* **2021**, *118*, 2109256118.
[238] K. Su, L. Shi, T. Sheng, X. Yan, L. Lin, C. Meng, S. Wu, Y. Chen, Y. Zhang, C. Wang, Z. Wang, J. Qiu, J. Zhao, T. Xu, Y. Ping, Z. Gu, S. Liu, *Nat. Commun.* **2024**, *15*, 5659.
[239] The role of helper lipids in lipid nanoparticles (LNPs) designed for oligonucleotide delivery-PubMed, https://pubmed.ncbi.nlm.nih.gov/26900977/, Accessed: Aug. 25, **2025**.
[240] D. Witzigmann, J. A. Kulkarni, J. Leung, S. Chen, P. R. Cullis, R. van der Meel, *Adv. Drug Delivery Rev.* **2020**, *159*, 344.
[241] M. D. Buschmann, M. J. Carrasco, S. Alishetty, M. Paige, M. G. Alameh, D. Weissman, *Vaccines* **2021**, *9*, 65.
[242] E. Fang, X. Liu, M. Li, Z. Zhang, L. Song, B. Zhu, X. Wu, J. Liu, D. Zhao, Y. Li, *Signal Transduction Targeted Ther.* **2022**, *7*, 94.
[243] A. August, H. Z. Attarwala, S. Himansu, S. Kalidindi, S. Lu, R. Pajon, S. Han, J.-M. Lecerf, J. E. Tomassini, M. Hard, L. M. Ptaszek, J. E. Crowe, T. Zaks, *Nat. Med.* **2021**, *27*, 2224.
[244] Y. Zhao, L. Gan, D. Ke, Q. Chen, Y. Fu, *J. Transl. Med.* **2023**, *21*, 693.
[245] D. Zhang, H. Liu, Y. Zhong, *New Biotechnol.* **2025**, *90*, 163.
[246] Y. Huang, Y. Zhang, X. Yang, Z. Lin, *Trends Biotechnol.* **2025**, *43*, 476.
[247] NIAID Visual & Medical Arts. (6/4/2025). RNA. NIAID NIH BIOART Source. https://bioart.niaid.nih.gov/bioart/452.
[248] NIAID Visual & Medical Arts. (6/4/2025). DNA. NIAID NIH BIOART Source. https://bioart.niaid.nih.gov/bioart/123.

**Ana Clara Barbosa Antonelli** received her Bachelor's degree in Biotechnology and a Master's degree in Tropical Medicine and Public Health with a focus on Immunology from the Federal University of Goiás. She is currently pursuing her PhD, generating monoclonal antibodies against flaviviruses using phage display libraries. During her doctoral studies, she completed a visiting PhD period at the Ragon Institute of MGH, MIT, and Harvard. Her research focuses on immunology and molecular biology, with an emphasis on antibody discovery and therapeutic applications.

**Lucas Silva Rodrigues** graduated in Biological Sciences from the University of Brasília in 2021 and earned a Master's degree in Molecular Pathology from the same institution. His research focuses on molecular biology and immunology, particularly the discovery and characterization of monoclonal antibodies selected by phage display. He has experience in protein expression and purification, ELISA, neutralization assays, and in vitro transcription. He is currently pursuing a PhD in Molecular Biology at the University of Brasília, investigating in vivo antibody expression using nucleic-acidbased delivery platforms, including DNA vectors and IVT-mRNA.


**Maria Clara Moura Pinheiro** is an undergraduate Biotechnology student at the University of Brasília (UnB) with experience in Cell Biology, Molecular Biology, and Immunology, focusing on heterologous expression of human monoclonal antibodies. She is a Scientific Initiation fellow in the Molecular Immunology Laboratory, where she develops neutralizing antibodies against flaviviruses such as Zika and Dengue. Her work earned an Honorable Mention award in 2024 and a nomination for the Scientific Initiation Excellence Award in 2025. She also served as an instructor in the "Design of Therapeutical Proteins" module at LymphoRioMove 2025.

**Sylvia Barbosa Pinhate** is a Biologist and MSc in Molecular Biology from the University of Brasília (UnB). Her research background includes molecular biology, microbiology, and immunology, with a recent focus on engineered probiotics for therapeutic antibody delivery in models of inflammatory bowel disease.

**Marcelo de Macedo Brígido**, Full Professor at the University of Brasília, is a molecular immunologist with substantial contributions to genomics, recombinant antibodies, and bioinformatics. He holds a PhD from USP and has published over 100 scientific articles. He is the Principal Investigator of the Molecular Immunology Group at UnB. His academic impact includes supervising 47 master's students, 18 doctoral candidates, six postdoctoral fellows, and over 50 additional trainees. His work spans antibody engineering, gene expression systems, and computational analysis of immune-related sequences.

**Andréa Queiroz Maranhão** is a full professor of Cell Biology at the University of Brasília, specializing in molecular immunology, antibody engineering, and CAR design. She has published 73 articles, holds seven patents, and has supervised 25 master's, 12 PhD, two postdoctoral researchers, and 47 trainees. As vice-leader of UnB's Molecular Immunology Group, she advances therapeutic antibody research, including humanization strategies, phage display libraries, optimized expression systems, and innovative biotechnological routes for developing high-complexity drugs.